

University of Windsor

## Scholarship at UWindor

---

Electronic Theses and Dissertations

Theses, Dissertations, and Major Papers

---

2014

# New Materials, Methods, and Molecules for Microelectronic and Molecular Electronic Devices

Michael Stephen Miller  
*University of Windsor*

Follow this and additional works at: <https://scholar.uwindsor.ca/etd>

 Part of the [Biochemistry, Biophysics, and Structural Biology Commons](#)

---

### Recommended Citation

Miller, Michael Stephen, "New Materials, Methods, and Molecules for Microelectronic and Molecular Electronic Devices" (2014). *Electronic Theses and Dissertations*. 5053.  
<https://scholar.uwindsor.ca/etd/5053>

This online database contains the full-text of PhD dissertations and Masters' theses of University of Windsor students from 1954 forward. These documents are made available for personal study and research purposes only, in accordance with the Canadian Copyright Act and the Creative Commons license—CC BY-NC-ND (Attribution, Non-Commercial, No Derivative Works). Under this license, works must always be attributed to the copyright holder (original author), cannot be used for any commercial purposes, and may not be altered. Any other use would require the permission of the copyright holder. Students may inquire about withdrawing their dissertation and/or thesis from this database. For additional inquiries, please contact the repository administrator via email ([scholarship@uwindsor.ca](mailto:scholarship@uwindsor.ca)) or by telephone at 519-253-3000ext. 3208.

# **New Materials, Methods, and Molecules for Microelectronic and Molecular Electronic Devices**

By

Michael Stephen Miller

A Dissertation

Submitted to the Faculty of Graduate Studies  
through the Department of Chemistry and Biochemistry  
in Partial Fulfillment of the Requirements for  
the Degree of Doctor of Philosophy at the  
University of Windsor

Windsor, Ontario, Canada

2014

© 2014 Michael Stephen Miller

**New Materials, Methods and Molecules for Microelectronic and Molecular  
Electronic Devices**

by

Michael Miller

APPROVED BY:

---

G. Kane Jennings, External Examiner  
Vanderbilt University

---

A. Alpas  
Mechanical and Materials Engineering

---

S.H. Eichhorn  
Department of Chemistry & Biochemistry

---

S. Loeb  
Department of Chemistry & Biochemistry

---

T. Carmichael, Advisor  
Department of Chemistry & Biochemistry

December 18, 2013

# **Declaration of Co-Authorship / Previous Publication**

## **I. Co-Authorship Declaration**

I hereby declare that this thesis incorporates material that is a result of joint research, as follows: This thesis incorporates the outcome of the research undertaken in Dr. Tricia Carmichael's research group. I acknowledge my colleague Dr. Ronan R. San Juan for the synthesis of dialkyldithiophosphinic acids in Chapter 5, Chapter 6, and Chapter 7 and Chapter 8. I acknowledge Dr. Christopher J. Allan and Dr. Charles L. B. Macdonald for undertaking the computational investigation presented in Chapter 8. I acknowledge all colleagues listed on the manuscripts, each of whom contributed to this thesis through raw data acquisition (Dr. Gregory J. E. Davidson, Heather L. Filiatrault, Dr. Ronan R. San Juan, Minmin Luo, Michael-Anthony Ferrato, Jessica C. O'Kane, Adrian Niec, and R. Stephen Carmichael). I am aware of the University of Windsor Senate Policy on Authorship and I certify that I have properly acknowledged the contribution of other researchers to my thesis, and have obtained written permission from each of the co-author(s) to include the above material(s) in my thesis. I certify that, with the above qualification, this thesis, and the research to which it refers, is the product of my own work.

## II. Declaration of Previous Publication

This thesis includes 5 original papers that have been previously published / submitted for publication in peer reviewed journals, as follows:

Thesis Chapter	Publication Title / Full Citation	Publication Status
Chapter 2	Miller, M. S.; Filiatrault, H. L.; Davidson, G. J. E.; Luo, M.; Carmichael, T. B. "Selectively Metallized Polymeric Substrates by Microcontact Printing an Aluminum(III) Porphyrin Complex" <i>J. Am. Chem. Soc.</i> <b>2010</b> , <i>132</i> , 765-772.	Published
Chapter 3	Miller, M. S.; O'Kane, J. C.; Niec, A.; Carmichael, R. S.; Carmichael, T. B. "Silver Nanowire/Optical Adhesive Coatings as Transparent Electrodes for Flexible Electronics" <b>2013</b> , <i>5</i> , 10165-10172.	Published
Chapter 4	Miller, M. S.; Davidson, G. J. E.; Carmichael, T. B. "Templated Self Assembly of Glass Microspheres into Ordered Two-Dimensional Arrays under Dry Conditions" <i>Langmuir</i> <b>2010</b> , <i>26</i> , 5286-90.	Published
Chapter 5	Miller, M. S.; San Juan, R. R.; Ferrato, M.-A.; Carmichael, T. B. "New Dialkyldithiophosphinic Acid Self-Assembled Monolayers (SAMs): Influence of Gold Substrate Morphology on Adsorbate Binding and SAM Structure" <i>Langmuir</i> <b>2011</b> , <i>27</i> , 10019-10026.	Published
Chapter 6	Miller, M. S.; San Juan, R. R.; Ferrato, M.-A.; Carmichael, T. B. "The Unusual Self-Organization of Dialkyldithiophosphinic Acid Self-Assembled Monolayers on Ultrasoother Gold" <b>2013</b> , <i>J. Am. Chem. Soc.</i> ID: ja-2013-11140j.	Submitted
Chapter 7	Miller, M. S.; Carmichael, T. B. "Ultra Smooth Gold Substrates Prepared by Chemical Mechanical Polishing: A New Substrate for Measuring Charge Transport in Metal-SAM//Ga <sub>2</sub> O <sub>3</sub> /EGaIn Junctions" ( <i>J. Am. Chem. Soc.</i> ).	In preparation
Chapter 8	Miller, M. S.; Carmichael, T. B. "Electronic Properties of Diphenyldithiophosphinic Acid Self-Assembled Monolayers" ( <i>J. Am. Chem. Soc.</i> ).	In preparation

I declare that the work presented in Chapter 4, and published in *Langmuir* in 2010, contains material (particularly Figure 2.2 b-e) that resulted from a thesis submitted to the Department of Chemistry and Biochemistry in 2008 in partial fulfillment of the degree of B.Sc. Honours Chemistry with Thesis at the University of Windsor. I declare that a significant amount of the work presented in Chapter 4, including the preparation of the manuscript published in *Langmuir*, was a result of work completed during my registration as a graduate student at the University of Windsor.

I certify that I have obtained a written permission from the copyright owner(s) to include the above published material(s) in my thesis. I certify that the above material describes work completed during my registration as graduate student at the University of Windsor.

I declare that, to the best of my knowledge, my thesis does not infringe upon anyone's copyright nor violate any proprietary rights and that any ideas, techniques, quotations, or any other material from the work of other people included in my thesis, published or otherwise, are fully acknowledged in accordance with the standard referencing practices. Furthermore, to the extent that I have included copyrighted material that surpasses the bounds of fair dealing within the meaning of the Canada Copyright Act, I certify that I have obtained a written permission from the copyright owner(s) to include such material(s) in my thesis.

I declare that this is a true copy of my thesis, including any final revisions, as approved by my thesis committee and the Graduate Studies office, and that this thesis has not been submitted for a higher degree to any other University or Institution.

# Abstract

This dissertation reports a variety of new methods and materials for the fabrication of electronic devices. Particular emphasis is placed on low-cost, solution based methods for flexible electronic device fabrication, and new substrates and molecules for molecular electronic tunnel junctions.

Chapter 2 reports a low-cost, solution based method for depositing patterned metal circuitry onto a variety of flexible polymer substrates. Microcontact printing an aluminum (III) porphyrin complex activates selected areas of an oxidized polymer substrate to electroless copper metallization.

Chapter 3 reports a new transparent conductive electrode for use in optoelectronic devices. A highly conductive, transparent silver nanowire network is embedded at the surface of an optical adhesive, which can be applied to a variety of rigid and flexible polymer substrates.

Chapter 4 describes a new approach to the self-assembly of mesoscale components into two-dimensional arrays. Unlike most previously reported self-assembly motifs, this method is completely dry; eliminating solvent makes this method compatible with the assembly of electronic components.

Chapter 5 describes a new class of self-assembled monolayer (SAM) on gold formed from dihexadecyldithiophosphinic acid ( $((C_{16})_2DTPA)$ ) adsorbate molecules. The binding and structure  $(C_{16})_2DTPA$  SAMs is dependent upon the roughness and morphology of the underlying gold substrate.

Chapter 6 investigates the influence of chain length on the binding and structure of dialkyl-DTPA SAMs on smooth, template-stripped (TS) gold. Binding of the DTPA head group is independent of the length of the alkyl chain, while the structure of the organic layer has a counter-intuitive dependence: As the length of the alkyl chain increases, these SAMs become more disordered and liquid-like.

Chapter 7 describes the fabrication of ultra smooth gold substrates using chemical mechanical polishing (CMP). These substrates are smooth, uniform, and prove to be ideal

candidates for bottom electrodes within SAM-based molecular electronic tunnel junctions.

Chapter 8 investigates the charge transport properties of new diphenyldithiophosphinic acid ( $\text{Ph}_2\text{DTPA}$ ) SAMs on TS gold within metal-SAM// $\text{Ga}_2\text{O}_3$ /EGaIn molecular tunnel junctions. A computational investigation provides insight into the electronic structure of the junction.

# Dedication

This dissertation is dedicated to the memories of my two Grandfathers,  
Donald Knight Sr. and Steve Miller

# Acknowledgments

I would like to thank my parents, Len and June Miller, my sister, Lindsay Branovacki, and my girlfriend of nearly eight years, Jennifer O'Brien for their unending support and encouragement throughout my time at the University of Windsor. You have all been there for me in good times and bad, and have always been understanding of the time and energy investment required to complete this degree.

I would like to thank my advisor, Dr. Tricia Carmichael, for the many years of support, encouragement, and mentorship. I joined the Carmichael research group in 2005 without a lab, equipment, co-workers, or any idea of what 'research' really meant. Eight years later, I leave with a feeling of great academic and personal growth, and for that I am truly thankful.

I would also like to thank Steve Carmichael, not only for his contributions to my research, but also for his contributions to my knowledge of good BBQ.

I would like to thank my lab mates, particularly Heather Filiatrault and Dr. Ronan San Juan who have been by my side for the past seven years. I could write an entire chapter on all the things we've experienced together over the years and how much I appreciate your support (both in the lab, and out), and for that I thank you. I thank Stan, Akhil, Michael-Anthony, Gyllian, Jess, Paul and all other current and past members of the Carmichael group for all of the good times and laughs shared over the years. I also thank former colleagues Dr. Greg Davidson and Dr. Jan Muller for their guidance and encouragement, as well as Dr. Darren Mercer for all the conversations we've had over an XL double-double and an XL black. I'd also like to thank the numerous students who have passed through Essex hall over the past nine years for the social atmosphere that makes this department special.

I would like to thank all of the technicians who have helped with my research, including Dr. Mark Biesinger at Surface Science Western, Sharon Lackie at GLIER, and Dr. Rick Glew, Dr. Tim Goldhawk, and Dr. Todd Simson at the Western Ontario Nanofab.

Finally, I would like to thank my committee members, Dr. Steve Loeb, Dr. S. Holger Eichhorn, Dr. Ahmet Alpas, and Dr. G. Kane Jennings for reading this dissertation and providing me with the criticisms required to make it right.

# Table of Contents

Declaration of Co-Authorship/Previous Publication .....	iii
Abstract .....	vi
Dedication .....	viii
Acknowledgments .....	ix
List of Figures .....	xix
List of Tables .....	xxxiv
List of Schemes .....	xxxvii
List of Abbreviations .....	xxxviii
1. Chapter 1 - Introduction .....	1
1.1. Flexible Electronic Devices .....	2
1.1.1. Low-Cost Metallization of Polymeric Substrates .....	2
1.1.1.1. Physical Vapour Deposition .....	3
1.1.1.2. Electroless Metal Deposition .....	6
1.1.2. Flexible, Transparent Conductive Electrodes .....	7
1.1.2.1. ITO – The Industry Standard .....	7
1.1.2.2. Silver Nanowire Films as a Drop-in Replacement for ITO ...	8
1.1.3. Assembly of Device Components .....	12
1.1.3.1. Self-Assembly .....	13
1.1.3.2. Self-Assembly using Capillary Interactions .....	14
1.2. Molecular Electronics .....	18
1.2.1. Charge Transport Properties of Molecules .....	18
1.2.1.1. Coherent Tunneling .....	19
1.2.1.2. Incoherent Tunneling .....	20
1.2.1.3. Activated Transport (Hopping) .....	21
1.2.2. Molecular Junctions .....	22
1.2.3. Challenges with Molecular Junctions .....	23
1.2.4. The Molecular Monolayer .....	24
1.2.4.1. Self-Assembled Monolayers .....	26

1.2.4.2. Charge Transport through <i>n</i> -alkanethiolate SAMs .....	29
1.2.4.3. Chelating SAMs for use in Molecular Electronics .....	31
1.2.5. The Top Electrode .....	33
1.2.5.1. The Hanging Mercury Drop Electrode .....	34
1.2.5.2. The EGaIn Tip Electrode .....	35
1.2.6. The Bottom Electrode.....	37
1.3. Dissertation Objectives .....	43
1.3.1. Simple, Low-Cost Fabrication of Thin Film Device Components .....	43
1.3.2. New Molecules and Substrates for use in Molecular Electronic Devices .....	44
1.4. References .....	46
2. Chapter 2 - Selectively Metallized Polymeric Substrates by Microcontact Printing an Aluminum (III) Porphyrin Complex .....	56
2.1. Introduction .....	57
2.2. Experimental Section .....	62
2.2.1. Materials .....	62
2.2.2. Substrate Preparation .....	63
2.2.3. Stamp Inking and Printing .....	63
2.2.4. Electroless Metallization .....	63
2.2.5. Reaction of TPPAl-(benzoate) with HCl.....	63
2.2.6. Tape Test .....	64
2.2.7. Fabrication of Copper Wires and Electrical Testing .....	64
2.2.8. Characterization.....	64
2.3. Results and Discussion.....	65
2.3.1. A Single Process Selectively Deposits Copper on a Variety of Oxidized Polymeric Substrates .....	65
2.3.2. Microcontact Printing Transfers a TPPAl-OMe Multilayer to Oxidized Polymeric Substrates .....	66
2.3.3. Rinsing Removes Physisorbed TPPAl-OMe and Leaves a TPPAl- (carboxylate) Monolayer on Oxidized Polymeric Substrates.....	69

2.3.4. Pd/Sn Colloids Adsorb from Solution on TPPAI-(carboxylate) Monolayers .....	71
2.3.5. Pd/Sn Colloids Adsorbed to Microntact-Printed TPPAI-(carboxylate) Monolayers Initiate Electroless Metallization.....	73
2.3.6. Copper Wires Fabricated on Oxidized PEN are Resilient to Mechanical Stress.....	74
2.4. Conclusions .....	77
2.5. References .....	78
2.6. Supporting Information .....	85
2.6.1. Procedures for the Preparation and Oxidation of Polymer Substrates	85
2.6.1.1. Polyethylene Terephthalate and Polyethylene Naphthalate	85
2.6.1.2. Polyimide .....	85
2.6.1.3. Polyethylene and Polypropylene .....	85
2.6.1.4. Polytetrafluoroethylene .....	85
2.6.1.5. Polymethylmethacrylate.....	86
2.6.1.6. SU-8.....	86
2.6.2. Supporting Figures and Tables .....	87
3. Chapter 3 - Silver Nanowire/Optical Adhesive Coatings as Transparent Electrodes for Flexible Electronics .....	90
3.1. Introduction .....	91
3.2. Experimental Section .....	93
3.2.1. Preparation of Glass, PET, and Oxidized PDMS Substrates.....	93
3.2.2. Fabrication AgNW-OA Films on Glass, PET, and oxidized PDMS..	94
3.2.3. Fabrication of LEECs .....	95
3.2.4. Characterization.....	95
3.3. Results and Discussion.....	96
3.3.1. Fabrication of AgNW-OA Coatings .....	96
3.3.2. Optical and Electrical Performance of AgNW-OA Coatings .....	98
3.3.3. Structural Characterization of AgNW-OA Coatings.....	100
3.3.4. Resilience of AgNW-OA Coatings .....	102

3.3.5. Flexible, Light-Emitting Electrochemical Cells using AgNW-OA	
Anodes.....	108
3.4. Conclusions.....	110
3.5. References.....	112
4. Chapter 4 - Templated Self-Assembly of Glass Microspheres into Ordered Two-Dimensional Arrays under Dry Conditions.....	116
4.1. Introduction.....	117
4.2. Experimental Section.....	119
4.2.1. Materials.....	119
4.2.2. Template Fabrication.....	120
4.2.3. Microsphere Self-Assembly.....	120
4.2.4. Fabrication of Binary Lattices of Microspheres.....	120
4.2.5. Characterization.....	121
4.3. Results and Discussion.....	121
4.3.1. Fabrication of the Template.....	121
4.3.2. Self-Assembly of Glass Microspheres.....	124
4.3.3. Defects in the Self-Assembled Structures.....	126
4.3.4. Fabrication of Binary Lattices of Microspheres.....	129
4.4. Conclusions.....	132
4.5. References.....	133
5. Chapter 5 - New Dialkyldithiophosphinic Acid Self Assembled Monolayers (SAMs): The Influence of Gold Substrate Morphology on Adsorbate Binding and SAM Structure.....	136
5.1. Introduction.....	137
5.2. Experimental Section.....	139
5.2.1. Dihexadecylphosphine Oxide.....	140
5.2.2. Dihexadecyldithiophosphinic Acid ((C <sub>16</sub> ) <sub>2</sub> DTPA).....	140
5.2.3. Gold Substrate Preparation.....	141
5.2.4. SAM Formation.....	141
5.2.5. Sample Preparation for Lateral Force Microscopy.....	142

5.2.6. Atomic Force Microscopy (AFM) and Lateral Force Microscopy (LFM) .....	142
5.2.7. X-Ray Photoelectron Spectroscopy (XPS) .....	142
5.2.8. Infrared Spectroscopy .....	143
5.2.9. Contact Angle Measurements .....	143
5.2.10. Electrochemical Impedance Spectroscopy (EIS) .....	143
5.2.11. Thermal Desorption .....	143
5.3. Results and Discussion	
5.3.1. Gold Substrate Fabrication and SAM Formation .....	144
5.3.2. (C <sub>16</sub> ) <sub>2</sub> DTPA Head Group Binding on As-Dep and TS Substrates....	145
5.3.3. Organization of the Organic Layers .....	149
5.3.4. Frictional Properties of (C <sub>16</sub> ) <sub>2</sub> DTPA SAMs on As-Dep and TS Gold	153
5.3.5. Electrochemical Barrier Properties of (C <sub>16</sub> ) <sub>2</sub> DTPA SAMs on As-Dep and TS Gold .....	155
5.3.6. Thermal Stability .....	157
5.4. Conclusions .....	159
5.5. References .....	161
5.6. Supporting Information and Figures .....	164
6. Chapter 6 - The Unusual Self-Organization of Dialkyldithiophosphinic Acid Self-Assembled Monolayers on Ultrasoother Gold .....	168
6.1. Introduction .....	169
6.2. Experimental Section .....	173
6.2.1. Gold Substrate Preparation .....	173
6.2.2. SAM Formation .....	173
6.2.3. Sample Preparation for Lateral Force Microscopy .....	174
6.2.4. Atomic Force Microscopy (AFM) and Lateral Force Microscopy (LFM) .....	174
6.2.5. X-Ray Photoelectron Spectroscopy .....	174
6.2.6. Infrared Spectroscopy .....	175
6.2.7. Contact Angle Measurements .....	175

6.2.8. Electrochemical Impedance Spectroscopy.....	175
6.3. Results and Discussion.....	175
6.3.1. Substrate and R <sub>2</sub> DTPA Preparation.....	175
6.3.2. <i>Binding</i> of the DTPA Head Group to the Gold Surface .....	176
6.3.3. Organization of the Alkyl Chains .....	179
6.3.4. Frictional Properties.....	188
6.3.5. Electrochemical Barrier Properties .....	192
6.4. Conclusions .....	196
6.5. References .....	197
6.6. Supporting Information and Figures .....	201
7. Chapter 7 - Ultra Smooth Gold Substrates Prepared by Chemical Mechanical Polishing: A New Substrate for Measuring Charge Transport in Metal- SAM//Ga <sub>2</sub> O <sub>3</sub> /EGaIn Junctions.....	209
7.1. Introduction .....	210
7.2. Experimental Section .....	217
7.2.1. Preparation of CMP Polishing Slurry .....	217
7.2.2. CMP of Gold Substrates .....	217
7.2.3. Cleaning of Au <sup>CMP</sup> Substrates.....	218
7.2.4. Preparation of Au <sup>TS</sup> Substrates .....	218
7.2.5. Atomic Force Microscopy and Uniformity Study .....	219
7.2.6. Substrate Characterization.....	219
7.2.7. Formation of Dihexadecyldithiophosphinic Acid SAMs on Au <sup>CMP</sup> Substrates .....	219
7.2.8. Formation of <i>n</i> -Alkanethiolate SAMs on Au <sup>CMP</sup> Substrates .....	220
7.2.9. Formation of <i>n</i> -Alkanethiolate SAMs on Au <sup>TS</sup> Substrates .....	220
7.2.10. X-Ray Photoelectron Spectroscopy (XPS) .....	220
7.2.11. Electrical Measurements of <i>n</i> -Alkanethiolate SAMs on Gold .....	221
7.2.12. Solvent Compatibility Study.....	222
7.3. Results and Discussion.....	222
7.3.1. Ultra Smooth Gold Films Fabricated using CMP.....	222

7.3.2. Uniformity of Au <sup>CMP</sup> Substrates .....	226
7.3.3. Composition of the Au <sup>CMP</sup> Surface.....	228
7.3.4. Binding of (C <sub>16</sub> ) <sub>2</sub> DTPA SAMs on AuCMP Substrates .....	233
7.3.5. Electrical Characterization of <i>n</i> -Alkanethiolate SAMs on Au <sup>TS</sup> and Au <sup>CMP</sup> Substrates .....	234
7.3.5.1. Forming Au-SAM//Ga <sub>2</sub> O <sub>3</sub> /EGaIn Junctions.....	234
7.3.5.2. Non-Shorting Yields of <i>n</i> -Alkanethiolate SAMs are Higher on AuCMP Substrates than on AuTS Substrates .....	235
7.3.5.3. Tunneling is the Primary Charge Transport Mechanism for <i>n</i> -Alkanethiolate SAMs formed on Au <sup>CMP</sup> and Au <sup>TS</sup> .....	236
7.3.5.4. $\mu_{\log}$ , $\sigma_{\log}$ , $\beta$ , and $\log J_0$ for <i>n</i> -Alkanethiolate SAMs formed on AuCMP Substrates and AuTS Substrates are Statistically Indistinguishable .....	237
7.3.6. Solvent Compatibility of Au <sup>CMP</sup> and Au <sup>TS</sup> Substrates.....	243
7.4. Conclusions .....	245
7.5. References .....	247
7.6. Supporting Information .....	253
7.6.1. Thickogram Calculation .....	253
7.6.2. Synthesis of 1-Tridecanethiol .....	254
7.6.3. <sup>1</sup> H NMR Spectra of Purified <i>n</i> -Alkanethiols .....	255
8. Chapter 8 – Electronic Properties of Diphenyldithiophosphinic Acid Self-Assembled Monolayers.....	264
8.1. Introduction .....	265
8.2. Experimental Section .....	267
8.2.1. Gold Substrate Preparation .....	268
8.2.2. SAM Formation.....	268
8.2.3. X-Ray Photoelectron Spectroscopy .....	268
8.2.4. Contact Angle Goniometry .....	269
8.2.5. Electrochemical Impedance Spectroscopy (EIS).....	269
8.2.6. Electrical Characterization of Ph <sub>2</sub> DTPA SAMs .....	269

8.2.7. Density Functional Theory (DFT) Calculations .....	270
8.3. Results and Discussion.....	271
8.3.1. Gold Substrate Fabrication and SAM formation .....	271
8.3.2. Ph <sub>2</sub> DTPA Head Group Binding.....	271
8.3.3. Contact Angle Measurements .....	272
8.3.4. Electrochemical Barrier Properties .....	274
8.3.5. Electrical Properties of Ph <sub>2</sub> DTPA SAMS on TS Gold.....	278
8.4. Conclusions .....	286
8.5. References .....	289
9. Chapter 9 - Conclusions and Outlook.....	293
9.1. Conclusions .....	294
9.2. Outlook.....	300
9.2.1. Stretchable Electronics .....	300
9.2.2. Molecular Junctions formed from DTPA SAMs.....	300
9.2.3. New Applications of CMP .....	301
9.4. References .....	302
Appendices – Copyright Permissions .....	303
Vita Auctoris.....	329

# List of Figures

Figure 1.01.	Image of a completed plastic active matrix backplane circuit. The inset shows an optical micrograph of a typical transistor.....	4
Figure 1.02	(a) Scanning electron micrograph (SEM) of printed Au (20 nm thick, 300 nm wide) lines on top of Au nanochannels. (b) SEM image of a cross section of a sample with 10 consecutively printed layers of 100 nm gold channels. For each step the stamps were rotated 90° with respect to the direction of the channels of the underlying layer. In both structures, the first layer adheres to the GaAs substrate through covalent bonds to the dithiol monolayer. Cold welding bonds the subsequent Au layers to each other. ....	5
Figure 1.03.	Morphology characterizations of as-prepared Ag NWs. (a) SEM image of top view of as-prepared AgNWs on a silicon substrate and their suspensions in alcohol (inset). (b) High-magnification SEM image of AgNWs. ....	9
Figure 1.04.	Top-view SEM images of AgNW-coated films with different densities, in which the AgNWs are shown to be a continuous network. ....	10
Figure 1.05.	The measurement of sheet resistance during 10 000 bending cycles with a 2 mm bending amplitude for a AgNW transparent electrode transferred onto Xerox paper. ....	11

Figure 1.06.

Examples of two-dimensional (A and B) and three-dimensional (C–F) structures, self-assembled in systems of macroscopic components interacting via capillary interactions. Open hexagonal array (A) and hexagonal lattice formed around circular templates (B) self-assembled from poly(dimethylsiloxane) plates floating at the interface between perfluodecalin and water. (C) Spherical structure formed by self-assembly of hexagonal metal plates on the surface of a drop of perfluodecalin in water. (D) Compact 3D structure formed by self-folding of a string of tethered, polymeric polyhedra. (E) Large crystal self-assembled from micrometer-sized hexagonal metal plates. (F) Aggregate with electrical connectivity self-assembled from polyhedral, polymer components bearing solder patterns of wires and dots .....15

Figure 1.07.

Photograph of the operating display after the alignment of the top electrode. The display contains 113 LEDs that are assembled in an interleaved fully addressable array. ....17

Figure 1.08.

Illustration of the coherent tunneling electron transport mechanism.....20

Figure 1.09.

Illustration of the incoherent tunneling mechanism .....21

Figure 1.10.

Illustration of a single molecule bridging two electrodes to form a single molecule junction .....22

Figure 1.11.

Illustration of a monolayer bridging two electrodes to form an ensemble junction .....23

Figure 1.12.

Schematic diagram of an ideal, single-crystalline alkanethiolate SAM formed on a gold (111) surface.....27

Figure 1.13.	Schematic diagram depicting the $(\sqrt{3} \times \sqrt{3})R30^\circ$ overlayer and $c(4 \times 2)$ super lattice of <i>n</i> -alkanethiolate SAMs formed on Au (111).....	29
Figure 1.14.	The terphenyl compounds with a DTC head group (a) and a thiol head group (b) shown bound to gold. c) Mesomeric forms of the DTC head group on gold.....	32
Figure 1.15	Illustration of the damage that can be caused to a SAM by the hot metal atoms present during evaporation. a) Chemical reaction between the organic molecules and the metal atoms. b) Formation of a metallic filament through the SAM. c) Formation of a metal adlayer on the surface of the substrate bearing the SAM. d) Formation of metal-oxide impurities on the surface of the substrate .....	34
Figure 1.16.	Photograph (left) and model (right) of a Hg-drop junction formed from <i>n</i> -alkanethiolate SAMs on Hg and Au .....	35
Figure 1.17.	A series of photographs of the formation of a conical tip of EGaIn.....	36
Figure 1.18.	Schematic illustration of the different types of defects seen for SAMs formed on polycrystalline gold substrates .....	38

Figure 1.19.

Schematic diagrams of several possible defects in SAMs of  $SC_{12}$  on silver (bottom electrode) and at the interface with a SAM of  $SC_{12}$  on mercury (top electrode): (a) a defect-free junction; (b) isolated (un-annealed) vacancies; (c) impurities in the silver film that cause local disorder in the SAM; (d) steps at the edge of annealed vacancy islands; (e) small, raised vacancy islands; and (f) defects at the grain boundaries of the silver supporting disordered SAMs. The molecules in between the SAMs are intercalated or trapped solvent (e.g., hexadecane) or solute (e.g.,  $HSC_{12}$ ). ...39

Figure 1.20.

Contact-mode AFM images of the topography of the (a) As-deposited silver film and (b) TS silver film. The root-mean-square roughnesses of a  $25 \mu m^2$  area of the silver films are  $5.1 \pm 0.4$  nm for As-deposited and  $1.2 \pm 0.1$  nm for TS. The white circles indicate the approximate size of the largest grains in each film and have diameters of (a) As-deposited, 80 nm, and (b) TS, 1  $\mu m$ .....40

Figure 1.21.

(Left) Plots of the average  $|J|$ -V curves (log-mean, bold black lines) and all  $|J|$ -V curves (light gray lines) measured on the TS junctions Ag- $SC_n//CnS$ -Hg ( $n = 10, 12, 14$ ), except for the initial traces that had a current density several orders of magnitude below the remaining traces, and traces directly preceding and following amalgamation. (Right) The same set of traces for the corresponding junction using As-Deposited silver.

Figure 2.1.	Reaction of TPPAI-OMe with carboxylic acid groups on the surface of an oxidized polymeric substrate .....	62
Figure 2.2.	Characterization of a TPPAI-OMe film transferred by microcontact printing to the surface of an oxidized PET substrate. (a) UV-vis absorption spectrum of a TPPAI-OMe film transferred by microcontact printing to the surface of oxidized PET before (red) and after rinsing with isopropanol (blue). (b) RAIRS spectra ( $3000 - 2800 \text{ cm}^{-1}$ and $1800 - 1200 \text{ cm}^{-1}$ ) of a TPPAI-OMe film transferred by microcontact printing to the surface of an MHDA SAM on gold before (red) and after rinsing in dichloromethane (blue).....	68
Figure 2.3.	UV-vis absorption spectra of two samples of TPPAI-(carboxylate) monolayers on oxidized PET exposed to a solution of Pd/Sn colloids for 1 min. The first sample was rinsed with water (red), then accelerated in 1 M HCl and rinsed with water (blue). The second sample was rinsed with isopropanol (yellow), then accelerated in 1 M HCl and rinsed with isopropanol (black) .....	72
Figure 2.4.	Optical and SEM images of patterned copper films on oxidized PET. (a) Optical image of an arbitrary copper pattern. (b) SEM image of a portion of the metallized substrate in (a). In both images, the light areas are copper; these areas correspond to the raised portion of the PDMS microcontact printing stamp .....	74
Figure 2.5.	Electrical characterization of copper wires fabricated on PEN. (a) Photograph of copper wires ( $l = 5.0 \text{ cm}$ , $w = 1.0 \text{ mm}$ , $h = 40 \text{ nm}$ ) fabricated on a $75\text{-}\mu\text{m}$ -thick PEN substrate. (b) Resistivity of copper wires ( $l = 1.0 \text{ cm}$ , $w = 1.0 \text{ mm}$ , $h = 40 \text{ nm}$ ) as a function of bending radius.....	76

Figure S2.1.	RAIRS spectrum of a 16-mercaptohexadecanoic acid SAM on gold.....	87
Figure S2.2.	UV-vis absorption spectrum of a TPPAI-(carboxylate) monolayer covered with a film of physisorbed TPPAI-OMe on oxidized PET before (red) and after (blue) exposure to a solution of Pd/Sn colloids for 1 min.....	88
Figure S2.3.	Contact-mode AFM images of native PET (left) and oxidized PET (right). The root-mean-square roughness of the PET substrates increases from 0.96 nm for native PET to 10.4 nm for oxidized PET .....	89
Figure 3.1.	Electrical and optical properties of AgNW-OA coatings. (a) Photograph of an AgNW-OA coating on PDMS ( $14 \Omega/\square$ ). (b) Transmittance spectra of AgNW-OA coatings on glass, with corresponding sheet resistances .....	99
Figure 3.2.	Structural features of AgNW-OA coatings. (a, b) Cross-sectional SEM images of a freeze-fractured AgNW-OA coating on glass ( $4 \Omega/\square$ ). (c, d) SEM images of the surface of an AgNW-OA coating ( $4 \Omega/\square$ ) on glass ....	101
Figure 3.3.	AFM images (z-scale = 150 nm) with root-mean-squared (RMS) roughness measurements and corresponding profile measurements of AgNW-OA films ( $9 \Omega/\square$ ) on (a, b) Glass; (c, d) PDMS; (e, f) PET .....	101
Figure 3.4.	Comparison of surface roughness of AgNW-OA coatings and drop-cast AgNW films. (a, b) AFM image and corresponding profile measurements of an AgNW-OA ( $14 \Omega/\square$ ) coating on PDMS. (c, d) AFM image and corresponding profile measurements of an AgNW film on a silicon wafer formed by drop casting .....	102

Figure 3.5.

AgNW-OA coatings subjected to bending. (a) Photograph of a flexed AgNW-OA coating ( $14 \Omega/\square$ ) on PDMS. The solid line indicates that axis of bending; the dashed line indicates the perpendicular axis. (b) Change in resistance of AgNW-OA coatings ( $4 \Omega/\square$ ) on PDMS as a function of increasing tensile strain. (c) Change in resistance of AgNW-OA coatings ( $4 \Omega/\square$ ) on PET as a function of increasing tensile strain. (d) Change in resistance of AgNW-OA coatings ( $4 \Omega/\square$ ) on PDMS with repetitive cycles of 15% tensile strain measured with a four-point probe oriented to inject current along the bending axis (squares) and along the perpendicular axis (diamonds).....105

Figure 3.6.

a) Photograph of serrated alligator clips clamping onto a AgNW-OA ( $4 \Omega/\square$ ) coating on glass. b) Dark field optical micrograph showing ITO on glass after 100 clamping cycles. c) Dark field optical micrograph showing a AgNW-OA ( $4 \Omega/\square$ ) coating on glass after 100 clamping cycles. d) Resistance of AgNW-OA ( $4 \Omega/\square$ ) coatings on glass (squares) and ITO on glass (diamonds) measured after repetitive cycles of clamping and unclamping the same area with alligator clips.....107

Figure 3.7.

Photographs of flexible LEECs fabricated with AgNW-OA ( $14 \Omega/\square$ ) transparent anodes on PDMS, bent to radii of (a) 7.0 mm; (b) 3.0 mm; (c) 1.5 mm.....109

Figure 3.8.

Characterization of unstrained devices and devices subjected to cycles of tensile strain. (a) Temporal evolution of current (solid line) and radiance (dotted line) of a typical unstrained device operated under a 5 V bias in ambient conditions. (b) Temporal evolution of EQE of a typical unstrained device operated under a 5 V bias in ambient conditions. (c) Temporal evolution of current (solid line) and radiance (dotted line) of a typical

device after 20 bending cycles of 25% tensile strain operated under a 5 V bias in ambient conditions. (d) Temporal evolution of EQE of a typical device after 20 bending cycles of 25% tensile strain operated under a 5 V bias in ambient conditions. ....110

Figure 4.1.

Fabrication of templates of liquid adhesive drops for self-assembly. a) Schematic of the process used to fabricate an array of adhesive drops on hydrophilic SiO<sub>2</sub> squares surrounded by a hydrophobic HDT SAM on gold, with optical micrograph of NOA 73 assembled on a hexagonal lattice consisting of 40 μm hydrophilic squares distributed in a background of an HDT SAM on gold. b) Plot showing the approximately linear relationship between adhesive viscosity and the height of adhesive drops deposited on a template consisting of a square lattice of 40-μm hydrophilic squares.....122

Figure 4.2.

Self-assembly of glass microspheres of 100 μm diameter on templates of liquid adhesive drops of NOA 73. a) Schematic of the experimental setup. The clamp holding the upper and lower filtration frits together is not shown for clarity. b – e) Optical micrographs of glass microspheres self-assembled on square lattice templates (b, c), and hexagonal lattice templates (d, e).....125

Figure 4.3.

Self-assembly of a binary lattice of microspheres. a) Schematic of the process steps. b) Optical microscopy image of a hexagonal array fabricated from clear and black glass microspheres (100-μm diameter) deposited along diagonal lines. Note that there is some variation in the size of the microspheres.....131

Figure 5.1.	AFM topographic images recorded in contact mode of the (a) As-Dep gold film and (b) TS gold film. In both images the vertical scale is 20 nm. The white line shows the region that corresponds to the cross-sectional-profile depicted beside each image.....	145
Figure 5.2.	HR-XPS spectra of the S 2p region for (C <sub>16</sub> ) <sub>2</sub> DTPA SAMs formed on (a) As-Dep gold and (b) TS gold.....	147
Figure 5.3.	RAIR spectra (2975 - 2825 cm <sup>-1</sup> ) of (C <sub>16</sub> ) <sub>2</sub> DTPA SAMs on As-Dep gold (red) and TS gold (blue) .....	152
Figure 5.4.	LFM images of alternating lines of C <sub>16</sub> SH and (C <sub>16</sub> ) <sub>2</sub> DTPA SAMs patterned onto (a) As-Dep gold and (b) TS gold. Bright areas correspond to regions of higher friction. Z-scale is 250 mV for both images.....	154
Figure 5.5.	Bode plot of (C <sub>16</sub> ) <sub>2</sub> DTPA SAMs formed on As-Dep gold (red) and TS gold (blue). Inset (upper right): Randles circuit model used to fit raw EIS data	156
Figure 5.6.	Thermal desorption of (C <sub>16</sub> ) <sub>2</sub> DTPA SAMs on As-Dep gold (red) and TS gold (blue) plotted as the static contact angle of water as a function of immersion time in 70 °C decahydronaphthalene. Desorption of C <sub>16</sub> SH SAMs on As-Dep gold (black) and TS gold (green) is shown for reference	159

Figure S5.1.

XPS survey spectra for  $(C_{16})_2DTPA$  SAMs formed for 24 hours on a) As-Dep gold and b) TS gold. Please note that when comparing the atomic percentages of sulphur and phosphorus that the phosphorus percentage is routinely lower than expected relative to sulphur. There are three reasons for this discrepancy: First, the phosphorus signal has a lower cross-section compared to sulphur (relative sensitivity factors of 0.486 and 0.668 respectively). Second, the P 2p peak is mixed in with the large inelastic background of the Au 4f peaks, which puts the peak on a slope that alters the applied Shirley background to give a smaller peak area than should be expected. Third, since we are at or near the detection limit for phosphorus any noise in the background strongly affects the amount of phosphorus reported. For these reasons, there is a significant amount of error (+/-) associated with the P numbers. Conversely, the sulfur peak is stronger due to its larger cross-section and the fact that there is more sulfur present, and it is not affected as greatly by the Au 4f background (much less slope. Therefore, much less error associated with it .....166

Figure S5.2.

High resolution XPS spectra of the P 2p region for  $(C_{16})_2DTPA$  SAMs formed for 24 hours on a) As-Dep gold and b) TS gold.....166

Figure S5.3.

High resolution XPS spectra of the S 2p region for  $(C_{16})_2DTPA$  SAMs formed for 5 minutes on a) As-Dep gold and b) TS gold. ....167

Figure 6.1.

AFM topographic image recorded in contact mode of a typical TS gold film. The vertical scale is 20 nm. The white line shows the region that corresponds to the cross-sectional profile depicted beside the image. ....176

Figure 6.2.	HR-XPS spectra of the S 2p region for $[\text{CH}_3(\text{CH}_2)_n]_2\text{DTPA}$ SAMs on TS gold. ....	178
Figure 6.3	RAIR spectra ( $2970 - 2820 \text{ cm}^{-1}$ ) of $[\text{CH}_3(\text{CH}_2)_n]_2\text{DTPA}$ ( $n = 5, 9, 11, 13, 15$ ) SAMs formed on TS gold. Dashed lines correspond to symmetric ( $2850 \text{ cm}^{-1}$ ) and asymmetric ( $2918 \text{ cm}^{-1}$ ) methylene C-H stretches of $\text{C}_{16}\text{SH}$ SAMs formed on TS gold. ....	180
Figure 6.4.	Hexadecane (a) and water (b) contact angles of $\text{R}_2\text{DTPA}$ ( $n = 5, 9, 11, 13, 15$ ) SAMs on TS gold (squares) and As-Dep gold (diamonds) plotted as a function of the number of methylene groups in the alkyl chains.....	188
Figure 6.5.	Bode LFM images of alternating lines of $\text{C}_{16}\text{SH}$ and $\text{R}_2\text{DTPA}$ ( $n = 5, 9, 11, 13, 15$ ) SAMs patterned on TS gold (left) and As-Dep gold (right). Bright areas correspond to regions of higher friction. White lines correspond to representative profile measurements depicting the change in friction across the image. Z-scale is 250 mV for all images .....	191
Figure 6.6.	Bode magnitude plots for $\text{R}_2\text{DTPA}$ SAMs formed on TS gold showing the raw data (dotted lines) and data derived from circuit modeling (solid lines).	192
Figure 6.7.	Randles circuit models used to fit raw EIS data of $\text{R}_2\text{DTPA}$ SAMs on TS gold. a) Circuit model used to model impedance data of $\text{R}_2\text{DTPA}$ SAMs with $n = 9, 11, 13, 15$ . b) Circuit model used to model impedance data of $(\text{C}_6)_2\text{DTPA}$ SAMs.....	193

Figure 6.8.	EIS parameters calculated from fitting raw impedance data to the appropriate Randles equivalent circuit model for R <sub>2</sub> DTPA ( <i>n</i> = 5, 9, 11, 13, 15) SAMs on TS gold. (a) Resistance, (b) capacitance, and (c) thickness plotted as a function of the number of methylene groups in the alkyl chains. ....	195
Figure S6.1.	XPS survey scans for SAMs formed from a) (C <sub>6</sub> ) <sub>2</sub> DTPA, b) (C <sub>10</sub> ) <sub>2</sub> DTPA, c) (C <sub>12</sub> ) <sub>2</sub> DTPA, d) (C <sub>14</sub> ) <sub>2</sub> DTPA, and e) (C <sub>16</sub> ) <sub>2</sub> DTPA on TS gold.....	205
Figure S6.2.	Nyquist plots of R <sub>2</sub> DTPA SAMs on TS gold for <i>n</i> = a) 5 b) 9 c) 11 d) 13 e) 15. ....	207
Figure 7.1.	a-b) AFM topographic images of an Au <sup>As-Dep</sup> and Au <sup>CMP</sup> gold film with corresponding line scan profiles shown below (c-d). e) SEM image of a Au <sup>CMP</sup> film. The z-scale for the AFM images is 20 nm. ....	225
Figure 7.2.	Three dimensional 1 μm x 1 μm AFM images (a – b) and corresponding height profile measurements (c – d) of Au <sup>CMP</sup> , and Au <sup>TS</sup> films. The z-scale in the AFM images is 20 nm.....	226
Figure 7.3.	Histogram detailing the RMS surface roughness values of Au <sup>CMP</sup> substrates collected from 60 1 μm x 1 μm AFM images.....	227
Figure 7.4.	XPS survey scan of a Au <sup>CMP</sup> substrate .....	230
Figure 7.5.	Graphical representation of the thickogram calculation used to determine the thickness of the AuI overlayer on a Au <sup>CMP</sup> substrate. Details of the thickogram calculation are available in the supporting information .....	231

Figure 7.6.	XPS survey scan of a Au <sup>CMP</sup> substrate after the formation of a 1-hexadecanethiolate SAM.....	232
Figure 7.7.	HR-XPS spectrum of the S 2p region of a (C <sub>16</sub> ) <sub>2</sub> DTPA SAM formed on a Au <sup>CMP</sup> substrate. ....	234
Figure 7.8.	Average traces (a), beta plot (b) and histograms with unimodal Gaussian fit (c) of log J for <i>n</i> -alkanethiolate SAMs formed on Au <sup>CMP</sup> substrates. Beta plot and histograms are shown for a bias of -0.5 V. Trendlines in the beta plot for <i>n</i> -alkanethiolate SAMs with even (red) and odd (black) number of carbons have been separated to illustrate the odd-even effect. Beta and log J <sub>0</sub> values are calculated by treating all chain lengths as a single series. The y-axis of the Gaussian distributions corresponds to the number of counts for a given statistical bin.....	240
Figure 7.9.	Average traces (a), beta plot (b) and histograms with unimodal Gaussian fit (c) of log J for <i>n</i> -alkanethiolate SAMs formed on Au <sup>TS</sup> substrates. Beta plot and histograms are shown for a bias of -0.5 V. Trendlines in the beta plot for <i>n</i> -alkanethiolate SAMs with even (red) and odd (black) number of carbons have been separated to illustrate the odd-even effect. Beta and log J <sub>0</sub> values are calculated by treating all chain lengths as a single series. The y-axis of the Gaussian distributions corresponds to the number of counts for a given statistical bin.....	242
Figure 7.10.	Optical micrographs of Au <sup>CMP</sup> (a) and Au <sup>TS</sup> (b) substrates after immersion in ethanol, toluene, chloroform, and dichloromethane for various time intervals .....	244

Figure S7.1.	$^1\text{H}$ NMR spectrum of 1-nonanethiol after purification by column chromatography .....	256
Figure S7.2.	$^1\text{H}$ NMR spectrum of 1-decanethiol after purification by column chromatography .....	257
Figure S7.3.	$^1\text{H}$ NMR spectrum of 1-undecanethiol after purification by column chromatography .....	258
Figure S7.4.	$^1\text{H}$ NMR spectrum of 1-dodecanethiol after purification by column chromatography .....	259
Figure S7.5.	$^1\text{H}$ NMR spectrum of 1-tridecanethiol after purification by column chromatography .....	260
Figure S7.6.	$^1\text{H}$ NMR spectrum of 1-tetradecanethiol after purification by column chromatography .....	261
Figure S7.7.	$^1\text{H}$ NMR spectrum of 1-pentadecanethiol after purification by column chromatography .....	262
Figure S7.8.	$^1\text{H}$ NMR spectrum of 1-hexadecanethiol after purification by column chromatography .....	263
Figure 8.1.	HR-XPS spectra of the S 2p region of a Ph <sub>2</sub> DTPA SAM formed on TS gold .....	272
Figure 8.2.	Bode magnitude plots (a) and Nyquist plots (b) of Ph <sub>2</sub> DTPA SAMs on TS gold. 8.2a inset: Randles circuit model used to fit raw EIS data .....	275

Figure 8.3.	Average $J(V)$ traces of PhSH SAMs (blue) and Ph <sub>2</sub> DTPA SAMs (red) on TS gold .....	279
Figure 8.4.	Histograms and corresponding Gaussian fit of PhSH SAMs (blue) and Ph <sub>2</sub> DTPA SAMs (blue) on TS gold.....	280
Figure 8.5.	Illustration of the HOMO and LUMO energy levels of the Ph <sub>2</sub> DTPA (a) and PhSH (b) model systems with respect to the work function of the metal electrodes .....	284
Figure S8.1.	XPS survey scan of a Ph <sub>2</sub> DTPA SAM formed on TS gold .....	292

# List of Tables

Table 1.1.	Variety of molecular junctions used to measure $\beta$ and $J_0$ of alkanes .....	24
Table 1.2.	Types of interactions at metal – molecule interfaces.....	26
Table 2.1.	Assignments of selected absorption bands in the RAIRS spectra of an MHDA SAM on gold, a TPPAI-OMe multilayer printed on the MHDA SAM, and a TPPAI-OMe multilayer printed on the MHDA SAM after rinsing with dichloromethane .....	70
Table 3.1.	Electrical and optical properties of AgNW-OA coatings on glass .....	99
Table 3.2.	Change in resistance of AgNW-OA films ( $4 \Omega/\square$ ) on PDMS subjected to durability tests.....	106
Table 4.1.	Defect Rates <sup>[a]</sup> for Arrays <b>1</b> – <b>4</b> showing the effect of adhesive drop height and template geometry.....	128
Table 5.1.	S 2p and P 2p doublet binding energies in eV, abundances, and peak assignments for (C <sub>16</sub> ) <sub>2</sub> DTPA SAMs formed on As-Dep gold and TS Gold Substrates.....	148
Table 5.2.	RAIRS absorption bands and contact angle data <sup>[a]</sup> for (C <sub>16</sub> ) <sub>2</sub> DTPA and C <sub>16</sub> SH SAMs formed on As-Dep and TS gold.....	152

Table 5.3.	Electrical parameters of (C <sub>16</sub> ) <sub>2</sub> DTPA and C <sub>16</sub> SH SAMs formed on As-Dep gold and TS gold calculated by fitting raw EIS data using the Randles simple circuit model .....	157
Table 6.1.	S 2p <sub>3/2</sub> binding energies of [CH <sub>3</sub> (CH <sub>2</sub> ) <sub>n</sub> ] <sub>2</sub> DTPA SAMs on TS gold .....	178
Table 6.2.	Comparison of asymmetric and symmetric methylene C-H stretching frequencies for R <sub>2</sub> DTPA (n = 5, 15) SAMs on TS gold, RSH (n = 5, 15) SAMs on TS gold, and R <sub>2</sub> DTPA (n = 5, 15) SAMs on As-Dep gold .....	181
Table S6.1.	Position and intensity of methyl and methylene C-H stretches of R <sub>2</sub> DTPA SAMs on TS gold as determined by RAIRS .....	206
Table S6.2.	Position of methylene C-H stretches of R <sub>2</sub> DTPA SAMs on As-Dep gold as determined by RAIRS.....	206
Table S6.3.	Static water and hexadecane contact angles of R <sub>2</sub> DTPA SAMs on As-Dep and TS gold.....	207
Table S6.4.	Resistance, capacitance, and thickness values of R <sub>2</sub> DTPA SAMs on TS gold calculated from Randles equivalent circuit analysis.....	208
Table 7.1.	Summary of the Au <sup>CMP</sup> surface roughness uniformity study.....	228
Table 7.2.	Summary of charge transport measurements of <i>n</i> -alkanethiolate SAMs formed on Au <sup>CMP</sup> substrates .....	239

Table 7.3.	Summary of charge transport measurements of <i>n</i> -alkanethiolate SAMs formed on Au <sup>TS</sup> substrates .....	241
Table 8.1.	Electrochemical barrier parameters of Ph <sub>2</sub> DTPA SAMs on TS gold calculated by fitting raw EIS data using the Randles simple circuit model	276
Table 8.2.	Charge transport data of PhSH and Ph <sub>2</sub> DTPA SAMs on TS gold .....	279
Table 8.3.	Calculated electronic properties of Ph <sub>2</sub> DTPA and PhSH model systems ..	283

# List of Schemes

Scheme 2.1.	Schematic of the process steps used to fabricate patterned copper films on oxidized polymeric substrates.....	66
Scheme 3.1.	Process used to fabricate AgNW-OA coatings.....	97
Scheme 3.2.	Diagram of the device test structure .....	109
Scheme 5.1.	Dialkyldithiophosphinic acid bound to a gold surface. (a) Monodentate binding. (b) Bidentate binding.....	137
Scheme 5.2.	Process used to pattern alternating lines of $(C_{16})_2DTPA$ and $C_{16}SH$ SAMs on gold substrates .....	154
Scheme 6.1.	$R_2DTPA$ adsorbates bound to gold with (a) monodentate binding and (b) chelation.....	172
Scheme 6.2.	Diagrams depicting two possibilities for the self-organization of $(C_6)_2DTPA$ adsorbates in SAMs on TS gold. a) $(C_6)_2DTPA$ adsorbates aligned laterally. b) $(C_6)_2DTPA$ adsorbates oriented to enable interdigitation of the alkyl chains .....	185
Scheme 6.3.	Process used to pattern alternating lines of $R_2DTPA$ and $C_{16}SH$ SAMs on TS and As-Dep gold substrates.....	189
Scheme 8.1.	$Ph_2DTPA$ (a) and $PhSH$ (b) adsorbate molecules shown bound to a gold surface.....	267

# List of Abbreviations

%	percent
%T	percent transmittance
&	and
~	approximately
<	less than
>	greater than
°	degrees
°C	degrees celcius
A	amp
Å	angstrom
AFM	atomic force microscopy
AgNW	silver nanowire
As-Dep	as-deposited
ASTM	American society for testing and materials
at.%	atomic percent
Au(111)	111 plane of gold
Au <sup>As-Dep</sup>	as-deposited gold
Au <sup>CMP</sup>	polished gold
Au <sup>TS</sup>	template-stripped gold
Avg	average
β	beta
BEs	binding energies
bpy	bipyridal
CA	contact angle
c	centi-
cm <sup>-1</sup>	wavenumbers
CMOS	complementary metal oxide semiconductor
CMP	chemical mechanical polishing
cps	centipoise

$C_{\text{SAM}}$	self-assembled monolayer capacitance
$d$	tunneling distance
decalin	decahydronaphthalene
dialkyl-DTPA	dialkyldithiophosphinic acid
DOS	density of states
$\Delta\theta$	contact angle hysteresis
dtb	ditertbutyl
DTC	dithiocarbamate
DTCA	dithiocarboxylic acid
DTP	dithiophosphate
DTPA	dithiophosphinic acid
$\varepsilon$	permittivity
$e$	Euler's number
e-beam	electron-beam
EGaIn	eutectic of gallium indium
EIS	electrochemical impedance spectroscopy
ELD	electroless deposition
EQE	external quantum efficiency
EtOH	ethanol
eV	electron-volt
F	Faraday
FWHM	full width at half max
$g$	gram
$h$	Planck's constant
h or hrs	hours
HD	hexadecane
HDT	1-hexadecanethiol
Hg-Drop	mercury drop
HOMO	highest occupied molecular orbital
HR-XPS	high resolution x-ray photoelectron spectroscopy

Hz	hertz
I	intensity
IC	integrated circuit
ITO	tin-doped indium oxide
I-V	current-voltage
J	current density
K	Kelvin
k	kilo
kcal	kilocalorie
kJ	kilojoule
k $\Omega$	kilo ohm
$\lambda$	lambda
LB	Langmuir-Blodgett
LED	light-emitting diode
LEEC	light-emitting electrochemical cell
LFM	lateral force microscopy
log	logarithm
LUMO	lowest unoccupied molecular orbital
m	meter
M	molar
$\mu$	micro-
m	milli-
$\mu$ CP	microcontact printing
mg	milligram
MHDA	mercaptohexadecanoic acid
MIM	metal-insulator-metal
min or mins	minutes
mL	milliliter
$\mu$ L	microliter
$\mu_{\log}$	average logarithm

mm	millimeter
$\mu\text{m}$	micrometer
mM	millimolar
mV	millivolt
$\text{M}\Omega$	mega ohm
nm	nanometer
n	nano-
$\mu\Omega$	micro ohm
$\nu_{\text{as}}$	asymmetric stretching frequency
$n_{\text{C}}$	number of carbons
NIST	national institute of standards and technology
nm	nanometer
NMR	nuclear magnetic resonance
NOA	norland optical adhesive
$\nu_{\text{s}}$	symmetric stretching frequency
nTP	nanotransfer printing
OA	optical adhesive
OLED	organic light-emitting diode
OMe	methoxy
OTS	octadecyltrichlorosilane
PDMS	polydimethylsiloxane
PE	polyethylene
PEDOT:PSS	poly(3,4-ethylenedioxythiophene) poly(styrenesulfonate)
PET	polyethylene terephthalate
pH	power of hydrogen
PI	polyimide
PLED	polymer light-emitting diode
PMMA	polymethyl methacrylate
PP	polypropylene

ppm	parts per million
PS	polystyrene
psi	pounds per square inch
Pt <sup>As-Dep</sup>	as-deposited platinum
Pt <sup>CMP</sup>	polished platinum
PTFE	polytetrafluoroethylene
PVA	polyvinyl alcohol
PVD	physical vapour deposition
q	charge of an electron
$\theta(\text{H}_2\text{O})$	water contact angle
$\theta(\text{HD})$	hexadecane contact angle
R/R <sub>0</sub>	relative change in resistance
R <sub>2</sub> DTPA	dialkyldithiophosphinic acid
RAIRS	reflection absorption infrared spectroscopy
RMS	root mean squared
R <sub>SAM</sub>	self-assembled monolayer resistance
RSH	alkanethiolate
s	second
$\sigma$	standard deviation
SAM	self-assembled monolayer
SEM	scanning electron microscopy
Silicon (100)	100 plane of silicon
$\sigma_{\log}$	standard deviation of the logarithm
STM	scanning tunneling microscopy
t	thickness
TCE	transparent conductive electrode
THF	tetrahydrofuran
TPDTC	terphenyldithiocarbamate
TPP	tetraphenylporphyrin
TS	template-stripped
UV-vis	ultraviolet-visible

V	volt
$\Omega$	ohm
W	watt
$\Omega/\square$	ohms per square
wt. %	weight percent
XPS	x-ray photoelectron spectroscopy

# **Chapter 1**

## **Introduction**

## 1.1. Flexible Electronic Devices

Advances in thin film device technology over the past four decades have sparked exciting innovations for displays, sensors, and energy conversion.<sup>1</sup> These innovations have traditionally been fueled by the need for devices that are faster, smaller, and lighter, with a recent push for devices that are portable and more compatible with the human body.<sup>1-4</sup> Unfortunately, the latter set of requirements cannot be met by traditional device fabrication methods; high-performance electronics are fabricated using single crystal inorganic materials that are inherently rigid and planar.<sup>2,3,5</sup> Replacing solid-state device technology with flexible, organic analogues opens the door to devices that bend, roll, fold, and match the contours of the human body.<sup>1,2,6</sup> This field of research – collectively known as ‘flexible electronics’ – has produced exciting proof of concept devices such as flexible displays,<sup>7</sup> memory storage,<sup>8</sup> solar cells,<sup>9</sup> and radio frequency-identification systems.<sup>10</sup> Despite this great research effort, the commercialization of this technology has been markedly slow; it has taken ~ 20 years since the filing of the first polymer light-emitting device (PLED) patent for this technology to slowly trickle into market.<sup>1</sup> A major challenge that inhibits mass commercialization of flexible electronics is the requirement that each part of the device – including the electrodes, active components, and interconnects – function under tensile and compressive strain. Designing flexible device components with performance characteristics comparable to that of single crystal inorganic materials is the fundamental challenge of this field.

### *1.1.1. Low-Cost Metallization of Polymeric Substrates*

Flexible electronic devices require the deposition of patterned metal interconnects and contacts onto polymer substrates. Conventional fabrication methods rely on a combination of physical vapour deposition (PVD) and photolithography to deposit and pattern such films. Both of these methods have high capital and operating costs which fall out of line with the low-cost nature of polymer electronics. As a result, two general schemes have emerged as low-cost alternatives to conventional fabrication: In the first approach, low-cost patterning methods are used in conjunction with metal films that have been deposited using PVD;<sup>11-21</sup> the second approach eliminates PVD entirely by employing solution-based metal deposition.<sup>22-28</sup>

#### 1.1.1.1. Physical Vapour Deposition

Various low-cost patterning methods, both additive and subtractive, have been integrated with PVD to produce functioning metal circuitry on polymeric substrates. The simplest of the patterning techniques involves depositing a metal film through a physical mask, known as a ‘shadow mask’. Shadow masking provides a straightforward means of patterning; however, it suffers from poor resolution due to edge distortion and cannot fabricate closed geometric patterns without the use of multiple masks.<sup>11</sup>

A popular method of subtractive patterning involves first depositing a blanket film of metal using PVD, patterning an etch resist using a technique known as microcontact printing ( $\mu$ CP), and using wet chemical etching to remove the unprotected areas of the film.<sup>12-15</sup>  $\mu$ CP is a technique pioneered by Whitesides and Kumar that uses an elastomeric stamp to transfer a pattern (features as small as 1  $\mu$ m) of chemical ‘ink’ to a substrate via the formation of a self-assembled monolayer (SAM); the stamp bears a relief pattern that is formed by pouring liquid pre-polymer over the surface of a lithographically patterned silicon wafer, followed by curing the stamp, and peeling it away.<sup>29,30</sup>

Rogers et al. showcased this method by fabricating an array of 256 thin film transistors on a plastic substrate (Mylar) which used a backplane consisting of gold source/drain contacts patterned by  $\mu$ CP (Figure 1.01).<sup>12</sup> The source/drain contacts were fabricated in four steps. First, a blanket film of Ti/Au was deposited onto a Mylar substrate using PVD (electron beam evaporation). Second, an etch resist (1-hexadecanethiolate SAM) was patterned in the positive tone of the desired source/drain contacts using  $\mu$ CP. Third, wet chemical etching using a ferri-/ferrocyanide solution removed the gold film from the areas that were not protected by the etch resist, revealing the gold source/drain pattern. Finally, the etch resist was removed from the source/drain contacts using heat.

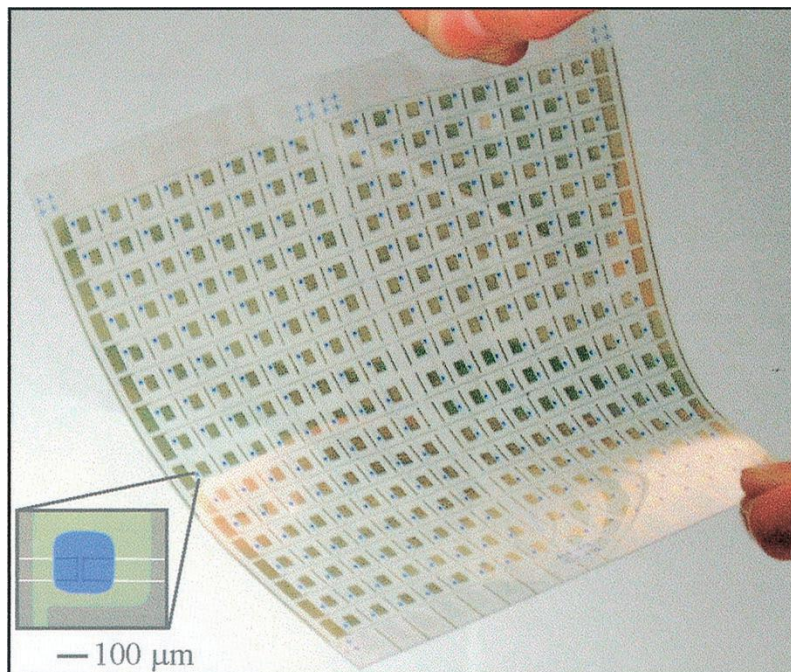


**Figure 1.01.** Image of a completed plastic active matrix backplane circuit. The inset shows an optical micrograph of a typical transistor. Adapted from reference 12. Copyright the National Academy of Sciences.

A popular additive method known as nanotransfer printing (nTP) uses an elastomeric stamp to directly transfer a patterned metal film – with feature sizes as low as 100 nm and edge resolutions of 15 nm – to a receiving substrate; the transfer process is driven by strong adhesion between the metal film and the receiving substrate, usually through the formation of covalent bonds.<sup>16-19,31</sup> Zaumseil et al. used nTP to create three-dimensional, multi-layer gold structures by successively employing a two-step process. First, a patterned elastomeric stamp bearing a thin (20 nm) gold film is brought into contact with a 1,8-alkanedithiol SAM-coated GaAs substrate; covalent linkage of the gold film to the SAM results in its transfer to the GaAs substrate upon removal of the stamp. Then, a second gold-coated elastomeric stamp is brought into contact with the surface of the substrate, resulting in cold welding of the two gold films. This process can be repeated until the desired multilayer architecture is achieved (Figure 1.02).<sup>31</sup> In a later publication, a similar process used non-covalent interactions to transfer multilayer metal stacks to a

variety of polymer substrates including polyethylene terephthalate (PET), polyimide (PI) and polypropylene (PP).<sup>17</sup>

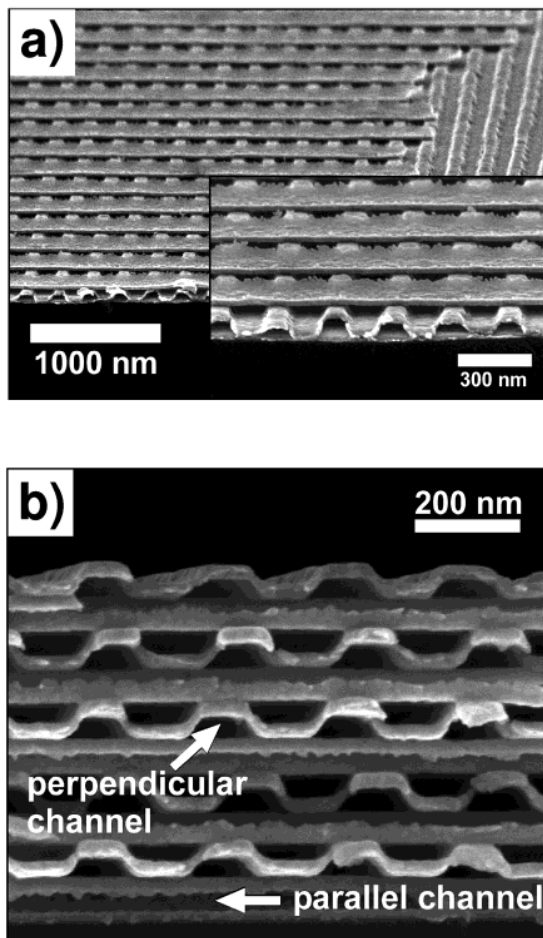


**Figure 1.02.** (a) Scanning electron micrograph (SEM) of printed Au (20 nm thick, 300 nm wide) lines on top of Au nanochannels. (b) SEM image of a cross section of a sample with 10 consecutively printed layers of 100 nm gold channels. For each step the stamps were rotated 90° with respect to the direction of the channels of the underlying layer. In both structures, the first layer adheres to the GaAs substrate through covalent bonds to the dithiol monolayer. Cold welding bonds the subsequent Au layers to each other. Adapted with permission from reference 31.

### 1.1.1.2. Electroless Metal Deposition

Eliminating PVD is the only way to develop a truly ‘low-cost’ method of patterned metal deposition. One potential PVD replacement - electroless deposition (ELD) – is a solution-based metallization technique that is capable of depositing copper, silver, nickel, gold, and cobalt onto a variety of different substrates, and is widely used in the microelectronics industry.<sup>32</sup> The ELD process involves the reduction of metal ions in solution to produce thin metal films. In the first step of the process, a Pd catalyst on the substrate surface catalyzes the initial reduction of metal ions in solution. Once a thin layer of metal is deposited, the process becomes autocatalytic and metal ions continue to be reduced as a reducing agent in the plating solution is oxidized.  $\mu$ CP has been combined with ELD in both subtractive<sup>33</sup> and additive<sup>34-37</sup> processes to generate patterned metal films using a fully solution-based approach.

A subtractive patterning method by Tate et al. used a three step process to fabricate patterned silver source/drain electrodes for use in organic transistors.<sup>33</sup> First, a blanket film of silver was deposited onto the gate dielectric using a commercially available ELD plating bath. Then,  $\mu$ CP was used to pattern an etch resist (SAM of 1-hexadecanethiolate) onto the silver film in the desired source/drain pattern. Finally, the unprotected areas of the silver film were removed using a ferri-/ferrocyanide wet chemical etch process, followed by removal of the etch resist. This method produced functional source/drain electrodes with a spacing of only 1 micron, and minimal edge roughness.

Additive ELD processes use  $\mu$ CP to pattern the Pd catalyst prior to metal deposition. Patterning is achieved in one of two ways: In the first approach,  $\mu$ CP is used to directly print a patterned film of Pd catalyst onto a polymer substrate; subsequent ELD deposits metal only in the printed areas. This approach was used by Hidber et al. to deposit patterned films of electroless copper onto various polymer substrates including PI, polystyrene (PS), and polyethylene (PE).<sup>34</sup> In the second approach,  $\mu$ CP is used to pattern an organosilane SAM that can either promote or inhibit the binding of Pd catalyst during solution deposition. For example, Prissanaroon et al. patterned an amino-terminated organosilane adhesion promoter onto the surface of plasma-modified polytetrafluoroethylene (PTFE) using  $\mu$ CP; exposing the substrate to a solution of Pd

colloids resulted in catalyst binding only in the areas defined by the SAM, which subsequently catalyzed ELD of copper.<sup>35</sup> Using a similar approach, Zschieschang et al. patterned a hydrophobic fluoropolymer onto the surface of polyethylene naphthalate (PEN) that acted as an adhesion inhibitor; exposure to aqueous Pd catalyst solution led to binding only in areas *not* defined by SAM, which subsequently catalyzed ELD of nickel.<sup>37</sup>

All of the aforementioned patterning/deposition methods demonstrate that metal circuitry can be deposited onto flexible polymer substrates without the need for expensive PVD or photolithography. Despite these advances, a clear frontrunner has yet to emerge as the ‘standard method’ for depositing patterned metals for flexible electronic devices.

### *1.1.2. Flexible, Transparent Conductive Electrodes*

Optoelectronic devices such as organic light-emitting diodes (OLEDs) and solar cells require an anode that is both conductive – to facilitate charge injection through the device, as well as transparent – to allow the passage of light through the device. Traditionally, transparent conductive electrodes (TCEs) have been fabricated using thin films of transparent metal oxides such as aluminum-doped zinc oxide, gadolinium indium oxide, fluorine-doped indium oxide, tin oxide, as well as many others.<sup>38</sup> Despite a diverse catalogue of transparent conductive oxides, the industry workhorse since the 1960s has been tin-doped indium oxide (ITO).

#### *1.1.2.1. ITO – The Industry Standard*

ITO has several characteristics that make it such a strong candidate as a TCE. First, ITO is highly transparent and conductive; ITO films on glass have sheet resistance values of  $< 20 \Omega/\square$  with a transparency of  $> 85\%$ . Sheet resistance can be thought of as a measure of resistivity averaged over the sample thickness, and has the units ohms/square ( $\Omega/\square$ ).<sup>39</sup> Typical sheet resistance requirements are  $\sim 15 \Omega/\square$  for displays, and up to  $100 \Omega/\square$  for touch screens.<sup>38</sup> Second, the scale up of dc magnetron sputter deposition methods has made the large scale fabrication of ITO coatings for thin film solar cells or flat panel displays a routine process.<sup>38</sup> Finally, roll-to-roll processing facilitates large scale (roll sizes up to 7 feet wide) deposition of ITO onto thin polymer substrates such as PET;<sup>38</sup>

befittingly, the market for ITO-coated polymer substrates is growing at an estimated 10% per year.<sup>40</sup>

Despite its advantages over other TCEs, ITO has two major limitations that hinder its integration into flexible electronic devices. First, the high temperature processing conditions required to produce highly transparent and conductive ITO films are not compatible with most polymer substrates. As a result, the sheet resistance values of ITO on PET are higher than on glass (60 – 400  $\Omega/\square$  and 80% transparent), which is undesirable for large area flat panel display technology.<sup>38</sup> Second, ITO is a brittle ceramic that cracks under very low (< 2%) tensile strains, and incurs irreversible damage when subjected to repetitive bending cycles.<sup>41,42</sup> A requirement of flexible electronic devices is that each component of the device – including the TCE – are able to withstand the strain associated with bending, folding, and rolling; the inability of ITO to withstand large amounts of tensile strain would severely limit the flexibility of any practical device.

#### *1.1.2.2. Silver Nanowire Films as a Drop-in Replacement for ITO*

A large research community has been developing potential replacements for ITO that possess its beneficial optoelectronic properties (low sheet resistance and high transparency) without compromising the mechanical and electrical properties of devices formed on flexible polymer substrates.<sup>43</sup> Examples of technologies that are currently being explored as ITO replacements include metallic grids,<sup>9,44-46</sup> conductive polymers,<sup>47-49</sup> reduced graphene oxide,<sup>50,51</sup> single-walled carbon nanotubes,<sup>52</sup> and metallic nanowires.<sup>41,53-74</sup>

Many view thin films of silver nanowires (AgNWs) as the most promising replacement for ITO for the following reasons: First, silver is the most conductive of the elements; highly conductive nanowires lead to films with low sheet resistance values. Second, AgNWs have extremely high aspect ratios (>  $10^3$ ); the high aspect ratio results in numerous interwire junctions within the AgNW films – reducing the sheet resistance of the film – while maintaining enough void space to allow the passage of light – essential for high transparency (Figure 1.03).<sup>75</sup> Third, the transparency and sheet resistance of the films can be tuned by varying the density of AgNWs; increasing the number of nanowires leads to more interwire connections, but consequently less void space for the

transmission of light (Figure 1.04).<sup>76</sup> Finally, there are a variety of methods available for depositing AgNW films including vacuum filtration,<sup>60,61</sup> drop casting,<sup>53,54</sup> Meyer rod coating,<sup>56,57</sup> and spray deposition.<sup>58,59,71,72</sup>

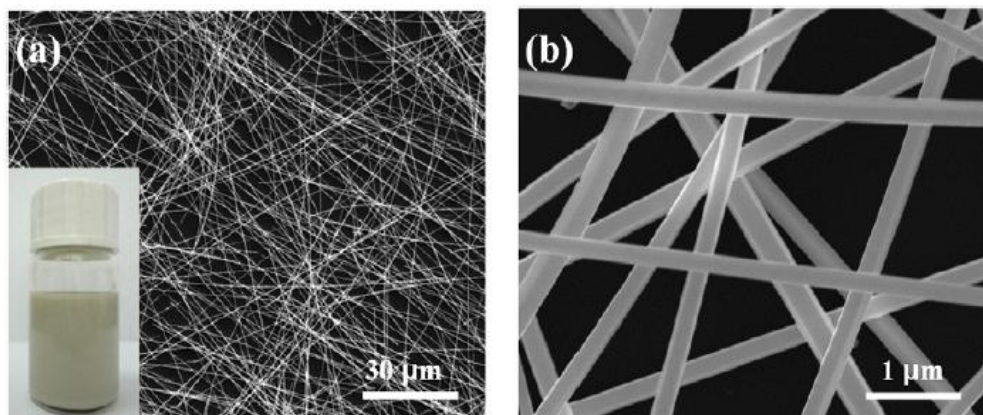


**Figure 1.03.** Morphology characterizations of as-prepared Ag NWs. (a) SEM image of top view of as-prepared AgNWs on a silicon substrate and their suspensions in alcohol (inset). (b) High-magnification SEM image of AgNWs. Adapted with permission from reference 75. © IOP Publishing. Reproduced by permission of IOP Publishing. All rights reserved.

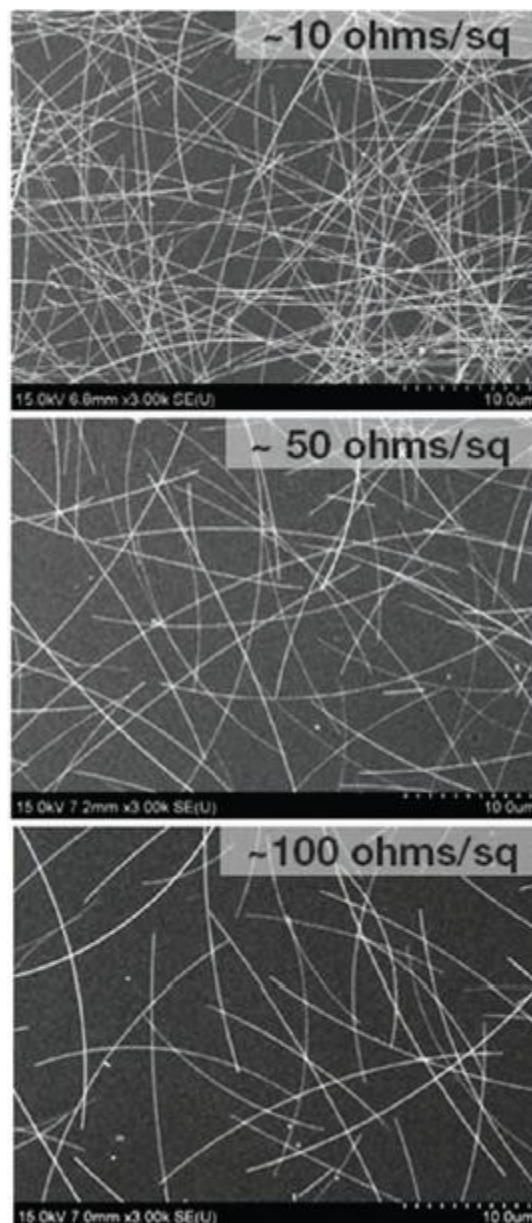


**Figure 1.04.** Top-view SEM images of AgNW-coated films with different densities, in which the AgNWs are shown to be a continuous network. Adapted with permission from reference 76.

AgNW films not only have optoelectronic properties that rival, if not surpass, those of ITO (85% transparent,  $20 \Omega/\square$ ), but they have also been deposited onto a variety of polymer substrates to make flexible TCEs that can withstand the tensile and compressive strain associated with bending, rolling, and folding.<sup>41,55,57,60,63,68,71,72,75,77,78</sup> For example, a

recent publication by Song et al. fabricated AgNW films on flexible PET plastic that had transparencies greater than 90% and sheet resistance values less than  $15 \Omega/\square$ .<sup>78</sup> These AgNW films were able to withstand up to 12.5% compressive strain (being bent to a radius of 0.2 mm), as well as over 1000 cycles of repetitive strain (being bent to a radius of 1.5 mm) without experiencing any change in electrical performance. These AgNW films were showcased as TCEs in flexible organic solar cells. Zhu et al. demonstrated the remarkable versatility of AgNW films by fabricating transparent conductive electrodes (91% transparent,  $13 \Omega/\square$  on glass) on a variety of substrates including flat and curved glass, flexible PET plastic, rough cloth, Xerox paper, a ceramic plate, and even a bamboo leaf.<sup>75</sup> AgNW films on paper substrates withstood over 10 000 cycles of repetitive strain (being bent to a radius of 2 mm) without any significant increase in sheet resistance (Figure 1.05)

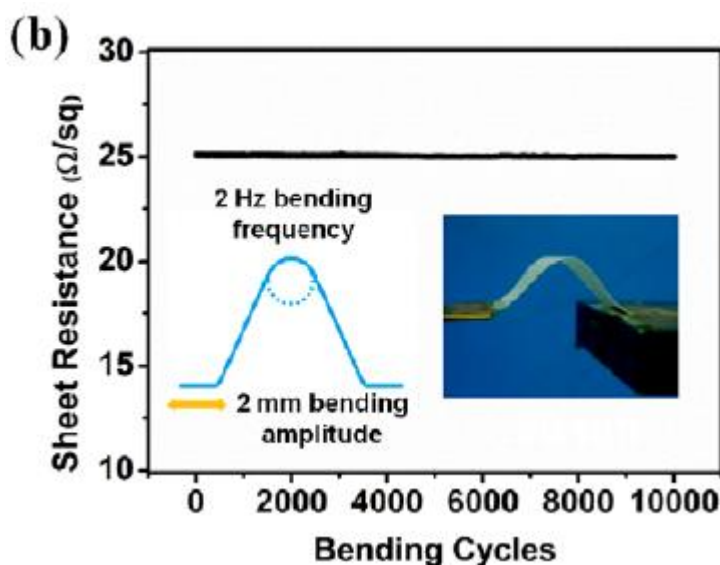


**Figure 1.05.** The measurement of sheet resistance during 10 000 bending cycles with a 2 mm bending amplitude for a AgNW transparent electrode transferred onto Xerox paper. Adapted with permission from reference 75. © IOP Publishing. Reproduced by permission of IOP Publishing. All rights reserved.

Despite the impressive optical, electrical, and mechanical performance of AgNW films, there are two major limitations that inhibit their integration into real flexible electronic devices. First, many of the techniques used to deposit AgNWs do so haphazardly, producing uncontrolled piles of nanowires that protrude from the substrate surface. These protrusions, which can often be  $> 100$  nm in height, may not be compatible with thin film devices in which the layer thickness is often  $< 100$  nm;<sup>54,57</sup> protruding AgNWs could provide a pathway for electrical shorts. Second, these haphazard piles of AgNWs are often not adhered to the surface, making them very fragile.<sup>64</sup> One potential solution to these problems is to embed AgNWs into a polymer film; embedding the wires not only provides adhesion to the substrate, but also reduces the height variations that can cause device shorts. This approach has been used to fabricate flexible OLEDs,<sup>64</sup> PLEDs,<sup>41</sup> polymer solar cells,<sup>63</sup> and capacitive strain sensors<sup>70</sup> using polymer embedded AgNWs as the TCE, truly highlighting these materials as the frontrunner for replacing ITO.

### *1.1.3. Assembly of Device Components*

Microelectronic devices are not limited to layered thin films, but can also be comprised of a series of electrical or optical components that have been integrated into a single system.<sup>79</sup> A significant challenge in the manufacture of these types of devices is assembling the components into their desired location with high reproducibility.<sup>80</sup> Traditionally, this has been accomplished using serial ‘pick-and-place’ fabrication in which robotic manipulators assemble each of the components individually, followed by serial wire-bonding and serial packaging.<sup>81</sup> According to Moore’s law, the number of electrical components (transistors) that can fit onto an integrated circuit (IC) chip doubles approximately every two years.<sup>4</sup> Consequently, the size of electrical components found in microelectronic devices must shrink at an equivalent rate. As the size of these components reaches the meso- and nanoscale (objects with dimensions ranging from 100  $\mu\text{m}$  to several nm), several limitations inhibit the usefulness of pick-and-place assembly in device fabrication. First, pick-and-place assembly is slow and inefficient for the assembly of very large numbers of components. Second, the adhesive and electrostatic forces that are negligible for the assembly of macroscopic components become dominant at the meso- or nanoscale; these forces can cause sticking between the micromanipulator

and the components, reducing efficiency and yield.<sup>81</sup> Finally, pick-and-place assembly is not compatible with non-planar substrate surfaces, or the assembly of components in three dimensions.<sup>79</sup>

#### *1.1.3.1. Self-Assembly*

The limitations of serial pick-and-place fabrication methods have pushed researchers towards developing new, parallel methods for assembling large numbers of device components in a single step.<sup>80</sup> The most popular of the parallel assembly methods – self assembly – has been ubiquitous in chemistry and biology long before the advent of IC technology.<sup>80</sup> Self-assembly, defined as the spontaneous aggregation of components into larger, ordered structures without human intervention,<sup>82</sup> is responsible for basic biological processes such as the formation of lipid membranes, folded proteins, structured nucleic acids, and protein aggregates, to name a few.<sup>80</sup> The same principles that make self-assembly nature's choice for forming biological structures also make it attractive for fabricating electronic devices. First, self-assembly is a parallel technique which can assemble a large number of components very quickly. Second, self-assembly allows access to highly ordered structures that cannot be fabricated using any other methods.<sup>80</sup>

Whitesides defines five important features that determine the success of any self-assembling system (these features are specific to molecular self-assembly, though in principle they extend to all length scales):<sup>80</sup>

*The components* – self-assembling systems consist of large numbers of components that may be identical or different, and their interaction with each other leads from a less ordered state (such as solution or disordered aggregate) to a more ordered state (such as a crystal).

*The interactions* – self-assembly is a result of the balance between repulsive and attractive interactions between the components. These interactions are usually weak and non-covalent, such as van der Waals interactions and hydrophobic interactions.

*Reversibility* – generating highly ordered structures requires that the interaction between the components is reversible, or weak enough to allow them to adjust their position within the structure after it is formed. This means that the forces holding the components together must be comparable to the forces that disrupt them.

*The environment* – self-assembly is usually carried at an interface or in solution; the interaction of the components with the environment, much like the interaction of the components with each other, can strongly influence the assembly process.

*Mass transport and agitation* – self-assembly requires that the components of the system are mobile, and come into contact. For molecular self-assembly, the thermal motion of molecules in solution is enough to facilitate contact; for nano-, meso-, and macroscopic systems, assuring mobility of the components is often more challenging.

These five design criteria, though initially applied to molecular self-assembling systems, can provide a useful framework for systems in which the component sizes extend to the meso- and macroscale.

### *1.1.3.2. Self-Assembly using Capillary Interactions*

Though a variety of interactions have been used as the driving force for the self-assembly of meso- and macroscopic components (e.g. magnetism<sup>83</sup> or electrostatics<sup>84,85</sup>), capillary interactions have emerged as the most popular. These self-assembly motifs usually involve components that are floated at a liquid/liquid or liquid/air interface, or components that have been coated with a hydrophobic liquid and suspended in water.<sup>80</sup> In the first case, the capillary forces can be controlled by changing the shape of the menisci at the interface between the components and the liquid. In the second case, capillary forces drive the components together to minimize the surface free energy of the hydrophobic liquid coating. If the liquid coating is an adhesive, the components can be made into permanent structures after self-assembly.<sup>86-90</sup> Electrical conductivity is important for any self-assembling microelectronic system; the use of molten solder as a liquid coating allows for assembly schemes that yield permanent, electrically connected structures.<sup>80,91-93</sup> Capillary bonds formed during the assembly process are strong enough to hold nanometer-,<sup>94-96</sup> micrometer-,<sup>97,98</sup> and millimeter<sup>99,100</sup> sized components together, and have yielded a variety of interesting two-dimensional<sup>101,102</sup> and three-dimensional<sup>88,91,103,104</sup> structures (Figure 1.06).

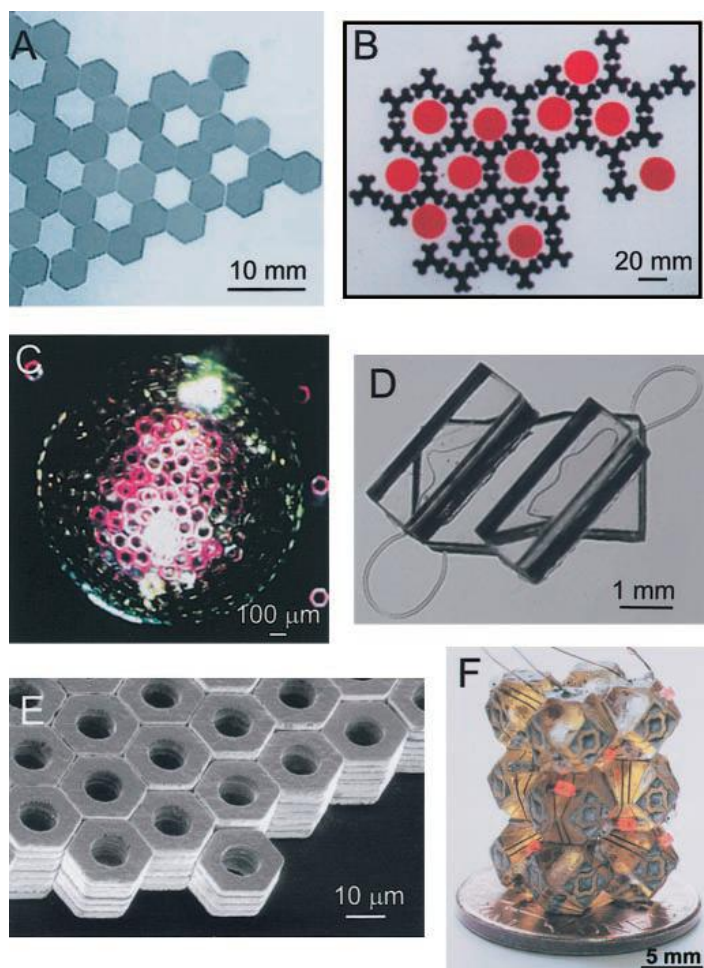


**Figure 1.06.** Examples of two-dimensional (A and B) and three-dimensional (C–F) structures, self-assembled in systems of macroscopic components interacting via capillary interactions. Open hexagonal array (A) and hexagonal lattice formed around circular templates (B) self-assembled from poly(dimethylsiloxane) plates floating at the interface between perfluodecalin and water. (C) Spherical structure formed by self-assembly of hexagonal metal plates on the surface of a drop of perfluodecalin in water. (D) Compact 3D structure formed by self-folding of a string of tethered, polymeric polyhedra. (E) Large crystal self-assembled from micrometer-sized hexagonal metal plates. (F) Aggregate with electrical connectivity self-assembled from polyhedral, polymer components bearing solder patterns of wires and dots. All images adapted with permission from the original copyright owners (references 33, 48, 49, 54, 36, 42 found within reference 80).

All of the structures in Figure 1.06 are assembled by minimizing the interfacial free energies of the components and forming closed-packed structures; however, these motifs do not permit control over the spacing between components. One way to control the spacing and geometry of the final structure is to incorporate the use of a template. Within the context of capillary induced self-assembly, templates can be fabricated using adhesive drops that have been patterned using SAMs to alter the surface free energy of specific areas of the template substrate.<sup>79,105</sup> Passing the substrate through a thin film of hydrophobic adhesive floating at an air/water interface deposits small adhesive drops in the hydrophobic regions to minimize the surface free energy. Following this step, hydrophobic components suspended in water can be flowed towards the substrate and will stick to the adhesive drops upon impingement.

Another approach to templated self-assembly – in which the surface tension between a metal electrode and a drop of molten solder is used to drive the assembly process – was used elegantly by Jacobs et al. to fabricate a fully functioning cylindrical display (Figure 1.07).<sup>79</sup> The display was fabricated in two steps: First, a series of GaAs/GaAlAs LED chips ( $\sim 280 \mu\text{m} \times 280 \mu\text{m} \times 200 \mu\text{m}$ ) – each with a large square gold anode on the backside of the chip and a small round gold cathode on the frontside of the chip – were assembled onto square shaped molten solder drops that had been patterned onto a copper template; this assembly process took place in aqueous media and was driven by the minimization of interfacial free energies of the molten solder and the gold anode. Next, both the small gold cathodes of the LED chips and a top electrode consisting of patterned copper wire were dip coated with molten solder and immersed into water; minimization of the free energy of the molten solder led to registration between the top electrode and the chips. After cooling the molten solder below its melting temperature, the LEDs were permanently anchored in place within a fully functional, addressable array.



**Figure 1.07.** Photograph of the operating display after the alignment of the top electrode. The display contains 113 LEDs that are assembled in an interleaved fully addressable array. Adapted with permission from reference 79.

Despite the versatility of templated self-assembly methods, they rely on the use of solvents (usually water) to minimize the effects of gravity and deliver the components to the template; wet conditions may not be compatible with the assembly of electronic components without requiring special packaging. Dry templated assembly methods have been proposed – such as the electrostatic assembly of spherical polystyrene particles into two-dimensional arrays by Winkleman et al.<sup>85</sup> – but anchoring the assembled structure in place requires that it be transferred to a polymer matrix such as optical adhesive, epoxy, or elastomer. Furthermore, this method is limited to the assembly of a single type of component.

## 1.2. Molecular Electronics

Since Aviram and Ratner first proposed the idea of a ‘molecular rectifier’ in 1974,<sup>106</sup> a large research effort has been put forth investigating the possibility of integrating individual molecules as the active or passive components in electronic devices.<sup>107-117</sup> This field of research, now known collectively as ‘molecular electronics’, has grown quickly over the past decade. The study of molecular electronics is driven by the rapid progression of electronic device miniaturization and the fundamental size limitations imposed by current complementary metal-oxide semiconductor (CMOS) technology.<sup>116</sup> As previously noted, Moore’s law states that the number of transistors on an integrated circuit chip grows exponentially, doubling about every two years.<sup>4,113</sup> In order for this trend to continue, the size of microelectronic circuit elements must soon approach the molecular and atomic scale.<sup>114</sup> The use of single molecules as active device elements is attractive for two reasons. First, the molecular length scale (several nm) is small enough to produce device elements that can extend the Moore’s law predictions. Second, advances in synthetic chemistry provide innumerable potential molecules for creating a ‘molecular toolbox’ that can be used to construct different device elements.<sup>113</sup>

### *1.2.1. Charge Transport Properties of Molecules*

Sandwiching molecules or molecular monolayers between two metal electrodes allows for characterization of their charge transport properties. The inherently small size of molecules leads to charge transport characteristics that are drastically different from those seen for bulk materials. A simple calculation of the energy dissipation across a single molecule during charge transport is often employed to express this point: Passing 500 fA of current at a bias of 0.5 V through a single alkane molecule with a heat capacity of 350 J·mol<sup>-1</sup>·K<sup>-1</sup> would lead to a temperature increase of ~10<sup>8</sup> K per molecule.<sup>110</sup> This calculation does not apply to molecules because they are smaller than the inelastic mean free path of electrons in typical metals, invalidating the concept of bulk resistivity. A variety of mechanisms has been considered for charge transport through the backbone of a molecule within a molecular electronic device. The mechanism that dominates charge transport depends on several factors including temperature, molecular size and structure, coupling of the molecule to the top and bottom electrodes, and the position of the

electrode Fermi energy levels with respect to the molecular orbitals of the molecule.<sup>108,113</sup>

Three primary charge transport mechanisms are applied to molecular junctions: coherent tunneling, incoherent tunneling, and charge hopping.

### 1.2.1.1. Coherent Tunneling

Classical quantum mechanical electron tunneling, often referred to as ‘coherent’ tunneling, is based on the probability of an electron traversing a barrier with a given height and thickness.<sup>108</sup> The tunneling rate exponentially decreases as the thickness of the barrier is increased, according to the Simmons equation, where  $J$  is the current density ( $\text{A}\cdot\text{cm}^{-2}$ ),  $q$  is the charge of the electron,  $V$  is the applied voltage,  $h$  is Planck’s constant,  $m$  is the mass of an electron,  $\Phi$  is the height of the tunneling barrier, and  $d$  is the barrier thickness:<sup>118,119</sup>

$$J = \frac{q^2 V}{h^2 d} \exp\left[\frac{-4\pi d}{h} 2m\Phi^{1/2}\right] \quad (\text{Eq. 1.1})$$

The Simmons equation can be simplified for practical experimentation by implementing a constant,  $J_0$ , to replace the pre-exponential term, and a term  $\beta$  that has units of inverse length (often  $\text{\AA}^{-1}$ ) that is proportional to the square root of the barrier height:

$$J = J_0 e^{-\beta d} \quad (\text{Eq. 1.2})$$

Within the context of a molecular junction, coherent tunneling is the most likely charge transport mechanism for a system in which the electron cannot access any electronic states on the molecule. In this case, the electron is forced to tunnel through the space between the two electrodes. The thickness of this tunneling barrier,  $d$ , is defined by the length of the molecule, while the height of the tunneling barrier is defined by difference between the Fermi energy level of the electrode, and the energy level of the closest molecular orbital (Figure 1.08).<sup>113</sup> One defining characteristic of coherent tunneling is the temperature independence of the rate of charge transport; measuring the rates of transport at various temperatures for a given molecular junction can aid in identifying coherent tunneling as the primary mechanism at work.

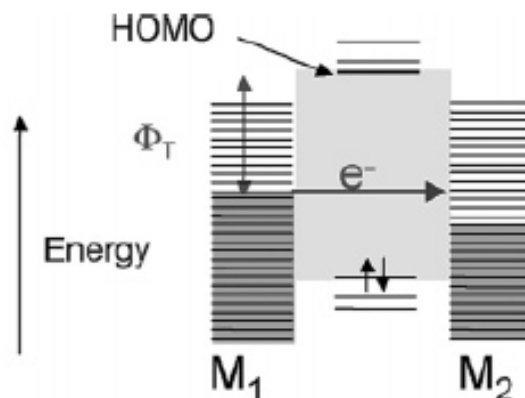


**Figure 1.08.** Illustration of the coherent tunneling electron transport mechanism, adapted with permission from reference 108.

#### 1.2.1.2. Incoherent Tunneling

It is generally accepted that coherent tunneling mechanisms apply only to systems in which the barrier is less than 25 Å thick, due to the exponential decay of tunneling probability as a function of barrier thickness.<sup>108</sup> As a result, the measurement of electron tunneling through a 40 Å thick insulating DNA helix in the 1990s came as a shock to many researchers in the field.<sup>120,121</sup> This result led to the proposal a new charge transport mechanism known as ‘incoherent’ tunneling, in which the electron no longer coherently tunnels through the barrier, but rather incoherently tunnels through a series of potential wells that exist along the barrier (Figure 1.09).<sup>108</sup> Tunneling from one of these discrete potential wells to the next occurs via a coherent tunneling process, making the incoherent tunneling process also independent of temperature.

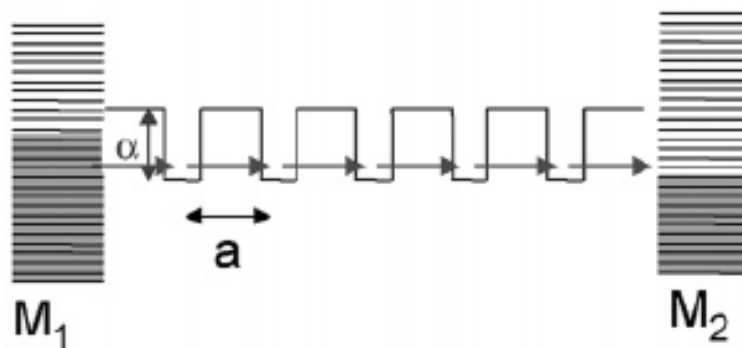


**Figure 1.09.** Illustration of the incoherent tunneling mechanism, adapted with permission from reference 108.

### 1.2.1.3. Activated Transport (Hopping)

Activated transport, or ‘hopping’, is a mechanism by which the electron travels over the tunneling barrier rather than through it.<sup>108</sup> Charge hopping occurs when the tunneling barrier is either deformed by an applied bias, or more commonly, by thermal nuclear motion that leads to a molecular geometry with a decreased barrier height.<sup>108,113</sup> In an ideal system, complete hybridization of the electrode Fermi levels and the molecular orbitals of the molecule would lead to a ‘molecular wire’ in which the electron could hop directly from one electrode to the other.<sup>113</sup> In reality, the offset between the Fermi energy levels of the electrodes from the molecular orbitals of the molecule and the discrete energy states present along the molecular backbone lead to a series of electrical sites to which the electron must hop in order to cross the molecular junction.<sup>113</sup> Electron hopping between relatively stable sites along the molecular backbone leads to a tunneling probability that is dependent upon  $d^{-1}$ , rather than exponentially dependent as is the case for coherent tunneling. Because charge hopping is an activated process, it is strongly dependent upon temperature and applied bias; increasing either of these parameters lowers the tunneling barrier height.

### 1.2.2. Molecular Junctions

While Aviram and Ratner's theoretical study of unidirectional electron transport through a single molecule sparked great interest in the field of molecular electronics, the development of nanotechnology capable of measuring such properties was not realized until the 1990s.<sup>107</sup> Charge transport through molecules is typically measured using a two-terminal junction in which the molecule of study is sandwiched between two conductive electrodes. There are generally two types of molecular junctions: single molecule, and ensemble.<sup>108</sup> Single molecule junctions (Figure 1.10) have been defined as those in which individual molecules make up the layer that bridges the two electrodes. Ensemble junctions (Figure 1.11) are those in which a large number of molecules ( $10^3 - 10^{12}$ ) make up a highly ordered monolayer that bridges the two electrodes.<sup>122</sup> Single molecule junctions can be extremely elegant, and also represent the lowest limit to the miniaturization of microelectronic components; however, their fabrication and characterization are extremely intricate and experimentally demanding.<sup>108</sup> As such, the remainder of this discussion and the work presented in this dissertation will focus on ensemble junctions.

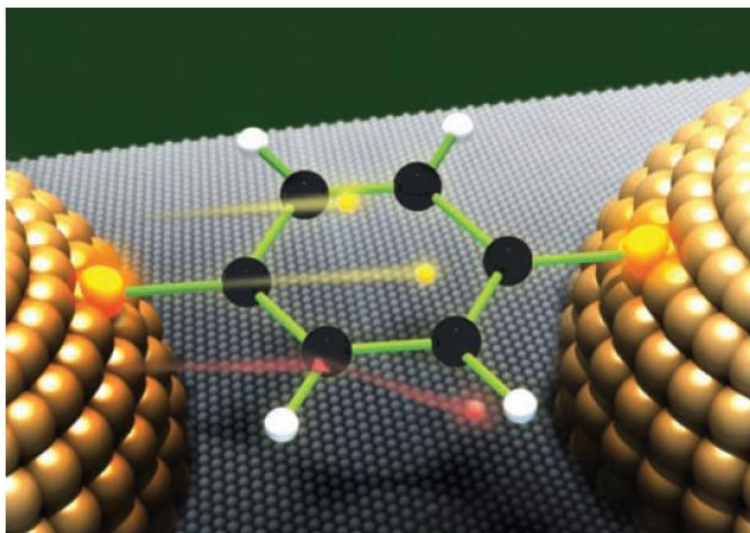


**Figure 1.10.** Illustration of a single molecule bridging two electrodes to form a single molecule junction, adapted with permission from reference 116.

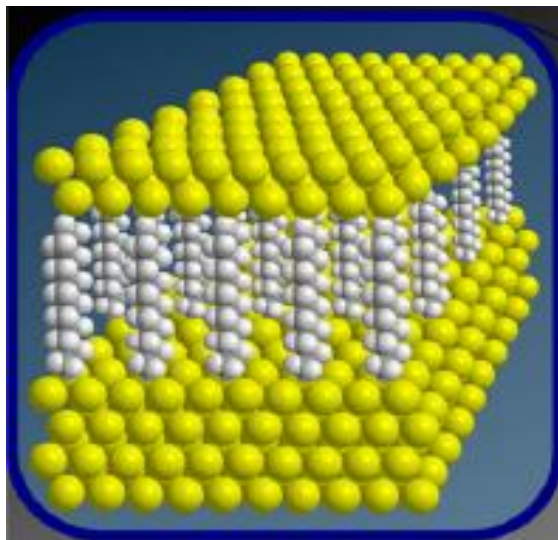


**Figure 1.11.** Illustration of a monolayer bridging two electrodes to form an ensemble junction, adapted with permission from reference 122.

### 1.2.3. Challenges with Molecular Junctions

The literature describing charge transport through molecules using molecular junctions has been plagued by inconsistent, irreproducible, and often contradictory results. This lack of coherency within the field can be attributed to the fact that nearly every research group studying molecular electronics fabricates their junctions differently.<sup>112</sup> Ensemble molecular junctions have three primary structures: the top electrode, the molecular monolayer, and the bottom electrode. A variety of different materials and deposition methods are available for producing each of these structures, leading to innumerable possibilities for the makeup of a molecular junction. Table 1.1 highlights this point by illustrating a variety of different molecular junction systems used to measure coherent tunneling through simple alkane molecules.<sup>123</sup> Across these different studies, the measured values of  $\beta$  range from 0.47 – 0.90 Å<sup>-1</sup>, and the measured values of  $J_0$  range from  $\sim 10^1 - 10^8$  A·cm<sup>-2</sup>. Recently, a large research effort has been put forth to minimize, if not eliminate the inconsistencies associated with measuring charge transport properties of molecules by developing reliable protocols for data collection and analysis.<sup>124-126</sup> A set of reliable experimental protocols requires careful consideration of the material and method of deposition used to fabricate the molecular monolayer, the bottom electrode,

and the top electrode. Furthermore, these three structures do not operate independently of each other; the relative position of the electrode Fermi energy levels with respect to the molecular orbitals of the molecules can have drastic implications on the charge transport properties of the system.

**Table 1.1.** Variety of molecular junctions used to measure  $\beta$  and  $J_0$  of alkanes, reproduced with permission from reference 123.

type of junction	top electrode	bottom electrode	values of $n$	$J_0$ (A/cm <sup>2</sup> )	$\beta$ (Å <sup>-1</sup> )	ref
(1) Au-SAM//polymer/Au <sup>a</sup>	conductive polymer	AS-DEP <sup>g</sup>	8, 10, 12, 14	$\sim 10^{5h}$	$0.47 \pm 0.1$	26
(2) Au-SAM//polymer/Hg <sup>b</sup>	conductive polymer	AS-DEP <sup>g</sup>	8, 10, 12, 14, 16	$\sim 10^{2h}$	$0.90 \pm 0.03$	55
(3) Hg-SAM//Hg <sup>c</sup>	liquid metal	liquid metal	9, 10, 11, 12, 15, 16, 18	$\sim 10^{6h}$	$0.85 \pm 0.06$	56
(4) Au-SAM//graphene	graphene	AS-DEP <sup>g</sup>	8, 12, 16	$2 \times 10^8$	$0.84 \pm 0.1$	57
(5) Au-SAM-Au	direct deposition of Au	AS-DEP <sup>g</sup>	8, 12, 16	$\sim 10^8$	$0.80 \pm 0.03$	58
(6) Ag-SAM//Ga <sub>2</sub> O <sub>3</sub> /EGaIn	liquid metal (cross-bar)	TS	12, 14, 16, 18	$\sim 340$	$0.78 \pm 0.2$	1, this paper
(7a) Ag-SAM//Ga <sub>2</sub> O <sub>3</sub> /EGaIn <sup>d,e</sup>	liquid metal (cone)	TS	10, 12, 14, 16, 18	$339 \pm 1$	$0.792 \pm 0.01$	21
(7b) Ag-SAM//Ga <sub>2</sub> O <sub>3</sub> /EGaIn <sup>d,e</sup>	liquid metal (cone)	TS	9, 11, 13, 15, 17	$91 \pm 1$	$0.819 \pm 0.01$	21
(8) Ag-SAM//Ga <sub>2</sub> O <sub>3</sub> /EGaIn <sup>d</sup>	liquid metal (cone)	TS	12, 14, 16	$(\sim 0.2)^f$	$(0.43 \pm 0.2)^f$	19
(9) Ag-SAM//Ga <sub>2</sub> O <sub>3</sub> /EGaIn <sup>d,f</sup>	liquid metal (cone)	TS	10, 12, 14, 16	$\sim 10^3$	$0.88 \pm 0.2$	2, 19
(10) Ag-SAM//SAM-Hg	liquid metal	TS	20, 24, 28	$\sim 10^3$	0.64	30
(11) Si/SiO <sub>2</sub> //SAM-Hg	liquid metal	Si/SiO <sub>2</sub>	10, 12, 14, 18	NA	0.82	59
(12) Si-SAM//Hg	liquid metal	Si	12, 14, 16, 18	$1.5 \times 10^{4h}$	0.78	60
(13) Hg-SAM//SAM-Hg	liquid metal	liquid metal	18, 20, 22, 24, 28	$\sim 10^{2h}$	0.71	48
(14) Ag-SAM//SAM-Hg	liquid metal	AS-DEP <sup>g</sup>	24, 26, 28, 30, 32	$4 \times 10^5$	0.86	54

### 1.2.4. The Molecular Monolayer

There are two types of molecular monolayers used as the active component in molecular electronic devices: Langmuir-Blodgett (LB) films and SAMs. LB films are formed by spreading a molecular film at an air/water interface and compressing the film to a desired molecular density.<sup>127</sup> Pulling a solid substrate through the interface results in a complete transfer of the molecular film. LB films have several beneficial characteristics that make them interesting candidates for molecular electronics applications.<sup>112</sup> First, the LB method provides fine control over the packing density of molecules in the film. Molecular packing density of LB films is largely independent of the substrate, allowing for tightly packed monolayers of a variety of different types of molecules. Second, the LB method allows for easy fabrication of bilayer or multilayer molecular films by simply repeating the process several times. Finally, the LB method does not require the formation of a covalent bond between the molecules in the film and the substrate surface,

making it compatible with a wide variety of different substrate materials. One particularly interesting study by Collier et al. used LB films of rotaxane molecules to fabricate molecular junctions that were capable of acting as logic gates.<sup>128</sup> However, one crucial drawback to the LB method is that the molecules are physisorbed – and thus only weakly coupled – to the surface of the metal electrode.<sup>129</sup> The nature of the interaction between the molecular anchoring group and the metal electrode surface is one of the most important parameters that dictate the charge transport through a molecular junction. It has previously been shown for alkyl-thiol systems that the current flow through the alkyl chain can be up to four orders of magnitude higher for a system that is covalently linked to the electrode surface versus a system that is physisorbed.<sup>130,131</sup> Unlike LB films, SAMs provide a route to highly ordered monolayers in which the molecules comprising the film are covalently linked to the electrode surface, thus improving the metal-molecule coupling.<sup>132</sup> Table 1.2 outlines the different types of interactions between a molecule and an electrode surface within a molecular junction.<sup>129</sup>

**Table 1.2.** Types of interactions at metal – molecule interfaces, adapted with permission from reference 129. © IOP Publishing. Reproduced by permission of IOP Publishing. All rights reserved.

Increasing interaction strength ↓	Metal–molecule interface	Interaction type	Schematic
	Noble gas atoms or saturated, non-polar molecules on clean metal surfaces	Physisorption, absence of charge transfer	
	$\pi$ -conjugated molecules on passivated metal surfaces	Physisorption, possible integer electron charge transfer through tunneling	
	Polarizable molecules or molecules with intrinsic dipole moment on clean metal surfaces	Physisorption, rearrangement of electron densities, attraction through image forces	
	Molecules with free electron pairs on clean metal surfaces	Weak chemisorptions, possible partial charge transfer	
	Molecules with anchoring groups on clean metal surfaces	Strong chemisorption, covalent bonds, (partial) charge transfer, surface dipole	

#### 1.2.4.1. Self-Assembled Monolayers

SAMs are highly ordered, single layer molecular films formed from the adsorption of organic molecules onto a solid or liquid surface. Adsorbate molecules spontaneously organize on the surface to produce crystalline or semi-crystalline domains. The anatomy and characteristics of a SAM are highlighted in Figure 1.12.<sup>132</sup>

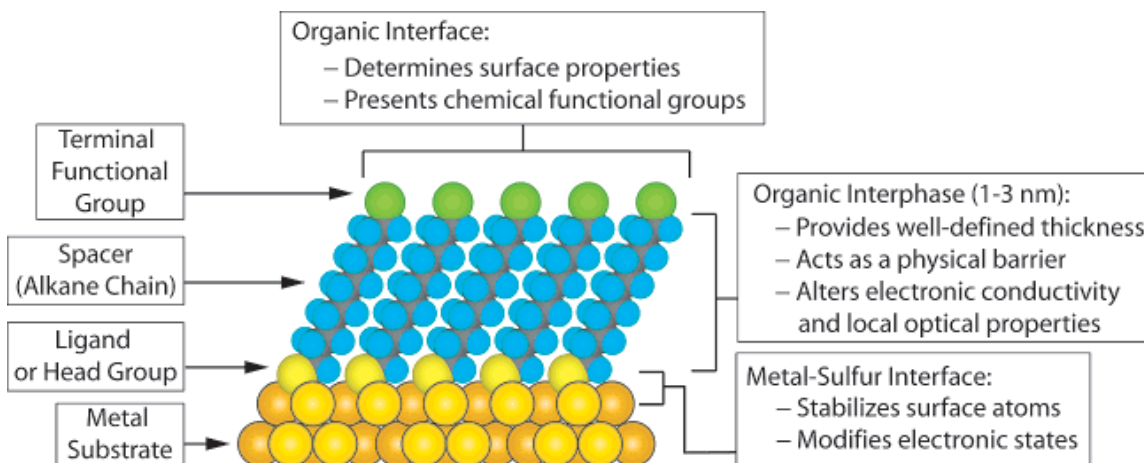


**Figure 1.12.** Schematic diagram of an ideal, single-crystalline alkanethiolate SAM formed on a gold (111) surface, adapted with permission from reference 132.

The primary driving force for SAM formation is the interaction between the substrate (which for the purpose of this discussion will be restricted to metals, though metal-oxides and semiconductor surfaces can also be used for SAM formation), and the reactive ligand or ‘head group’ of the adsorbate molecule. The head group has a highly specific affinity for the metal substrate which leads to an overall lowering of the interfacial free energy upon adsorption. Adsorption happens via the formation of a covalent bond between the molecule and the metal surface (chemisorption), and is exothermic.<sup>132</sup>

Self-assembly of adsorbate molecules into tightly packed domains on the surface of the metal is also driven by van der Waals interactions between neighbouring molecules. Isolated van der Waals interactions are much weaker than the covalent bonds that anchor the molecule to the metal surface;<sup>133</sup> however, extending these interactions between neighbouring molecules across an infinite two-dimensional network significantly lowers the free energy of the organic layer.<sup>132,134</sup>

Although the self-assembly process is driven by the free energy minimization associated with chemisorption of the head group and van der Waals interactions between neighbouring molecules, the interfacial properties of the SAM are often dictated by the terminal functional groups that are present at the organic interface. Interfacial properties (e.g. wettability) and tribological properties (e.g. adhesion, friction, and lubrication) of

the SAM are all affected by the nature of the functional group that presents at the surface of the layer.<sup>82,132</sup>

A variety of different metals can be used as substrates for the formation of SAMs, with the most popular choice being the series of coinage metals (Au, Ag, Cu, Pt, Pd). Of the coinage metals, gold has historically been the most heavily studied SAM-bearing substrate for three major reasons. First, gold is inert; it does not oxidize in ambient conditions like copper or silver,<sup>135</sup> and it does not react with most chemicals. Second, thin gold films can easily be deposited onto a variety of substrates using well established methods such as physical vapour deposition, sputtering, or electrodeposition.<sup>132</sup> Finally, the interaction between gold and sulfur is highly favourable ( $\sim 30$  kcal/mol<sup>136-138</sup>); adsorption of organosulfur compounds such as alkanethiols, dialkylsulfides, and dialkyldisulfides have all been shown to produce robust, well ordered SAMs.<sup>139-143</sup>

The surface structure of *n*-alkanethiolate SAMs on Au (111) (Figure 1.13) is based on a  $(\sqrt{3} \times \sqrt{3})R30^\circ$  overlayer in which the sulfur atoms bind at the three-fold hollows of the crystal lattice.<sup>144,145</sup> Each unit cell has two non-equivalent alkyl chains that result in a secondary structure with a  $c(4 \times 2)$  superlattice.<sup>146</sup> For *n*-alkanethiolate SAMs on gold with long ( $>10$  methylene units) alkyl chains, chain orientation within the organic layer can be described by two parameters: the angle of tilt for the linear backbone away from the surface normal ( $\alpha$ ), and the angle of rotation about the long axis of the molecule ( $\beta$ ).<sup>132</sup> Due to the separation of sulfur atoms on the surface ( $4.99 \text{ \AA}$ )<sup>133</sup>, alkyl chains tilt and rotate to maximize both packing density and the number of van der Waals interactions between neighbouring molecules. The values of  $\alpha$  and  $\beta$  are strongly dependent upon the substrate; for example *n*-alkanethiolate SAMs have a tilt angle of  $\sim 30^\circ$  when formed on Au (111), and a tilt angle of  $\sim 10^\circ$  when formed on Ag (111).<sup>132</sup>

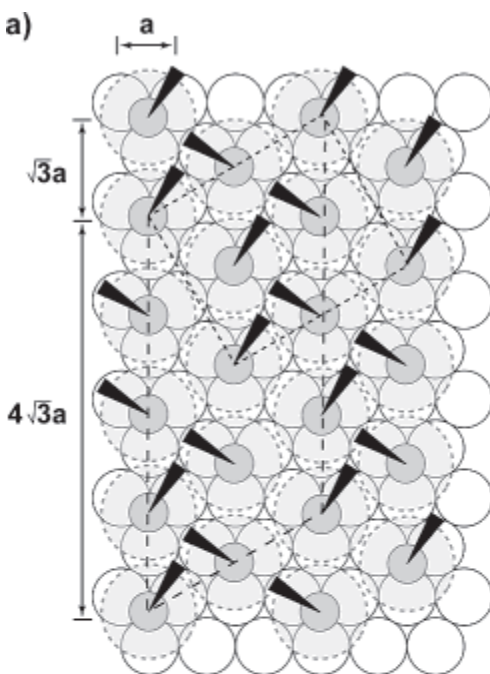


**Figure 1.13.** Schematic diagram depicting the  $(\sqrt{3} \times \sqrt{3})R30^\circ$  overlayer and  $c(4 \times 2)$  superlattice of *n*-alkanethiolate SAMs formed on Au (111), adapted with permission from reference 132.

There are a myriad of applications in nanoscience and technology for *n*-alkanethiolate SAMs,<sup>132</sup> however it is the use of these SAMs as the active component in molecular electronic devices that is the application of greatest interest to this discussion and this dissertation.

#### 1.2.4.2. Charge Transport through *n*-Alkanethiolate SAMs

Attempts to rectify the aforementioned problems associated with characterizing charge transport through molecules has forced many researchers to take a step back to the simplest of systems: a monolayer of alkane molecules sandwiched between two metal electrodes.<sup>112</sup> *n*-alkanethiolate SAMs on coinage metal surfaces provide the simplest method for producing this system, and have thus been the most extensively studied class of molecules within the field. There is a general consensus that charge transport through SAMs comprised of insulating alkanes, such as SAMs formed from *n*-alkanethiols, occurs via non-resonant, coherent tunneling according to the simplified Simmons

equation (Eq. 1.2).<sup>118,131,147-149</sup> The height of the tunneling barrier is defined by the large HOMO-LUMO gap for these systems ( $\sim 8 - 10$  eV), and the thickness of the tunneling barrier is defined by the length of the molecule.<sup>125</sup>

Within the context of metal-insulator-metal (MIM) molecular junctions formed from *n*-alkanethiolate SAMs on gold, the parameters of the Simmons equation begin to take on a more meaningful form. The current density,  $J$ , is calculated by measuring the current across a molecular junction with an applied bias, and then normalizing the current to the effective area of contact between the two electrodes and the SAM. The thickness of the tunneling barrier,  $d$ , is determined by the molecular length. It is important to note that the thickness of the tunneling barrier is not equivalent to the thickness of the SAM; coherent tunneling is thought to occur across the length of the carbon backbone (through bond) and not across the shortest distance between the two electrodes (through space).<sup>149</sup> This point becomes important when comparing *n*-alkanethiolate SAMs formed on two different metal substrates; an increase in the average tilt angle of the alkyl chains can lead to a thinner SAM, reducing the distance between the two electrodes; however, the length of the carbon backbone is constant.

$\beta$  describes the exponential decay in tunneling probability as a function of increasing molecular length, and is often expressed in units of per carbon ( $n_C^{-1}$ ). Theoretically,  $\beta$  depends only on the molecular orbitals of the molecules comprising the SAM, and should be independent of the contacts at the electrode surface.<sup>108</sup> One assumption in the Simmons equation is that the molecular orbitals, and consequently  $\beta$ , are independent of molecular length. The values of  $\beta$  reported in the literature for *n*-alkanethiolate SAMs ranges from  $0.51 - 1.13 n_C^{-1}$ ,<sup>125</sup> with most values falling in the range of  $0.75 - 1.1 n_C^{-1}$ .<sup>150-152</sup>

$J_0$  is an expression of the theoretical current density through a molecular junction with no tunneling barrier (e.g. an *n*-alkanethiolate SAM with no carbons). The value of  $J_0$  is a reflection of the nature of the interface between the SAM and the electrode surface. An important factor that influences the magnitude of  $J_0$  is the coupling strength; strong molecule-electrode coupling is usually achieved via chemisorption, and can lead to broadening and overlap of the HOMO/LUMO of the molecule and the Fermi energy

levels of the electrodes, lowering the barrier to charge injection. Weak coupling, usually associated with physisorbed molecules, leads to discrete HOMO/LUMO energy levels that do not mix with electronic states at the electrode surface.<sup>111</sup>  $J_0$  is not always reported in the literature because of its strong dependence on the choice of the top and bottom electrode.

#### 1.2.4.3. Chelating SAMs for use in Molecular Electronics

*n*-Alkanethiolate SAMs provide a simple, well-understood system for developing reliable protocols for fabricating and characterizing molecular junctions; however, two major limitations may prevent their use in real electronic devices.<sup>153</sup> First, the sulfur 3p orbitals involved in the metal-thiolate bond are localized, restricting charge transport through the molecule.<sup>154,155</sup> Second, a low energy barrier to molecular diffusion and desorption<sup>156</sup> causes poor stability and could limit the lifetime of a real device. von Wrochem et al. studied an elegant system that solves each of these problems using SAMs on gold formed from terphenyldithiocarbamate (TPDTC) adsorbate molecules.<sup>153</sup> The DTC head group (Figure 1.14 a) chelates to the gold surface leading to stronger metal-molecule coupling and improved thermal stability versus a thiol analogue (Figure 1.14 b). The combination of head group chelation and the aromatic nature of the terphenyl backbone causes delocalization of the molecular orbitals (Figure 1.14 c), with a high density of states (DOS) near (-0.6 eV) the Fermi level of the gold surface. Notably, molecular junctions formed using a mercury drop top electrode and a TPDTC SAM on gold showed values of  $J$  that were two orders of magnitude higher than the non-chelating thiol analogue (terphenylthiol).<sup>153</sup> Similar studies also show, both experimentally and theoretically, that the chelation of conjugated dithiocarboxylic acid (DTCAs) molecules to the gold surface improves the metal-molecule coupling and reduces the charge injection barrier in a molecular junction.<sup>157,158</sup>

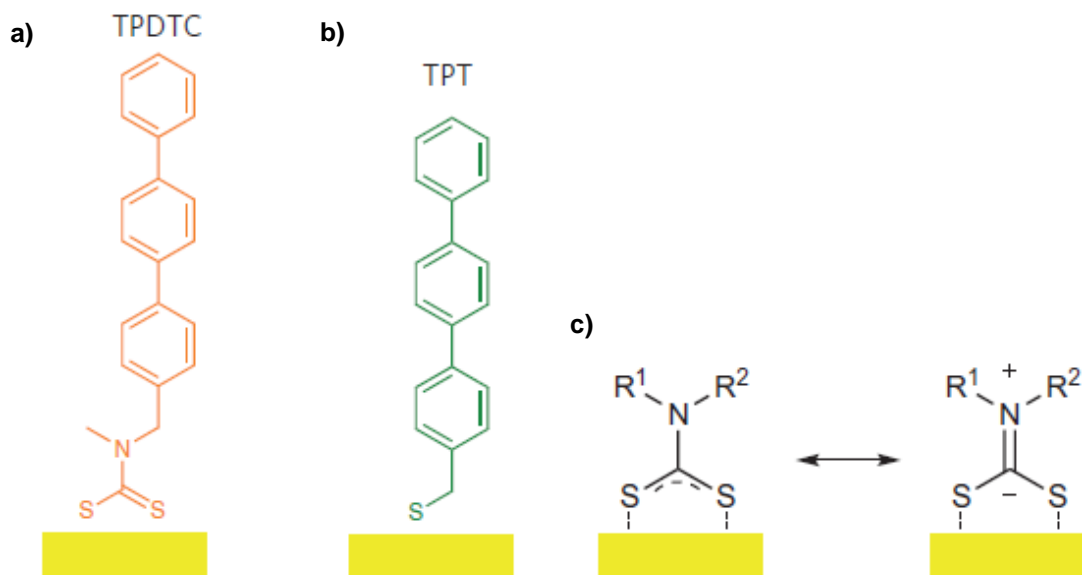


**Figure 1.14.** The terphenyl compounds with a DTC head group (a) and a thiol head group (b) shown bound to gold. c) Mesomeric forms of the DTC head group on gold. Adapted with permission from reference 153.

In addition to DTCs and DTCAs, a variety of other adsorbate molecules have been shown to form SAMs on gold in which the head group binds in a multidentate fashion.<sup>159</sup> Though multidentate binding of an adsorbate molecule improves the stability of the SAM, reducing the charge injection barrier requires strong coupling that is only achieved through mixing and overlap of the molecular orbitals with the Fermi energy levels of the metal surface.<sup>153,157,158</sup> Delocalized bonding to the gold surface for DTC and DTCA adsorbates provides orbital mixing and overlap; however, other systems of this nature have yet to be studied within the context of molecular electronics.

One potentially interesting candidate for use as an anchoring group in SAM-based molecular junctions is the dithiophosphinic acid (DTPA). Dialkyl-DTPA molecules have previously been used in industrial applications for the selective separation of precious metals from sulfide ores.<sup>160</sup> Though little is known about the ability of the DTPA anchoring group to form SAMs on metal surfaces<sup>161-163</sup>, the potential for chelation with resonance between the two sulfur atoms<sup>162</sup> makes this class of molecules interesting for molecular electronics applications.

### 1.2.5. The Top Electrode

As previously discussed, establishing electrical contact between molecules and the bottom electrode in ensemble molecular junctions can be achieved by forming SAMs.<sup>132</sup> Therefore, the biggest challenge in completing the junction is finding a suitable method to contact the organic interface or ‘top’ of the SAM.<sup>164</sup> Chiechi et al. define four important characteristics for an ideal top electrode. First, the electrode should form physical, conformal, but non-damaging contact to the SAM. Second, the electrode should form small area (micron scale) contact to the SAM to minimize the contribution of defects to the measured current densities. Third, the top electrode should be fabricated in a way that does not require the use of specialized equipment or access to a cleanroom. Finally, the material should be non-toxic.<sup>165</sup> A variety of different top electrodes have been investigated including mechanical break junctions, scanning probe (scanning tunneling microscopy (STM) and conductive probe atomic force microscopy (AFM)) junctions, evaporated metal junctions, conductive polymer junctions, and liquid metal junctions.<sup>124</sup>

Break junctions and scanning probe junctions are used to probe contact areas of only a few molecules, and do not fall within the boundaries of an ensemble measurement. Evaporating thin metal films directly onto the surface of the SAM leads to intimate metal-molecule contact; however, the hot metal atoms present during evaporation can damage the organic layer or cause the formation of metallic filaments (Figure 1.15).<sup>132</sup> The formation of metallic filaments can be prevented by the deposition of a conductive polymer interlayer between the SAM and electrode;<sup>166</sup> however, these polymers often require high annealing temperatures that are not compatible with *n*-alkanethiolates.<sup>156,165</sup> Liquid metal contacts, such as the hanging mercury drop electrode and the EGaIn (a liquid eutectic alloy, 75.5 wt % Ga and 24.5 wt % In) tip electrode, form reproducible, non-damaging contact to the SAM surface, making them ideal candidates for top electrodes in SAM based junctions.

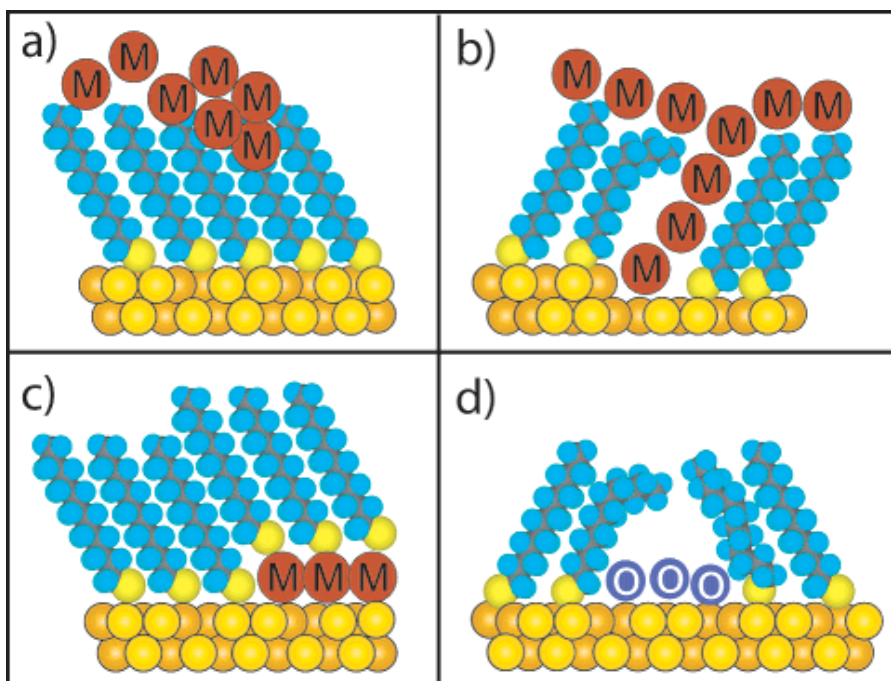


**Figure 1.15.** Illustration of the damage that can be caused to a SAM by the hot metal atoms present during evaporation. a) Chemical reaction between the organic molecules and the metal atoms. b) Formation of a metallic filament through the SAM. c) Formation of a metal adlayer on the surface of the substrate bearing the SAM. d) Formation of metal-oxide impurities on the surface of the substrate. Adapted with permission from reference 132.

#### 1.2.5.1. The Hanging Mercury Drop Electrode

One of the most well studied top electrodes for use in molecular junctions, pioneered by Majda et al.,<sup>167-170</sup> is the hanging mercury drop (Hg-drop). Since its inception in 1997, there have been numerous reports of charge transport measurements through SAMs using the Hg-drop test bed.<sup>148,171-178</sup> To fabricate Hg-drop junctions, a SAM is formed on the surface of a metal substrate which is then immersed into a solvent bath containing secondary adsorbate molecules. Then, a drop of mercury – which has been stabilized by the formation of a SAM from the secondary adsorbate – is lowered into mechanical contact with the metal surface.<sup>109</sup> Hg-drop junctions can also be fabricated by bringing into contact the surfaces of two SAM coated drops of mercury in a thiol-containing

solvent bath.<sup>173</sup> One defining characteristic of the Hg-drop junction is that the interface is SAM-SAM (Figure 1.16), rather than SAM-electrode.

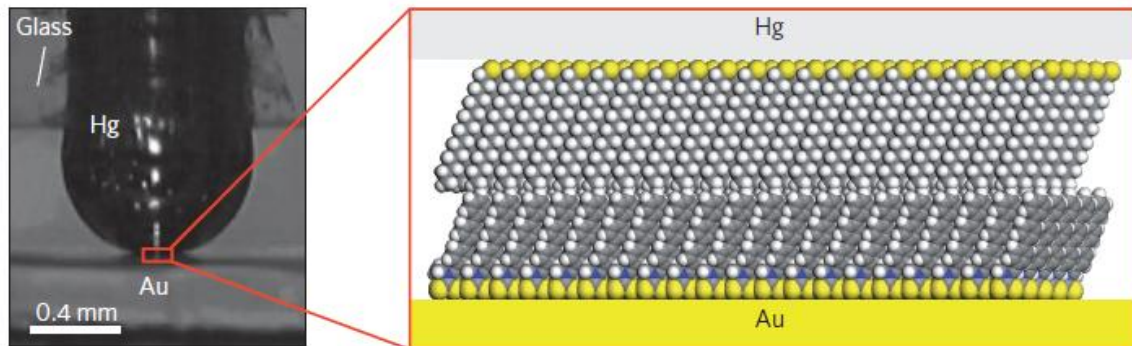


**Figure 1.16.** Photograph (left) and model (right) of a Hg-drop junction formed from *n*-alkanethiolate SAMs on Hg and Au. Adapted with permission from reference 153.

There are several benefits to using the Hg-drop electrode: First, junctions can be fabricated quickly and easily, allowing the collection of large pools of data for statistical analysis.<sup>108</sup> Second, the high surface tension of mercury reduces the likelihood of filament formation through the SAM. Finally, the interface allows for the study of asymmetric (Hg-SAM<sub>1</sub>-SAM<sub>2</sub>-metal) junctions with a variety of different molecular structures.<sup>179</sup> There are also several drawbacks to the Hg-drop top electrode: First, the area of contact is large ( $\sim 250 \mu\text{m}^2$ ),<sup>124</sup> amplifying the contribution of defects in the SAM which can result in a large number of electrical shorts.<sup>180</sup> Second, the environmental effects associated with measuring charge transport properties in a solvent bath are unclear.<sup>181</sup> Finally, integrating the Hg-drop electrode into a real microelectronic device is not practical; mercury is both mechanically unstable and highly toxic.<sup>108,180</sup>

#### 1.2.5.2. The EGaIn Tip Electrode

Recently, a new liquid metal top electrode formed from conically shaped tips of EGaIn has emerged.<sup>180</sup> Like the Hg-drop electrode, the EGaIn tip makes conformal, non-damaging contact to the surface of a SAM coated metal substrate. However unlike the Hg-drop electrode, EGaIn is non-toxic,<sup>180</sup> it can be formed into non-spherical shapes with

small (1 – 100  $\mu\text{m}$ ) diameter contact areas,<sup>180</sup> it does not require a solvent bath or secondary SAM to act as a protective barrier layer at the metal surface (this purpose is served by a thin ( $\sim 0.7$  nm) self-limiting skin of  $\text{Ga}_2\text{O}_3$  that spontaneously forms in ambient conditions)<sup>124</sup> and it can be formed into stable liquid metal microstructures,<sup>182,183</sup> increasing the likelihood of it being integrated into real microelectronic devices.

The process for fabricating a conical EGaIn tip is shown in Figure 1.17. First, a drop of EGaIn is extruded from a syringe and brought into contact with a bare metal substrate (to which it adheres) using a micromanipulator. Second, the syringe is slowly pulled away from the surface, forming an hourglass shape; the interesting rheological properties of EGaIn are attributed to the spontaneous formation of  $\text{Ga}_2\text{O}_3$  ‘skin’ which is non-compressible.<sup>183</sup> The syringe continues to be pulled away from the metal surface until the EGaIn bifurcates into a distinct conical tip.<sup>180</sup> Bringing the conical tip into contact with the surface of a SAM coated metal substrate completes the molecular junction.



**Figure 1.17.** A series of photographs of the formation of a conical tip of EGaIn. Adapted with permission from reference 180.

A number of interesting phenomena have been observed using the EGaIn tip electrode, including coherent tunneling,<sup>180</sup> molecular rectification,<sup>184</sup> the ‘odd-even’ effect,<sup>125</sup> quantum interference,<sup>185</sup> and very recently, the influence of changing a single atom on the charge transport properties of SAMs.<sup>164</sup> Despite its versatility, there have been questions about the nature of the  $\text{Ga}_2\text{O}_3$  layer that makes up the surface of the tip, specifically the

contributions to the resistance of the electrode from i) the oxide layer, ii) any adventitious organics that adsorb onto the oxide layer, and iii) experimental and environmental processing conditions.<sup>124</sup> A recent study by Cademartiri et al. answered many of these questions by concluding that i) handling conditions had no influence on the structure and composition of the tip, ii) adsorption of adventitious organics under normal laboratory conditions did not significantly affect charge transport measurements, and iii) for all systems tested, the resistance of the junction is dominated by the SAM and not the tip; the resistance of the tip is estimated to be several orders of magnitude lower than the most conductive SAM measured in this study.<sup>124</sup> The EGeIn tip electrode provides a fast, safe, and simple way to collect large amounts of reproducible charge transport data, making it one of the most attractive top electrodes currently available.

### *1.2.6. The Bottom Electrode*

The most popular choice of bottom electrode for ensemble molecular junctions is a thin coinage metal film, more specifically, silver or gold.<sup>112</sup> Well understood thiol chemistry provides ease with which reproducible, well ordered SAMs can be formed on these substrates.<sup>132</sup> One drawback however, is that polycrystalline coinage metal films produced by electron beam evaporation (As-deposited) have a surface morphology that is dominated by intergrain boundaries comprised of several atomic steps, as well as a variety of different structural irregularities.<sup>132</sup> SAMs formed on these substrates exhibit various defects, many of which are highlighted in Figure 1.18, that are strongly influenced by the surface morphology of the metal film.

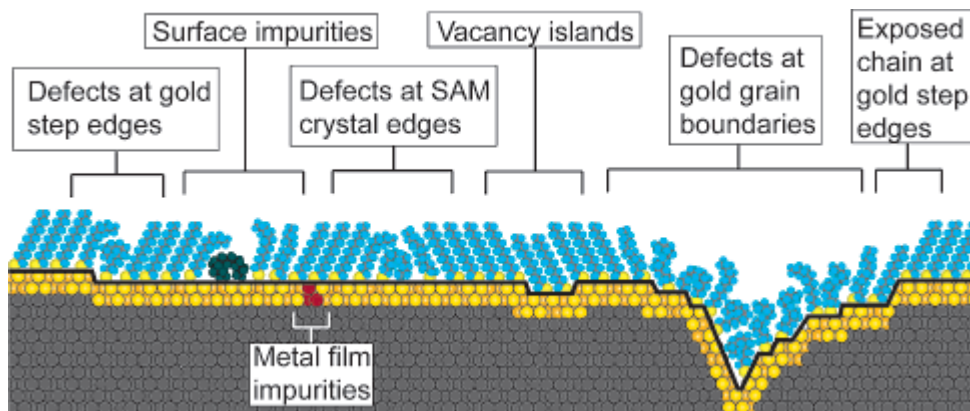


**Figure 1.18.** Schematic illustration of the different types of defects seen for SAMs formed on polycrystalline gold substrates. Adapted with permission from reference 132.

Within the context of a molecular junction, defects present in SAMs can lead to variation in the measured current densities as a result of ‘thin’ and ‘thick’ areas (as illustrated for a Hg-SAM-SAM-Ag junction in Figure 1.19) that change the thickness of the tunneling barrier,  $d$ .<sup>171</sup> Thick area defects include those in which a solvent or solute molecule has intercalated the interface between the SAM and the top electrode; the presence of these contaminants leads to additional van der Waals interfaces through which charge must tunnel, causing a decrease in the measured current densities. Thin area defects are caused by local disorder in the SAM as a result of misalignment between neighbouring alkyl chains, resulting in a decrease in the thickness of the tunneling barrier, and consequently an increase in the measured current densities.<sup>171</sup> Substrate induced defects, both thick and thin, are randomly distributed throughout the SAM leading to a normal distribution of  $d$ .<sup>126</sup> For systems that obey the Simmons equation – in which  $J$  is exponentially dependent upon  $d$  – a normal distribution of  $d$  leads to a log-normal distribution of  $J$ ; statistical analysis of  $\log J$  is much more useful than analysis of  $J$ .<sup>126</sup>

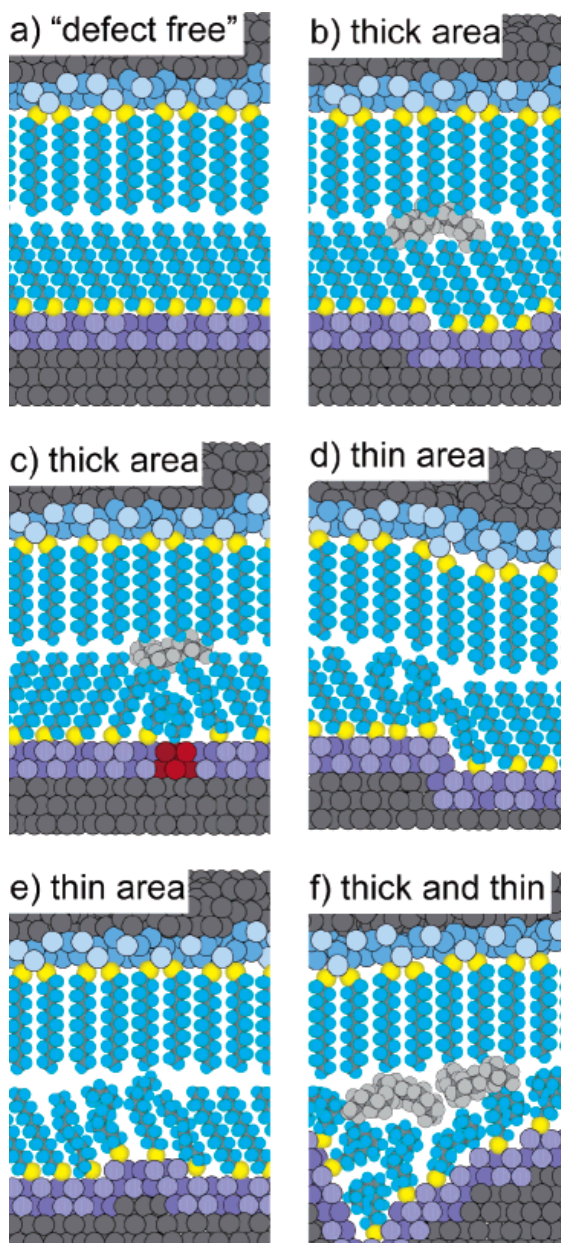


**Figure 1.19.** Schematic diagrams of several possible defects in SAMs of  $SC_{12}$  on silver (bottom electrode) and at the interface with a SAM of  $SC_{12}$  on mercury (top electrode): (a) a defect-free junction; (b) isolated (un-annealed) vacancies; (c) impurities in the silver film that cause local disorder in the SAM; (d) steps at the edge of annealed vacancy islands; (e) small, raised vacancy islands; and (f) defects at the grain boundaries of the silver supporting disordered SAMs. The molecules in between the SAMs are intercalated or trapped solvent (e.g., hexadecane) or solute (e.g.,  $HSC_{12}$ ). Adapted with permission from reference 171.

A potential solution for reducing the density of substrate induced defects in SAM based molecular junctions is to replace rough, As-deposited metal substrates with ultra smooth metal substrates.<sup>171,186</sup> Ultra smooth coinage metal substrates are fabricated using a process known as ‘template stripping’,<sup>187,188</sup> in which a metal film is deposited onto a smooth template (usually silicon or mica) and subsequently stripped away to reveal its smooth underside. Template-stripped (TS) metal substrates are smooth (RMS surface roughness values of  $\sim 2 - 3 \text{ \AA}$ ) and have a surface comprised of large (50 – 500 nm), atomically flat terraces that differ by only a few atoms in height.<sup>187-190</sup> Figure 1.20 highlights the differences between the surface of As-deposited, and TS silver films. *n*-Alkanethiolate SAMs formed on TS metal surfaces have fewer substrate induced defects, owing to the improved alignment of neighbouring alkyl chains.<sup>191,192</sup>

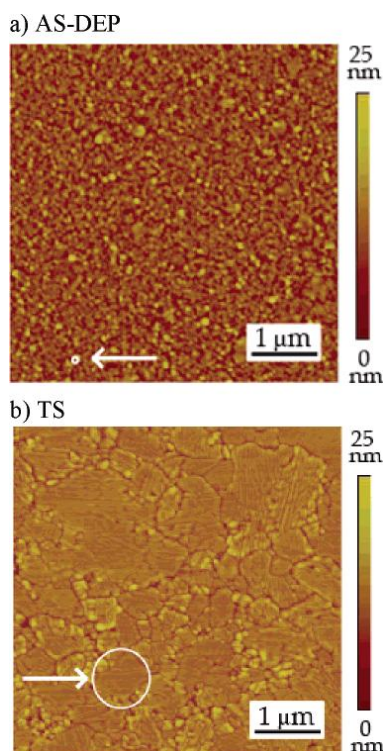


**Figure 1.20.** Contact-mode AFM images of the topography of the (a) As-deposited silver film and (b) TS silver film. The root-mean-square roughnesses of a  $25 \mu\text{m}^2$  area of the silver films are  $5.1 \pm 0.4 \text{ nm}$  for As-deposited and  $1.2 \pm 0.1 \text{ nm}$  for TS. The white circles indicate the approximate size of the largest grains in each film and have diameters of (a) As-deposited, 80 nm, and (b) TS, 1  $\mu\text{m}$ . Adapted with permission from reference 171.

Molecular junctions formed from *n*-alkanethiolate SAMs on TS metal substrates show a decrease in the variance of  $\log J$  and an increase in the non-shortening device yield.<sup>171,186</sup> Fewer substrate induced defects (both thin and thick area) in SAMs formed on TS substrates lowers the distribution of the tunneling barrier thickness across the area of the junction, resulting in narrower distributions of  $\log J$ . Reducing the number of thin area defects also helps prevent the formation of metallic filaments, improving the junction yield.<sup>171</sup> Weiss et al. showed that Hg-drop junctions formed using *n*-alkanethiolate SAMs on TS silver had variance in the measured current densities several orders of magnitude lower than for junctions that used as-deposited silver (Figure 1.21). Hg-drop junctions on As-deposited silver also failed 3.5 times more often than those on TS silver.<sup>171</sup> A similar study by Engelkes et al. demonstrated that conductive probe AFM junctions formed using *n*-alkanethiolate SAMs on TS Au had a several orders of magnitude decrease in the variance of the measured current densities compared to As-deposited Au.<sup>186</sup> These studies are important because they demonstrate the profound influence of substrate morphology on the measurement of current density through SAMs, regardless of the bottom electrode material (gold or silver) or the choice of top electrode (Hg-drop or conductive probe AFM).

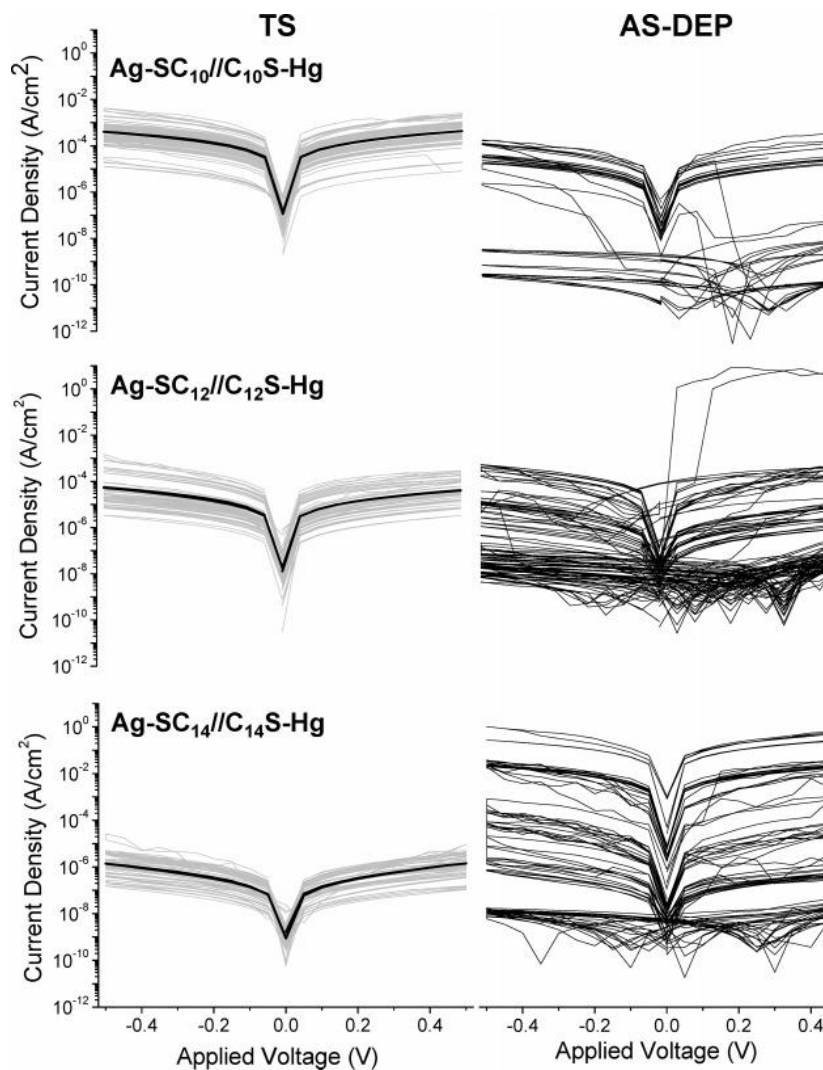


**Figure 1.21.** (Left) Plots of the average  $|J|$ -V curves (log-mean, bold black lines) and all  $|J|$ -V curves (light gray lines) measured on the TS junctions Ag-SC<sub>n</sub>//C<sub>n</sub>S-Hg ( $n = 10, 12, 14$ ), except for the initial traces that had a current density several orders of magnitude below the remaining traces, and traces directly preceding and following amalgamation. (Right) The same set of traces for the corresponding junction using As-Deposited silver. Adapted with permission from reference 171.

Ultrasooth metal films can also be fabricated using chemical mechanical polishing (CMP) – a well known technology within the semiconductor manufacturing industry. CMP uses a synergistic combination of wet chemical etching and mechanical polishing to remove surface defects, such as roughness or scratching, from metallic films.<sup>193</sup> Islam et al. demonstrated that alkoxyphthalenethiol monolayers on polished platinum electrodes showed greatly improved molecular packing and orientation compared to those formed on As-deposited platinum.<sup>194</sup> Molecular switching devices fabricated from monolayers on the polished platinum electrodes showed a remarkable 100% device yield. Apart from this proof of concept study, the use of polished metal electrodes as substrates for SAM based molecular junctions remains relatively unexplored.

### 1.3. Dissertation Objectives

#### *1.3.1. Simple, Low-Cost Fabrication of Thin Film Device*

##### *Components*

The first half of this dissertation focuses on the development of simple, low-cost methods for fabricating thin film device components. We seek replacements for traditional fabrication methods that rely on the need for high capital equipment and specialized facilities, or that are incompatible with emerging technologies such as flexible and stretchable electronics.

First, we examine a general solution-based method for patterned metal deposition onto a variety of rigid and flexible polymer substrates. Traditionally, metal is deposited onto polymer substrates using expensive PVD techniques such as electron beam evaporation or sputtering. These metals are typically patterned using photolithography. We replace PVD and photolithography with a combination of electroless copper deposition and soft lithographic patterning using an aluminum porphyrin complex, thereby reducing cost and complexity. This work is presented in Chapter 2.

Second, we examine the use of AgNW / optical adhesive composite films as transparent conductive electrodes in flexible photovoltaic devices. Lightweight, flexible photovoltaic devices are fabricated on polymeric substrates that can be bent, rolled, or folded. ITO, the universal TCE, fails under the compressive and tensile strain

experienced by flexible electronic devices. We look to replace brittle ITO with a durable, flexible AgNW-based transparent conductive coating that can be applied to a variety of substrates including glass, plastic, and elastomer. We also examine the functionality of these coatings as TCEs in flexible light-emitting devices. This work is presented in Chapter 3.

Finally, we examine a two-dimensional mesoscale self-assembly method in which the need for a solvent carrier medium has been eliminated. A method in which particle self-assembly takes place under dry conditions is compatible with the assembly of electronic components; under wet conditions, the electronic components would likely require special protective packaging. This work is presented in Chapter 4.

### *1.3.2. New Molecules and Substrates for use in Molecular Electronic Devices*

The second half of this dissertation focuses on developing new tools for creating molecular electronic devices. Molecular electronic devices are comprised of an active component, typically a molecule or group of molecules, sandwiched between two metal electrodes. We describe a new series of molecules as potential active components in molecular electronic devices, as well as a new class of metal substrates as potential electrodes in molecular electronic devices.

First, we examine new SAMs on gold formed from dihexadecyldithiophosphinic acid ((C<sub>16</sub>)<sub>2</sub>DTPA) adsorbate molecules. The DTPA head group, bearing two sulfur moieties, can potentially chelate to the gold surface. Chelation of the DTPA head group would improve coupling between the molecule and the metal surface, potentially reducing the barrier to charge transport through the SAM in a molecular electronic device. This study focuses on the influence of substrate morphology on the ability of the head group to chelate to the gold surface, and the consequential implications on the structure of the organic layer. This work is presented in Chapter 5.

Second, we examine a series of SAMs on gold formed from dialkyl-DTPAs with varying alkyl chain lengths (C<sub>6</sub>, C<sub>10</sub>, C<sub>12</sub>, C<sub>14</sub>, C<sub>16</sub>). This study focuses on the influence of

alkyl chain length on the head group binding, molecular packing density, and organic layer organization of dialkyl-DTPA SAMs. This work is presented in Chapter 6.

Third, we examine the use of chemical mechanical polishing in the fabrication of ultra smooth gold substrates for use as electrodes in molecular electronic devices. This study focuses on the development and characterization of the CMP process with respect to surface roughness, surface uniformity, and surface composition. Furthermore, we compare the charge transport properties through a series of *n*-alkanethiolate SAMs ( $n = 9 - 16$ ) formed on polished gold substrates to SAMs formed on TS gold substrates; TS substrates are widely accepted to be the standard substrate for use as a bottom electrode in SAM-based molecular electronic devices. This work is presented in Chapter 7.

Finally, we examine the charge transport properties of new diphenyldithiophosphinic acid ( $\text{Ph}_2\text{DTPA}$ ) SAMs within molecular tunnel junctions. This study begins with the characterization of the head group binding, wettability, and electrochemical barrier properties of  $\text{Ph}_2\text{DTPA}$  SAMs formed on TS gold. Then, we form and characterize metal-SAM// $\text{Ga}_2\text{O}_3$ /EGaIn molecular junctions using both chelating  $\text{Ph}_2\text{DTPA}$  SAMs and monodentate analogue thiophenol ( $\text{PhSH}$ ) SAMs to determine the effect of head group chelation on charge transport properties. We conclude with a computational investigation detailing the electronic structure of these two systems, providing important insight into the ability of the adsorbate molecules to couple to the underlying gold surface. This work is presented in Chapter 8.

## 1.4. References

- (1) Nathan, A.; Ahnood, A.; Cole, M. T.; Lee, S.; Suzuki, Y.; Hiralal, P.; Bonaccorso, F.; Hasan, T.; Garcia-Gancedo, L.; Dyadyusha, A.; Haque, S.; Andrew, P.; Hofmann, S.; Moultrie, J.; Chu, D. P.; Flewitt, A. J.; Ferrari, A. C.; Kelly, M. J.; Robertson, J.; Amaratunga, G. A. J.; Milne, W. I. *Proc. IEEE* **2012**, *100*, 1486.
- (2) Kim, D. H.; Ghaffari, R.; Lu, N. S.; Rogers, J. A. In *Annual Review of Biomedical Engineering, Vol 14*; Yarmush, M. L., Ed.; Annual Reviews: Palo Alto, 2012; Vol. 14, p 113.
- (3) Vogel, E. M. *Nat. Nanotechnol.* **2007**, *2*, 25.
- (4) Moore, G. E. In *Electronics Magazine* 1965; Vol. 38.
- (5) Streetman, B. G.; Banerjee, S.; 6th ed.; Prentice Hall: Upper Saddle River, NJ, 2005.
- (6) Bao, Z. N. In *Polymers for Microelectronics and Nanoelectronics*; Lin, Q., Pearson, R. A., Hedrick, J. C., Eds.; Amer Chemical Soc: Washington, 2004; Vol. 874, p 1.
- (7) Gelinck, G. H.; Huitema, H. E. A.; Van Veenendaal, E.; Cantatore, E.; Schrijnemakers, L.; Van der Putten, J.; Geuns, T. C. T.; Beenhakkers, M.; Giesbers, J. B.; Huisman, B. H.; Meijer, E. J.; Benito, E. M.; Touwslager, F. J.; Marsman, A. W.; Van Rens, B. J. E.; De Leeuw, D. M. *Nat. Mater.* **2004**, *3*, 106.
- (8) Darbanian, N.; Venugopal, S. M.; Gopalan, S. G.; Allee, D. R.; Clark, L. T. *J. Soc. Inf. Disp.* **2010**, *18*, 346.
- (9) Krebs, F. C. *Org. Electron.* **2009**, *10*, 761.
- (10) Myny, K.; Steudel, S.; Vicca, P.; Beenhakkers, M. J.; van Aerle, N.; Gelinck, G. H.; Genoe, J.; Dehaene, W.; Heremans, P. *Solid-State Electron.* **2009**, *53*, 1220.
- (11) Klauk, H. *Org. Electron.: Materials, Manufacturing, and Applications*; Wiley-VCH: Weinheim, Germany, 2006.
- (12) Rogers, J. A.; Bao, Z.; Baldwin, K.; Dodabalapur, A.; Crone, B.; Raju, V. R.; Kuck, V.; Katz, H.; Amundson, K.; Ewing, J.; Drzaic, P. *Proc. Natl. Acad. Sci. U. S. A.* **2001**, *98*, 4835.
- (13) Mach, P.; Rodriguez, S. J.; Nortrup, R.; Wiltzius, P.; Rogers, J. A. *Appl. Phys. Lett.* **2001**, *78*, 3592.
- (14) Rogers, J. A.; Bao, Z. N.; Dodabalapur, A.; Makhija, A. *IEEE Electron Device Lett.* **2000**, *21*, 100.
- (15) Rogers, J. A.; Bao, Z. N.; Makhija, A.; Braun, P. *Adv. Mater.* **1999**, *11*, 741.

- (16) Cosseddu, P.; Bonfiglio, A. *Appl. Phys. Lett.* **2006**, *88*.
- (17) Hur, S. H.; Khang, D. Y.; Kocabas, C.; Rogers, J. A. *Appl. Phys. Lett.* **2004**, *85*, 5730.
- (18) Wang, Z.; Xing, R. B.; Zhang, J.; Yuan, J. F.; Yu, X. H.; Han, Y. C. *Appl. Phys. Lett.* **2004**, *85*, 831.
- (19) Loo, Y. L.; Willett, R. L.; Baldwin, K. W.; Rogers, J. A. *Appl. Phys. Lett.* **2002**, *81*, 562.
- (20) Loo, Y. L.; Someya, T.; Baldwin, K. W.; Bao, Z. N.; Ho, P.; Dodabalapur, A.; Katz, H. E.; Rogers, J. A. *Proc. Natl. Acad. Sci. U. S. A.* **2002**, *99*, 10252.
- (21) Guo, T. F.; Pyo, S.; Chang, S. C.; Yang, Y. *Adv. Funct. Mater.* **2001**, *11*, 339.
- (22) Gray, C.; Wang, J.; Duthaler, G.; Ritenour, A.; Drzaic, P. In *Organic Field Effect Transistors*; Fichou, D., Bao, Z., Eds. 2001; Vol. 4466, p 89.
- (23) van Osch, T. H. J.; Perelaer, J.; de Laat, A. W. M.; Schubert, U. S. *Adv. Mater.* **2008**, *20*, 343.
- (24) Smith, P. J.; Shin, D. Y.; Stringer, J. E.; Derby, B.; Reis, N. *Journal of Materials Science* **2006**, *41*, 4153.
- (25) Dearden, A. L.; Smith, P. J.; Shin, D. Y.; Reis, N.; Derby, B.; O'Brien, P. *Macromol. Rapid Comm.* **2005**, *26*, 315.
- (26) Kamyshny, A.; Ben-Moshe, M.; Aviezer, S.; Magdassi, S. *Macromol. Rapid Comm.* **2005**, *26*, 281.
- (27) Redinger, D.; Molesa, S.; Yin, S.; Farschi, R.; Subramanian, V. *IEEE Trans. Electron Devices* **2004**, *51*, 1978.
- (28) Szczech, J. B.; Megaridis, C. M.; Gamota, D. R.; Zhang, J. *IEEE Trans. Electron. Packag. Manuf.* **2002**, *25*, 26.
- (29) Kumar, A.; Whitesides, G. M. *Appl. Phys. Lett.* **1993**, *63*, 2002.
- (30) Kumar, A.; Biebuyck, H. A.; Whitesides, G. M. *Langmuir* **1994**, *10*, 1498.
- (31) Zaumseil, J.; Meitl, M. A.; Hsu, J. W. P.; Acharya, B. R.; Baldwin, K. W.; Loo, Y. L.; Rogers, J. A. *Nano Lett.* **2003**, *3*, 1223.
- (32) *Electroless Plating: Fundamentals and Applications*; Mallory, G. O.; Hajdum, J. B., Eds.; Electroplaters and Surface Finishers Society: Orlando, Florida, 1990.
- (33) Tate, J.; Rogers, J. A.; Jones, C. D. W.; Vyas, B.; Murphy, D. W.; Li, W. J.; Bao, Z. A.; Slusher, R. E.; Dodabalapur, A.; Katz, H. E. *Langmuir* **2000**, *16*, 6054.
- (34) Hidber, P. C.; Helbig, W.; Kim, E.; Whitesides, G. M. *Langmuir* **1996**, *12*, 1375.

- (35) Prissanaroon, W.; Brack, N.; Pigram, P. J.; Hale, P.; Kappen, P.; Liesegang, J. *Thin Solid Films* **2005**, *477*, 131.
- (36) Li, Y.; Chen, D. S.; Lu, Q. H.; Qian, X. F.; Zhu, Z. K.; Yin, J. *Appl. Surf. Sci.* **2005**, *241*, 471.
- (37) Zscheschang, U.; Klauk, H.; Halik, M.; Schmid, G.; Dehm, C. *Adv. Mater.* **2003**, *15*, 1147.
- (38) Brian G. Lewis, D. C. P. *MRS Bull.* **2000**, *25*, 22.
- (39) Schroder, D. K. *Semiconductor Material and Device Characterization*; John Wiley and Sons Inc.: Hoboken, 2006.
- (40) Cornia, R. L.; Fenn, J. B.; Memarian, H.; Ringer, R. *Proc. 41st Annu. Tech. Conf. (Society of Vacuum Coaters, Boston, 1998)* **1998**, 452.
- (41) Yu, Z. B.; Zhang, Q. W.; Li, L.; Chen, Q.; Niu, X. F.; Liu, J.; Pei, Q. B. *Adv. Mater.* **2011**, *23*, 664.
- (42) Park, S. K.; Han, J. I.; Moon, D. G.; Kim, W. K. *Jpn. J. Appl. Phys., Part 1* **2003**, *42*, 623.
- (43) Kumar, A.; Zhou, C. W. *ACS Nano* **2010**, *4*, 11.
- (44) Krebs, F. C. *Sol. Energy Mater. Sol. Cells* **2009**, *93*, 1636.
- (45) Galagan, Y.; Rubingh, J.-E. J. M.; Andriessen, R.; Fan, C.-C.; Blom, P. W. M.; Veenstra, S. C.; Kroon, J. M. *Sol. Energy Mater. Sol. Cells* **2011**, *95*, 1339.
- (46) Kang, M.-G.; Kim, M.-S.; Kim, J.; Guo, L. J. *Adv. Mater.* **2008**, *20*, 4408.
- (47) Chang, Y.-M.; Wang, L.; Su, W.-F. *Org. Electron.* **2008**, *9*, 968.
- (48) Colsmann, A.; Stenzel, F.; Balthasar, G.; Do, H.; Lemmer, U. *Thin Solid Films* **2009**, *517*, 1750.
- (49) Do, H.; Reinhard, M.; Vogeler, H.; Puetz, A.; Klein, M. F. G.; Schabel, W.; Colsmann, A.; Lemmer, U. *Thin Solid Films* **2009**, *517*, 5900.
- (50) Becerril, H. A.; Mao, J.; Liu, Z.; Stoltenberg, R. M.; Bao, Z.; Chen, Y. *ACS Nano* **2008**, *2*, 463.
- (51) Eda, G.; Fanchini, G.; Chhowalla, M. *Nat. Nanotechnol.* **2008**, *3*, 270.
- (52) Cao, Q.; Rogers, J. A. *Adv. Mater.* **2009**, *21*, 29.
- (53) Gaynor, W.; Burkhard, G. F.; McGehee, M. D.; Peumans, P. *Adv. Mater.* **2011**, *23*, 2905.
- (54) Lee, J. Y.; Connor, S. T.; Cui, Y.; Peumans, P. *Nano Lett.* **2008**, *8*, 689.
- (55) Madaria, A. R.; Kumar, A.; Ishikawa, F. N.; Zhou, C. W. *Nano Research* **2010**, *3*, 564.
- (56) Liu, C. H.; Yu, X. *Nanoscale Res. Lett.* **2011**, *6*, 75.
- (57) Hu, L. B.; Kim, H. S.; Lee, J. Y.; Peumans, P.; Cui, Y. *ACS Nano* **2010**, *4*, 2955.
- (58) Scardaci, V.; Coull, R.; Lyons, P. E.; Rickard, D.; Coleman, J. N. *Small* **2011**, *7*, 2621.

- (59) Akter, T.; Kim, W. S. *ACS Appl. Mater. Interfaces* **2012**, *4*, 1855.
- (60) De, S.; Higgins, T. M.; Lyons, P. E.; Doherty, E. M.; Nirmalraj, P. N.; Blau, W. J.; Boland, J. J.; Coleman, J. N. *ACS Nano* **2009**, *3*, 1767.
- (61) Lee, P.; Lee, J.; Lee, H.; Yeo, J.; Hong, S.; Nam, K. H.; Lee, D.; Lee, S. S.; Ko, S. H. *Adv. Mater.* **2012**, *24*, 3326.
- (62) Azulai, D.; Belenkova, T.; Gilon, H.; Barkay, Z.; Markovich, G. *Nano Lett.* **2009**, *9*, 4246.
- (63) Yang, L. Q.; Zhang, T.; Zhou, H. X.; Price, S. C.; Wiley, B. J.; You, W. *ACS Appl. Mater. Interfaces* **2011**, *3*, 4075.
- (64) Zeng, X. Y.; Zhang, Q. K.; Yu, R. M.; Lu, C. Z. *Adv. Mater.* **2010**, *22*, 4484.
- (65) Hu, W.; Niu, X.; Li, L.; Yun, S.; Yu, Z.; Pei, Q. *Nanotechnology* **2012**, *23*, 344002.
- (66) Xu, F.; Zhu, Y. *Adv. Mater.* **2012**, *24*, 5117.
- (67) Leem, D. S.; Edwards, A.; Faist, M.; Nelson, J.; Bradley, D. D.; de Mello, J. C. *Adv. Mater.* **2011**, *23*, 4371.
- (68) Li, L.; Yu, Z.; Hu, W.; Chang, C. H.; Chen, Q.; Pei, Q. *Adv. Mater.* **2011**, *23*, 5563.
- (69) Rathmell, A. R.; Wiley, B. J. *Adv. Mater.* **2011**, *23*, 4798.
- (70) Hu, W. L.; Niu, X. F.; Zhao, R.; Pei, Q. B. *Appl. Phys. Lett.* **2013**, *102*.
- (71) Kim, T.; Canlier, A.; Kim, G. H.; Choi, J.; Park, M.; Han, S. M. *ACS Appl. Mater. Interfaces* **2013**, *5*, 788.
- (72) Choi, D. Y.; Kang, H. W.; Sung, H. J.; Kim, S. S. *Nanoscale* **2013**, *5*, 977.
- (73) Naito, K.; Yoshinaga, N.; Tsutsumi, E.; Akasaka, Y. *Synth. Met.* **2013**, *175*, 42.
- (74) Tien, H. W.; Hsiao, S. T.; Liao, W. H.; Yu, Y. H.; Lin, F. C.; Wang, Y. S.; Li, S. M.; Ma, C. C. M. *Carbon* **2013**, *58*, 198.
- (75) Zhu, S.; Gao, Y.; Hu, B.; Li, J.; Su, J.; Fan, Z.; Zhou, J. *Nanotechnology* **2013**, *24*.
- (76) Kim, T.; Kim, Y. W.; Lee, H. S.; Kim, H.; Yang, W. S.; Suh, K. S. *Adv. Funct. Mater.* **2013**, *23*, 1250.
- (77) Wang, Y. J.; Feng, T.; Wang, K.; Qian, M.; Chen, Y. W.; Sun, Z. *J. Nanomater.* **2011**.
- (78) Song, W.; You, D. S.; Lim, K.; Park, S.; Jung, S.; Kim, C. S.; Kim, D.-H.; Kim, D.-G.; Kim, J.-K.; Park, J.; Kang, Y.-C.; Heo, J.; Jin, H.-S.; Park, J. H.; Kang, J.-W. *Adv. Funct. Mater.* **2013**.
- (79) Jacobs, H. O.; Tao, A. R.; Schwartz, A.; Gracias, D. H.; Whitesides, G. M. *Science* **2002**, *296*, 323.
- (80) Whitesides, G. M.; Boncheva, M. *Proc. Natl. Acad. Sci. U. S. A.* **2002**, *99*, 4769.

- (81) Cohn, M. B.; Bohringer, K. F.; Noworolski, J. M.; Singh, A.; Keller, C. G.; Goldberg, K. Y.; Howe, R. T. In *Materials and Device Characterization in Micromachining*; Friedrich, C. R., Vladimirsky, Y., Eds.; Spie-Int Soc Optical Engineering: Bellingham, 1998; Vol. 3512, p 2.
- (82) Whitesides, G. M. *Sci. Am.* **1995**, *273*, 146.
- (83) Miyashita, S.; Pfeifer, R. *Adapt. Behav.* **2012**, *20*, 117.
- (84) Grzybowski, B. A.; Winkleman, A.; Wiles, J. A.; Brumer, Y.; Whitesides, G. M. *Nat. Mater.* **2003**, *2*, 241.
- (85) Winkleman, A.; Gates, B. D.; McCarty, L. S.; Whitesides, G. M. *Adv. Mater.* **2005**, *17*, 1507.
- (86) Terfort, A.; Bowden, N.; Whitesides, G. M. *Nature* **1997**, *386*, 162.
- (87) Tien, J.; Breen, T. L.; Whitesides, G. M. *J. Am. Chem. Soc.* **1998**, *120*, 12670.
- (88) Clark, T. D.; Tien, J.; Duffy, D. C.; Paul, K. E.; Whitesides, G. M. *J. Am. Chem. Soc.* **2001**, *123*, 7677.
- (89) Breen, T. L.; Tien, J.; Oliver, S. R. J.; Hadzic, T.; Whitesides, G. M. *Science* **1999**, *284*, 948.
- (90) Boncheva, M.; Bruzewicz, D. A.; Whitesides, G. M. *Langmuir* **2003**, *19*, 6066.
- (91) Gracias, D. H.; Tien, J.; Breen, T. L.; Hsu, C.; Whitesides, G. M. *Science* **2000**, *289*, 1170.
- (92) Boncheva, M.; Gracias, D. H.; Jacobs, H. O.; Whitesides, G. M. *Proc. Natl. Acad. Sci. U. S. A.* **2002**, *99*, 4937.
- (93) Gracias, D. H.; Boncheva, M.; Omoregie, O.; Whitesides, G. M. *Appl. Phys. Lett.* **2002**, *80*, 2802.
- (94) Yamaki, M.; Higo, J.; Nagayama, K. *Langmuir* **1995**, *11*, 2975.
- (95) Dushkin, C. D.; Lazarov, G. S.; Kotsev, S. N.; Yoshimura, H.; Nagayama, K. *Colloid Polym. Sci.* **1999**, *277*, 914.
- (96) Nikoobakht, B.; Wang, Z. L.; El-Sayed, M. A. *J. Phys. Chem. B* **2000**, *104*, 8635.
- (97) Denkov, N. D.; Velev, O. D.; Kralchevsky, P. A.; Ivanov, I. B.; Yoshimura, H.; Nagayama, K. *Nature* **1993**, *361*, 26.
- (98) Lazarov, G. S.; Denkov, N. D.; Velev, O. D.; Kralchevsky, P. A.; Nagayama, K. *Journal of the Chemical Society-Faraday Transactions* **1994**, *90*, 2077.
- (99) Choi, I. S.; Bowden, N.; Whitesides, G. M. *Angew. Chem. Int. Ed.* **1999**, *38*, 3078.
- (100) Bowden, N.; Arias, F.; Deng, T.; Whitesides, G. M. *Langmuir* **2001**, *17*, 1757.

- (101) Bowden, N.; Terfort, A.; Carbeck, J.; Whitesides, G. M. *Science* **1997**, *276*, 233.
- (102) Choi, I. S.; Weck, M.; Xu, B.; Jeon, N. L.; Whitesides, G. M. *Langmuir* **2000**, *16*, 2997.
- (103) Huck, W. T. S.; Tien, J.; Whitesides, G. M. *J. Am. Chem. Soc.* **1998**, *120*, 8267.
- (104) Clark, T. D.; Boncheva, M.; German, J. M.; Weck, M.; Whitesides, G. M. *J. Am. Chem. Soc.* **2001**, *124*, 18.
- (105) Srinivasan, U.; Liepmann, D.; Howe, R. T. *J. Microelectromech. Syst.* **2001**, *10*, 17.
- (106) Aviram, A.; Ratner, M. A. *Chem. Phys. Lett.* **1974**, *29*.
- (107) McCreery, R. L.; Yan, H. J.; Bergren, A. J. *Phys. Chem. Chem. Phys.* **2013**, *15*, 1065.
- (108) McCreery, R. L. *Chem. Mater.* **2004**, *16*, 4477.
- (109) McCreery, R. L.; Bergren, A. J. *Adv. Mater.* **2009**, *21*, 4303.
- (110) Salomon, A.; Cahen, D.; Lindsay, S.; Tomfohr, J.; Engelkes, V. B.; Frisbie, C. D. *Adv. Mater.* **2003**, *15*, 1881.
- (111) Jia, C. C.; Guo, X. F. *Chem. Soc. Rev.* **2013**, *42*, 5642.
- (112) Heath, J. R. In *Annual Review of Materials Research* 2009; Vol. 39, p 1.
- (113) Erbe, A.; Verleger, S. *Acta Phys. Polon. A* **2009**, *115*, 455.
- (114) Joachim, C. G., J. K. Aviram, A. *Nature* **2000**, *408*, 541.
- (115) Del Nero, J.; de Souza, F. M.; Capaz, R. B. *J. Comp. Theor. Nanosci.* **2010**, *7*, 503.
- (116) Song, H.; Reed, M. A.; Lee, T. *Adv. Mater.* **2011**, *23*, 1583.
- (117) Tsutsui, M.; Taniguchi, M. *Sensors* **2012**, *12*, 7259.
- (118) Simmons, J. G. *Conduction in Thin Films*; Mills and Boon Ltd.: London, 1971.
- (119) Lamb, D. R. *Electrical Conduction Measurements in Thin Insulating Films*; Methuen and Co.: London, 1968.
- (120) O'Neill, M. A.; Dohno, C.; Barton, J. K. *J. Am. Chem. Soc.* **2004**, *126*, 1316.
- (121) Murphy, C. J.; Arkin, M. R.; Jenkins, Y.; Ghatlia, N. D.; Bossmann, S. H.; Turro, N. J.; Barton, J. K. *Science* **1993**, *262*, 1025.
- (122) Ricoeur, G.; Lenfant, S.; Guerin, D.; Vuillaume, D. *J. Phys. Chem. C* **2012**, *116*, 20722.
- (123) Nijhuis, C. A.; Reus, W. F.; Barber, J. R.; Whitesides, G. M. *J. Phys. Chem. C* **2012**, *116*, 14139.
- (124) Cademartiri, L.; Thuo, M. M.; Nijhuis, C. A.; Reus, W. F.; Tricard, S.; Barber, J. R.; Sodhi, R. N. S.; Brodersen, P.; Kim, C.; Chiechi, R. C.; Whitesides, G. M. *J. Phys. Chem. C* **2012**, *116*, 10848.

- (125) Thuo, M. M.; Reus, W. F.; Nijhuis, C. A.; Barber, J. R.; Kim, C.; Schulz, M. D.; Whitesides, G. M. *J. Am. Chem. Soc.* **2011**, *133*, 2962.
- (126) Reus, W. F.; Nijhuis, C. A.; Barber, J. R.; Thuo, M. M.; Tricard, S.; Whitesides, G. M. *J. Phys. Chem. C* **2012**, *116*, 6714.
- (127) Schwartz, D. K. *Surf. Sci. Rep.* **1997**, *27*, 245.
- (128) Collier, C. P.; Wong, E. W.; Belohradksy, M.; Raymo, F. M.; Stoddart, J. F.; Kuekes, P. J.; Williams, R. S.; Heath, J.R. *Science* **1999**, *285*, 391.
- (129) Karthaus, S. *J. Phys.-Condes. Matter* **2011**, *23*.
- (130) Cui, X. D.; Primak, A.; Zarate, X.; Tomfohr, J.; Sankey, O. F.; Moore, A. L.; Moore, T. A.; Gust, D.; Harris, G.; Lindsay, S. M. *Science* **2001**, *294*, 571.
- (131) Selzer, Y.; Salomon, A.; Cahen, D. *J. Am. Chem. Soc.* **2002**, *124*, 2886.
- (132) Love, C. J. E., Lara A.; Kriebel, J. K. N., Ralph G.; Whitesides, G. M. *Chem. Rev.* **2005**, *105*, 1103.
- (133) Ulman, A. *Ultrathin Organic Films*; Academic Press: San Diego, 1991.
- (134) Bareman, J. P.; Klein, M. L. *J. Phys. Chem.* **1990**, *94*, 5202.
- (135) Laibinis, P. E.; Whitesides, G. M.; Allara, D. L.; Tao, Y. T.; Parikh, A. N.; Nuzzo, R. G. *J. Am. Chem. Soc.* **1991**, *113*, 7152.
- (136) Nuzzo, R. G.; Zegarski, B. R.; Dubois, L. H. *J. Am. Chem. Soc.* **1987**, *109*, 733.
- (137) Lavrich, D. J.; Wetterer, S. M.; Bernasek, S. L.; Scoles, G. *J. Phys. Chem. B* **1998**, *102*, 3456.
- (138) Fischer, D.; Curioni, A.; Andreoni, W. *Langmuir* **2003**, *19*, 3567.
- (139) Nuzzo, R. G.; Allara, D. L. *J. Am. Chem. Soc.* **1983**, *105*.
- (140) Biebuyck, H. A.; Bian, C. D.; Whitesides, G. M. *Langmuir* **1994**, *10*, 1825.
- (141) Jung, C.; Dannenberger, O.; Xu, Y.; Buck, M.; Grunze, M. *Langmuir* **1998**, *14*, 1103.
- (142) Strong, L.; Whitesides, G. M. *Langmuir* **1988**, *4*, 546.
- (143) Bain, C. D.; Biebuyck, H. A.; Whitesides, G. M. *Langmuir* **1989**, *5*, 723.
- (144) Dubois, L. H.; Zegarski, B. R.; Nuzzo, R. G. *J. Chem. Phys.* **1993**, *98*, 678.
- (145) Dubois, L. H.; Nuzzo, R. G. *Ann. Rev. Phys. Chem.* **1992**, *43*, 437.
- (146) Poirier, G. E.; Tarlov, M. J. *Langmuir* **1994**, *10*, 2853.
- (147) Cai, L. T.; Skulason, H.; Kushmerick, J. G.; Pollack, S. K.; Naciri, J.; Shashidhar, R.; Allara, D. L.; Mallouk, T. E.; Mayer, T. S. *J. Phys. Chem. B* **2004**, *108*, 2827.

- (148) Tran, E.; Duati, M.; Ferri, V.; Mullen, K.; Zharnikov, M.; Whitesides, G. M.; Rampi, M. A. *Adv. Mater.* **2006**, *18*, 1323.
- (149) Weiss, E. A.; Kriebel, J. K.; Rampi, M. A.; Whitesides, G. M. *Philos. Trans. R. Soc. A-Math. Phys. Eng. Sci.* **2007**, *365*, 1509.
- (150) Kim, T. W.; Wang, G. N.; Lee, H.; Lee, T. *Nanotechnology* **2007**, *18*.
- (151) Akkerman, H. B.; de Boer, B. *J. Phys.-Condes. Matter* **2008**, *20*.
- (152) Akkerman, H. B.; Kronemeijer, A. J.; van Hal, P. A.; de Leeuw, D. M.; Blom, P. W. M.; de Boer, B. *Small* **2008**, *4*, 100.
- (153) von Wrochem, F.; Gao, D.; Scholz, F.; Nothofer, H.-G.; Nelles, G.; Wessels, J. M. *Nat. Nanotechnol.* **2010**, *5*, 618.
- (154) Nitzan, A.; Ratner, M. A. *Science* **2003**, *300*, 1384.
- (155) Xue, Y. Q.; Datta, S.; Ratner, M. A. *J. Chem. Phys.* **2001**, *115*, 4292.
- (156) Schreiber, F.; Eberhardt, A.; Leung, T. Y. B.; Schwartz, P.; Wetterer, S. M.; Lavrich, D. J.; Berman, L.; Fenter, P.; Eisenberger, P.; Scoles, G. *Phys. Rev. B* **1998**, *57*, 12476.
- (157) Xing, Y. P., Tae-Hong Venkatramani, Ravindra Keinan, Shahar Beratan, David Therien, Michael J.; Borguet, E. *J. Am. Chem. Soc.* **2010**, *132*, 7946.
- (158) Tivanski, A. V.; He, Y. F.; Borguet, E.; Liu, H. Y.; Walker, G. C.; Waldeck, D. H. *J. Phys. Chem. B* **2005**, *109*, 5398.
- (159) Chinwangso, P.; Jamison, A. C.; Lee, T. R. *Acc. Chem. Res.* **2011**, *44*, 511.
- (160) Kim, D. S. *Bull. Korean Chem. Soc.* **1995**, *16*, 321.
- (161) Hope, G. A.; Woods, R.; Watling, K. *J. Appl. Electrochem.* **2001**, *31*, 1285.
- (162) Hope, G. A.; Woods, R.; Boyd, S.; Watling, K. *Colloids Surf., A* **2003**, *214*, 77.
- (163) Hope, G. A.; Woods, R.; Watling, K. *Colloids Surf., A* **2003**, *214*, 87.
- (164) Fracasso, D.; Muglali, M. I.; Rohwerder, M.; Terfort, A.; Chiechi, R. C. *J. Phys. Chem. C* **2013**, *117*, 11367.
- (165) Chiechi, R. C.; Weiss, E. A.; Dickey, M. D.; Whitesides, G. M. *Angew. Chem. Int. Ed.* **2008**, *47*, 142.
- (166) Akkerman, H. B.; Blom, P. W. M.; de Leeuw, D. M.; de Boer, B. *Nature* **2006**, *441*, 69.
- (167) Slowinski, K.; Chamberlain, R. V.; Bilewicz, R.; Majda, M. *J. Am. Chem. Soc.* **1996**, *118*, 4709.
- (168) Slowinski, K.; Fong, H. K. Y.; Majda, M. *J. Am. Chem. Soc.* **1999**, *121*, 7257.
- (169) Slowinski, K.; Majda, M. *J. Electroanal. Chem.* **2000**, *491*, 139.

- (170) Slowinski, K.; Chamberlain, R. V.; Miller, C. J.; Majda, M. *J. Am. Chem. Soc.* **1997**, *119*, 11910.
- (171) Weiss, E. A.; Chiechi, R. C.; Kaufman, G. K.; Kriebel, J. K.; Li, Z.; Duati, M.; Rampi, M. A.; Whitesides, G. M. *J. Am. Chem. Soc.* **2007**, *129*, 4336.
- (172) Ashwell, G. J.; Mohib, A.; Miller, J. R. *J. Mater. Chem.* **2005**, *15*, 1160.
- (173) Tran, E.; Rampi, M. A.; Whitesides, G. M. *Angew. Chem. Int. Ed.* **2004**, *43*, 3835.
- (174) York, R. L.; Slowinski, K. *J. Electroanal. Chem.* **2003**, *550*, 327.
- (175) Chabinyk, M. L.; Holmlin, R. E.; Haag, R.; Chen, X. X.; Ismagilov, R. F.; Rampi, M. A.; Whitesides, G. M. In *Molecules as Components of Electronic Devices*; Lieberman, M., Ed.; Amer Chemical Soc: Washington, 2003; Vol. 844, p 16.
- (176) Anariba, F.; McCreery, R. L. *J. Phys. Chem. B* **2002**, *106*, 10355.
- (177) Haag, R.; Rampi, M. A.; Holmlin, R. E.; Whitesides, G. M. *J. Am. Chem. Soc.* **1999**, *121*, 7895.
- (178) Simeone, F. C.; Rampi, M. A. *Chimia* **2010**, *64*, 362.
- (179) Holmlin, R. E.; Haag, R.; Chabinyk, M. L.; Ismagilov, R. F.; Cohen, A. E.; Terfort, A.; Rampi, M. A.; Whitesides, G. M. *J. Am. Chem. Soc.* **2002**, *124*, 8762.
- (180) Chiechi, R. C.; Weiss, E. A.; Dickey, M. D.; Whitesides, G. M. *Angew. Chem.* **2008**, *120*, 148.
- (181) Fatemi, V.; Kamenetska, M.; Neaton, J. B.; Venkataraman, L. *Nano Lett.* **2011**, *11*, 1988.
- (182) Nijhuis, C. A.; Reus, W. F.; Barber, J. R.; Dickey, M. D.; Whitesides, G. M. *Nano Lett.* **2010**, *10*, 3611.
- (183) Dickey, M. D.; Chiechi, R. C.; Larsen, R. J.; Weiss, E. A.; Weitz, D. A.; Whitesides, G. M. *Adv. Funct. Mater.* **2008**, *18*, 1097.
- (184) Nijhuis, C. A.; Reus, W. F.; Whitesides, G. M. *J. Am. Chem. Soc.* **2010**, *132*, 18386.
- (185) Fracasso, D.; Valkenier, H.; Hummelen, J. C.; Solomon, G. C.; Chiechi, R. C. *J. Am. Chem. Soc.* **2011**, *133*, 9556.
- (186) Engelkes, V. B.; Beebe, J. M.; Frisbie, C. D. *J. Phys. Chem. B* **2005**, *109*, 16801.
- (187) Hegner, M.; Wagner, P.; Semenza, G. *Surf. Sci.* **1993**, *291*, 39.
- (188) Weiss, E. A.; Kaufman, G. K.; Kriebel, J. K.; Li, Z.; Schalek, R.; Whitesides, G. M. *Langmuir* **2007**, *23*, 9686.
- (189) Naumann, R.; Schiller, S. M.; Giess, F.; Grohe, B.; Hartman, K. B.; Karcher, I.; Koper, I.; Lubben, J.; Vasilev, K.; Knoll, W. *Langmuir* **2003**, *19*, 5435.

- (190) Wagner, P.; Zaugg, F.; Kernen, P.; Hegner, M.; Semenza, G. J. *Vac. Sci. Technol., B* **1996**, *14*, 1466.
- (191) Gupta, P.; Ulman, A.; Fanfan, S.; Korniaikov, A.; Loos, K. *J. Am. Chem. Soc.* **2005**, *127*, 4.
- (192) Gupta, P.; Loos, K.; Korniaikov, A.; Spagnoli, C.; Cowman, M.; Ulman, A. *Angew. Chem. Int. Ed.* **2004**, *43*, 520.
- (193) *Microelectronic Applications of Chemical Mechanical Planarization*; Li, Y., Ed.; John Wiley & Sons Inc.: Hoboken, 2007.
- (194) Islam, M. S.; Jung, G. Y.; Ha, T.; Stewart, D. R.; Chen, Y.; Wang, S. Y.; Williams, R. S. *Appl. Phys. A: Mater. Sci. Process.* **2005**, *80*, 1385.

## **Chapter 2**

# **Selectively Metallized Polymeric Substrates by Microcontact Printing an Aluminum (III) Porphyrin Complex**

## 2.1. Introduction

This chapter describes a simple, low-cost method based on microcontact printing and electroless metal deposition (ELD) to fabricate metallic contacts and wires on polymeric substrates for use in lightweight plastic electronic devices. Plastic electronics span a wide range of applications and polymeric substrates: Flexible polymers, such as polyethylene terephthalate (PET), polyethylene naphthalate (PEN), and polyimide (PI), enable the fabrication of devices such as conformal displays, wearable electronics, and bioelectronic devices such as sensors and artificial nerves.<sup>1-5</sup> Rigid polymers that can be rapidly molded or lithographically patterned into thick, high-aspect-ratio structures, such as polymethylmethacrylate (PMMA) or the epoxy-based negative-tone photoresist SU-8, are useful as structural materials for microanalytical and microfluidic systems.<sup>6</sup> Coating these rigid structures with metal enables the transmission of electrical signals in devices such as microactuators,<sup>7</sup> electrochemical detectors,<sup>8</sup> millimeter-wave antennae for broadband wireless communications,<sup>9</sup> and radio frequency conductors for MEMS.<sup>10</sup>

The selective metallization method described in this chapter is applicable to the range of substrates used for plastic electronics, as well as to inert polymers such as polyethylene (PE), polypropylene (PP), and poly(tetrafluoroethylene) (PTFE). Oxidizing these polymer surfaces generates a common surface chemistry consisting of surface-bound carboxylic acid groups. We use microcontact printing to form a patterned monolayer of an aluminum porphyrin complex that binds to the oxidized surface of the polymer through a covalent aluminum carboxylate bond and subsequently captures a palladium-tin colloidal catalyst from solution, which initiates the electroless deposition (ELD) of copper from solution. This selective metallization process reduces fabrication costs by replacing complex and expensive processes - conventional photolithography and physical vapor deposition (PVD) of metals - with the simple, low-cost methods of microcontact printing and ELD. We demonstrate the process by fabricating patterned copper films on a variety of both flexible and rigid polymers with minimum feature sizes of 2  $\mu\text{m}$  over 2- $\text{cm}^2$  substrates. We also establish an important practical advantage to this process by demonstrating that copper wires fabricated on flexible PEN substrates withstand

substantial mechanical deformation without a loss in performance: Wire resistivity is unaffected by bending the metallized PEN around a cylinder of radius  $< 1$  mm.

The emergence of plastic electronic products has intensified the drive to reduce the cost and complexity of their fabrication. Academic research leads this effort by developing fabrication processes that replace conventional technologies such as photolithography and PVD, both of which are slow processes with high capital and operating expenses, with simple patterning methods such as microcontact printing, ink-jet printing, or screen printing, and fast materials deposition methods from solution such as spin-coating or dip-coating.<sup>11-12</sup> For the deposition of metallic wires and contacts on polymeric substrates, researchers have developed several low-cost printing methods to replace photolithography; however, many of these methods rely on metal PVD. Examples include patterning methods based on shadow masks,<sup>13</sup> microcontact printing and etching,<sup>14-17</sup> nanotransfer printing,<sup>18-21</sup> and lamination.<sup>22-23</sup> These methods have all successfully contributed to the fabrication of flexible devices on polymeric substrates; in addition, Rogers *et al.* demonstrated that microcontact printing and etching can produce high-quality plastic electronics over large substrate areas.<sup>14</sup>

To further reduce costs, however, it is necessary to eliminate our dependence on PVD and instead combine a low-cost patterning method with solution-based metal deposition. One approach is to directly pattern a conductive metallic ink or a suspension of metallic nanoparticles. Conductive silver inks have been patterned using screen printing, which uses a physical mask to block the flow of the ink.<sup>24</sup> Although this method is compatible with large-area patterning, it is limited by the relatively modest resolution that can be achieved ( $\sim 75$   $\mu\text{m}$ ).<sup>12</sup> Solutions of metallic nanoparticles have been patterned using inkjet printing<sup>25-30</sup> and direct ink writing.<sup>31</sup> Annealing the printed nanoparticles to create conductive metallic films can be accomplished at relatively low temperatures due to melting point depression of metal nanoparticles, making this process compatible with many polymeric substrates. A second approach is to combine a low-cost patterning method such as inkjet printing or microcontact printing with a solution-based metal deposition process such as ELD.<sup>32</sup>

ELD is widely used in the microelectronics industry to form patterned conducting lines and interlevel connections on printed circuit boards, to cap copper damascene interconnects in semiconductor devices, and to fabricate thin metal etch masks.<sup>33-38</sup> It can be used to deposit metals such as copper, nickel, gold, silver, and cobalt onto either metallic or insulating substrates. In ELD, metal ions in the electroless plating solution are chemically reduced to metal by a Pd catalyst chemisorbed on the surface of the substrate. After metallization is initiated, the initial layer of deposited metal autocatalyzes further metal deposition as a reducing agent in the electroless plating solution is oxidized. Inkjet printing and microcontact printing have both been used with ELD to fabricate metal contacts and wires on plastic substrates. Inkjet printing of either a Pd catalyst<sup>39-40</sup> or a polyelectrolyte adhesion layer that subsequently binds a Pd catalyst from solution,<sup>41-42</sup> followed by ELD, has been demonstrated on PET substrates. Microcontact printing has been used with ELD in either subtractive or additive patterning approaches. Subtractive patterning uses ELD to deposit a blanket metal film that is then patterned by microcontact printing an alkanethiol SAM and wet etching.<sup>43</sup> Although this approach is presumably compatible with plastic substrates, the process of depositing and then removing metal generates waste. Additive patterning eliminates this drawback by using microcontact printing to define a chemical pattern on a polymeric substrate and then depositing metal within that pattern using ELD. There are few reports of additive patterning methods on polymeric substrates, and they can be divided into two categories: The first category uses microcontact printing to directly transfer the Pd catalyst to the surface of a polymeric substrate, followed by ELD. Whitesides et al. demonstrated this approach by microcontact printing tetraalkylammonium bromide-stabilized Pd nanoparticles to a polymeric substrate that had previously been oxidized and treated with an organosilane bearing amino or thiol groups.<sup>44</sup> The organosilane is an adhesion promoter: it covalently binds to the oxidized surface and presents amino or thiol groups that bind the Pd catalyst. In the second category, it is the organosilane layer that is initially patterned by microcontact printing; Pd or Pd/Sn colloids subsequently bind from solution selectively either within or outside the patterned organosilane. For example, Prissanaroon et al. used microcontact printing of an organosilane adhesion promoter bearing an amino group and subsequent binding of Pd colloids from aqueous solution to selectively metallize plasma-

modified PTFE.<sup>45</sup> Li et al. also used microcontact printing to pattern an organosilane adhesion promoter for the selective metallization of PI; however, this method was only applicable to a siloxane-containing polyimide substrate.<sup>46</sup> Zschieschang et al. used microcontact printing to transfer a patterned fluorinated organosilane to the surface of a PEN substrate; the fluorinated layer subsequently acted as a resist to Pd catalyst adsorption, allowing for the selective deposition of nickel gate electrodes on the PEN surface and fabrication of flexible circuits.<sup>47</sup>

The problem with the reported additive approaches to selective electroless metallization is the incompatibility of PDMS stamps used in microcontact printing with the solvents used to suspend Pd nanoparticles, with polar catalysts like Pd or Pd/Sn colloids, and with organosilanes. Tetraalkylammonium bromide-stabilized Pd nanoparticles require the use of solvents such as toluene or THF, which swell the stamp<sup>48</sup> and lead to distortion of the metallized pattern. Distortion is highly detrimental to device fabrication, where registration between patterned materials layers is crucial. Pd/Sn colloids or other polar catalysts use aqueous solvents that inhibit the deposition of the catalyst onto the surface of the hydrophobic PDMS stamp. Rendering the PDMS surface hydrophilic by plasma oxidation is only a temporary solution due to the tendency of PDMS to undergo hydrophobic recovery over a period of only a few hours.<sup>49</sup> Microcontact printing of functionalized organosilanes also requires plasma oxidation of the stamp to enable inking, and additionally presents a serious manufacturing problem: The hydrolytic instability of alkyltrichloro- and alkyltrialkoxysilanes results in crosslinking on the surface of the PDMS stamp, curtailing its lifetime.

Our approach to the selective electroless metallization of polymeric substrates incorporates the economic advantages of microcontact printing and ELD with a new microcontact printing ink – an aluminum (III) porphyrin complex – to eliminate the problems plaguing previous methods that use unsuitable printing inks. In the past, applications of metalloporphyrins immobilized on solid substrates have predominantly been based on the optical and electrochemical properties of the metalloporphyrin: Optical and photoelectrochemical sensors,<sup>50-52</sup> molecular electronics,<sup>53-55</sup> and sensitizers in dye-sensitized solar cells<sup>56-57</sup> are all well-studied examples. Our work exploits different

metalloporphyrin properties – solubility, hydrophobicity, and chemical reactivity at the metal center – to demonstrate that tetraphenylporphyrinato-aluminum (III) methoxide (TPPAI-OMe) is an ideal microcontact printing ink when paired with oxidized polymeric substrates bearing carboxylic acid groups. There are four important advantages to using TPPAI-OMe as a microcontact printing ink and subsequent foundation for ELD: First, TPPAI-OMe is soluble in isopropanol, an ideal solvent for microcontact printing because it minimizes swelling and distortion of the PDMS stamp. Second, TPPAI-OMe is a hydrophobic material that can effectively wet the surface of a native PDMS stamp, eliminating the need for stamp surface modification. Third, the reaction of TPPAI-OMe with carboxylic acid groups at the interface between the inked stamp and oxidized polymer occurs rapidly to form highly stable aluminum carboxylate bonds that covalently anchor the TPPAI monolayer to the substrate (Figure 2.1). The by-product of the reaction, methanol, evaporates or dissipates into the PDMS stamp, but does not cause swelling or distortion. The reactivity of aluminum (III) porphyrin complexes is well-established in solution: TPPAI-OH reacts rapidly with benzoic acid to generate the five-coordinate aluminum benzoate complex TPPAI-(benzoate) and liberate an equivalent of water.<sup>58</sup> The axially-bound benzoate ligand is highly stable. It is not displaced by alcohols or water; rather, it requires a competitive carboxylic acid to be present in excess. Fourth, the TPPAI-(carboxylate) monolayer rapidly binds Pd/Sn colloids from solution to subsequently initiate ELD.

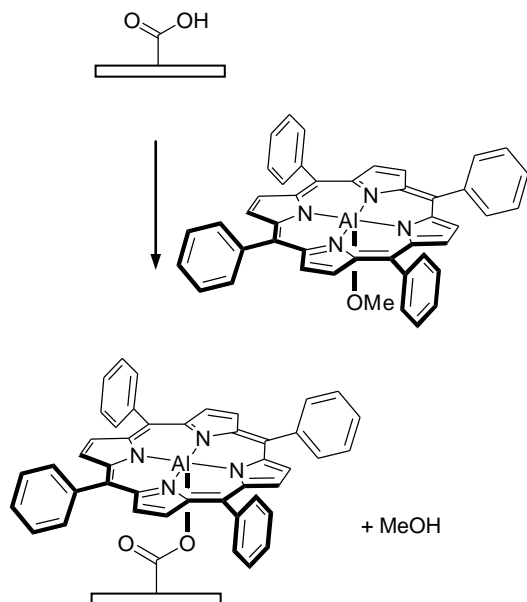


**Figure 2.1.** Reaction of TPPAl-OMe with carboxylic acid groups on the surface of an oxidized polymeric substrate.

## 2.2. Experimental Section

### 2.2.1. Materials

All materials and chemicals were purchased commercially and used as received. PDMS stamps were prepared by casting PDMS prepolymer against photolithographic masters according to published procedures.<sup>59</sup> Tetraphenylporphyrinato-aluminum(III) methoxide (TPPAl-OMe) was prepared using the literature method reported for TPPAl-OEt,<sup>60</sup> but the reaction was quenched with methanol rather than ethanol. Tetraphenylporphyrinato-aluminum(III) benzoate (TPPAl-(benzoate)) was prepared according to the literature method. The following polymer films were purchased from Goodfellow (Oakdale, PA) and used as received (thickness of polymer films in parentheses): polyethylene terephthalate (75  $\mu\text{m}$ ), polyethylene naphthalate (75  $\mu\text{m}$ ), polyimide (75  $\mu\text{m}$ ), polypropylene (75  $\mu\text{m}$ ), polyethylene (125  $\mu\text{m}$ ),

poly(tetrafluoroethylene) (100  $\mu\text{m}$ ) and polymethylmethacrylate (500  $\mu\text{m}$ ). SU-8 films were prepared as directed by manufacturer. For details, see the Supporting Information.

### *2.2.2. Substrate Preparation*

The surfaces of PET,<sup>61</sup> PEN,<sup>61</sup> PI,<sup>62</sup> PE,<sup>63</sup> PP,<sup>63</sup> PTFE,<sup>64</sup> PMMA,<sup>65</sup> and SU-8<sup>66</sup> were oxidized according to literature methods. For details, see the Supporting Information.

### *2.2.3. Stamp Inking and Printing*

An ink solution of TPPAI-OMe in isopropanol (1 mg/mL) was filtered through a 0.2- $\mu\text{m}$  PTFE Acrodisc syringe filter. The surface of a PDMS stamp was flooded with the filtered ink solution and left for 30 s. A stream of nitrogen was used to first blow off excess solution and then to thoroughly dry the stamp for 30 s, leaving a film of neat TPPAI-OMe. Inked stamps were placed on the surface of oxidized polymeric substrates using tweezers, left for 1 min, and then removed. Porphyrin multilayers were removed by rinsing the printed substrate with isopropanol for 1 min.

### *2.2.4. Electroless Metallization*

The patterned polymeric substrate was immersed in a Pd/Sn colloidal catalyst solution (Cataposit 44 and Cataprep 404 (Shipley), prepared as directed by the manufacturer) for 1 min, accelerator solution (1 M HCl) for 1 min, and then metallized in the copper ELD bath (10:1 v:v mixture of solutions A (copper (II) sulfate pentahydrate (4.5 g/L), sodium potassium tartrate tetrahydrate (21.0 g/L), and sodium hydroxide (6.0 g/L) in water) and B (37.2 % formaldehyde in water)). Plating times were typically 3-5 min.

### *2.2.5. Reaction of TPPAI-(benzoate) with HCl*

0.03 mmol TPPAI-(benzoate) was dissolved in 3.0 mL  $\text{CH}_2\text{Cl}_2$  and 2.0 mL of 1 M HCl was added and the mixture was shaken vigorously for 3 min. The mixture was allowed to stand for 3 h; the organic layer was then separated and dried over sodium sulfate. The solvent was removed by evaporation under vacuum and the residue dissolved in  $\text{CDCl}_3$

for  $^1\text{H}$  NMR spectroscopic analysis, which showed only the presence of TPPAl-(benzoate).

### *2.2.6. Tape Test*

Adhesion of copper films deposited by ELD was tested using the ASTM D3359B-02 tape test.<sup>67</sup> A 30 x 30 mm copper film was metallized on a polymeric substrate as described (a flat slab of PDMS was used as the microcontact printing stamp). A cutter equipped with 11 blades spaced by 1 mm was used to cut a lattice pattern measuring 20 x 20 mm in the copper film. Pressure-sensitive tape was applied to the cut area and then removed. Adhesion was assessed qualitatively on a 0 – 5 scale according to ASTM guidelines.<sup>67</sup>

### *2.2.7. Fabrication of Copper Wires and Electrical Testing*

Copper wires on PEN were fabricated with  $l = 1.0$  cm,  $w = 1.0$  mm,  $h = 40$  nm. A small drop of Eutectic Gallium-Indium (EGaIn) was applied to each end of the wire. The wire was then bent around a metal cylinder with the desired radius of curvature, and then electrical contact was made via the EGaIn drops using stainless steel probes connected to a Keithley 2601 Source Meter (Keithley Instruments, Cleveland, OH). The resistance of the wire was measured at 0.005 V increments as the voltage was swept from -0.5 V to +0.5 V. The average of these 210 measurements was used, and three separate measurements were taken for two wires at each radius of curvature. Radii of curvature ranged from 12.5 mm to 100  $\mu\text{m}$ .

### *2.2.8. Characterization*

UV/vis absorption spectra were collected using a CARY 50 Conc UV/Visible Spectrophotometer. RAIRS spectra were collected using a Bruker IFS 66/v spectrometer equipped with an MCT detector and Harrick Autoseagull accessory. The p-polarized light was incident at  $85^\circ$  from the surface normal; 1024 scans were collected at a resolution of  $2\text{ cm}^{-1}$ . Water contact angles were measured using the sessile drop method on a Rame-Hart contact angle goniometer. Three readings from at least two samples

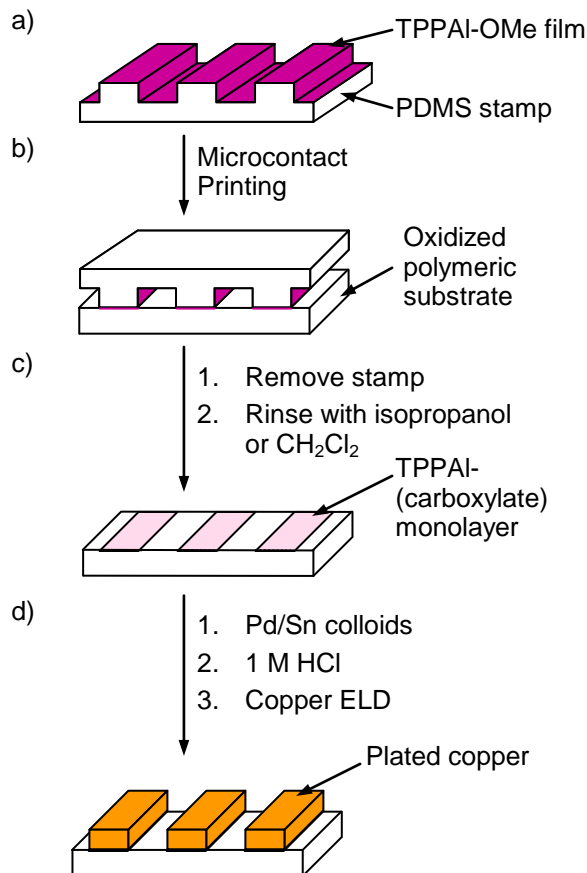
were averaged.  $^1\text{H}$  NMR spectroscopy was performed using a Bruker DRX spectrometer operating at 500 MHz in  $\text{CDCl}_3$ , using residual  $\text{CHCl}_3$  as the internal reference. Optical inspection was performed using an Olympus BX51 microscope. SEM images were obtained using a FEI Quanta 200 scanning electron microscope. AFM measurements were made using a Digital Instruments Multimode atomic force microscope.

## 2.3. Results and Discussion

### *2.3.1. A Single Process Selectively Deposits Copper on a Variety of Oxidized Polymeric Substrates*

We used a single process for the selective electroless metallization of flexible polymers (PET, PEN, and PI), rigid polymers (PMMA, SU-8), and polymers with low surface free energies (PE, PP, and PTFE). This process begins with oxidation of the polymer surfaces to create surface carboxylic acid groups. Scheme 2.1 outlines the subsequent process steps: (a) Inking a PDMS stamp with TPPAI-OMe forms a film of TPPAI-OMe on the surface of the stamp; (b) Microcontact printing brings the film of TPPAI-OMe in contact with the surface carboxylic acid groups of the substrate to form a TPPAI-(carboxylate) monolayer and an equivalent of methanol, as depicted in Figure 2.1. It also transfers a film of unreacted TPPAI-OMe to the surface; (c) Rinsing with dichloromethane or isopropanol removes the physisorbed TPPAI-OMe, leaving the TPPAI-(carboxylate) monolayer covalently bound to the surface; (d) Immersion in a solution of Pd/Sn colloids, which consist of a Pd-rich core protected from oxidation by a hydrolyzed  $\text{Sn}^{2+}/\text{Sn}^{4+}$  shell, binds the colloids selectively to the TPPAI-(carboxylate) monolayer. The acceleration step uses 1 M HCl to dissolve a portion of the  $\text{Sn}^{2+}/\text{Sn}^{4+}$  protective shell to expose the catalytic, Pd-rich core of the bound Pd/Sn colloids.<sup>68-73</sup> Immersion in an electroless copper plating bath deposits copper selectively over the catalyzed regions of the substrate.

*Selectively Metallized Polymeric Substrates by Microcontact Printing an Aluminum (III) Porphyrin Complex*



**Scheme 2.1.** Schematic of the process steps used to fabricate patterned copper films on oxidized polymeric substrates.

*2.3.2. Microcontact Printing Transfers a TPPAI-OMe Multilayer to Oxidized Polymeric Substrates*

Ultraviolet-visible (UV-vis) absorption spectra of printed TPPAI-OMe films on oxidized PET confirm the initial formation of a multilayer of TPPAI-OMe and are consistent with the removal of physisorbed TPPAI-OMe by rinsing with dichloromethane or isopropanol to leave a TPPAI-(carboxylate) monolayer on the surface (Figure 2.2a). For these experiments we used a flat slab of PDMS as the printing stamp to create a printed area on oxidized PET for UV-vis absorption spectroscopy. The very broad Soret band at 432 nm in the UV-vis spectrum of the as-printed layer is due to the random

orientation of TPPAI-OMe molecules in the multilayered film: The absorption spectrum is the sum of the absorption bands resulting from the various types of excitonic couplings between molecules in the film.<sup>74</sup> Two Q-bands at 555 nm and 602 nm are also visible. After repeatedly rinsing the printed film with either dichloromethane or isopropanol, the Q-bands are no longer detectable and the Soret band diminishes in absorbance and narrows relative to the Soret band of the unrinsed film, consistent with the removal of physisorbed TPPAI-OMe. The bathochromic shift of the Soret band (426 nm) relative to the solution spectrum (414 nm) is typical of head-to-tail dipolar interactions between  $\pi$ -systems of neighboring adsorbates,<sup>75</sup> and is thus consistent with the formation of a TPPAI-(carboxylate) monolayer.

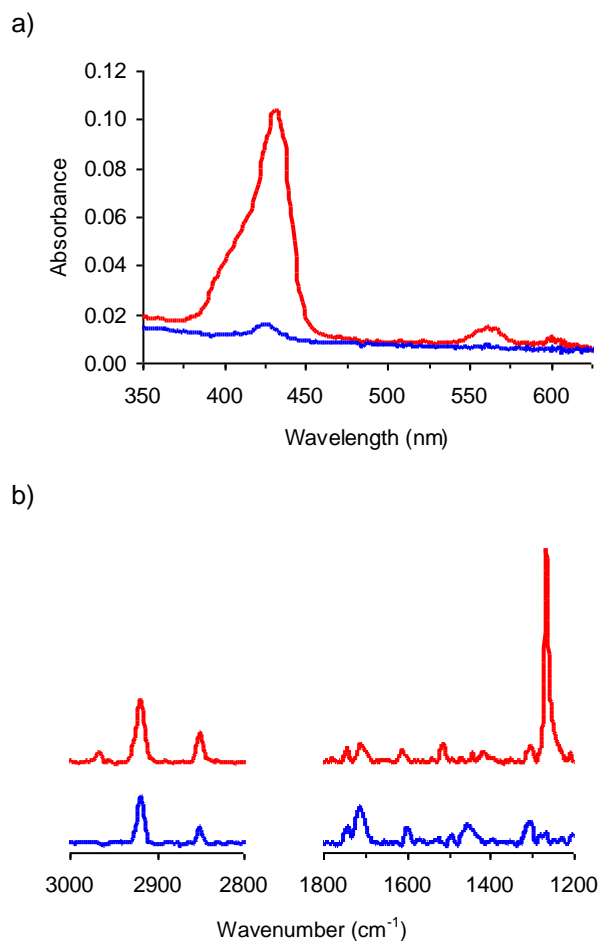


**Figure 2.2.** Characterization of a TPPAI-OMe film transferred by microcontact printing to the surface of an oxidized PET substrate. (a) UV-vis absorption spectrum of a TPPAI-OMe film transferred by microcontact printing to the surface of oxidized PET before (red) and after rinsing with isopropanol (blue). (b) RAIRS spectra (3000 – 2800  $\text{cm}^{-1}$  and 1800 – 1200  $\text{cm}^{-1}$ ) of a TPPAI-OMe film transferred by microcontact printing to the surface of an MHDA SAM on gold before (red) and after rinsing in dichloromethane (blue).

### *2.3.3. Rinsing Removes Physisorbed TPPAI-OMe and Leaves a TPPAI-(carboxylate) Monolayer on Oxidized Polymeric Substrates*

We used reflection-absorption infrared spectroscopy (RAIRS) to confirm that rinsing removes physisorbed TPPAI-OMe from microcontact-printed multilayers and leaves a TPPAI-(carboxylate) monolayer on the surface. The RAIRS spectrum of a printed TPPAI-OMe multilayer formed on a 16-mercaptohexadecanoic acid (MHDA) SAM on gold – a reflective model surface for oxidized polymeric substrates – and the RAIRS spectrum of a multilayer rinsed with dichloromethane both contain characteristic bands that confirm the presence of the MHDA SAM and the porphyrin ring (Figure 2.2b, Table 2.1). The presence of free and hydrogen-bonded carbonyl stretches of the MHDA carboxylic acid group indicates that the large size of the aluminum porphyrin precludes a 1:1 reaction between TPPAI-OMe and MHDA carboxylic acid groups. The decrease in the average water contact angle from 82.8° for a multilayer printed on oxidized PET to 53.9° after rinsing with isopropanol supports this model: When the multilayer is rinsed off, the water drop then senses the underlying hydrophilic carboxylic acid groups, thus reducing the contact angle. The bands due to MHDA and the porphyrin ring likely obscure one of the two carboxylate stretches expected for the TPPAI-(carboxylate) monolayer covalently bonded to the MHDA surface; nonetheless, we are able to assign the absorption band at 1510 cm<sup>-1</sup> in the spectrum of the unrinsed film and 1520 cm<sup>-1</sup> in the spectrum of the rinsed film to a carboxylate stretch since it does not appear in either the RAIRS spectrum of the MHDA SAM or the transmission spectrum of TPPAI-OMe.<sup>77</sup> Although observation of both the symmetric and antisymmetric carboxylate stretches is necessary to establish the binding mode of the carboxylate to aluminum,<sup>78</sup> we propose a unidentate coordination mode for this carboxylate in agreement with the crystal structure reported for TPPAI-(benzoate).<sup>58</sup> The major change that occurs upon rinsing is the loss of absorption bands due to the methoxy group bound to aluminum ( $\nu_{as}(\text{CH}_3)$  at 2963 cm<sup>-1</sup> and  $\nu(\text{C-O})$  at 1265 cm<sup>-1</sup>) in TPPAI-OMe. This loss confirms that physisorbed TPPAI-OMe is completely removed by rinsing.

**Table 2.1.** Assignments of selected absorption bands in the RAIRS spectra of an MHDA SAM on gold, a TPPAI-OMe multilayer printed on the MHDA SAM, and a TPPAI-OMe multilayer printed on the MHDA SAM after rinsing with dichloromethane.<sup>a</sup>

wavenumber (cm <sup>-1</sup> )			
MHDA SAM	As-printed TPPAI-OMe multilayer	TPPAI-OMe multilayer after rinsing	Assignment
	2963		$\nu_{as}(\text{CH}_3)$ (from Al-OMe)
2917	2917	2917	$\nu_{as}(\text{CH}_2)$
2849	2849	2849	$\nu_s(\text{CH}_2)$
1742	1740	1739	$\nu(\text{C}=\text{O})$ (free)
1709	1706	1709	$\nu(\text{C}=\text{O})$ (H-bonded)
	1607	1594	$\nu(\text{C}=\text{C})$ (phenyl)
	1510	1520	$\nu(\text{C}=\text{O})$ (from Al-CO <sub>2</sub> -R)
	1486	1488	$\delta(\text{C}-\text{H})$ (pyrrole)
1303	1297	1300	$\nu(\text{C}-\text{O})$ (from C-OH of MHDA)
	1265		$\nu(\text{C}-\text{O})$ (from Al-OMe)

<sup>a</sup> Assignments taken from Yan, L.; Marzolin, C.; Terfort, A.; Whitesides, G. M. *Langmuir* **1997**, *13*, 6704 and Thomas, D. W.; Martell, A. E. *J. Am. Chem. Soc.* **1959**, *81*, 5111.

#### *2.3.4. Pd/Sn Colloids Adsorb from Solution on TPPAl- (carboxylate) Monolayers*

The selective adsorption of Pd/Sn colloids on TPPAl-(carboxylate) monolayers patterned on oxidized polymeric substrates – the foundation of selective ELD – was established by UV-vis absorption spectroscopy (Figure 2.3). We exposed unmodified oxidized polymeric substrates and oxidized polymeric substrates bearing a TPPAl-(carboxylate) monolayer (formed using a flat PDMS stamp) to an aqueous solution of Pd/Sn colloids for one minute and rinsed with water. The former substrates showed no evidence of colloid adsorption in the UV-vis absorption spectrum; the latter substrates showed the Soret band at 426 nm of the TPPAl-(carboxylate) monolayer riding on top of the broad absorption continuum extending through the visible-ultraviolet range that is characteristic of Pd/Sn colloids. After acceleration in 1 M HCl, the absorption due to the Pd/Sn colloids diminished due to colloid loss during the acceleration process, which is typically due to overetching of the Sn<sup>2+</sup>/Sn<sup>4+</sup> shell,<sup>68-73</sup> but the Soret band remains at 426 nm.

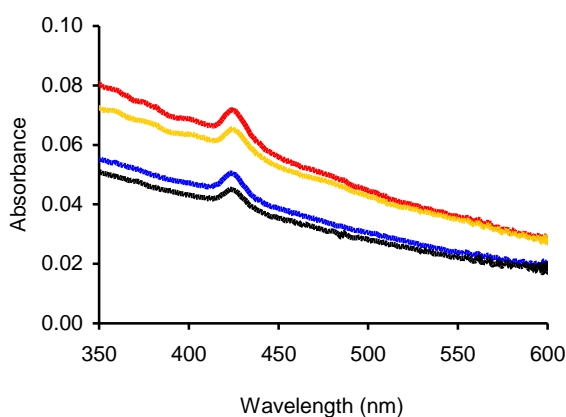


**Figure 2.3.** UV-vis absorption spectra of two samples of TPPAl-(carboxylate) monolayers on oxidized PET exposed to a solution of Pd/Sn colloids for 1 min. The first sample was rinsed with water (red), then accelerated in 1 M HCl and rinsed with water (blue). The second sample was rinsed with isopropanol (yellow), then accelerated in 1 M HCl and rinsed with isopropanol (black).

Although the nature of the interaction between Pd/Sn colloids and the TPPAl-(carboxylate) monolayer remains unclear, we were able to establish that Pd/Sn colloids adsorb on an intact TPPAl-(carboxylate) monolayer. Exposure to HCl, present in both the Pd/Sn colloid and accelerator solution, does not protonate the aluminum carboxylate bond or the Al-N bonds of the aluminum porphyrin to liberate  $\text{AlCl}_3$  and leave physisorbed  $\text{H}_4\text{TPP}^{2+}$  on the surface. It is plausible that physisorbed  $\text{H}_4\text{TPP}^{2+}$  could bind Pd/Sn colloids: Chloride ions associated with the  $\text{Sn}^{2+}/\text{Sn}^{4+}$  colloidal shell give Pd/Sn colloids a net negative charge that inhibits aggregation and allows the colloids to be electrostatically bound to cationic functional groups on a substrate.<sup>68-73</sup> Two studies eliminated this possibility: First, rinsing TPPAl-(carboxylate) monolayers with isopropanol after Pd/Sn colloid adsorption and after acceleration should easily remove physisorbed  $\text{H}_4\text{TPP}^{2+}$ . UV-vis absorption spectra show an increased loss of Pd/Sn colloids relative to samples rinsed with water, but still exhibit the Soret band at 426 nm (Figure 2.3). Second, a solution study that used TPPAl-(benzoate) as a model for surface bound TPPAl-(carboxylate) showed no reaction with excess HCl. The  $^1\text{H}$  NMR spectrum showed only the presence of unchanged TPPAl-(benzoate),<sup>58</sup> with no trace of benzoic acid or  $\text{H}_4\text{TPP}^{2+}$ .

### *2.3.5. Pd/Sn Colloids Adsorbed to Microcontact-Printed TPPAl-(carboxylate) Monolayers Initiate Electroless Metallization*

Pd/Sn colloids adsorbed on patterned TPPAl-(carboxylate) monolayers initiate copper metal deposition in the ELD solution. We used 2-cm<sup>2</sup> PDMS stamps bearing an arbitrary pattern with feature sizes ranging from 200 to 2 μm to create TPPAl-(carboxylate) monolayers on oxidized polymeric substrates. After adsorption of the Pd/Sn colloids and acceleration, the samples were plated with copper by immersion in the copper ELD solution for 3 - 5 minutes. Optical and scanning electron microscope (SEM) images show that copper deposits exclusively within the printed regions for all oxidized polymeric substrates in this study (shown in Figure 2.4 for selectively metallized oxidized PET).<sup>76</sup> Defects in the metallized patterns are limited to errors associated with microcontact printing: Dust particles or air bubbles trapped between the stamp and substrate prevent the deposition of TPPAl-(carboxylate), producing unmetallized voids; collapse of recessed regions of the PDMS stamp deposits TPPAl-(carboxylate) in unwanted areas, producing superfluous metallized areas. These defects can be avoided by engineering the microcontact printing process, such as conducting the experiments in a cleanroom to eliminate dust particles and incorporating nonfunctional support posts in the PDMS stamp to prevent collapse.

Contact mode atomic force microscopy (AFM) studies of the copper films indicate that a plating time of 3 minutes yields patterned copper films that are 40 nm thick. Longer plating times yield thicker metal films, but > 5 minutes in the ELD bath resulted in the formation of large, dome-shaped blisters and eventual delamination of the copper film. The formation of blisters during copper ELD has been widely observed and is attributed to incorporation of hydrogen gas that evolves during copper plating.<sup>79</sup> Although blistering can be remedied through manipulation of the ELD bath chemistry and deposition temperature, keeping plating times < 5 min produced uniform, blister-free copper films on oxidized polymeric substrates that we used for further characterization.

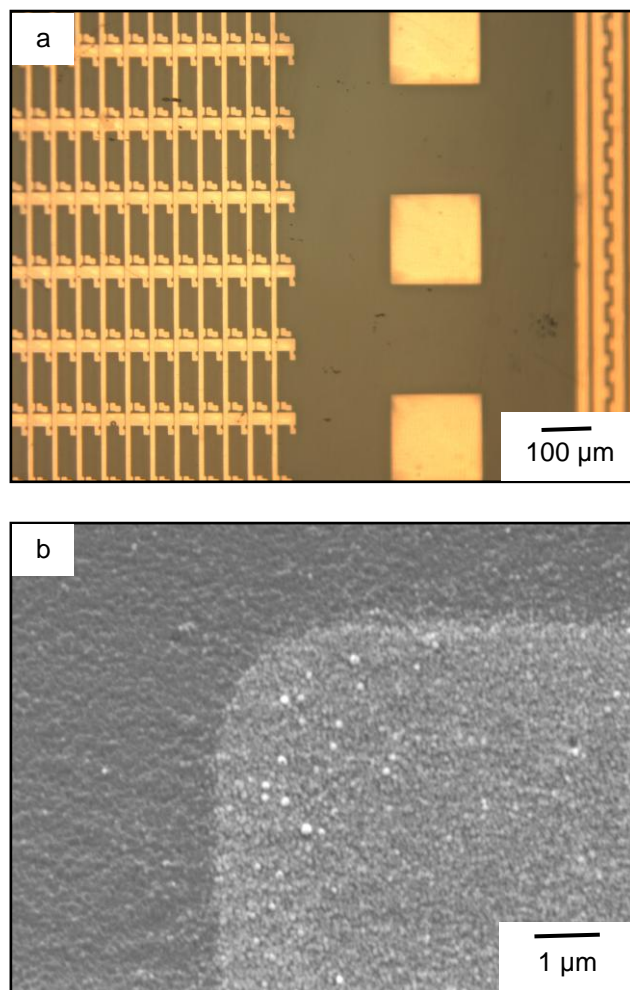
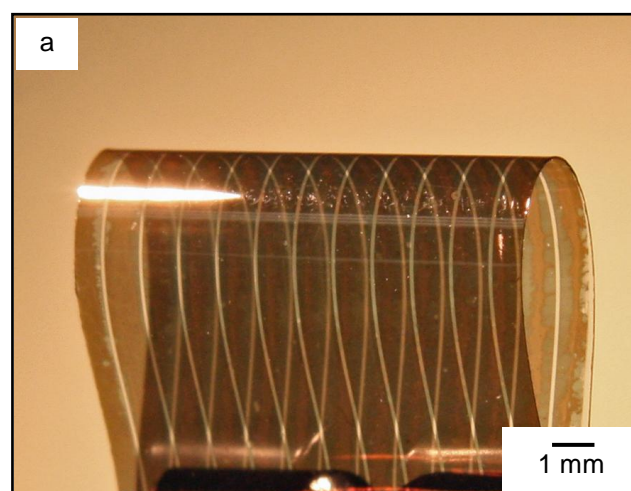


**Figure 2.4.** Optical and SEM images of patterned copper films on oxidized PET. (a) Optical image of an arbitrary copper pattern. (b) SEM image of a portion of the metallized substrate in (a). In both images, the light areas are copper; these areas correspond to the raised portion of the PDMS microcontact printing stamp.

### *2.3.6. Copper Wires Fabricated on Oxidized PEN are Resilient to Mechanical Stress*

Copper wires fabricated by selective ELD on flexible polymeric substrates retain their conductivity even when subjected to substantial mechanical deformation. The average resistivity of unstrained copper wires fabricated on flexible PEN substrates was  $2.7 \pm 0.27 \mu\Omega \text{ cm}$ , which compares well with the reported resistivity for ELD copper ( $\sim 2 \mu\Omega \text{ cm}$ ).<sup>80</sup>

Inducing tensile strain in the wire by bending the PEN substrate around cylinders with radii decreasing from 12.5 mm to 500  $\mu\text{m}$  did not increase the resistivity (Figure 2.5), indicating that the wires deform with the PEN substrate and that the testing process, which subjected the wires to  $\sim 30$  cycles of repetitive strain, did not induce metal fatigue. We observed a modest increase in resistivity (to 4.3  $\mu\Omega\text{ cm}$ ) only when the PEN substrate was creased, corresponding to a radius of curvature of  $\sim 100\ \mu\text{m}$ . Permanent damage to the PEN substrate occurs before copper wires fabricated on the surface cease to function electrically.



b)

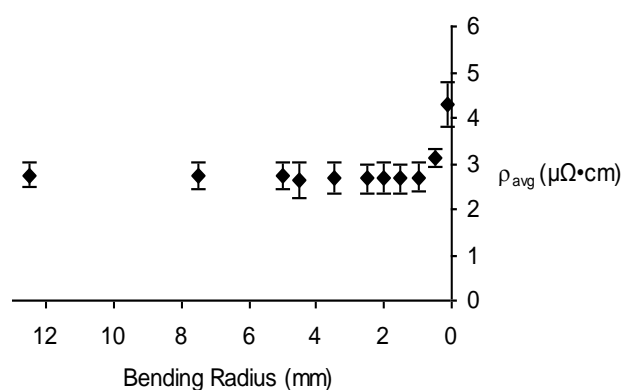


**Figure 2.5.** Electrical characterization of copper wires fabricated on PEN. (a) Photograph of copper wires ( $l = 5.0$  cm,  $w = 1.0$  mm,  $h = 40$  nm) fabricated on a 75- $\mu\text{m}$ -thick PEN substrate. (b) Resistivity of copper wires ( $l = 1.0$  cm,  $w = 1.0$  mm,  $h = 40$  nm) as a function of bending radius.

We attribute the ability of copper wires on PEN to tolerate high tensile strain to strong adhesion between the wire and the substrate. Strong adhesion is essential to strain tolerance because it distributes the strain over the entire area of the wire, thus allowing the wire and substrate to deform together. We tested the adhesion of copper films deposited on oxidized polymeric substrates using the ASTM D3359B-02 tape test.<sup>67</sup> There was no removal of copper after scoring the copper films into 1 mm x 1 mm

squares, applying tape to the cut surface, and peeling it off. Copper films deposited on all polymeric substrates achieved the highest ASTM adhesion classification (5B). This strong adhesion is likely due to both chemical and mechanical adhesion: Chemical adhesion is caused by strong bonds between the interfaces present in the film. A significant contribution to chemical adhesion may be from the TPPAI-(carboxylate) monolayer, which is covalently bound to the oxidized polymeric substrate. Mechanical adhesion is caused by physical interlocking between the metal film and a rough substrate. Roughening of the polymeric substrates used in this work is a result of surface oxidation. For example, the root-mean-square roughness of PET substrates increases from 0.96 nm to 10.4 nm after oxidation, as measured by AFM (Figure S2.2).<sup>81</sup>

## 2.4. Conclusions

In conclusion, we have shown that TPPAI-OMe is an ideal material for the selective electroless metallization of a wide range of polymeric substrates: It is inexpensive, stable, compatible with native PDMS stamps, and it reacts quickly with surface carboxylic acid groups to form robust TPPAI-(carboxylate) monolayers that are stable to the harsh processing conditions of electroless copper deposition, particularly the low pH of Pd/Sn colloidal catalyst solutions. The use of TPPAI-(carboxylate) monolayers as a base for selective electroless metallization is also applicable to the selective electroless deposition of other metals that are initiated by Pd/Sn colloids, such as nickel and cobalt. Copper wires fabricated in this way exhibit remarkable adhesion to polymeric substrates, allowing the copper/polymer to withstand substantial deformation without a negative impact on electrical performance. This simple, inexpensive fabrication method is well-suited to the fabrication of low-cost plastic electronic devices, such as flexible displays. It is adaptable for use in the fabrication of large-area plastic electronic devices by simply scaling up the size of the microcontact printing stamp.

## 2.5. References

- (1) Special issue on “Flexible Electronics”, *Mater. Today* **2006**, 9 24.
- (2) Special issue on “Macroelectronics”, *Mater. Res. Soc. Bull.* **2006**, 31 (6), 447.
- (3) Special issue on “Flexible Electronics Technology, Part 1: Systems and Applications”, *Proc. IEEE* **2005**, 93 (7), 1235.
- (4) Special issue on “Flexible Electronics Technology, Part 2: Materials and Devices”, *Proc. IEEE* **2005**, 93 (8), 1391.
- (5) Someya, T.; Sekitani, T.; Iba, S.; Kato, Y.; Kawaguchi, H.; Sakurai, T. *Proc. Natl. Acad. Sci.* **2004**, 101, 9966.
- (6) Velten, T.; Ruf, H. H.; Barrow, D.; Aspragathos, N.; Lazarou, P.; Jung, E.; Malek, C. K.; Richter, M.; Kruckow, J.; Wackerle, M. *IEEE Trans. Adv. Packaging* **2005**, 28, 533.
- (7) Dai, W.; Wang, W. *Proc. SPIE Int. Opt. Eng.* **2007**, 6464, 64640I
- (8) Henry, A. C.; McCarley, R. L. *J. Phys. Chem. B* **2001**, 105, 8755.
- (9) Yoon, Y. -K.; Pan, B.; Papapolymerou, J.; Tentzeris, M.; Allen, M. G. *International Conference on Solid-State Sensors, Actuators, and Microsystems (Transducers '05)* **2005**, 1986.
- (10) Yoon, Y. -K.; Allen, M. G. *J. Microelectromech. Syst.* **2005**, 14, 886.
- (11) Menard, E.; Meitl, M. A.; Sun, Y.; Park, J. -U.; Shir, D. J.; Nam, Y. -S.; Jeon, S.; Rogers, J. A. *Chem. Rev.* **2007**, 107, 1117.
- (12) Ling, M. M.; Bao, Z. *Chem. Mater.* **2004**, 16, 4824.
- (13) H. Klauk, Ed. *Organic Electronics: Materials, Manufacturing and Applications* Wiley VCH, Weinheim, Germany **2006**.

- (14) Rogers, J. A.; Bao, Z.; Baldwin, K.; Dodabalapur, A.; Crone, B.; Raju, V. R.; Kuck, V.; Katz, H.; Amundson, K.; Ewing, J.; Drzaic, P. *Proc. Nat. Acad. Sci.* **2001**, *98*, 4835.
- (15) Mach, P.; Rodriguez, S. J.; Nortrup, R.; Wiltzius, P.; Rogers, J. A. *Appl. Phys. Lett.* **2001**, *78*, 3592.
- (16) Rogers, J. A.; Bao, Z.; Dodabalapur, A. *IEEE Elect. Dev. Lett.* **2000**, *21*, 100.
- (17) Rogers, J. A.; Bao, Z. N.; Makhija, A.; Braun, P. *Adv. Mater.* **1999**, *11*, 741.
- (18) Cosseddu, P.; Bonfiglio, A. *Appl. Phys. Lett.* **2006**, *88*, 023506.
- (19) Hur, S. H.; Khang, D. Y.; Kocabas, C.; Rogers, J. A. *Appl. Phys. Lett.* **2004**, *85*, 5730.
- (20) Wang, Z.; Xing, R. B.; Zhang, J.; Yuan, J. F.; Yu, X. H.; Han, Y. C. *Appl. Phys. Lett.* **2004**, *85*, 831.
- (21) Loo, Y. L.; Willett, R. L.; Baldwin, K. W.; Rogers, J. A. *Appl. Phys. Lett.* **2002**, *81*, 562.
- (22) Loo, Y. L.; Someya, T.; Baldwin, K. W.; Bao, Z. N.; Ho, P.; Dodabalapur, A.; Katz, H. E.; Rogers, J. A. *Proc. Natl. Acad. Sci. U.S.A.* **2002**, *99*, 10252.
- (23) Guo, T. F.; Pyo, S.; Chang, S. C.; Yang, Y. *Adv. Funct. Mater.* **2001**, *11*, 339.
- (24) Gray, C.; Wang, J.; Duthaler, G.; Ritenour, A.; Drzaic, P. S. *Proc. SPIE* **2001**, *4466*, 89.
- (25) van Osch, T. H. J.; Perelaer, J.; de Laut, A. W. M.; Schubert, U. S. *Adv. Mater.* **2008**, *20*, 343.
- (26) Smith, P. J.; Shin, D. -Y.; Stringer, J. E.; Derby, B. *J. Mater. Sci.* **2006**, *41*, 4153.
- (27) Deardon, A. L.; Smith, P. J.; Shin, D. -Y.; Reis, N.; Derby, B.; O'Brien, P. *Macromol. Rapid Commun.* **2005**, *26*, 315.

- (28) Kamyshny, A.; Ben-Moshe, M.; Aviezer, S.; Magdassi, S. *Macromol. Rapid Commun.* **2005**, *26*, 281.
- (29) Redinger, D.; Molesa, S.; Yin, S.; Farschi, R.; Subramanian, V. *IEEE Trans. Electron.* **2004**, *51*, 1978.
- (30) Szczech, J. B.; Megaridis, C. M.; Gamota, D. R.; Zhang, J. *IEEE Trans. Electron. Packag. Manuf.* **2002**, *25*, 26.
- (31) Ahn, B. Y.; Duoss, E. B.; Motala, M. J.; Guo, X.; Park, S.; Xiong, Y.; Yoon, J.; Nuzzo, R. G.; Rogers, J. A.; Lewis, J. A. *Science* **2009**, *323*, 1590.
- (32) G. O. Mallory, J. B. Hajdum, Eds. *Electroless Plating: Fundamentals and Applications* American Electroplaters and Surface Finishers Society, Orlando, Florida **1990**.
- (33) Nakano, H.; Itabashi, T.; Akahoshi, H. *J. Electrochem. Soc.* **2005**, *152*, C163.
- (34) Mak, C. Y. *MRS Bull.* **1994**, August, 55.
- (35) Cho, J. S. H.; Kang, H.-K.; Wong, S. S.; Shachem-Diamand, Y. *MRS Bull.* **1993**, June, 31.
- (36) Li, J.; Blewer, R.; Mayer, J. W. *MRS Bull.* **1993**, June, 18.
- (37) Ting, C. H.; Paunovic, M.; Pai, P. L.; Chiu, G. J. *J. Electrochem. Soc.* **1989**, *136*, 462.
- (38) Ting, C. H.; Paunovic, M. *J. Electrochem. Soc.* **1989**, *136*, 456.
- (39) Cheng, K.; Yang, M. -H.; Chiu, W. W. W.; Huang, C. -Y.; Chang, J.; Ying, T. -F.; Yang, Y. *Macromol. Rapid Commun.* **2005**, *26*, 247.
- (40) Shah, P.; Kevrekidis, Y.; Benziger, J. *Langmuir* **1999**, *15*, 1584.
- (41) Wang, T. C.; Chen, B.; Rubner, M. F.; Cohen, R. E. *Langmuir* **2001**, *17*, 6610.
- (42) Guo, R. -F.; Chang, S. -C.; Pyo, S.; Yang, Y. *Langmuir* **2002**, *18*, 8142.

- (43) Tate, J.; Rogers, J. A.; Jones, C. D. W.; Vyas, B.; Murphy, D. W.; Li, W.; Bao, Z.; Slusher, R. E.; Dodabalapur, A.; Katz, H. E. *Langmuir* **2000**, *16*, 6054.
- (44) Hidber, P. C.; Helbig, W.; Kim, E.; Whitesides, G. M. *Langmuir* **1996**, *12*, 1375.
- (45) Prissanaroon, W.; Brack, N.; Pigram, P. J.; Hale, P.; Kappen, P.; Liesegang, J. *Thin Solid Films* **2005**, *477*, 131.
- (46) Li, Y.; Chen, D.; Lu, Q.; Qian, X.; Zhu, Z.; Yin, J. *Appl. Surf. Sci.* **2005**, *241*, 471.
- (47) Zschieschang, U.; Klauk, H.; Halik, M.; Schmid, G.; Dehm, C. *Adv. Mater.* **2003**, *15*, 1147.
- (48) Lee, J. N.; Park, C.; Whitesides, G. M. *Anal. Chem.* **2003**, *75*, 6544.
- (49) Kim, J.; Chaudhury, M. K.; Owen, M. J.; Orbeck, T. *J. Coll. Interface Sci.* **2001**, *244*, 200.
- (50) Spadavecchia, J.; Rella, R.; Siciliano, P.; Manera, M. G.; Alimelli, A.; Paolesse, R.; DiNatale, C.; D'Amico, A. *Sens. Actuators, B* **2006**, *115*, 12.
- (51) Andersson, M.; Holmberg, M.; Lundstrom, I.; Lloyd-Spetz, A.; Martensson, P.; Paolesse, R.; Falconi, C.; Proietti, E.; DiNatale, C.; D'Amico, A. *Sens. Actuators, B* **2001**, *77*, 567.
- (52) Flink, S.; van Veggel, F. C. J. M.; Reinhoudt, D. N. *Adv. Mater.* **2000**, *12*, 1315.
- (53) Li, C.; Ly, J.; Lei, B.; Fan, W.; Zhang, D.; Han, J.; Meyyappan, M.; Thompson, M.; Zhou, C. *J. Phys. Chem. B* **2004**, *108*, 9646.
- (54) Yasserli, A. A.; Syomin, D.; Malinovskii, V. L.; Loewe, R. S.; Lindsey, J. S.; Zaera, F.; Bocian, D. F. *J. Am. Chem. Soc.* **2004**, *126*, 11944.
- (55) Roth, K. M.; Dontha, N.; Dabke, R. B.; Gryko, D. T.; Clausen, C.; Lindsey, J. S. *J. Vac. Sci. Technol. B* **2000**, *18*, 2359.
- (56) Imahori, H.; Umeyama, T.; Ito, S. *Acc. Chem. Res.* **2009**, *42*, 1809.

- (57) Campbell, W. M.; Burrell, A. K.; Officer, D. L.; Jolley, K. W. *Coord. Chem. Rev.* **2004**, *248*, 1363.
- (58) Davidson, G. J. E.; Tong, L. H.; Raithby, P. R.; Sanders, J. K. M. *Chem. Commun.* **2006**, 3087.
- (59) Kumar, A.; Biebuyck, H. A.; Whitesides, G. M. *Langmuir* **1994**, *10*, 1498.
- (60) Davidson, G. J. E.; Lane, L. A.; Raithby, P. R.; Warren, J. E.; Robinson, C. V.; Sanders, J. K. M. *Inorg. Chem.* **2008**, *47*, 8721.
- (61) Roux, S.; Demoustier-Champagne, S. *J. Polym. Sci. A* **2003**, *42*, 1347.
- (62) Stephans, L. E.; Myles, A.; Thomas, R. R. *Langmuir* **2000**, *16*, 4706.
- (63) Rasmussen, J. R.; Stedronsky, E. R.; Whitesides, G. M. *J. Am. Chem. Soc.* **1977**, *99*, 4736.
- (64) Kim, S. R. *J. Appl. Polym. Sci.* **2000**, *77*, 1913.
- (65) Brown, L.; Koerner, T.; Horton, J. H.; Oleschuk, R. D. *Lab Chip* **2006**, *6*, 66.
- (66) Walther, F.; Davydovskaya, P.; Zurcher, S.; Kaiser, M.; Herberg, H.; Gigler, A. M.; Stark, R. W. *J. Micromech. Microeng.* **2007**, *17*, 524.
- (67) *ASTM Annual Book of Standards, Volume 06.01*; American Society for Testing and Materials International, West Conshohocken, PA, 2002.
- (68) Horkans, J.; Kim, J.; McGrath, C.; Romankiw, L. T. *J. Electrochem. Soc.* **1987**, *134*, 300.
- (69) Osaka, T.; Nagasaka, H.; Goto, F. *J. Electrochem. Soc.* **1980**, *127*, 2343.
- (70) Osaka, T.; Rakematsu, H.; Hikei, K. *J. Electrochem. Soc.* **1980**, *127*, 1021.
- (71) Cohen, R. L.; Meek, R. L. *J. Colloid Interface Sci.* **1976**, *55*, 156.

- (72) Feldstein, N.; Schlesinger, M.; Hedgecock, N. E.; Chow, S. L. *J. Electrochem. Soc.* **1974**, *121*, 738.
- (73) Cohen, R.; West, K. W. *J. Electrochem. Soc.* **1973**, *120*, 502.
- (74) Satake, A.; Kobuke, Y. *Org. Biomol. Chem.* **2007**, *5*, 1679.
- (75) Zak, J.; Yuan, H.; Ho, M.; Woo, L. K.; Porter, M. D. *Langmuir* **1993**, *9*, 2772.
- (76) In principle, unrinsed TPPAI-(carboxylate) monolayers that are covered with a film of physisorbed TPPAI-OMe can also be used for the selective deposition of copper. UV-vis spectra of printed multilayers on PET after exposure to Pd/Sn colloids (Figure S3.2) show a slight reduction of the Soret band absorbance, indicating that the physisorbed TPPAI-OMe layers do not desorb to an appreciable extent in the colloidal solution. However, the economic advantage of using ELD diminishes if contamination of the plating solutions – particularly for Pd/Sn colloids – reduces their lifetime. For this reason, we have focused on the use of TPPAI-(carboxylate) monolayers as a base for selective ELD.
- (77) IR of AlTPP-OMe (KBr pellet,  $\text{cm}^{-1}$ ): 1723 (br), 1594 (br), 1486 (w), 1441 (w), 1405 (sh), 1384 (s), 1351 (m), 1321 (sh), 1260 (m), 1203 (m), 1174 (w), 1108 (br), 1069 (m), 1008 (s).
- (78) Alcock, N. W.; Tracy, V. M.; Waddington, T. C. *J. C. S. Dalton* **1976**, 2243.
- (79) Nakahara, S.; Okinaka, Y. *Annu. Rev. Mater. Res.* **1991**, *21*, 93.
- (80) Li, T.; Seidel, T. E.; Mayer, J. W. *MRS Bull.* **1994**, August, 15.
- (81) It is interesting to note that copper deposited on unrinsed TPPAI-(carboxylate) monolayers covered with a film of physisorbed TPPAI-OMe achieves the same ASTM adhesion classification (5B) as copper deposited on TPPAI-(carboxylate) monolayers. The presence of physisorbed TPPAI-OMe introduces a potentially weak interface since physisorbed TPPAI-OMe multilayers are held together by weak intermolecular forces. The fact that the presence of this interface does not

*Selectively Metallized Polymeric Substrates by Microcontact  
Printing an Aluminum (III) Porphyrin Complex*

impact the adhesion of the copper likely indicates that the adhesion of copper films is dominated by mechanical interlock to the rough polymeric substrate.

## 2.6. Supporting Information

### *2.6.1. Procedures for the Preparation and Oxidation of Polymeric Substrates*

#### *2.6.1.1. Polyethylene terephthalate and polyethylene naphthalate*

PET and PEN substrates were sonicated in acetone for 5 min, dried then immersed in a 2 M NaOH solution at 70 °C for 30 min. The substrates were then immersed in acetic acid at 70 °C for 15 min, rinsed with water, and then immersed in a 60 °C, 1.2 N H<sub>2</sub>SO<sub>4</sub> solution containing 50 g L<sup>-1</sup> KMnO<sub>4</sub> for 1 h. The substrates were rinsed with water, then immersed in 0.1 M HCl solution for 5 min, in water for 5 min, and in THF for 5 min, and finally dried using a stream of nitrogen.

#### *2.6.1.2. Polyimide*

PI substrates were hydrolyzed in aqueous solution of 0.02 M NaOH and 0.4 M NaNO<sub>3</sub> at 30 °C for 35 min. The substrates were neutralized by immersion in 0.1 M acetic acid, extensively rinsed with water and then dried using a stream of nitrogen.

#### *2.6.1.3. Polyethylene and polypropylene*

PE and PP substrates were immersed in chromic acid solution (CrO<sub>3</sub>/H<sub>2</sub>O/H<sub>2</sub>SO<sub>4</sub> = 29:42:29 by weight) at 72 °C for 5 min to oxidize the polymer surface. After removing from the chromic acid solution, the substrates were rinsed three times with water.

#### *2.6.1.4. Polytetrafluoroethylene*

PTFE substrates were oxidized by immersion, with mild agitation, in commercially available FluoroEtch solution (Acton Technologies, Pittston, PA) at 50 °C for 60 s. The substrates were then rinsed with isopropanol and acidic water for 60 s and dried using a stream of nitrogen.

#### *2.6.1.5. Polymethylmethacrylate*

PMMA substrates were sonicated for 10 min in a 50% aqueous isopropanol solution and dried using stream of nitrogen. The PMMA substrates were then immersed in 3 M sulfuric acid at 60 °C for 20 minutes to catalyze the conversion of terminal ester groups to carboxylic acid groups. After removal, the PMMA substrates were rinsed with water and isopropanol and dried using a stream of nitrogen

#### *2.6.1.6. SU-8*

SU-8 films were prepared using SU-8 2050 (MicroChem, Newton, MA) on silicon (100) wafers as substrates. The silicon wafer was cleaned by sonication for 5 min in acetone and then 5 min in methanol. After drying using a stream of nitrogen, SU-8 2050 was spin-coated onto the surface at 500 rpm for 10 s and then the speed was increased to 3000 rpm for 30 s to give a film thickness of approximately 50  $\mu\text{m}$ . The film was pre-baked on a hotplate for 2 min at 65 °C and 7 min at 95 °C, and then exposed in a mask aligner (Karl Suss MJB3 Mask Aligner) at 10  $\text{mW cm}^{-2}$  at 365 nm for 20 s (total radiation dose 200  $\text{mJ cm}^{-2}$ ). After a post-exposure bake (1 min 30 s at 65 °C, then 6 min 30 s at 95 °C), the film was developed in SU-8 developer for 6 min with mild agitation. The SU-8 films were then oxidized in an oxygen plasma using a Harrick plasma cleaner (Harrick Plasma, Ithaca, NY) for 10 min on high.

*2.6.2. Supporting Figures and Tables*

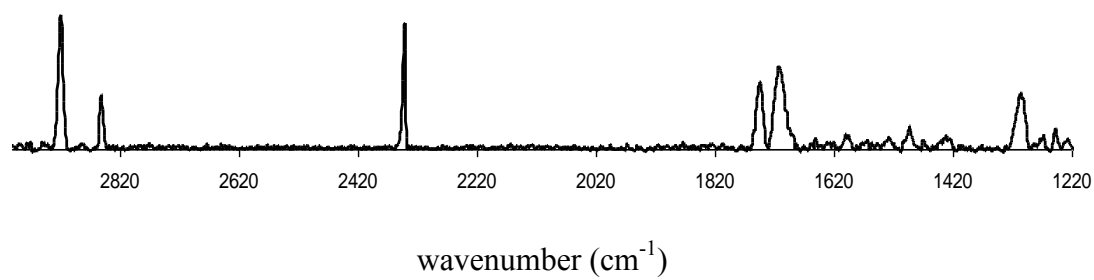


**Figure S2.1.** RAIRS spectrum of a 16-mercaptohexadecanoic acid SAM on gold

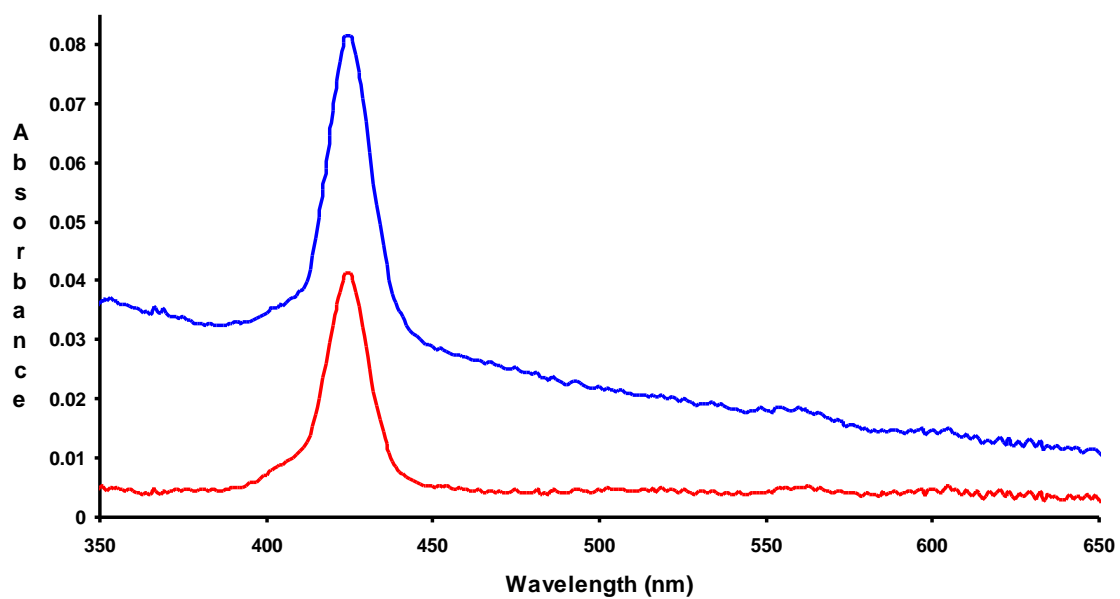


**Figure S2.2.** UV-vis absorption spectrum of a TPPAI-(carboxylate) monolayer covered with a film of physisorbed TPPAI-OMe on oxidized PET before (red) and after (blue) exposure to a solution of Pd/Sn colloids for 1 min.

*Selectively Metallized Polymeric Substrates by Microcontact  
Printing an Aluminum (III) Porphyrin Complex*

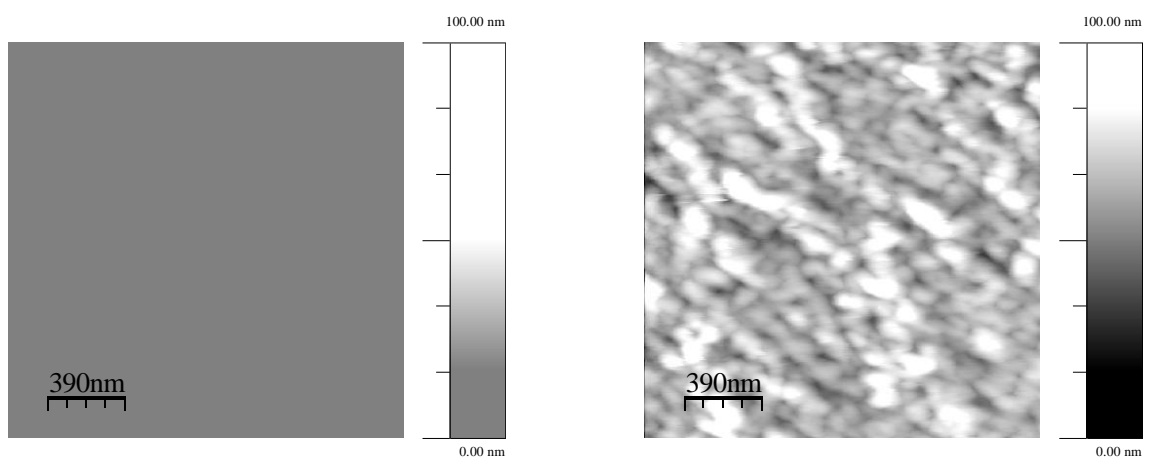


**Figure S2.3.** Contact-mode AFM images of native PET (left) and oxidized PET (right). The root-mean-square roughness of the PET substrates increases from 0.96 nm for native PET to 10.4 nm for oxidized PET.

## **Chapter 3**

# **Silver Nanowire/Optical Adhesive Coatings as Transparent Electrodes for Flexible Electronics**

### 3.1. Introduction

Flexible displays of organic light-emitting devices (OLEDs) on lightweight plastics are nearing commercial reality.<sup>1</sup> Despite years of research and development, however, the flexibility of these displays is still limited by reliance on the transparent conductor indium tin oxide (ITO).<sup>2</sup> ITO is universally used in rigid optoelectronic devices, but it is completely unsuitable for flexible devices because it is a brittle ceramic. Here, we describe a new transparent conductive coating of silver nanowires (AgNWs) embedded in a transparent polyurethane optical adhesive (OA) that can be applied to a variety of substrates – rigid glass, flexible polyethylene terephthalate (PET), and even elastomeric polydimethylsiloxane (PDMS). AgNW-OA coatings not only rival the conductivity (sheet resistance  $< 20 \Omega/\square$ ) and transparency ( $> 85\%$ ) of ITO;<sup>3</sup> they also surpass ITO in flexibility and durability. We demonstrate their use as electrodes in flexible light emitting electrochemical cells (LEECs) and show that repeated bending does not affect the device properties.

Devices fabricated on lightweight, flexible plastics open the way to thin, lightweight displays, large-area lighting panels, and solar cells that can be rolled, folded, or mounted on curved surfaces. Flexibility requires that each layer of these thin-film devices – metal electrodes, transparent conductive electrodes (TCEs), active organic materials, and device interconnects – function under bending strains. We cannot rely on the universal standard TCE used in rigid optoelectronics – ITO – because it compromises both the electrical and mechanical performance of flexible devices. ITO films on glass boast low sheet resistance ( $< 20 \Omega/\square$ ) and high transparency ( $> 85\%$ ); however, the sheet resistance of ITO films on PET are higher ( $60 \Omega/\square$ , 80% transparency) due to the low processing temperatures required by plastic substrates.<sup>3</sup> Furthermore, ITO films on flexible plastics crack at relatively low bending strains (2 – 3%), and repeated bending leads to catastrophic electrical failure.<sup>2</sup> The onus is on the research community to develop drop-in replacements for ITO that can deliver conductivity and transparency as good as ITO on glass, combined with the ability to tolerate repeated cycles of bending. In response, researchers are pursuing a number of alternative TCE materials to replace ITO, such as

carbon nanotubes,<sup>4</sup> graphene,<sup>5,6</sup> conductive polymers,<sup>7-9</sup> metallic grids,<sup>10-13</sup> and metallic nanowires.<sup>14-31</sup>

Many view AgNW films as the most promising replacement for ITO, but substantial problems still hinder the adoption of these materials. AgNW networks deposited on substrates by drop-casting,<sup>14,15</sup> meyer rod coating,<sup>17,18</sup> spray coating,<sup>19,20</sup> and vacuum filtration<sup>21,22</sup> display optical and electrical properties similar to ITO and retain conductivity while bent; however, there are two crucial drawbacks that limit the use of these AgNW films in real devices. First, many of these techniques produce AgNW films that are not adhered to the substrate, making them fragile and easily displaced.<sup>25</sup> Second, these AgNW films consist of an irregular pile of AgNWs with individual AgNWs protruding > 100 nm from the surface. Since the films comprising thin-film devices are often ~ 100 nm in thickness, protruding AgNWs provide pathways for electrical shorts and thus are unsuitable for use as electrodes.<sup>15,18</sup>

Embedding AgNWs into polymer films is a promising way to improve adhesion and reduce height variation at the surface. Two methods have been reported: The first method embeds the AgNWs into the surface of specific polymeric substrates, such as polyvinyl alcohol (PVA),<sup>25</sup> or crosslinked polyacrylate.<sup>27</sup> The second method embeds the AgNWs in an uncrosslinked polymer layer, such as poly(3,4-ethylenedioxythiophene) poly(styrenesulfonate) (PEDOT:PSS), on top of a plastic substrate.<sup>14</sup> Both methods produce AgNW composites with conductivity and transparency competitive with ITO/PET or ITO/glass, low surface roughness of < 10 nm, and minimal increases in resistance after bending. Despite these impressive developments, these AgNW composites cannot yet be called drop-in replacements for ITO. ITO is a coating that can be applied to different substrates (e.g., PET, polyethylene naphthalate, polyimide),<sup>3</sup> as well as plastics treated with multilayer barrier coatings that are essential to reduce the permeation of moisture and air, which degrade organic electronic materials and severely limit operating device lifetime.<sup>32</sup> ITO is also impervious to common solvents used to deposit thin films of device materials by spin coating, making it compatible with low-cost solution processing. In contrast, existing AgNW composite films each lack at least one of

these important features. AgNW films embedded in specific polymer substrates will need to be integrated with gas-impermeable plastics to be useful for practical flexible organic electronics. These polymer substrates also may not have the desired mechanical properties. For example, polyacrylate substrates with embedded AgNWs must be heated to above the glass transition temperature (110 °C) for them to be flexible or stretchable.<sup>26,27</sup> AgNWs embedded in uncrosslinked polymers such as PEDOT:PSS<sup>14</sup> or PVA<sup>25</sup> also may not be compatible with solution processing of device thin films due to possible dissolution of the polymer in the solvent.

Our approach to flexible and transparent electrodes is to fabricate a coating consisting of an annealed AgNW film embedded in a transparent polyurethane optical adhesive that can be applied to the substrate of choice. The fabrication procedure is simple, inexpensive, and uses commercially available materials, which makes the coatings easily accessible as transparent electrodes for flexible device testing. The coatings are as conductive and transparent as ITO/glass, with a low surface roughness (< 10 nm) that makes them compatible with thin-film devices. Since optical adhesives are designed to bond components together, AgNW-OA coatings adhere to a variety of target substrates. We demonstrate AgNW-OA coatings on glass, PET, and PDMS substrates; these coatings should also be applicable to the impermeable plastics necessary for practical flexible electronics. Optical adhesives are crosslinked polymers, which imparts durability and solvent resistance to the AgNW-OA coatings, making them essentially unaffected by marring, scratching, or solvent exposure. They show a negligible increase in resistance after bending to tensile strains as high as 76% or after 250 cycles of bending to 15% tensile strain.

## 3.2. Experimental Section

### *3.2.1. Preparation of glass, PET, and oxidized PDMS substrates*

Glass microscope slides (VWR) and PET films (Goodfellow, thickness = 75 μm) were cut into 2 cm x 2 cm squares, sonicated (Branson Model 3510) for 10 minutes in deionized water, acetone, and then isopropanol, and dried under a stream of nitrogen.

Clean PET films were adhered to a glass microscope slide using double sided tape (3M). PDMS substrates were fabricated by casting liquid pre-polymer (Sylgard 184, Dow Chemical) against flat polystyrene Petri dishes and curing overnight in a 60 °C oven. Cured PDMS films were cut into 2 cm x 2 cm squares, removed from the Petri dish, and oxidized in air plasma (Harrick Plasma) for 40 seconds. Oxidized PDMS substrates were then rinsed with methanol and dried under a stream of nitrogen.

### *3.2.2. Fabrication of AgNW-OA films on glass, PET, and oxidized PDMS*

Silver nanowires with an average diameter of 90 nm and average length of 25  $\mu\text{m}$  dispersed in ethanol (10 mg/mL, SLV-NW-90, BlueNano Inc.) were diluted to 0.025 mg/mL with ethanol, and then ultrasonicated for 45 seconds. The desired volume of dilute AgNW solution was filtered through a piece of filter paper (Millipore Durapore Hydrophobic 0.22  $\mu\text{m}$ ) using a 25 mm outer diameter glass filter frit and a vacuum filter holder. An unoxidized PDMS carrier substrate was then brought into contact with the filter paper with slight pressure. Peeling off the filter paper transferred the AgNW film to the PDMS carrier surface. AgNW films on PDMS carriers were annealed at 200 °C for 20 min on a hot plate, cooled to room temperature, and then cut to the desired size/geometry (1 cm x 1 cm square for transmittance and sheet resistance, 1.5 cm x 0.2 cm strips for bending experiments, and 1.5 cm diameter circles for durability testing and LEEC fabrication) using a scalpel. A drop (5  $\mu\text{L}/\text{cm}^2$  of AgNW film) of optical adhesive (NOA 83H, Norland Optical) was then placed onto the surface of the AgNW film, and the target substrate (glass, PET, or oxidized PDMS) placed on top. The adhesive was allowed to spread for 1 minute, and then was cured under a 100 W mercury lamp for 15 minutes. The PDMS carrier was then removed, leaving the AgNW-OA coating on the target substrate.

### *3.2.3. Fabrication of LEECs*

AgNW-OA anodes were oxidized in an oxygen plasma for 45 seconds, and a PEDOT:PSS (Heraeus Clevios P) layer was spin-coated at 1000 rpm for 1 minute on the surface by sonicating aqueous PEDOT:PSS dispersion for 15 minutes, heating the dispersion to 90 °C for 15 minutes, and diluting with 30 % isopropanol. The PEDOT:PSS film was annealed on a hot plate at 100°C for 20 minutes. After cooling to room temperature, a Ru(dtb-bpy)<sub>3</sub>(PF<sub>6</sub>)<sub>2</sub> / PMMA emissive layer was deposited by spin-coating a 3:1 v:v mixture of a 40 mg/mL solution of Ru(dtb-bpy)<sub>3</sub>(PF<sub>6</sub>)<sub>2</sub> in acetonitrile and a 25 mg/mL solution of PMMA (Avg M<sub>w</sub> = 120 000) at 1500 rpm for 30 s. The film was annealed in a vacuum oven at 120 °C overnight. A eutectic gallium indium (EGaIn) cathode was deposited onto the surface of the Ru/PMMA film using a syringe, and then sealed in epoxy resin.

### *3.2.4. Characterization*

Optical inspection was performed using an Olympus BX51 microscope equipped with an Olympus Q-Color3 camera. SEM images were collected with a Hitachi S-4500 field emission SEM (Surface Science Western, London, ON, Canada). AFM images (40 μm x 40 μm) were collected using the dynamic force mode of a Park Systems XE-100 AFM (Surface Science Western). AFM images (10 μm x 10 μm) were collected using the tapping mode of a Digital Instruments Multimode AFM. Transmittance spectra were recorded using a Varian Cary 50 UV-Visible spectrophotometer. Sheet resistance values were measured using the four-point probe technique with a Keithley 2601 source meter and EGaIn contacts, with a minimum of three measurements for each sample. Bending experiments were performed by wrapping AgNW-OA films on PET or oxidized PDMS around cylindrical objects with radii varying from 13.5 mm to 0.65 mm and measuring the resistance of the film at each bending radius. A minimum of three measurements were averaged for each radius. AgNW-OA films on PET were subjected to high tensile strain by manually creasing the PET sheet to a radius of ~ 0.1 mm as measured by optical microscopy. The adhesive tape test was performed by measuring the resistance of the

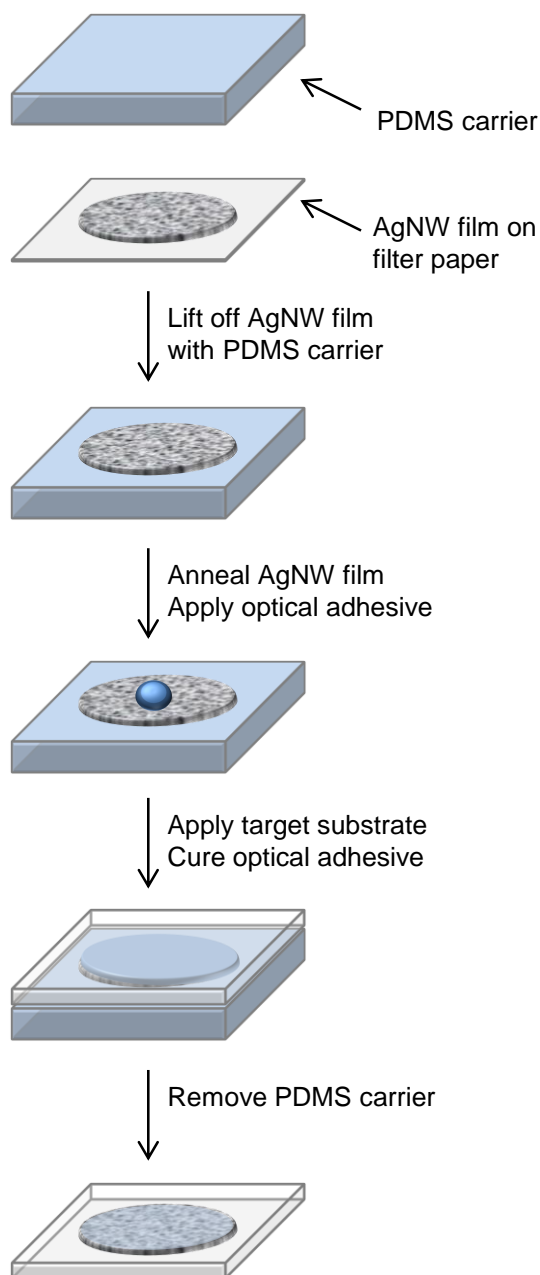
AgNW-OA film on PDMS before and after adhering and peeling off a 1 cm x 2 cm piece of tape (Permacel). The finger friction test was performed by measuring the resistance of an AgNW-OA film on PDMS before and after continuous rubbing with a gloved finger for 30 seconds. The solvent durability test was performed by measuring the resistance of the AgNW-OA film on PDMS before and after immersion into H<sub>2</sub>O and EtOH for 6 hours. EGaIn contacts were removed using a scalpel prior to solvent immersion. After immersion, new EGaIn contacts were placed onto the film and the resistance was normalized to the new length. The repetitive clamping test was performed by measuring the resistance of the AgNW-OA and ITO films on glass after a number of clamping and unclamping cycles of the same area of the film with alligator clips. LEEC devices were characterized using a Keithley 2601 source-measure unit to apply a DC bias voltage and measure the current. Radiance was measured with a calibrated UDT S470 optometer attached to an integrating sphere.

### 3.3. Results and Discussion

#### 3.3.1. Fabrication of AgNW-OA Coatings

The process to fabricate AgNW-OA coatings on glass, PET or PDMS substrates combines commercially available AgNWs with a polyurethane optical adhesive according to Scheme 3.1. Vacuum filtering an AgNW dispersion in ethanol (0.025 mg/mL) through hydrophobic filter paper produces a uniform AgNW film, which is then transferred to a flat PDMS carrier substrate and annealed to fuse the AgNWs at their intersection points.<sup>16</sup> We form AgNW coatings by depositing a drop (5  $\mu\text{L}/\text{cm}^2$ ) of optical adhesive onto the surface of the AgNW film on the PDMS carrier, and then placing a target substrate (glass, PET, or oxidized PDMS) on top. After curing the adhesive, the PDMS carrier substrate easily peels away to leave the cured AgNW-OA coating adhered to the target substrate. The PDMS carrier plays a significant role in the success of this process: First, PDMS can tolerate the high temperatures (200 °C) required to anneal the AgNW film. Second, the surface free energy of the PDMS carrier is ideal for both transfer processes.<sup>33</sup> It is higher than that of the hydrophobic filter paper, which allows the PDMS carrier to cleanly pick

up the AgNW network from the filter paper. It is also lower than that of the target substrates (glass, PET, oxidized PDMS), which enables the release of the AgNW-OA film from its surface to the target substrate. Finally, the PDMS surface provides a smooth template for what is ultimately the surface of the AgNW-OA coating after transfer to the target substrate.



**Scheme 3.1.** Process used to fabricate AgNW-OA coatings.

### *3.3.2. Optical and Electrical Performance of AgNW-OA Coatings*

AgNW-OA coatings on all three target substrates are highly transparent and conductive. A photograph of an AgNW-OA coating adhered to PDMS is shown in Figure 3.1a. By simply varying the volume of the AgNW dispersion passed through the filter paper, we prepared AgNW-OA coatings with sheet resistances of 4  $\Omega/\square$ , 9  $\Omega/\square$ , and 14  $\Omega/\square$ , and transmittances at 550 nm of 81%, 86%, and 89%, respectively. Figure 3.1b shows the transmission spectra for the AgNW-OA coatings on glass substrates, along with the spectrum of a film of the optical adhesive on glass. A summary of the data for AgNW-OA coatings on glass is provided in Table 3.1. The 4  $\Omega/\square$  and 9  $\Omega/\square$  coatings are as conductive and transparent as ITO/glass and also surpass other AgNW films embedded in polymers reported in the literature.<sup>14,21,25-27</sup> We believe that the low sheet resistance and high transparency exhibited by AgNW coatings is due to annealing the AgNW films, which is known to reduce the sheet resistance. In addition, annealing gives the AgNW film mechanical stability by fusing the AgNWs at their intersection points, allowing the network to be transferred to the target substrate without disruption. Annealing is essential to maintain the integrity of the AgNW network; without the annealing step, the resulting AgNW-OA coatings are not conductive.

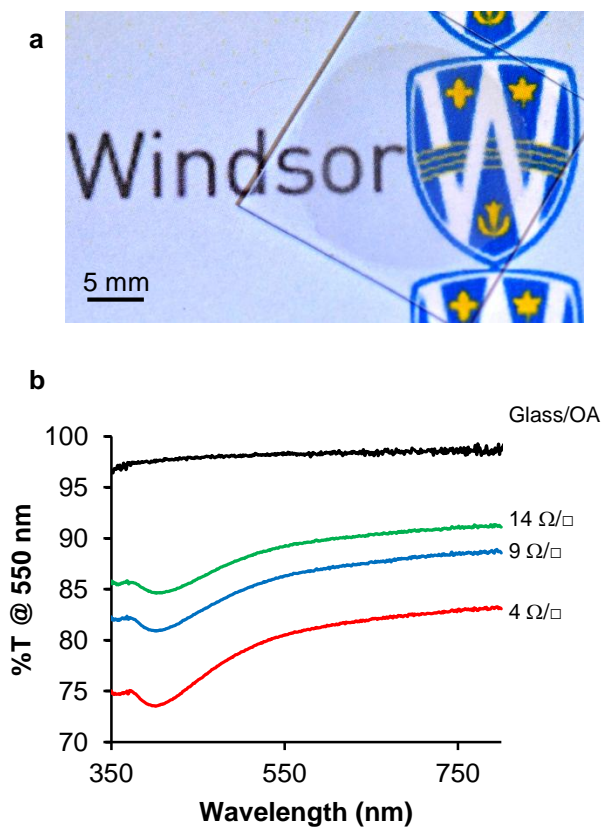


**Figure 3.1.** Electrical and optical properties of AgNW-OA coatings. (a) Photograph of an AgNW-OA coating on PDMS ( $14 \Omega/\square$ ). (b) Transmittance spectra of AgNW-OA coatings on glass, with corresponding sheet resistances.

**Table 3.1.** Electrical and optical properties of AgNW-OA coatings on glass.

$R_s$ ( $\Omega/\square$ )	%T (at 550 nm)
14.1 +/- 1.6	89.2
8.8 +/- 0.5	86.3
3.9 +/- 0.2	80.5

### *3.3.3. Structural Characterization of AgNW-OA Coatings*

Scanning electron microscopy (SEM) and atomic force microscopy (AFM) reveal that AgNW-OA coatings are uniform and smooth. Cross-sectional SEM images of an AgNW-OA ( $4 \Omega/\square$ ) coating on glass (Figure 3.2a and 3.2b) show that the AgNW network resides at the surface of a  $\sim 25\text{-}\mu\text{m}$ -thick film of optical adhesive adhered to the glass substrate. SEM views of the top of the film (Figure 3.2c and 3.2d) show a network of interconnected AgNWs embedded in, and not protruding from, the optical adhesive surface. AFM studies of AgNW-OA ( $9 \Omega/\square$ ) films formed on glass, PDMS, and PET substrates showed that the films have similar root-mean-square (RMS) roughness values (6.2 nm, 5.0 nm, and 7.5 nm, respectively) and maximum peak heights of  $\sim 30$  nm (Figure 3.3), indicating that the coating roughness is essentially independent of the substrate. We also compared how much the AgNWs protrude from the surface of an AgNW-OA ( $14 \Omega/\square$ ) coating on PDMS to AgNW films with a similar AgNW density deposited on a silicon wafer by drop casting.<sup>34</sup> The RMS roughness of the AgNW-OA film is 9.3 nm (Figure 3.4a), which is an order of magnitude lower than that of the drop-cast AgNW film (42.7 nm, Figure 3.4c). More importantly, AFM profile measurements (Figure 3.4b, d) reveal that the variation in maximum height over the scan area for the AgNW-OA film ( $< 25$  nm) makes these films suitable for use in thin-film devices. In contrast, AgNWs protrude from the drop-cast film up to 150 nm from the surface of the wafer.

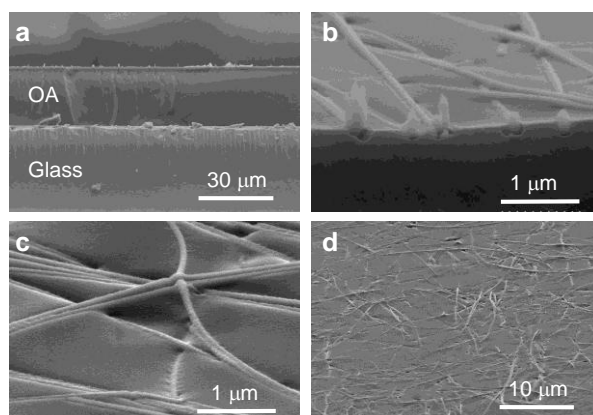


**Figure 3.2.** Structural features of AgNW-OA coatings. (a, b) Cross-sectional SEM images of a freeze-fractured AgNW-OA coating on glass ( $4 \Omega/\square$ ). (c, d) SEM images of the surface of an AgNW-OA coating ( $4 \Omega/\square$ ) on glass.

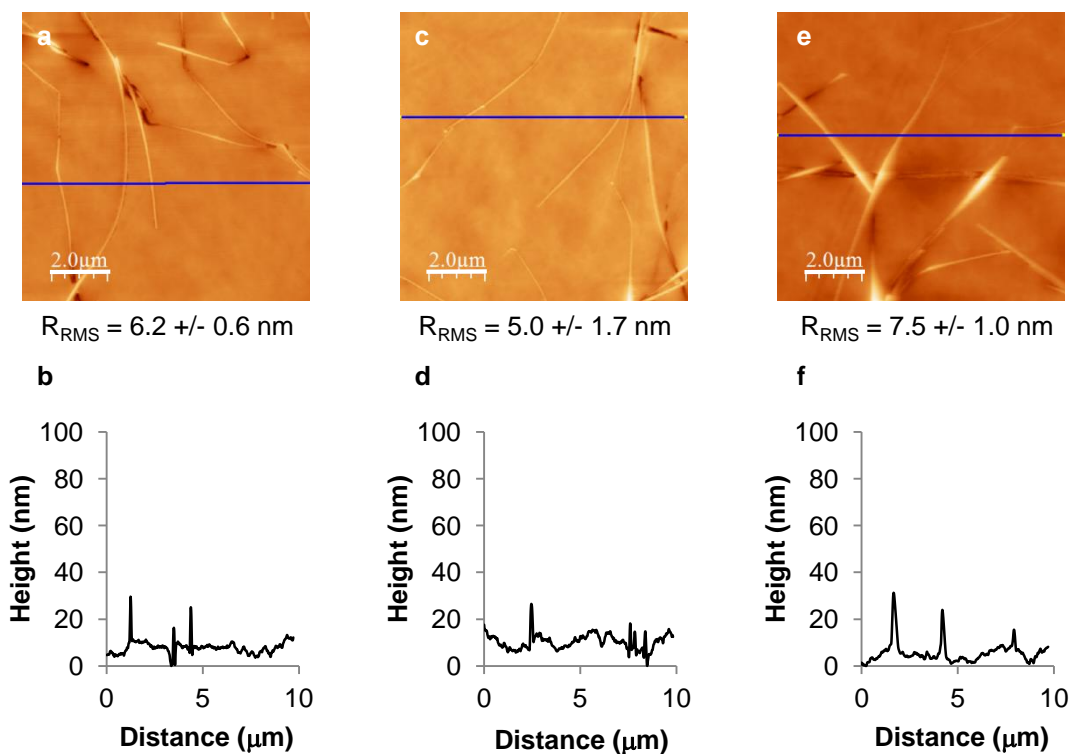


**Figure 3.3** AFM images ( $z$ -scale = 150 nm) with root-mean-squared (RMS) roughness measurements and corresponding profile measurements of AgNW-OA films ( $9 \Omega/\square$ ) on (a, b) Glass; (c, d) PDMS; (e, f) PET.

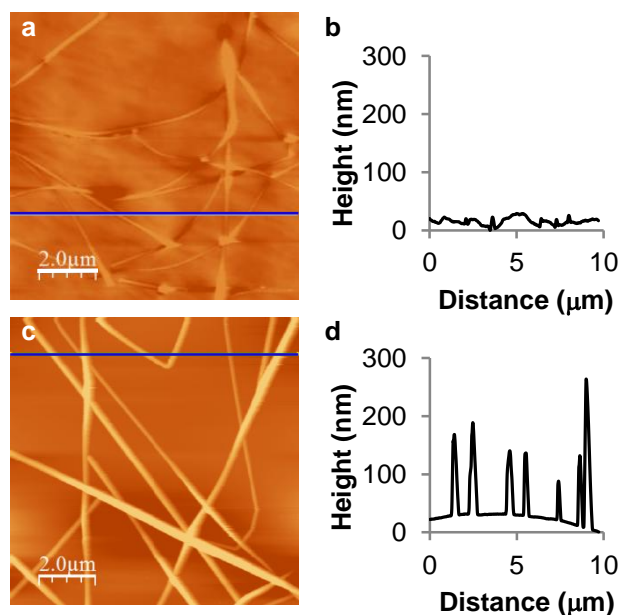


**Figure 3.4** Comparison of surface roughness of AgNW-OA coatings and drop-cast AgNW films. (a, b) AFM image and corresponding profile measurements of an AgNW-OA ( $14 \Omega/\square$ ) coating on PDMS. (c, d) AFM image and corresponding profile measurements of an AgNW film on a silicon wafer formed by drop casting.

### *3.3.4. Resilience of AgNW-OA Coatings*

AgNW-OA coatings are remarkably flexible. We measured the change in resistance of AgNW-OA ( $4 \Omega/\square$ ) coatings on 75- $\mu\text{m}$ -thick PET and 1-mm-thick PDMS substrates at various bending radii. A photograph of a bent AgNW-OA film on PDMS is shown in Figure 3.5a, and Figure 3.5b shows a plot of the change in resistance versus the tensile strain calculated according to the equation below:<sup>35</sup>

$$\varepsilon = d / 2r$$

where  $\varepsilon$  represents the tensile strain,  $d$  is the thickness of the substrate, and  $r$  is the radius of curvature. Remarkably, bending the films to radii as small as 0.65 mm produced a negligible change in resistance for AgNW-OA coatings on both PET (strain = 5.8 %)

and PDMS (strain = 76.9 %). The resistance of AgNW-OA films on PET increases less than two-fold ( $R/R_0 = 1.41 \pm 0.03$ ) when films are plastically deformed by creasing to a radius of  $\sim 0.1$  mm (37.5% tensile strain). In comparison, the resistance of ITO films on PET drastically increases to 88x the original value at 2% tensile strain;<sup>27</sup> that of AgNWs embedded into a polyacrylate substrate increases by 3.9x at 16% tensile strain.<sup>27</sup> We also tested the ability of AgNW-OA coatings to tolerate repeated bending by measuring the sheet resistance every 10 cycles for 250 cycles of 15% tensile strain (Figure 3.5c). We measured the sheet resistance in two directions by orienting a four-point probe to inject current parallel to, and then perpendicular to, the bending axis. Before bending, there was no difference in resistance in the two directions; however, we observed anisotropy in the resistance that increased with the number of strain cycles. After 250 cycles, the resistance parallel to the bending axis increased to 1.9x the initial value, whereas the resistance perpendicular to the bending axis decreased to 0.5x the initial value. We speculate that bending causes alignment of the AgNWs perpendicular to the bending axis, reducing the resistance. Similar effects have previously been reported for AgNWs deposited onto pre-stretched elastomeric substrates when the strain is released,<sup>36</sup> and for carbon nanotube fibers that have been embedded into a polymer matrix and uniaxially stretched.<sup>37,38</sup> Investigation of this possible alignment effect will be reported separately as it is beyond the scope of the present work.

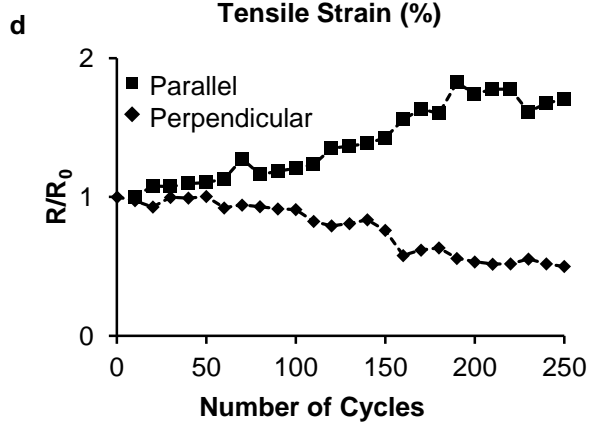
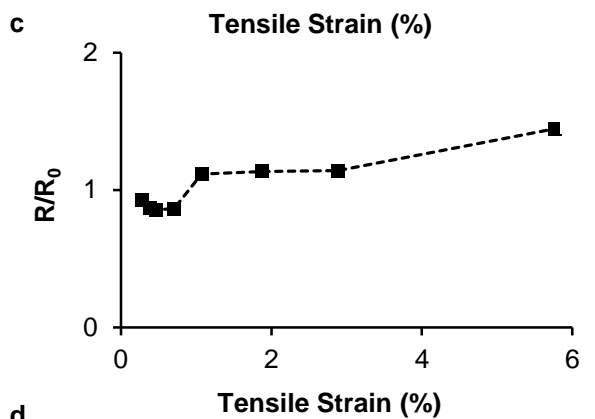
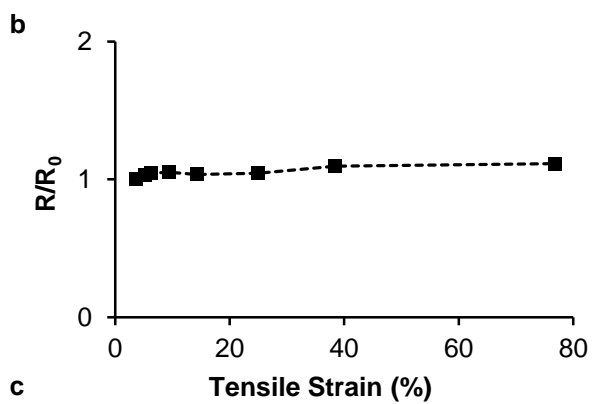
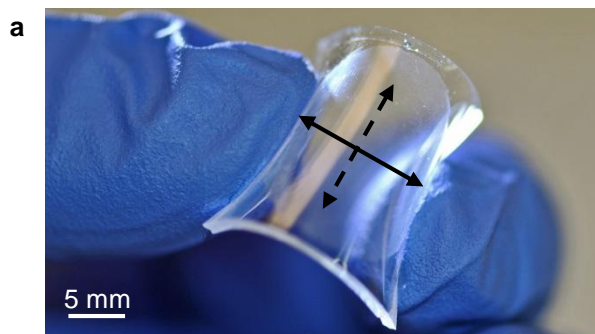


**Figure 3.5.** AgNW-OA coatings subjected to bending. (a) Photograph of a flexed AgNW-OA coating ( $14 \Omega/\square$ ) on PDMS. The solid line indicates that axis of bending; the dashed line indicates the perpendicular axis. (b) Change in resistance of AgNW-OA coatings ( $4 \Omega/\square$ ) on PDMS as a function of increasing tensile strain. (c) Change in resistance of AgNW-OA coatings ( $4 \Omega/\square$ ) on PET as a function of increasing tensile strain. (d) Change in resistance of AgNW-OA coatings ( $4 \Omega/\square$ ) on PDMS with repetitive cycles of 15% tensile strain measured with a four-point probe oriented to inject current along the bending axis (squares) and along the perpendicular axis (diamonds).

AgNW-OA coatings adhere strongly to the underlying substrate and are durable to marring, scratching, and solvent exposure. The AgNW-OA coatings pass the tape test without a change in resistance or deposition of observable residue on the adhesive surface of the tape. The resistance also remains constant after vigorous agitation with a gloved finger for 30 seconds (Table 3.2). We repetitively clamped and unclamped alligator clips with serrated edges to compare the effect of scratching on AgNW-OA coatings on glass to ITO/glass. Figure 3.6a shows a photograph of the alligator clips used for the testing clamped to an AgNW-OA film on glass; dark field optical micrographs in Figures 3.6b and 3.6c show the scratches on an AgNW-OA film on glass and an ITO film on glass, respectively, after 100 cycles of clamping and unclamping with the alligator clips. The resistance of AgNW-OA coatings on glass after cycles of repetitive clamping and unclamping of the same area of the film remained relatively constant through the testing cycles; after 200 cycles there was essentially no change in the resistance ( $R/R_0 = 1.23$ ). In contrast, the resistance of ITO films on glass showed greater variation in resistance with the testing cycles and a trend of increasing resistance. After 200 cycles, the resistance of the ITO film increased from  $48 \Omega$  to  $93 \Omega$ . Finally, we tested the effect of solvent exposure on AgNW-OA coatings on PDMS by immersion in water and ethanol for six hours. Similar to the other durability tests, solvent immersion had little effect on the resistance of the coating (Table 3.2).

**Table 3.2.** Change in resistance of AgNW-OA films ( $4 \Omega/\square$ ) on PDMS subjected to durability tests

	Adhesive Tape	Finger Friction	Immersion in Water	Immersion in EtOH
R/R <sub>0</sub>	1.02 +/- 0.02	0.99 +/- 0.03	0.93 +/- 0.10	0.97 +/- 0.15

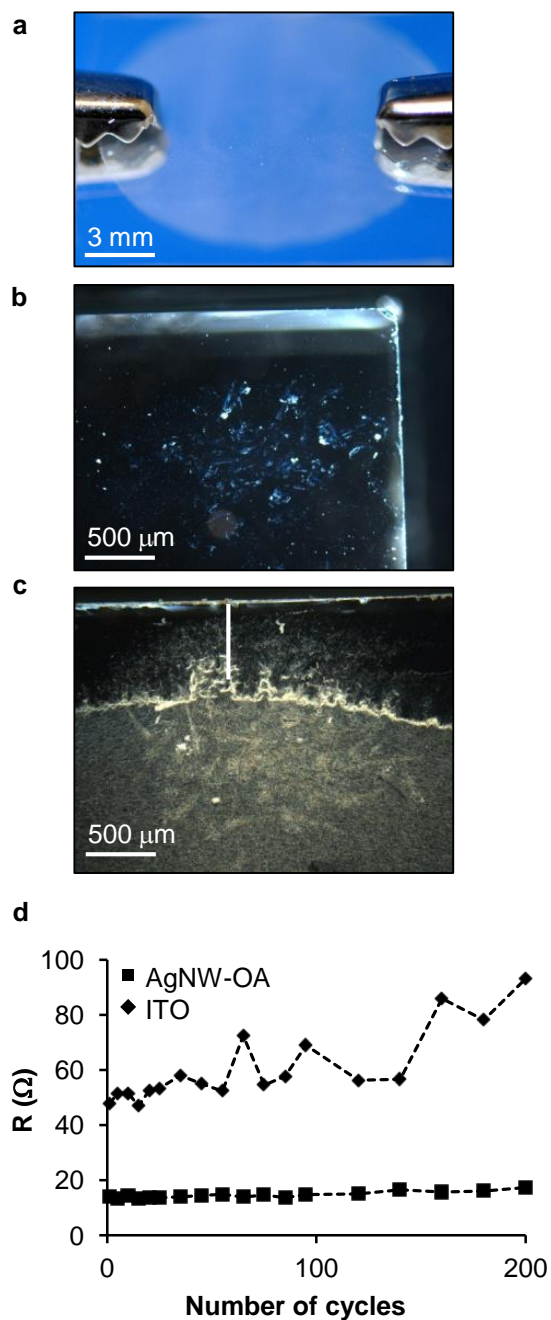


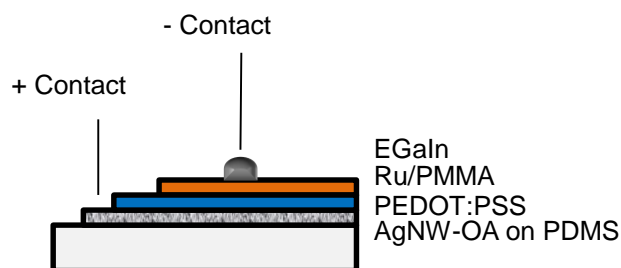
**Figure 3.6** a) Photograph of serrated alligator clips clamping onto a AgNW-OA ( $4 \Omega/\square$ ) coating on glass. b) Dark field optical micrograph showing ITO on glass after 100 clamping cycles. c) Dark field optical micrograph showing a AgNW-OA ( $4 \Omega/\square$ ) coating on glass after 100 clamping cycles. d) Resistance of AgNW-OA ( $4 \Omega/\square$ ) coatings on glass after 100 clamping cycles.

glass (squares) and ITO on glass (diamonds) measured after repetitive cycles of clamping and unclamping the same area with alligator clips.

### *3.3.5. Flexible, Light-Emitting Electrochemical Cells using AgNW-OA Anodes*

To demonstrate that the characteristics of AgNW-OA coatings make them well-suited for use in flexible devices, we fabricated flexible LEECs using AgNW-OA ( $14 \Omega/\square$ ) films on PDMS as the transparent anode and characterized the devices before and after cycles of bending. We chose the LEEC as our test structure due to its simple device architecture, which consists of a mixture of ionic and electronic conductors sandwiched between two metal electrodes.<sup>39,40</sup> The anode, cathode, and emissive layer support all three processes of charge injection, charge transport, and emissive recombination due to enhancement of charge injection that occurs at the electrodes.<sup>40-44</sup> This enhancement makes additional electron/hole injection, transport, and blocking layers unnecessary. The simplicity of the LEEC architecture has previously been exploited in the fabrication of intrinsically bendable and stretchable devices.<sup>27,30,45-47</sup> We fabricated flexible LEECs according to the device structure depicted in Scheme 3.2. The device consisted of the AgNW-OA anode with a spin-coated layer of PEDOT:PSS on the surface. The emissive layer was the ionic transition metal complex,  $\text{Ru}(\text{dtb-bpy})_3(\text{PF}_6)_2$ , dispersed in poly(methyl methacrylate) (PMMA). A drop of liquid gallium-indium eutectic (EGaIn) served as the cathode to complete the device. Unstrained devices produced bright, uniform emission over the entire area defined by the cathode. These devices continued to emit light when bent to radii of 7.0 mm, 3.0, and 1.5 mm (Figure 3.7). We compared the device characteristics of unstrained devices to devices subjected to 20 bending cycles of 25% tensile strain by recording the temporal evolution of current and radiance of the devices during ten minutes of operation at 5 V in ambient conditions and calculating the external quantum efficiencies (EQE) for the unstrained (Figure 3.8a and 3.8b) and strained devices (Figure 3.8c and d). Both devices reached their maximum EQE by < 90 s, followed by a decay in radiance over the testing period due to ambient moisture that degrades the ionic transition metal emitter.<sup>48</sup> Maximum EQEs of unstrained (0.57%) and

strained (0.82%) devices fall within the range of EQEs (0.4% - 0.9%) reported for LEECs with same emissive layer, an ITO anode on glass, and a gold laminated top contact.<sup>49</sup> Bending cycles thus do not negatively impact the device performance, indicating that the strain does not damage the components of the flexible LEECs.



**Scheme 3.2** Diagram of the device test structure

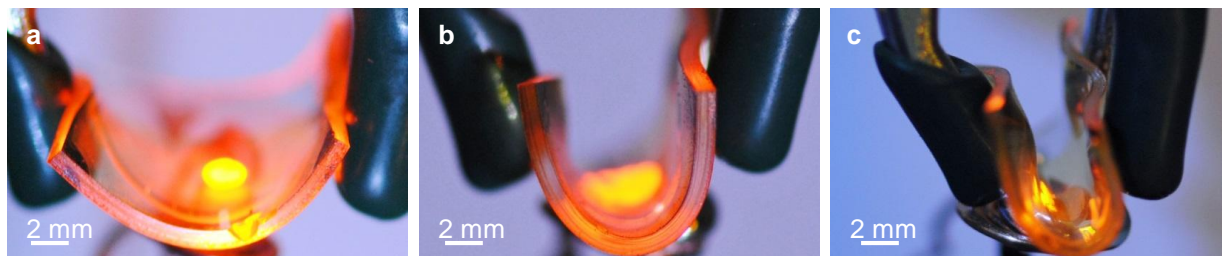


**Figure 3.7.** Photographs of flexible LEECs fabricated with AgNW-OA ( $14 \Omega/\square$ ) transparent anodes on PDMS, bent to radii of (a) 7.0 mm; (b) 3.0 mm; (c) 1.5 mm.

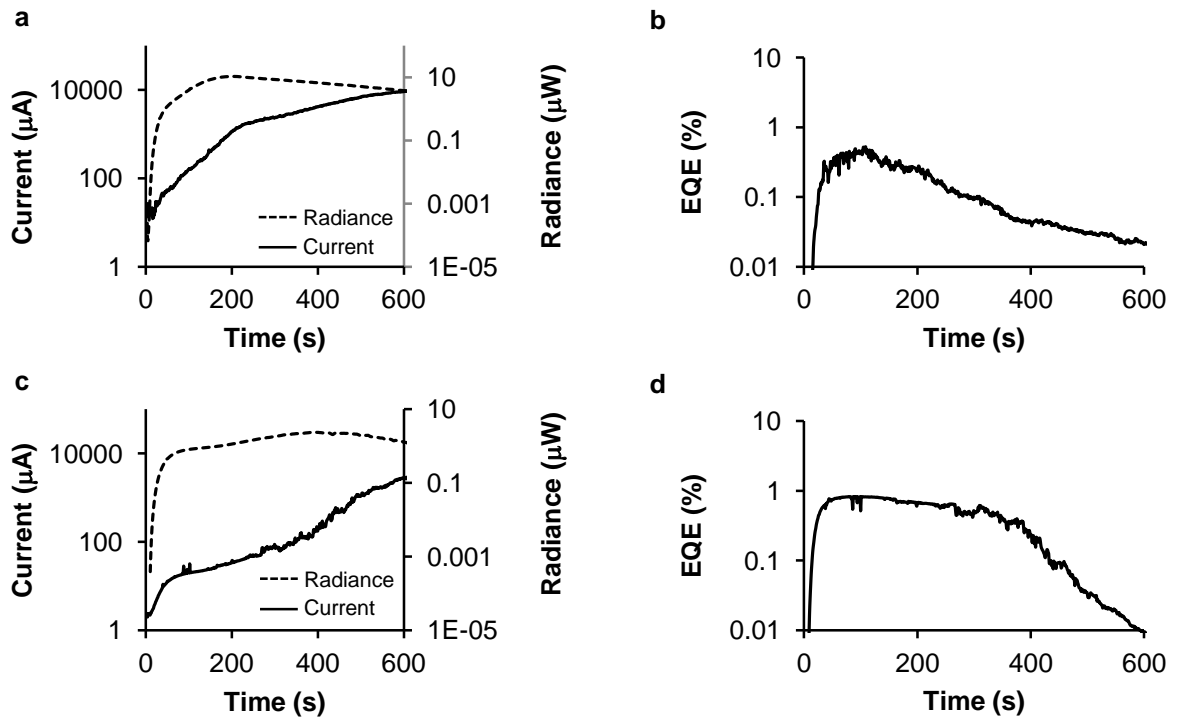


**Figure 3.8.** Characterization of unstrained devices and devices subjected to cycles of tensile strain. (a) Temporal evolution of current (solid line) and radiance (dotted line) of a typical unstrained device operated under a 5 V bias in ambient conditions. (b) Temporal evolution of EQE of a typical unstrained device operated under a 5 V bias in ambient conditions. (c) Temporal evolution of current (solid line) and radiance (dotted line) of a typical device after 20 bending cycles of 25% tensile strain operated under a 5 V bias in ambient conditions. (d) Temporal evolution of EQE of a typical device after 20 bending cycles of 25% tensile strain operated under a 5 V bias in ambient conditions.

### 3.4. Conclusions

Finding transparent conductive films to replace ITO is a highly active field of research that has generated a large body of literature. However, a successful replacement for ITO in flexible electronics must combine a number of essential features – high transparency, low sheet resistance, low surface roughness, good conductivity at high strains, and durability to repetitive strain – as well as being inexpensive and simple to fabricate. We

believe that AgNW-OA coatings can be instrumental in the development of flexible electronic devices because these coatings not only possess all of the essential features; they also use simple, commercially available materials in a straightforward and inexpensive fabrication scheme that can be applied to different flexible substrates, which potentially includes the highly impermeable plastics crucial to the development of flexible organic electronics. The ease of preparation and versatility of AgNW-OA coatings means they can easily be adopted by other research labs as flexible transparent electrodes to study new flexible electronic devices. Here, we have demonstrated their use as transparent electrodes in LEECs to show that the crosslinked optical adhesive of AgNW-OA coatings makes them compatible with the solvents used to fabricate the thin-film devices. Currently, the ideal application for AgNW-OA coatings is in lab-scale test structures due to the size of the AgNW-OA coatings that can be produced using the method described here, which is limited by the size of the filtration apparatus used to produce the initial AgNW network. We are currently developing methods to broaden the applicability of AgNW-OA coatings beyond the research lab by producing large-area AgNW networks that are compatible with our protocol for transferring and embedding in optical adhesive.

### 3.5. References

- (1) Mone, G. *Commun. ACM* **2013**, *56*, 16.
- (2) Cairns, D. R.; Crawford, G. P. *Proc. IEEE* **2005**, *93*, 1451.
- (3) Lewis, B. G.; Paine, D. C. *MRS Bull.* **2000**, *25*, 22.
- (4) Cao, Q.; Rogers, J. A. *Adv. Mater.* **2009**, *21*, 29.
- (5) Becerril, H. A.; Mao, J.; Liu, Z.; Stoltenberg, R. M.; Bao, Z.; Chen, Y. *ACS Nano* **2008**, *2*, 463.
- (6) Eda, G.; Fanchini, G.; Chhowalla, M. *Nat. Nanotechnol.* **2008**, *3*, 270.
- (7) Chang, Y.-M.; Wang, L.; Su, W.-F. *Org. Electron.* **2008**, *9*, 968.
- (8) Colsmann, A.; Stenzel, F.; Balthasar, G.; Do, H.; Lemmer, U. *Thin Solid Films* **2009**, *517*, 1750.
- (9) Do, H.; Reinhard, M.; Vogeler, H.; Puetz, A.; Klein, M. F. G.; Schabel, W.; Colsmann, A.; Lemmer, U. *Thin Solid Films* **2009**, *517*, 5900.
- (10) Krebs, F. C. *Org. Electron.* **2009**, *10*, 761.
- (11) Krebs, F. C. *Sol. Energy Mater. Sol. Cells* **2009**, *93*, 1636.
- (12) Galagan, Y.; Rubingh, J.-E. J. M.; Andriessen, R.; Fan, C.-C.; Blom, P. W. M.; Veenstra, S. C.; Kroon, J. M. *Sol. Energy Mater. Sol. Cells* **2011**, *95*, 1339.
- (13) Kang, M.-G.; Kim, M.-S.; Kim, J.; Guo, L. J. *Adv. Mater.* **2008**, *20*, 4408.
- (14) Gaynor, W.; Burkhard, G. F.; McGehee, M. D.; Peumans, P. *Adv. Mater.* **2011**, *23*, 2905.
- (15) Lee, J. Y.; Connor, S. T.; Cui, Y.; Peumans, P. *Nano Lett.* **2008**, *8*, 689.
- (16) Madaria, A. R.; Kumar, A.; Ishikawa, F. N.; Zhou, C. W. *Nano Res.* **2010**, *3*, 564.

- (17) Liu, C. H.; Yu, X. *Nanoscale Res. Lett.* **2011**, *6*, 75.
- (18) Hu, L. B.; Kim, H. S.; Lee, J. Y.; Peumans, P.; Cui, Y. *ACS Nano* **2010**, *4*, 2955.
- (19) Scardaci, V.; Coull, R.; Lyons, P. E.; Rickard, D.; Coleman, J. N. *Small* **2011**, *7*, 2621.
- (20) Akter, T.; Kim, W. S. *ACS Appl. Mater. Interfaces* **2012**, *4*, 1855.
- (21) De, S.; Higgins, T. M.; Lyons, P. E.; Doherty, E. M.; Nirmalraj, P. N.; Blau, W. J.; Boland, J. J.; Coleman, J. N. *ACS Nano* **2009**, *3*, 1767.
- (22) Lee, P.; Lee, J.; Lee, H.; Yeo, J.; Hong, S.; Nam, K. H.; Lee, D.; Lee, S. S.; Ko, S. H. *Adv. Mater.* **2012**, *24*, 3326.
- (23) Azulai, D.; Belenkova, T.; Gilon, H.; Barkay, Z.; Markovich, G. *Nano Lett.* **2009**, *9*, 4246.
- (24) Yang, L. Q.; Zhang, T.; Zhou, H. X.; Price, S. C.; Wiley, B. J.; You, W. *ACS Appl. Mater. Interfaces* **2011**, *3*, 4075.
- (25) Zeng, X. Y.; Zhang, Q. K.; Yu, R. M.; Lu, C. Z. *Adv. Mater.* **2010**, *22*, 4484.
- (26) Hu, W.; Niu, X.; Li, L.; Yun, S.; Yu, Z.; Pei, Q. *Nanotechnology* **2012**, *23*, 344002.
- (27) Yu, Z. B.; Zhang, Q. W.; Li, L.; Chen, Q.; Niu, X. F.; Liu, J.; Pei, Q. B. *Adv. Mater.* **2011**, *23*, 664.
- (28) Xu, F.; Zhu, Y. *Adv. Mater.* **2012**, *24*, 5117.
- (29) Leem, D. S.; Edwards, A.; Faist, M.; Nelson, J.; Bradley, D. D.; de Mello, J. C. *Adv. Mater.* **2011**, *23*, 4371.
- (30) Li, L.; Yu, Z.; Hu, W.; Chang, C. H.; Chen, Q.; Pei, Q. *Adv. Mater.* **2011**, *23*, 5563.

- (31) Rathmell, A. R.; Wiley, B. J. *Adv. Mater.* **2011**, *23*, 4798.
- (32) Burrows, P. E.; Graff, G. L.; Gross, M. E.; Martin, P. M.; Shi, M. K.; Hall, M.; Mast, E.; Bonham, C.; Bennett, W.; Sullivan, M. B. *Displays* **2001**, *22*, 65.
- (33) The static water contact angle of native PDMS was measured to be 114 °. The static water contact angle of glass, PET, and oxidized PDMS were measured to be < 10 °, 77 °, and < 10 °, respectively.
- (34) AgNW films made by drop-casting an identical AgNW volume and concentration on glass had a %T<sub>550nm</sub> = 89.6
- (35) Lewis, J. *Mater. Today* **2006**, *9*, 38.
- (36) Xu, F.; Durham, J. W.; Wiley, B. J.; Zhu, Y. *ACS Nano* **2011**, *5*, 1556.
- (37) Jin, L.; Bower, C.; Zhou, O. *Appl. Phys. Lett.* **1998**, *73*, 1197.
- (38) Iakoubovskii, K. *Cent. Eur. J. Phys.* **2009**, *7*, 645.
- (39) Slinker, J. D.; Rivnay, J.; Moskowitz, J. S.; Parker, J. B.; Bernhard, S.; Abruna, H. D.; Malliaras, G. G. *J. Mater. Chem.* **2007**, *17*, 2976.
- (40) Pei, Q. B.; Yu, G.; Zhang, C.; Yang, Y.; Heeger, A. J. *Science* **1995**, *269*, 1086.
- (41) Lenes, M.; Garcia-Belmonte, G.; Tordera, D.; Pertegas, A.; Bisquert, J.; Bolink, H. J. *Adv. Funct. Mater.* **2011**, *21*, 1581.
- (42) Slinker, J. D.; DeFranco, J. A.; Jaquith, M. J.; Silveira, W. R.; Zhong, Y. W.; Moran-Mirabal, J. M.; Craighead, H. G.; Abruna, H. D.; Marohn, J. A.; Malliaras, G. G. *Nat. Mater.* **2007**, *6*, 894.
- (43) deMello, J. C. *Phys. Rev. B* **2002**, *66*, 235210.
- (44) Rodovsky, D. B.; Reid, O. G.; Pingree, L. S. C.; Ginger, D. S. *ACS Nano* **2010**, *4*, 2673.

- (45) Filiatrault, H. L.; Porteous, G. C.; Carmichael, R. S.; Davidson, G. J. E.; Carmichael, T. B. *Adv. Mater.* **2012**, *24*, 2673.
- (46) Yu, Z. B.; Niu, X. F.; Liu, Z. T.; Pei, Q. B. *Adv. Mater.* **2011**, *23*, 3989.
- (47) Yu, Z. B.; Hu, L. B.; Liu, Z. T.; Sun, M. L.; Wang, M. L.; Gruner, G.; Pei, Q. B. *Appl. Phys. Lett.* **2009**, *95*, 203304.
- (48) Slinker, J. D.; Kim, J. S.; Flores-Torres, S.; Delcamp, J. H.; Abruna, H. D.; Friend, R. H.; Malliaras, G. G. *J. Mater. Chem.* **2007**, *17*, 76.
- (49) Bernards, D. A.; Biegala, T.; Samuels, Z. A.; Slinker, J. D.; Malliaras, G. G.; Flores-Torres, S.; Abruna, H. D.; Rogers, J. A. *Appl. Phys. Lett.* **2004**, *84*, 3675.

## **Chapter 4**

# **Templated Self-Assembly of Glass Microspheres into Ordered Two-Dimensional Arrays under Dry Conditions**

## 4.1. Introduction

This chapter describes a rapid, simple method for the self-assembly of ordered arrays of 100- $\mu\text{m}$  glass microspheres under dry conditions. We use a stream of nitrogen gas to deliver the microspheres to a template that consists of drops of liquid adhesive patterned on a solid surface; capillary bonds between the microspheres and the liquid drops hold the array in place. The geometry of the template defines the pattern of the microsphere array, which can be permanently fixed in place simply by curing the adhesive after self-assembly is complete. This work is the first example of a self-assembly process in which capillary bonds are used under dry conditions; in contrast, previous methods have relied on a liquid medium to suspend the components.<sup>1-2</sup> The problem with wet conditions is the potential incompatibility with electrically functional components, likely requiring the use of special protective packaging. The self-assembly method presented here is experimentally simple and rapidly produces ordered arrays of 100- $\mu\text{m}$  glass microspheres – simple models for electrically functional components – in a variety of 2D patterns over 2  $\text{cm}^2$  areas. Categorizing the types of defects in these arrays and relating their frequency to the density of binding sites in the template and the volume of the liquid adhesive drops provides insight into the self-assembly process and allows the template parameters and self-assembly conditions to be optimized, yielding 2D arrays with defect rates of  $\sim 4 - 5\%$ . We also demonstrate the versatility of this self-assembly method by manipulating the template to enable the sequential deposition of two different types of glass microspheres to produce ordered binary arrays.

Self-assembly is the spontaneous aggregation of components into larger, ordered structures without external intervention. It is an attractive fabrication methodology for two reasons: First, it creates arrays of components in parallel, making it faster and less expensive than serial pick-and-place component distribution. Second, a single self-assembly process can yield structures that are difficult or impossible to fabricate using conventional photolithography.<sup>3-5</sup> Of the many types of forces that have been used to drive self-assembly processes, capillary forces have been especially well-studied.<sup>1-2, 6-20</sup> Capillary forces between components exist due to interactions between the menisci that

form when components float on the surface of a liquid or are coated with a hydrophobic liquid and suspended in water. These capillary forces drive the components together to minimize the interfacial free energy of the system, resulting in the formation of capillary bonds that are strong enough to hold nanometre-<sup>6-8</sup>, micron-<sup>9-10</sup>, or even millimetre-scale<sup>11-12</sup> components together. When liquid films of adhesive or solder are used, the films can be solidified after self-assembly to yield permanent structures<sup>13-17</sup> and electrical connections.<sup>18-20</sup> Self-assembly schemes using capillary forces have yielded both 2D<sup>6-12</sup> and 3D<sup>13-20</sup> structures in which the particles form close-packed lattices, thus minimizing the free energy of the aggregate; however, these schemes do not provide control over the spacing of particles in the structure.

Templates that guide the placement of components are an effective way to dictate the final structure of self-assembled arrays. Self-assembly processes based on capillary forces have used surfaces bearing chemical patterns that define regions of differing surface free energies to successfully place components into specific array structures.<sup>21-22</sup> A typical experimental setup uses a template of adhesive drops fabricated by first patterning hydrophobic (hexadecanethiol, HDT) and hydrophilic (1-mercaptohexadecanoic acid) self-assembled monolayers (SAMs) on a gold film using microcontact printing. Passing the patterned substrate through a film of adhesive floating on water at a constant rate forms adhesive drops on the hydrophobic regions; this template binds hydrophobic components suspended in water to yield 2D particle arrays.

The main drawback with self-assembly methods that rely on capillary forces is that they have exclusively been used in schemes where the components are suspended in solution. This approach reduces gravitational forces and provides a convenient way to deliver the components to the template; however, wet conditions present a challenge for the self-assembly of electrically functional components, likely requiring encapsulation of the components to protect them from damage. In addition, the adhesive used to form the template must be less dense than water, eliminating many convenient photocurable epoxies and polyurethanes. Whitesides et al. have demonstrated dry self-assembly methods that eliminate the use of capillary forces, instead using electrostatic forces generated by an external applied electric field<sup>23-25</sup> to order glass microspheres on a

template. Although this method avoids the need for wet conditions, solidifying the resulting self-assembled structures into mechanically stable structures requires the transfer of the assembled structure into a secondary polymer matrix to provide mechanical stability. This method is also limited to the assembly of a single type of component across the template.

Our strategy for the self-assembly of extended 2D arrays uses gas flow to propel dry components – 100- $\mu\text{m}$  glass microspheres – toward a template of patterned liquid adhesive drops adhered to a solid surface. Microspheres that strike the dry portion of the template simply bounce off; those that impinge upon a drop of adhesive are first wet by the adhesive and then held in place via a capillary bond. This strategy combines three key attributes: First, it avoids the need for a liquidous medium, instead using dry conditions that are compatible with electrically functional components. Second, the capillary forces that hold components in place allow the assembly to be handled without disturbing the order of the array; the adhesive can then be cured to create a permanent structure. Third, the fabrication of the template can easily be manipulated to enable the sequential deposition of two different microsphere types to yield ordered binary lattices of microspheres.

## 4.2. Experimental Section

### *4.2.1. Materials*

All materials and chemicals were purchased from Aldrich used as received. Optical Adhesives NOA 83-H, NOA 89, NOA 73, or NOA 74 were purchased from Norland Products, Inc. (Cranbury, New Jersey). J-91 Epoxy was purchased from Summers Optical (Hatfield, Pennsylvania). 100- $\mu\text{m}$  glass microspheres (black and clear glass) were purchased from Whitehouse Scientific (Waverton, Chester, UK). PDMS stamps were prepared by casting PDMS prepolymer against photolithographic masters according to published procedures.<sup>26</sup>

#### *4.2.2. Template Fabrication*

Gold-coated silicon wafers were produced by depositing ~1 nm chromium as an adhesion promoter, followed by ~20 nm gold in an e-beam evaporator. Microcontact printing was used to pattern a hydrophobic HDT SAM on the gold surface. The pattern consisted of unmodified 40- $\mu\text{m}$  squares distributed in the HDT SAM according to the desired lattice geometry. The unprinted Cr/Au was removed by wet etching in a solution of 1 M KOH, 0.1 M  $\text{Na}_2\text{S}_2\text{O}_3$ , 0.01 M  $\text{K}_3\text{Fe}(\text{CN})_6$ , and 0.0001 M  $\text{K}_4\text{Fe}(\text{CN})_6$  for 20 minutes to expose hydrophilic  $\text{SiO}_2$  squares. A 0.5-mL drop of liquid adhesive (NOA 83-H, NOA 89, NOA 73, NOA 74, J-91 Epoxy) or molten polyethylene (PE, m.p. = 92 °C) was then applied to the patterned surface. Excess liquid was drained onto a paper towel, leaving a template of liquid adhesive or PE drops.

#### *4.2.3. Microsphere Self-Assembly*

A filtration frit with 15 mm diameter was loaded with 100 mg of glass microspheres (100  $\mu\text{m}$  diameter) and the template at a ~30° angle to the wall. A second filtration frit was clamped to the top of the first one and dry nitrogen (2 psi) was blown through the bottom frit for 1 minute. The microsphere array was removed from the apparatus. Templates made with UV-curable adhesives were cured under a 100 W mercury vapor lamp for 30 minutes. Templates made with PE were cooled to room temperature.

#### *4.2.4. Fabrication of Binary Lattices of Microspheres*

The template was fabricated from a substrate of  $\text{SiO}_2$  squares distributed in a background of an HDT SAM on gold (described above). Microcontact printing was used to transfer an OTS SAM to selected  $\text{SiO}_2$  squares by aligning an inked PDMS stamp by hand under an optical microscope. Molten PE was then assembled on the unpatterned squares and the template cooled to room temperature. The template was treated with an air plasma to remove the OTS and HDT SAMs, and then the HDT SAM was re-formed on the gold background by immersing the template in a 2 mM solution of HDT in ethanol for one hour. NOA 83-H was deposited on the remaining  $\text{SiO}_2$  squares and then clear

glass microspheres were assembled on these sites and the adhesive cured under a 100 W mercury vapour lamp for 30 minutes. Black glass microspheres were then assembled on the PE sites by heating the substrate to 100 °C during self-assembly to melt the PE.

#### *4.2.5. Characterization*

Optical inspection was performed using an Olympus BX51 microscope and a Leica MZ6 stereomicroscope. Profiles of cured drops were measured using a Dektak 3 Profilometer.

### 4.3 Results and Discussion

#### *4.3.1. Fabrication of the Template*

The template for self-assembly uses an underlying surface patterned with hydrophilic 40- $\mu\text{m}$  squares distributed in a hydrophobic background to direct the deposition of a liquid adhesive on the surface: The liquid wets regions with high surface free energy (the hydrophilic squares) and dewets from the hydrophobic background. This process has previously been used to fabricate arrays of microlenses<sup>27-29</sup> and waveguides<sup>30</sup> from liquid prepolymers. The initial hydrophilic/hydrophobic surface can be patterned by simply microcontact printing<sup>26</sup> a HDT SAM on a gold film to form the hydrophobic background, followed by removal of the unprinted Cr/Au using a ferricyanide/ferrocyanide wet etchant<sup>31</sup> to expose hydrophilic SiO<sub>2</sub> squares. A ~0.5 mL drop of UV-curable liquid adhesive (Norland Optical Adhesive (NOA) 83-H, 89, 73, or 74; Summers J-91 epoxy) or molten polyethylene (PE) applied to the hydrophobic/hydrophilic patterned surface initially covers the entire surface. Tilting the substrate and touching its edge to an absorbent cloth allows the liquid to drain from the surface; the liquid dewets from the hydrophobic background and remains on the hydrophilic squares, leaving a template of liquid adhesive drops selectively adhered to the hydrophilic squares (Figure 4.1a).

*Templated Self-Assembly of Glass Microspheres into Ordered Two-Dimensional Arrays Under Dry Conditions*

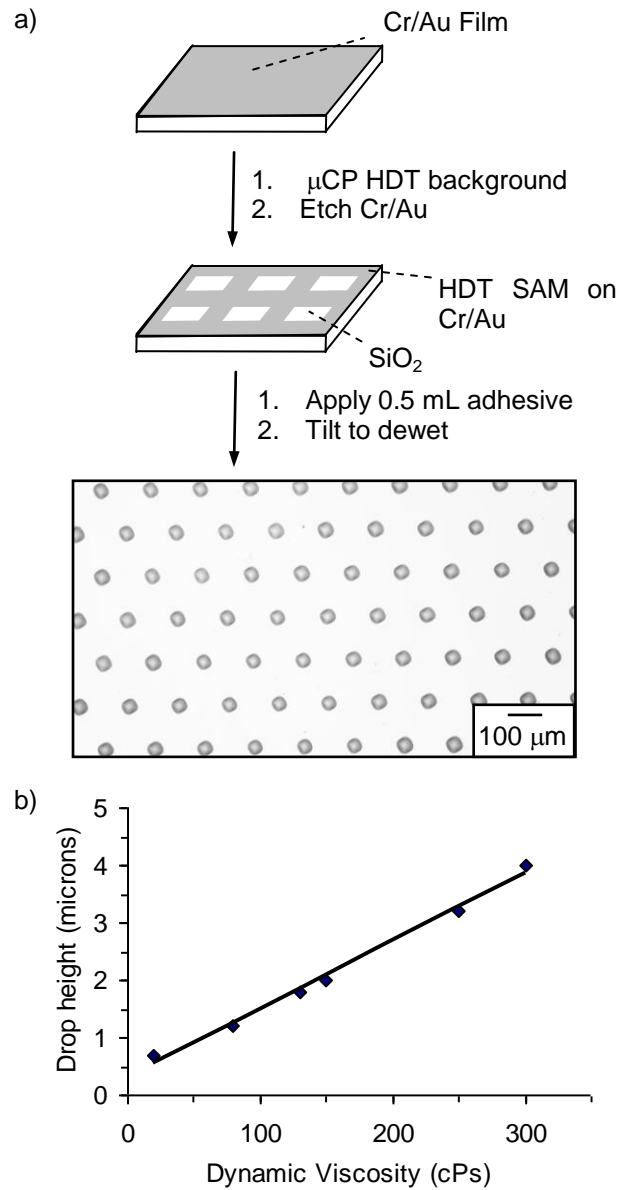


**Figure 4.1.** Fabrication of templates of liquid adhesive drops for self-assembly. a) Schematic of the process used to fabricate an array of adhesive drops on hydrophilic SiO<sub>2</sub> squares surrounded by a hydrophobic HDT SAM on gold, with optical micrograph of NOA 73 assembled on a hexagonal lattice consisting of 40  $\mu$ m hydrophilic squares distributed in a background of an HDT SAM on gold. b) Plot showing the approximately linear relationship between adhesive viscosity and the height of adhesive drops deposited on a template consisting of a square lattice of 40- $\mu$ m hydrophilic squares.

We characterized templates fabricated according to Figure 4.1a using optical microscopy and profilometry to determine how effectively liquid adhesive drops are confined to the hydrophilic squares and the uniformity of drop profiles across the template. Prior to inspection, the adhesive drops were solidified by exposing UV-curable adhesives to UV light from a mercury vapour lamp (100 W); the UV-curable adhesives exhibit only negligible volume and shape changes due to curing. Templates fabricated from molten PE were simply cooled to room temperature to solidify the drops. Inspection of the templates showed that drops of each type of adhesive uniformly fill the 40  $\mu\text{m}$  squares across the substrate. Adhesives do not deposit on the hydrophobic background, although occasional defects such as etch pits in the background gold film are sites for unwanted adhesive deposition. These defects are caused by air bubbles or dust particles that become trapped between the PDMS stamp and gold surface during microcontact printing. Drop profiles measured at several different locations over 2-cm<sup>2</sup> patterned substrates showed nearly identical adhesive structures with heights that depend on the viscosity of the liquid adhesive<sup>32</sup> used to fabricate the template. For example, NOA 89 (viscosity 20 cps) produced structures with a mean height of 0.7  $\mu\text{m}$ , whereas NOA 83-H (viscosity 250 cps) produced structures with a mean height of 3.2  $\mu\text{m}$ . In general, the height of the deposited drops is controlled by properties of the liquid (viscosity, surface tension, and density), variables associated with the coating procedure (the force pulling the liquid film down during dewetting and the angular orientation of the hydrophilic shapes with respect to the contact line of the dewetting liquid), and the geometry of the patterned surface (feature width and periodicity).<sup>33</sup> In our system, variables associated with the coating procedure and pattern geometry are constant and the drop height is controlled by the properties of the liquid adhesive. Although there is some variation in surface tension and density of the liquid adhesives, differences in viscosity are more significant. As the liquid adhesive dewets from the patterned surface, the viscosity of the adhesive resists the flow of the adhesive across the tilted substrate due to gravity: Adhesives with high viscosity resist this flow more strongly than adhesives with low viscosity, resulting in the deposition of a larger volume of liquid on the squares. The linear relationship between drop height (and hence the volume of adhesive deposited on

the surface) and adhesive viscosity is graphically represented in Figure 4.1b. Controlling the variables associated with template formation so that viscosity is the dominant factor influencing drop volume is a simple way to access templates with specific drop volumes and thus to evaluate the influence of adhesive drop volume on the quality of arrays of glass microspheres self-assembled on the templates.

### *4.3.2. Self-Assembly of Glass Microspheres*

We used the prepared templates for the self-assembly of dry glass microspheres with a 100  $\mu\text{m}$  diameter. A 2-cm<sup>2</sup> template and the microspheres were placed in a cylindrical glass chamber equipped at each end with a gas inlet/outlet and a fritted glass disc to prevent the microspheres from escaping (Figure 4.2a). A stream of nitrogen (2 psi) fluidized the microspheres, propelling them towards the template, which was held at a 30° angle to the chamber wall. Microspheres that strike an adhesive drop are wet by the adhesive and held in place by a capillary bond; those that strike the background region of the substrate simply bounce off. Self-assembly was complete after 1 minute; the array could be then be removed from the chamber and handled without damage due to the strong capillary bonds holding the microspheres in place. Curing the adhesive with UV light resulted in permanent, mechanically stable structures. Figure 4.2 b – e shows self-assembled arrays of glass microspheres demonstrated using templates with four different geometries: Arrays **1** and **2** (Figure 4.2b and 4.2c) are square lattices with distances between adjacent binding sites of 100  $\mu\text{m}$  and 500  $\mu\text{m}$ , respectively. Arrays **3** and **4** (Figure 4.2d and 4.2e) are hexagonal lattices with distances between binding sites of 100  $\mu\text{m}$  and 500  $\mu\text{m}$ , respectively.

*Templated Self-Assembly of Glass Microspheres into Ordered Two-Dimensional Arrays Under Dry Conditions*

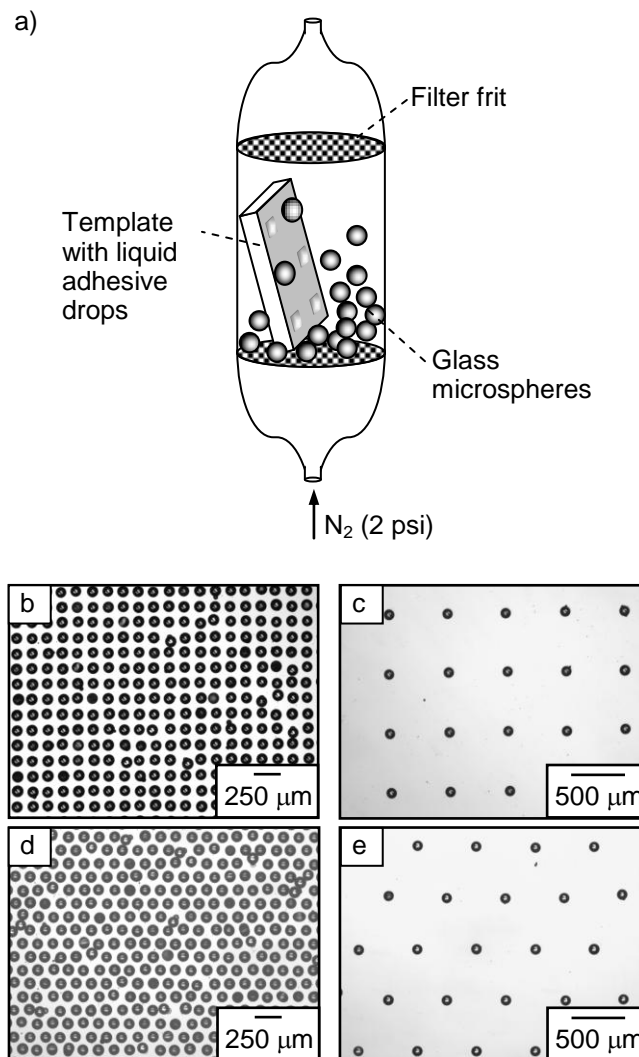


**Figure 4.2.** Self-assembly of glass microspheres of 100  $\mu\text{m}$  diameter on templates of liquid adhesive drops of NOA 73. a) Schematic of the experimental setup. The clamp holding the upper and lower filtration frits together is not shown for clarity. b – e) Optical micrographs of glass microspheres self-assembled on square lattice templates (b, c), and hexagonal lattice templates (d, e).

### *4.3.3. Defects in the Self-Assembled Structures*

The self-assembled structures have defects that appear even if self-assembly takes place over defect-free regions of the template, indicating that they arise during the self-assembly process. There are two categories of defects in the self-assembled structures: template binding sites lacking a bound microsphere (vacancies) and extra microspheres, which deposit on either the hydrophobic background or a binding site already occupied by a microsphere. We calculated overall defect rates ( $D$ ), in percent, for arrays **1** – **4** formed using adhesive drop heights of 0.7  $\mu\text{m}$  (Table 4.1) using Whitesides' method<sup>23-25</sup>:

$$D = (d/s) \times 100$$

where  $d$  is the number of defects and  $s$  is the number of sites. For each array, the number of defects and the number of sites were counted over a 7  $\text{mm}^2$  area of the template. Defect rates are averages of rates computed using three random areas on at least three different samples of each array. The defect rates for arrays with a dense packing of microspheres (**1** and **3**) are ~50 % lower than defect rates for arrays with a lower packing density (**2** and **4**). However, comparing defect rates for arrays with different packing densities can be misleading because small numbers of defects have a greater impact on defect rates for arrays with lower packing densities: For example, a single defect in a 7  $\text{mm}^2$  area of array **1**, which has 50 binding sites/ $\text{mm}^2$ , corresponds to a defect rate of 0.29 %, whereas a single defect in the same area of array **2**, which only has 4 binding sites/ $\text{mm}^2$ , corresponds to a defect rate of 3.6 %. Nonetheless, another contributing factor to the discrepancy in defect rates may be the greater background area available between binding sites in loosely-packed arrays **2** and **4**, which can accommodate more unwanted microspheres relative to the available background area in tightly-packed arrays **1** and **3**. We conducted a deeper investigation into this defect rate discrepancy by determining defect rates for each defect category for arrays **1** and **2** assembled on templates comprised of three different drop heights (Table 4.1). The detailed defect rate data for array **2** show that additional microspheres indeed dominate the overall defect rate and the defect rate due to additional microspheres increases dramatically as the adhesive drop height is

increased. Although this increase is much less dramatic for array **1**, additional microspheres still account for the majority of defects in these arrays.

The detailed defect rate study leads to two insights into the self-assembly process: First, the minor contribution that vacancies make to overall defect rates, regardless of the template geometry or adhesive drop height, indicates that the self-assembly process effectively delivers microspheres to the template that are held in place by capillary bonds. Second, the prevalence of extra microspheres in the absence of defects in the template indicates that the primary mechanism for defect formation must involve the redistribution of liquid adhesive during the self-assembly process. Control experiments using a “template” of an HDT SAM on gold without adhesive do not result in adhesion of glass microspheres to the surface, indicating that extra microspheres deposited in the background are held in place with adhesive. We believe the redistribution of adhesive occurs either when microspheres impinge on a liquid adhesive drop and bounce off, taking adhesive with them, or when they collide with a microsphere already bound to the template and knock it away. In either case, adhesive is transferred to mobile microspheres which may then collide with and adhere to background areas of the template. This hypothesis is supported by the observed increase in defect rates for array **2** as the adhesive drop height is increased: As the volume of adhesive increases, there is more adhesive available for redistribution. We do not observe the same defect rate increase in array **1**, which we attribute to the dense packing of microspheres in this array geometry that limits the binding of additional microspheres.

**Table 4.1.** Defect Rates<sup>[a]</sup> for Arrays **1 – 4** showing the effect of adhesive drop height and template geometry.

Array Geometry	Adhesive Drop Height ( $\mu\text{m}$ ) <sup>[b]</sup>	Defect Rate (Vacancies) (%) <sup>[c]</sup>	Defect Rate (Extra Microspheres) (%) <sup>[c]</sup>	Overall Defect Rate (%)
<b>1</b>	0.7	0.2	4.0	4.2
<b>1</b>	1.8	0.5	3.8	4.3
<b>1</b>	3.2	0.2	4.8	5.0
<b>2</b>	0.7	0.4	8.7	9.1
<b>2</b>	1.8	0.0	28.4	28.4
<b>2</b>	3.2	2.3	49.5	51.8
<b>3</b>	0.7	-	-	5.3
<b>4</b>	0.7	-	-	10.8

[a] Average defect rates determined using defect counts from a  $7\text{-mm}^2$  area of each array, repeated for three random areas on a minimum of three arrays, calculated using Whitesides' method.<sup>23-25</sup>

[b]  $0.7\ \mu\text{m}$  drops fabricated using NOA 89,  $1.8\ \mu\text{m}$  drops fabricated using NOA 73, and  $3.2\ \mu\text{m}$  drops fabricated using NOA 83-H

[c] Not obtained for arrays **3** and **4**

The defect rate study indicates that two modifications to the self-assembly process may reduce overall defect rates by preventing the redistribution of adhesive that leads to the inclusion of additional microspheres in the array. First, reducing the volume of adhesive drops comprising the template effectively lowers the defect rate. In this work, we have reduced this volume by simply reducing the viscosity of the adhesive. This approach does not allow optimization of the drop volume because adhesives with specific viscosities are not generally available. A better approach will be to reduce the area of the binding site, which will reduce the drop volume and may also reduce the incidence of multiple microspheres becoming bound to a single binding site. The second modification is the reduction of the kinetic energy of the microspheres, which must be low enough so that collisions between the microsphere and either an adhesive drop or a microsphere already bound to an adhesive drop do not result in redistribution of the adhesive. We have used the minimum gas pressure necessary to deliver the microspheres to the template in the self-assembly chamber. It is possible to reduce the kinetic energy of the microspheres further by lowering the nitrogen pressure; this modification will require redesigning the self-assembly chamber to bring the template closer to the microspheres. We envision a chamber in which the template is suspended parallel to the filtration frit holding the microspheres. In this way, the distance between template and microspheres, as well as the nitrogen pressure, could be optimized to produce arrays with low defect rates.

#### *4.3.4. Fabrication of Binary Lattices of Microspheres*

The dry self-assembly approach can be extended to fabricate binary lattices of two different particle types. There are few reported methods to integrate two different particle types in self-assembled arrays. Methods that use capillary forces between particles floating at a liquid-liquid interface<sup>34</sup> or contact electrification<sup>35</sup> between particles made of two different polymers produce only close-packed arrays. Other methods rely on the fabrication of sophisticated templates that integrate addressable electrical connections<sup>36</sup> or resistive heaters<sup>37</sup> to sequentially activate selected binding sites; a two-step self-assembly process yields the binary array. Our approach also uses the sequential

activation of binding sites and two-step self-assembly, but it benefits from simple and inexpensive template fabrication (Figure 4.3a). Beginning with hydrophilic SiO<sub>2</sub> squares distributed in a hydrophobic HDT-covered gold background, we use microcontact printing of octadecyltrichlorosilane (OTS) to render selected SiO<sub>2</sub> squares hydrophobic via formation of an OTS SAM. These squares are now “inactive”: Application of molten PE gives a template with PE drops assembled only on the unprinted SiO<sub>2</sub> squares. After solidifying the PE by cooling to room temperature, the OTS SAM is removed using air plasma and the HDT SAM is reformed on the gold background to render it hydrophobic. Since the solidified PE is also hydrophobic, subsequent application of the liquid adhesive NOA 83-H results in deposition only on the remaining hydrophilic SiO<sub>2</sub> squares. Self-assembly of microspheres takes place in two steps; we used two colors of glass microspheres to illustrate this process. First, clear glass microspheres are assembled on the liquid NOA 83-H binding sites and the adhesive cured using UV light. Second, black glass microspheres are assembled on the PE binding sites by heating the substrate during self-assembly to melt the PE. After cooling to room temperature, the self-assembled binary array is mechanically stable (Figure 4.3b).

*Templated Self-Assembly of Glass Microspheres into Ordered Two-Dimensional Arrays Under Dry Conditions*

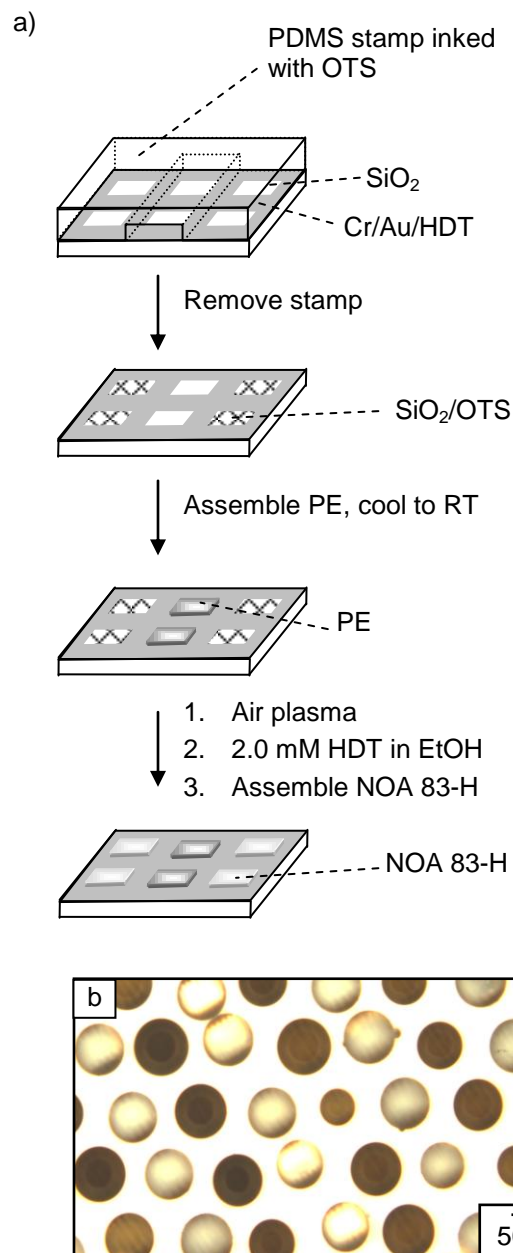


**Figure 4.3.** Self-assembly of a binary lattice of microspheres. a) Schematic of the process steps. b) Optical microscopy image of a hexagonal array fabricated from clear and black glass microspheres (100- $\mu\text{m}$  diameter) deposited along diagonal lines. Note that there is some variation in the size of the microspheres.

## 4.4. Conclusions

Our method for the self-assembly of microsphere arrays has several notable strengths: It is a rapid, economical way to generate component arrays and is potentially scalable to enable the self-assembly of large-area arrays. It uses dry conditions, making the process compatible with electrically functional components, in combination with capillary bonds to hold components in place and prevent misalignment of microspheres caused by handling. It uses a template to direct the self-assembly of the microspheres. This template can be designed to yield arrays of any geometry and can even be “encoded” to enable the self-assembly of two different particle types in a binary lattice. The main drawback to our self-assembly method is the incorporation of additional microspheres in the arrays, which causes high defect rates. We believe this problem can be solved via optimization of adhesive volume and microsphere kinetic energy.

## 4.5. References

- (1) Bowden, N. B.; Weck, M.; Choi, I. S.; Whitesides, G. M. *Acc. Chem. Res.* **2001**, *34*, 231.
- (2) Lin, C.; Tseng, F.; Chieng, C.-C. *J. Elec. Packaging* **2008**, *130*, 021005-1.
- (3) Wang, D.; Mohwald, H. *J. Mater. Chem.* **2004**, *14*, 459.
- (4) Parviz, B. A.; Ryan, D.; Whitesides, G. M. *IEEE Trans. Adv. Packag.* **2003**, *26*, 233.
- (5) Xia, Y.; Gates, B.; Yin, Y.; Lu, Y. *Adv. Mater.* **2000**, *12*, 693.
- (6) Yamaki, M.; Higo, J.; Nagayama, K. *Langmuir* **1995**, *11*, 2975.
- (7) Dushkin, C. D.; Lazarov, G. S.; Kotsev, S. N.; Yoshimura, H.; Nagayama, K. *Colloid. Polym. Sci.* **1999**, *277*, 914.
- (8) Nikoobakht, B.; Wang, Z. L.; El-Sayed, M. A. *J. Phys. Chem. B* **2000**, *104*, 8635.
- (9) Denkov, N. D.; Velev, O. D.; Kralchevsky, P. A.; Ivanov, I. B.; Yoshimura, H.; Nagayama, K. *Nature* **1993**, *361*, 26.
- (10) Lazarov, G. S.; Denkov, N. D.; Velev, O. D.; Kralchevsky, P. A. *J. Chem. Soc. Faraday Trans.* **1994**, *90*, 2077.
- (11) Bowden, N.; Choi, I. S.; Grzybowski, B. A.; Whitesides, G. M. *J. Am. Chem. Soc.* **1999**, *121*, 5373.
- (12) Bowden, N.; Arias, F.; Deng, T.; Whitesides, G. M. *Langmuir* **2001**, *17*, 1757.
- (13) Terfort, A.; Bowden, N.; Whitesides, G. M. *Nature* **1997**, *386*, 162.
- (14) Tien, J.; Breen, T. L.; Whitesides, G. M. *J. Am. Chem. Soc.* **1998**, *120*, 12670.
- (15) Clark, T. D.; Tien, J.; Duffy, D. C.; Paul, K. E.; Whitesides, G. M. *J. Am. Chem. Soc.* **2001**, *123*, 7677.

- (16) Breen, T. L.; Tien, J.; Oliver, S. R. J.; Hadzic, T.; Whitesides, G. M. *Science* **1999**, *284*, 948.
- (17) Boncheva, M.; Bruzewicz, D. A.; Whitesides, G. M. *Langmuir* **2003**, *19*, 6066.
- (18) Gracias, D. H.; Tien, J.; Breen, T. L.; Hsu, C.; Whitesides, G. M. *Science* **2000**, *289*, 1170.
- (19) Boncheva, M.; Gracias, D. H.; Jacobs, H. O.; Whitesides, G. M. *Proc. Nat. Acad. Sci.* **2002**, *99*, 4937.
- (20) Gracias, D. H.; Boncheva, M.; Omoregie, O.; Whitesides, G. M. *Appl. Phys. Lett.* **2002**, *80*, 2802.
- (21) Srinivasan, U.; Liepmann, D.; Howe, R. T. *J. Microelectromech. Syst.* **2001**, *10*, 17.
- (22) Jacobs, H. O.; Tao, A. R.; Schwartz, A.; Gracias, D. H.; Whitesides, G. M. *Science* **2002**, *296*, 323.
- (23) Winkleman, A.; Gates, B. D.; McCarty, L. S.; Whitesides, G. M. *Adv. Mater.* **2005**, *17*, 1507.
- (24) Zhu, T.; Suo, Z.; Winkleman, A.; Whitesides, G. M. *Appl. Phys. Lett.* **2006**, *88*, 144101.
- (25) Winkleman, A.; McCarty, L. S.; Zhu, T.; Weibel, D. B.; Suo, Z.; Whitesides, G. M. *J. Microelectromech. Syst.* **2008**, *17*, 900.
- (26) Xia, Y.; Whitesides, G. M. *Angew. Chem., Int. Ed. Engl.* **1998**, *37*, 550.
- (27) Biebuyck, H. A.; Whitesides, G. M. *Langmuir* **1994**, *10*, 2790.
- (28) Hartmann, D. M.; Kibar, O.; Esener, S. C. *Opt. Lett.* **2000**, *25*, 975.
- (29) Wu, M.-H.; Whitesides, G. M. *J. Micromech. Microeng.* **2002**, *12*, 747.

- (30) Kim, E.; Whitesides, G. M.; Lee, L. K.; Smith, S. P.; Prentiss, M. *Adv. Mater.* **1996**, *8*, 139.
- (31) Xia, Y.; Zhao, X.-M.; Kim, E.; Whitesides, G. M. *Chem. Mater.* **1995**, *7*, 2332.
- (32) Viscosities of adhesives: NOA 83-H (250 cps), NOA 73 (130 cps), NOA 74 (80 cps), NOA 89 (20 cps) Summers J-91 epoxy (300 cps), PE (150 cps)
- (33) Darhuber, A. A.; Troian, S. M.; Davis, J. M.; Miller, S. M.; Wagner, S. *J. Appl. Phys.* **2000**, *88*, 5119.
- (34) Choi, I. S.; Bowden, N.; Whitesides, G. M. *Angew. Chem., Int. Ed. Engl.* **1999**, *38*, 3078.
- (35) Grzybowski, B. A.; Winkleman, A.; Wiles, J. A.; Brumer, Y.; Whitesides, G. M. *Nature Mater.* **2003**, *2*, 241.
- (36) Xiong, X.; Hanein, Y.; Fang, J.; Wang, Y.; Wang, W.; Schwartz, D. T.; Bohringer, K. F. *J. Microelectromech. Syst.* **2003**, *12*, 117.
- (37) Sharma, R. *Langmuir* **2007**, *23*, 6843.

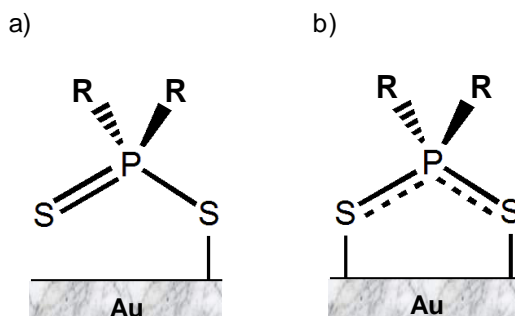
## **Chapter 5**

# **New Dialkyldithiophosphinic Acid Self Assembled Monolayers (SAMs): The Influence of Gold Substrate Morphology on Adsorbate Binding and SAM Structure**

## 5.1. Introduction

In this chapter we demonstrate that the morphology of the underlying gold substrate dictates the mode of head group binding and alkyl chain organization in new self-assembled monolayers (SAMs) of dialkyldithiophosphinic acids (dialkyl-DTPAs). Dialkyl-DTPA molecules are useful industrially as selective collectors for the flotation separation of precious metals from sulfide ores;<sup>1</sup> however, little is known about their ability to form SAMs on coinage metal surfaces.<sup>2-4</sup> As adsorbates, these molecules have two potential binding modes to gold surfaces: In the monodentate structure, the dialkyl-DTPA molecule is anchored by a single Au-S interaction; in the bidentate structure, a second Au-S interaction anchors the molecule at two points (Scheme 5.1). An important feature of the bidentate structure is the resonance generated between the two sulfur atoms,<sup>3</sup> making this binding mode applicable to molecular electronics. Here, we demonstrate that dihexadecyl-DTPA ((C<sub>16</sub>)<sub>2</sub>DTPA) molecules form stable SAMs on gold; furthermore, the roughness of the underlying gold surface is the cause of monodentate binding in the SAMs. Reducing the roughness of the gold substrate eliminates monodentate binding to produce SAMs in which all molecules exhibit the resonant bidentate structure. These morphology-induced differences in head group binding produce SAMs with distinctly different alkyl chain organizations, wettabilities, frictional responses, barrier properties, thickness, and thermal stabilities.

**Scheme 5.1.** Dialkyldithiophosphinic acid bound to a gold surface. (a) Monodentate binding. (b) Bidentate binding.



Gold films deposited by e-beam evaporation (As-Dep gold) are composed of a layer of contiguous grains with a dominant (111) texture.<sup>5</sup> Scanning tunneling microscopy (STM)<sup>6,7</sup> and atomic force microscopy (AFM)<sup>8,9</sup> studies have shown that although the tops of the grains are atomically flat, these terraces are relatively small and are separated by deep grain boundaries composed of atomic steps. These structural features lead to large root-mean-square (RMS) roughness values (30-50 Å).<sup>7-9</sup> When n-alkanethiolate SAMs are formed on As-Dep gold substrates, these atomic steps cause misalignment of adjacent alkyl chains and a consequent disruption of interchain van der Waals interactions.<sup>5</sup> In contrast, gold substrates produced by a process known as template stripping present a surface composed of larger, flatter grains; atomically-flat terraces possess diameters of 50-500 nm that differ by only 3-5 atomic steps in height.<sup>8-11</sup> This surface morphology results in a lower density of atomic steps and a lower RMS roughness (~ 3 Å) than As-Dep gold substrates. n-Alkanethiolate SAMs formed on template-stripped (TS) gold substrates exhibit better alignment of neighboring alkyl chains, which reduces the contact angle hysteresis.<sup>12,13</sup> Furthermore, forming molecular tunnel junctions using TS substrates reduces the large variance in junction resistance measurements and the incidence of failed junctions that is problematic with those formed using As-Dep substrates.<sup>14,15</sup>

Despite the influence of metal substrate morphology on n-alkanethiolate SAMs, there is a lack of research on how substrate morphology affects the binding and structure of SAMs comprised of adsorbates with head groups that are more complex than simple n-alkanethiols. On As-Dep metal substrates, the question is whether the deep grain boundaries disrupt optimal binding of the headgroup. For chelating adsorbates, this disruption may produce SAMs that incorporate monodentate adsorbates, which has an important consequence for molecular electronic devices: Monodentate species will diminish the molecule-metal coupling and consequently the electrical conductance.<sup>16</sup> High-resolution x-ray photoelectron spectroscopy (HR-XPS) of the S 2p spectral region of SAMs of chelating molecules such as dithiols,<sup>17,18</sup> trithiols,<sup>19,20</sup> dithiocarbamates,<sup>16,21-23</sup> dithiocarboxylic acids,<sup>24</sup> and xanthates<sup>25</sup> on As-Dep gold shows that these adsorbates chelate to the As-Dep gold surface, although this confirmation is difficult due to

problems with the low relative intensity of signals from surface-adsorbed species, resolution, and attenuation of the S 2p signal by the alkyl layer. Higher resolution and better signal-to-noise are achievable with synchrotron HR-XPS, which was used to establish that in SAMs of the chelating adsorbate di-isoamyl dithiophosphate (DTP) on As-Dep gold, a significant portion of surface-adsorbed species (40%) are monodentate.<sup>26</sup> Although the presence of monodentate adsorbates in these SAMs may be due to the geometry or steric demands of the DTP headgroup and alkyl substituents, the hypothesis that the morphology of the gold substrate plays a role in determining how the adsorbates bind to gold has not been tested. Here, we use a combination of techniques – HR-XPS, reflection-absorption infrared spectroscopy (RAIRS), contact angle measurements, lateral force microscopy (LFM), and electrochemical impedance spectroscopy (EIS) – to compare SAMs of chelating (C<sub>16</sub>)<sub>2</sub>DTPA molecules formed on both As-Dep and TS gold. We show that for these adsorbates, the different surface morphologies of As-Dep and TS gold produce SAMs with distinctly different properties. To our knowledge, this is the first study of the influence of substrate roughness on the structure of SAMs formed from chelating adsorbates.

## 5.2. Experimental Section

All chemicals were purchased commercially and used as received. Anhydrous tetrahydrofuran (THF), diethyl ether, and toluene were obtained from an Innovative Technologies solvent purification system. PDMS stamps were prepared by casting PDMS prepolymer against photolithographic masters according to published procedures.<sup>27</sup> Nuclear magnetic resonance (NMR) spectroscopic data were obtained and recorded on a Bruker Avance 300 MHz, a Bruker Avance 300 MHz Ultrashield or a Bruker Avance 500 MHz spectrometer at room temperature and reported in ppm. <sup>31</sup>P NMR spectra were referenced externally to 85% H<sub>3</sub>PO<sub>4</sub> ( $\delta = 0$  ppm). <sup>1</sup>H NMR spectra were referenced to residual proton peaks of CDCl<sub>3</sub> ( $\delta = 7.27$  ppm). <sup>13</sup>C NMR spectra were referenced to residual carbon peaks of CDCl<sub>3</sub> ( $\delta = 77.0$  ppm).

### 5.2.1. Dihexadecylphosphine Oxide

Magnesium turnings (2.0 g, 0.082 mol), 30 mL of anhydrous THF, and a crystal of iodine were added under nitrogen to a 250-mL, 3-neck round-bottom flask equipped with an addition funnel, a reflux condenser, and a gas adapter. 1-bromohexadecane (82.27 mmol) was then added dropwise, with stirring. After the mixture was refluxed overnight, it was cooled to room temperature and diethylphosphite (2.65 mL, 20.57 mmol) in 2.5 mL of anhydrous THF was added dropwise (Note: The addition of diethylphosphite is very exothermic; its addition to the reaction mixture must be done with caution). The solution was refluxed overnight, and the mixture was then cooled to room temperature and then it was slowly poured with stirring into 40 mL of 3 M hydrochloric acid. The THF was removed in vacuo, and then 40 mL of chloroform were added. After separation of the chloroform layer from the aqueous phase, the chloroform layer was washed with ~40 mL distilled water three times and dried with anhydrous Na<sub>2</sub>SO<sub>4</sub>. The solvent was evaporated under vacuum to yield dihexadecylphosphine oxide quantitatively. <sup>31</sup>P{<sup>1</sup>H} NMR (CDCl<sub>3</sub>, 202 MHz, 298 K): δ 35.7. <sup>1</sup>H NMR (CDCl<sub>3</sub>, 500 MHz, 298 K): δ 6.89 (d, |<sup>1</sup>J<sub>P-H</sub>| = 445 Hz, 1H, P-H), 1.86–1.70 (m, 4H, CH<sub>2</sub>), 1.64–1.52 (m, 4H, CH<sub>2</sub>), 1.44–1.41 (m, 4H, CH<sub>2</sub>), 1.33–1.26 (m, 48H, CH<sub>2</sub>), 0.88 (t, |<sup>3</sup>J<sub>H-H</sub>| = 6.93 Hz, 6H, CH<sub>3</sub>). <sup>13</sup>C{<sup>1</sup>H} NMR (CDCl<sub>3</sub>, 126 MHz, 298 K): δ 31.9 (s, CH<sub>2</sub>), 30.7 (d, |<sup>3</sup>J<sub>P-C</sub>| = 13.2 Hz, CH<sub>2</sub>), 29.3 (s, CH<sub>2</sub>), 28.4 (d, |<sup>1</sup>J<sub>P-C</sub>| = 63 Hz, CH<sub>2</sub>), 22.7 (s, CH<sub>2</sub>), 21.7 (s, CH<sub>2</sub>), 14.1 (s, CH<sub>3</sub>). Melting point range: 80–85°C.

### 5.2.2. Dihexadecylthiophosphinic Acid ((C<sub>16</sub>)<sub>2</sub>DTPA)

Dihexadecylphosphine oxide (1 g, 2.0 mmol) and LiAlH<sub>4</sub> (0.228 g, 6.01 mmol) were added under nitrogen to a 250-mL, 3-neck round bottom flask equipped with a gas adaptor, a reflux condenser and an addition funnel. 40 mL of anhydrous diethyl ether was then added dropwise, and the mixture refluxed overnight. The mixture was cooled to room temperature, and 40 mL of 3 M hydrochloric acid was added dropwise (vigorous bubbling occurs). After the bubbling ceases, a syringe equipped with a needle was used to remove the aqueous phase. Sulfur (0.129 g, 4.01 mmol) was then added to the organic

phase, followed by 40 mL of 3.5 M ammonium hydroxide solution. The mixture was heated to 50°C overnight and then cooled to room temperature. The organic phase was separated from the aqueous phase, acidified by slowly adding 20 mL of 6 M HCl solution, washed with distilled water three times, and dried over Na<sub>2</sub>SO<sub>4</sub>. The ether was removed by evaporation under vacuum and the product recrystallized from ethanol. Yield: 80%. <sup>31</sup>P {<sup>1</sup>H} NMR (CDCl<sub>3</sub>, 202 MHz, 298 K): δ 70.8. <sup>1</sup>H NMR (CDCl<sub>3</sub>, 500 MHz, 298 K): 2.17–2.08 (m, 4H, CH<sub>2</sub>), 1.73 (m, 5H, CH<sub>2</sub>, SH), 1.43–1.41 (m, 4H, CH<sub>2</sub>), 1.32–1.30 (m, 48H, CH<sub>2</sub>), 0.87 (t, |<sup>3</sup>J<sub>H-H</sub>| = 6.92 Hz, 6H, CH<sub>3</sub>). <sup>13</sup>C {<sup>1</sup>H} NMR (CDCl<sub>3</sub>, 126 MHz, 298 K): δ 38.8 (d, |<sup>1</sup>J<sub>P-C</sub>| = 50.3 Hz, CH<sub>2</sub>), 31.8 (s, CH<sub>2</sub>), 30.3 (d, |<sup>3</sup>J<sub>P-C</sub>| = 16.9 Hz, CH<sub>2</sub>), 29.3 (s, CH<sub>2</sub>), 22.9 (d, |<sup>2</sup>J<sub>P-C</sub>| = 4.39 Hz, CH<sub>2</sub>), 22.6 (s, CH<sub>2</sub>), 14.0 (s, CH<sub>3</sub>). Melting point range: 35–40°C. Anal. Calcd for C<sub>32</sub>H<sub>67</sub>PS<sub>2</sub>: C: 70.3%; H: 12.3%; P: 11.7%; S: 5.6%. Found: C: 70.9%; H: 12.3%; P: 11.1%; S: 4.8%.

### *5.2.3. Gold Substrate Preparation*

As-Dep gold films were produced by depositing 2 nm titanium as an adhesion promoter followed by ~200 nm gold onto silicon wafers using an e-beam evaporator. TS gold films were prepared according to published procedures.<sup>8</sup> 400 nm of gold was deposited onto silicon wafers, then a small drop (10 μL) of Norland Optical Adhesive 83-H was applied to the gold surface followed by a 2 cm x 2 cm glass substrate. After curing the adhesive using a UV lamp for 10 minutes the glass slide was stripped from the silicon wafer using a scalpel. Both As-Dep and TS gold films were used immediately after their fabrication to form SAMs to minimize surface contamination.

### *5.2.4. SAM Formation*

Approximately 2 cm x 2 cm As-Dep and TS gold substrates were immersed into a 1 mM (C<sub>16</sub>)<sub>2</sub>DTPA solution in anhydrous toluene or a 1 mM hexadecanethiol (C<sub>16</sub>SH) solution in anhydrous ethanol for 24 hours. Substrates were then removed from solution, rinsed with anhydrous toluene (for (C<sub>16</sub>)<sub>2</sub>DTPA SAMs) or anhydrous ethanol (for C<sub>16</sub>SH SAMs), and dried under a stream of nitrogen.

### *5.2.5. Sample Preparation for Lateral Force Microscopy*

Microcontact printing of C<sub>16</sub>SH onto gold substrates was carried out according to published procedures<sup>27</sup> using a PDMS stamp bearing 10- $\mu$ m-wide raised lines separated by 10- $\mu$ m-wide recesses. Printed gold substrates were rinsed with anhydrous ethanol, dried using a stream of nitrogen, and placed into a 2 mM toluene solution of (C<sub>16</sub>)<sub>2</sub>DTPA for 15 minutes. Substrates were removed from the solution, rinsed with anhydrous toluene and anhydrous ethanol, and dried under a stream of nitrogen.

### *5.2.6. Atomic Force Microscopy (AFM) and Lateral Force Microscopy (LFM)*

AFM and LFM images were obtained using a Digital Instruments Multimode atomic force microscope run in contact mode. Veeco type SNL (Silicon-tip on Nitride Lever) cantilevers were used with a nominal tip radius of 2 nm and a nominal force constant of 0.12 N/m. The back side of the cantilever was coated with 45 +/- 5 nm of Ti/Au. AFM images were collected over a 1  $\mu$ m x 1  $\mu$ m scan area using a scan rate of 0.5 Hz and a scanning resolution of 512 samples/line. LFM images were collected over a 75  $\mu$ m x 75  $\mu$ m scan area using a scan rate of 1.0 Hz, a scanning resolution of 512 samples/line, and a constant force of ~0.1 nN. Images were collected using Nanoscope 6 software, and processed using WSxM 5.0 Develop 1.0 software.<sup>28</sup>

### *5.2.7. X-Ray Photoelectron Spectroscopy (XPS)*

XPS spectra were collected at Surface Science Western (London, Ontario, Canada) using a Kratos Axis Nova X-ray photoelectron spectrometer with a monochromatic Al K $\alpha$  source. The detection limit of the instrument is 0.1 – 0.5 atomic percent. Both survey scan and high resolution analyses were carried out over a 300  $\mu$ m x 700  $\mu$ m scan area. Survey scan analyses were carried out with a pass energy of 160 eV, and high resolution analyses were carried out with a pass energy of 20 eV. Samples were analyzed at a 30 degree take-off angle (60 degree tilt). On both As-Dep and TS gold substrates, high resolution phosphorus line shapes were fit using one pair of spin-orbit split components

( $2p_{3/2}$  and  $2p_{1/2}$ ) assuming a Gaussian:Lorentzian (70%:30%) line shape and a fixed splitting energy of 0.84 eV with a 2:1 area ratio.<sup>29</sup> High resolution sulfur line shapes were fit using two pairs (As-Dep gold) or one pair (TS gold) of spin-orbit-split components ( $2p_{3/2}$  and  $2p_{1/2}$ ) assuming a Gaussian:Lorentzian (70%:30%) line shape and a fixed splitting energy of 1.18 eV with a 2:1 area ratio.<sup>29</sup>

### *5.2.8. Infrared Spectroscopy*

Reflection-absorption infrared (RAIR) spectra were collected using a Bruker IFS 66/v spectrometer equipped with an MCT detector and Harrick Autoseagull accessory. The p-polarized light was incident at 85° from the surface normal; 1024 scans were collected at a resolution of 2 cm<sup>-1</sup>.

### *5.2.9. Contact Angle Measurements*

Water and hexadecane contact angles were measured using the sessile drop method on a Rame-Hart contact angle goniometer. A minimum of three drops from three samples were averaged.

### *5.2.10. Electrochemical Impedance Spectroscopy (EIS)*

EIS spectra were collected using a BAS-Zahner IM6 ex impedance unit. A glass cell equipped with a calomel/saturated KCl reference electrode and a 1.0 mm Pt wire counter electrode was clamped to the working electrode, a 0.95-cm<sup>2</sup> area of the SAM on gold, and then filled with an aqueous solution of 1mM K<sub>3</sub>Fe(CN)<sub>6</sub>, 1mM K<sub>4</sub>Fe(CN)<sub>6</sub>·3H<sub>2</sub>O and 10 mM Na<sub>2</sub>SO<sub>4</sub>. The measurements were made at an open circuit potential set at 450 mV with a 10 mV ac perturbation that was controlled from 3.0×10<sup>-2</sup> to 1.0×10<sup>5</sup> Hz. SAM resistance and capacitance values were normalized to the area of the working electrode.

### *5.2.11. Thermal Desorption*

Gold substrates bearing (C<sub>16</sub>)<sub>2</sub>DTPA or C<sub>16</sub>SH SAMs were immersed into 50 mL of decahydronaphthalene at 70 °C. The decahydronaphthalene was stirred intermittently to maintain the desired temperature within +/- 2 °C, but not stirred while substrates were immersed. After the required immersion time, substrates were removed, immediately

rinsed with anhydrous ethanol, and dried under a stream of nitrogen. Contact angles were measured immediately after drying. A new substrate was used for each immersion time (i.e., substrates were not re-used after measuring contact angles), and a minimum of three measurements for each immersion time were averaged.

## 5.3. Results and Discussion

### 5.3.1. Gold Substrate Fabrication and SAM Formation

We prepared As-Dep gold films by e-beam evaporation on silicon wafers and TS gold films by template-stripping<sup>8</sup> for use as substrates for (C<sub>16</sub>)<sub>2</sub>DTPA SAMs. Characterization of the substrates by contact-mode AFM (Figure 5.1) showed the differences in surface morphologies of these two substrates. The As-Dep gold surfaces consisted of grains with an average size of ~50 nm, separated by boundaries as deep as 10 nm (Figure 5.1a). In contrast, the surface of TS gold is composed of large grains that range in size from 200-500 nm. The AFM cross-sectional profile of a 200-nm grain (Figure 5.1b) shows that the grains are separated by grain boundaries < 2 nm in depth. These different surface morphologies produce RMS roughness values of 27 Å for As-Dep gold surfaces and 5 Å for TS gold surfaces.

For SAM formation, As-Dep gold substrates were used immediately after removal from the e-beam evaporator and TS gold substrates were used immediately after template-stripping to minimize contamination of the gold surface. We used a modified synthetic route derived from Guoxin *et al.*<sup>30</sup> to prepare (C<sub>16</sub>)<sub>2</sub>DTPA in 80% yield and formed (C<sub>16</sub>)<sub>2</sub>DTPA SAMs on As-Dep and TS substrates by immersing the substrates in 1 mM (C<sub>16</sub>)<sub>2</sub>DTPA solutions in toluene for 24 hours.

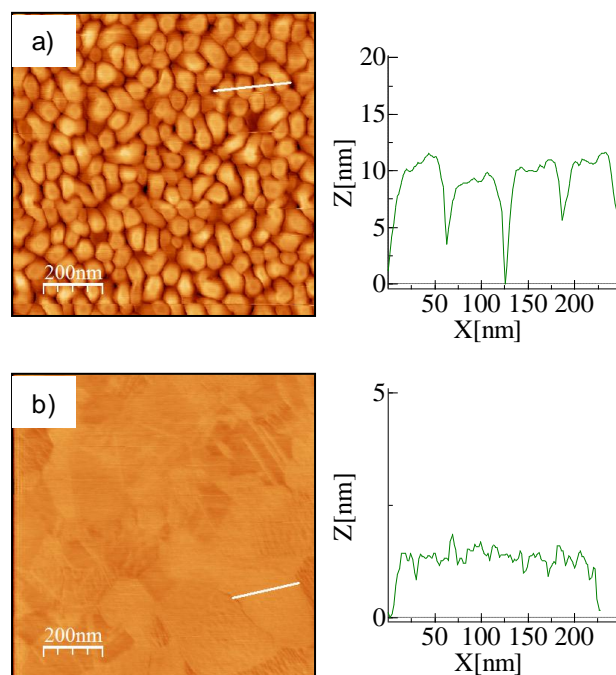


**Figure 5.1.** AFM topographic images recorded in contact mode of the (a) As-Dep gold film and (b) TS gold film. In both images the vertical scale is 20 nm. The white line shows the region that corresponds to the cross-sectional-profile depicted beside each image.

### 5.3.2. $(C_{16})_2DTPA$ Head Group Binding on As-Dep and TS

#### *Substrates*

XPS survey scans of  $(C_{16})_2DTPA$  SAMs on both As-Dep and TS substrates detected gold as well as the elements comprising the  $(C_{16})_2DTPA$  adsorbates (carbon, phosphorus, and sulfur) (Figure S5.1). The appearance of the O 1s line in both survey spectra indicates that SAM formation does not prevent the adsorption of a small amount of oxygen-containing species; however, HR-XPS spectra of the S 2p region of both SAMs did not show peaks due to oxidized sulfur species,<sup>31,32</sup> indicating that the  $(C_{16})_2DTPA$  adsorbate is not oxidized. HR-XPS of the S 2p region of the  $(C_{16})_2DTPA$  SAM on As-Dep gold (Figure 5.2a) showed a complex line shape that we fit using two pairs of spin-orbit-split components (S 2p<sub>3/2</sub> and S 2p<sub>1/2</sub>) by assuming a Gaussian:Lorentzian

(70%:30%) line shape and a splitting energy fixed at 1.18 eV.<sup>29</sup> In contrast, the HR-XPS spectrum of the S 2p region on TS gold (Figure 5.2b) showed a simpler line shape that we fit using only one spin-orbit-split pair. The binding energies and the relative concentrations of the sulfur species for SAMs on As-Dep and TS gold are listed in Table 5.1. Previous XPS studies of sulfur-containing SAMs on gold have clearly demonstrated that the electronic environment of the sulfur atom and the nature of the interaction between sulfur and gold surface atoms affect S 2p binding energies.<sup>33,34</sup> Based on these studies, we assign the S 2p<sub>3/2</sub> peak at 161.9 eV for the SAM on As-Dep gold and S 2p<sub>3/2</sub> peak at 161.5 eV for the SAM on TS gold to a sulfur species chemisorbed on gold. The second doublet found on As-Dep gold at 163.4 eV can be attributed to sulfur that is not interacting with the gold surface. On As-Dep gold, there are two possible explanations for the presence of both chemisorbed and non-interacting sulfur: The non-interacting sulfur could be due to physisorption or the formation of monodentate (C<sub>16</sub>)<sub>2</sub>DTPA adsorbates. Physisorption is unlikely due to the strong chemical bond that can form between the thiol group and gold substrate. Monodentate adsorption would produce one S 2p peak for the chemisorbed sulfur at low binding energy and one S 2p peak for the non-interacting sulfur at high binding energy, in a 1:1 ratio. The integrated atomic ratio of chemisorbed:non-interacting sulfur observed for the (C<sub>16</sub>)<sub>2</sub>DTPA SAM on As-Dep gold was 80:20, which corresponds to a SAM that contains both bidentate and monodentate (C<sub>16</sub>)<sub>2</sub>DTPA adsorbates in a 60:40 ratio. On TS gold, the absence of non-interacting sulfur indicates that all sulfur atoms are chemisorbed to gold, and hence all (C<sub>16</sub>)<sub>2</sub>DTPA molecules are bidentate.

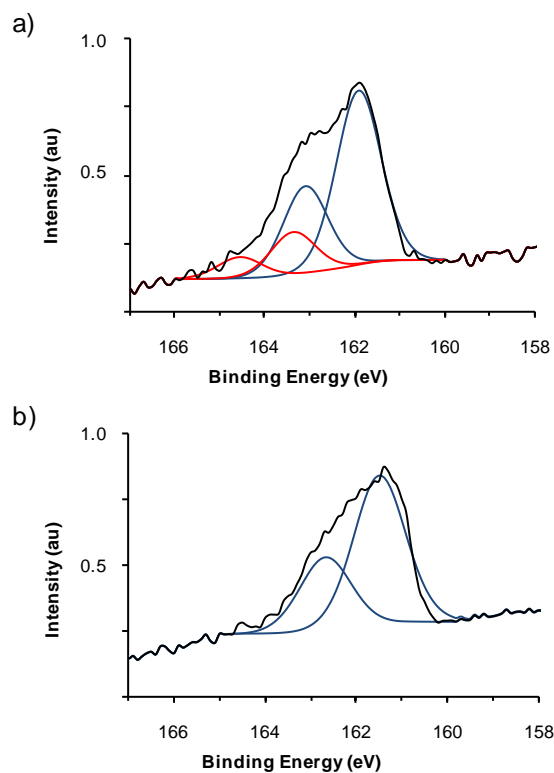


**Figure 5.2.** HR-XPS spectra of the S 2p region for  $(C_{16})_2$ DTPA SAMs formed on (a) As-Dep gold and (b) TS gold.

**Table 5.1.** S 2p and P 2p doublet binding energies in eV, abundances, and peak assignments for (C<sub>16</sub>)<sub>2</sub>DTPA SAMs formed on As-Dep gold and TS gold.<sup>[a]</sup>

	Binding Energy (eV)	Abundance (%)	Assignment
<i>(C<sub>16</sub>)<sub>2</sub>DTPA on As-Dep Gold</i>			
S 2p <sub>3/2</sub>	161.9 (blue)	80	Chemisorbed S
S 2p <sub>3/2</sub>	163.4 (red)	20	Non-interacting S
P 2p <sub>3/2</sub>	133.6	100	
<i>(C<sub>16</sub>)<sub>2</sub>DTPA on TS-Dep Gold</i>			
S 2p <sub>3/2</sub>	161.5 (blue)	100	Chemisorbed S
P 2p <sub>3/2</sub>	131.4	100	

<sup>[a]</sup> Doublet colors refer to fits in Figure 5.2.

The presence of monodentate binding in SAMs formed from chelating adsorbates on As-Dep gold substrates has previously been reported for the chelating adsorbate DTP,<sup>26</sup> which has the same P(S)(SH) headgroup as (C<sub>16</sub>)<sub>2</sub>DTPA. In this study, synchrotron HR-XPS provided higher resolution and better signal-to-noise than conventional HR-XPS, and enabled the fitting of the complex S 2p envelope with three S 2p doublets that were assigned to chemisorbed sulfur, a sulfur species chemisorbed in a low-density environment, and non-interacting sulfur. The overall ratio of chemisorbed:non-interacting sulfur was 80:20, corresponding to a ratio of bidentate to monodentate DTP adsorbates of 60:40, identical to what we have observed for (C<sub>16</sub>)<sub>2</sub>DTPA SAMs on As-Dep gold. The benefits of using a synchrotron source for XPS also enabled the fitting of three P 2p doublets, corresponding to three different types of DTP molecules: DTP

molecules chemisorbed in a low density environment, DTP molecules chemisorbed in a high-density environment, and monodentate DTP molecules. For our  $(C_{16})_2DTPA$  SAMs on As-Dep gold, the P 2p photoemission peaks in both spectra consisted of only a single P 2p doublet with the  $2p_{3/2}$  peak at 133.6 eV for SAMs on As-Dep gold and 131.4 eV for SAMs on TS gold (Figure S5.2). Although it was possible to resolve two sulfur species on As-Dep gold, the lower cross-section of phosphorus compared to sulfur (relative sensitivity factors of 0.486 and 0.668, respectively) means that for phosphorus, we are at or near the detection limit of our conventional XPS instrument. The poor signal-to-noise ratio achievable for the P 2p signal, combined with the fact that the P 2p signal is located along the large inelastic background of the Au 4f peaks, precluded the resolution of different phosphorus species.

Why are monodentate  $(C_{16})_2DTPA$  molecules present in  $(C_{16})_2DTPA$  SAMs on As-Dep gold and not on TS gold? There are two possibilities: The different morphologies of the two substrates may either affect the kinetics of SAM formation or directly affect how  $(C_{16})_2DTPA$  molecules bind to the surfaces. We can discount a kinetic effect: Forming  $(C_{16})_2DTPA$  SAMs by immersing As-Dep and TS gold substrates into 1 mM  $(C_{16})_2DTPA$  solutions in toluene for 5 minutes, 24 hours, and 48 hours consistently produced SAMs with 60% bidentate and 40% monodentate adsorbates on As-Dep gold and 100% bidentate adsorbates on TS gold (Figure S5.3). We propose that the dense network of deep grain boundaries on As-Dep gold prevents  $(C_{16})_2DTPA$  molecules from chelating at these sites; however, chelation can occur on the atomically-smooth tops of the gold grains. SAMs are thus comprised of both mono- and bidentate adsorbates. In contrast, the larger, flatter grains that make up TS gold substrates present a larger area of atomically-smooth surface that allows bidentate  $(C_{16})_2DTPA$  binding, and the grain boundaries are not deep or numerous enough to disrupt chelation.

### *5.3.3. Organization of the Organic Layers*

The different binding modes exhibited by  $(C_{16})_2DTPA$  molecules on As-Dep and TS gold substrates dramatically affect the packing and crystallinity of the hexadecyl chains, which we characterized using RAIRS and contact angle measurements. In the RAIR

spectra, peak frequencies of symmetric and asymmetric methylene stretches are an indication of the crystallinity of the alkyl chains.<sup>35</sup> RAIR spectra of (C<sub>16</sub>)<sub>2</sub>DTPA SAMs on both As-Dep and TS gold are shown in Figure 5.3; peak frequencies are given in Table 5.2.  $\nu_s(\text{CH}_2)$  and  $\nu_{as}(\text{CH}_2)$  appear at 2850 cm<sup>-1</sup> and 2918 cm<sup>-1</sup> for (C<sub>16</sub>)<sub>2</sub>DTPA SAMs on As-Dep gold, indicating that the alkyl chains are crystalline; in contrast, the  $\nu_s(\text{CH}_2)$  and  $\nu_{as}(\text{CH}_2)$  for (C<sub>16</sub>)<sub>2</sub>DTPA SAMs on TS gold appear at 2854 cm<sup>-1</sup> and 2925 cm<sup>-1</sup>, indicating a disordered, liquid-like alkyl layer that contains gauche defects. In comparison, RAIR spectra of hexadecanethiolate (C<sub>16</sub>SH) SAMs are not affected by the morphology of the substrate. On both As-Dep and TS gold substrates  $\nu_s(\text{CH}_2)$  and  $\nu_{as}(\text{CH}_2)$  appear at 2850 cm<sup>-1</sup> and 2918 cm<sup>-1</sup> respectively (Table 5.2). We contend that the difference in alkyl chain organization of (C<sub>16</sub>)<sub>2</sub>DTPA SAMs on As-Dep and TS gold is a consequence of the presence of monodentate DTPA molecules on the former substrate and the absence of this binding mode on the latter. Bidentate DTPA molecules are anchored at two points, preventing rotation about the Au-S bonds and fixing the Au-S-P bond angles; the tetrahedral geometry at phosphorus prevents the alkyl chains from packing closely. On TS gold, the presence of only bidentate DTPA molecules thus inhibits van der Waals interactions between alkyl chains, making this layer disordered and loosely packed. The monodentate DTPA molecules in the SAM on As-Dep gold, however, are anchored by a single point. The (C<sub>16</sub>)<sub>2</sub>DTPA molecules can rotate about the Au-S bond and the Au-S-P bond angle is no longer fixed; this flexibility enables alkyl group packing and increased van der Waals interactions. Relative peak intensities of methylene and methyl symmetric stretches support the notion that the average molecular tilt angle from the surface normal of (C<sub>16</sub>)<sub>2</sub>DTPA molecules on As-Dep gold is lower than that on TS gold. As the alkyl groups tilt further from the surface normal, the  $\nu_s(\text{CH}_2)$  peak intensity increases due to the surface selection rule.<sup>36</sup> The  $\nu_s(\text{CH}_2) : \nu_s(\text{CH}_3)$  intensity ratio is a way to compare the average molecular tilt between the two SAMs.<sup>37</sup> This ratio for (C<sub>16</sub>)<sub>2</sub>DTPA SAMs on As-Dep gold substrates (2.5) is lower than that (C<sub>16</sub>)<sub>2</sub>DTPA SAMs on TS gold (10.3), indicating that the crystalline alkyl groups of the (C<sub>16</sub>)<sub>2</sub>DTPA SAMs on As-Dep gold are less tilted than the liquid-like alkyl groups of the (C<sub>16</sub>)<sub>2</sub>DTPA SAMs on TS gold.

Contact angle data using water and hexadecane (HD) probe liquids (Table 5.2) are consistent with the RAIRS data. Contact angles of water for  $(C_{16})_2DTPA$  SAMs on As-Dep gold substrates ( $113^\circ$ ) are indistinguishable within experimental error from those measured for  $C_{16}SH$  SAMs ( $112^\circ$ ) on the same substrate, whereas the liquid-like  $(C_{16})_2DTPA$  SAMs on TS gold exhibit lower contact angles of water ( $98^\circ$ ). On TS gold, the water drop senses the exposed methylene chains rather than the terminal methyl group in a well-ordered SAM. Although contact angles of water depend on surface roughness<sup>38</sup> – they decrease for hydrophobic surfaces as surface roughness is reduced – the decrease observed for  $(C_{16})_2DTPA$  SAMs on As-Dep and TS gold ( $15^\circ$ ) is greater than that observed for  $C_{16}SH$  SAMs on As-Dep and TS gold ( $8^\circ$ ). HD drops are less sensitive to surface roughness and more sensitive to subtle differences in the organization of alkyl chains than water drops.<sup>39-41</sup> For  $C_{16}SH$  SAMs, static contact angles of HD are similar on both As-Dep ( $42^\circ$ ) and TS gold ( $45^\circ$ ), indicating that both SAMs present densely-packed methyl groups. For  $(C_{16})_2DTPA$  SAMs, the contact angle on As-Dep gold substrates ( $34^\circ$ ) also indicates the presence of a densely-packed methyl surface (albeit slightly less dense than  $C_{16}SH$  SAMs); however, HD wets  $(C_{16})_2DTPA$  SAMs on TS gold, indicating that the alkyl chains in this SAM are packed loosely enough to allow HD to penetrate the SAM.

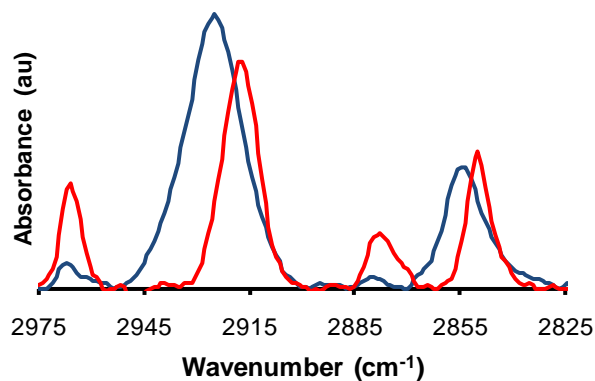


**Figure 5.3.** RAIR spectra (2975 - 2825  $\text{cm}^{-1}$ ) of  $(\text{C}_{16})_2\text{DTPA}$  SAMs on As-Dep gold (red) and TS gold (blue).

**Table 5.2.** RAIRS absorption bands and contact angle data<sup>[a]</sup> for  $(\text{C}_{16})_2\text{DTPA}$  and  $\text{C}_{16}\text{SH}$  SAMs formed on As-Dep and TS gold.

	$(\text{C}_{16})_2\text{DTPA}$ SAM on As-Dep Gold	$(\text{C}_{16})_2\text{DTPA}$ SAM on TS Gold	$\text{C}_{16}\text{SH}$ SAM on As-Dep Gold	$\text{C}_{16}\text{SH}$ SAM on TS Gold
$\nu_{as}(\text{CH}_2)$ ( $\text{cm}^{-1}$ )	2918	2925	2918	2918
$\nu_s(\text{CH}_2)$ ( $\text{cm}^{-1}$ )	2850	2854	2850	2850
$\theta(\text{H}_2\text{O})$ (deg) <sup>[a]</sup>	113 +/- 3	98 +/- 2	112 +/- 1	104 +/- 1
$\theta(\text{HD})$ (deg) <sup>[a]</sup>	34 +/- 1	< 10	42 +/- 1	45 +/- 1

[a] Static contact angles using the sessile drop method

### *5.3.4. Frictional Properties of (C<sub>16</sub>)<sub>2</sub>DTPA SAMs on As-Dep and TS gold*

We used LFM to illustrate the difference between ordered, crystalline (C<sub>16</sub>)<sub>2</sub>DTPA SAMs on As-Dep gold and disordered, liquid-like (C<sub>16</sub>)<sub>2</sub>DTPA SAMs on TS gold. LFM is a scanning probe technique that maps the frictional forces exerted on a cantilever tip as it moves across the SAM. SAMs in which the alkyl groups are liquid-like expose a greater number of methylene groups to the tip and consequently exert greater frictional forces on the tip than SAMs in which the alkyl groups are ordered and crystalline.<sup>42</sup> We used a C<sub>16</sub>SH SAM, in which the alkyl chains are organized and crystalline on both As-Dep and TS gold, as a standard to compare (C<sub>16</sub>)<sub>2</sub>DTPA SAMs on these substrates. LFM sample preparation (Scheme 5.2) begins with microcontact printing<sup>27</sup> to pattern 10- $\mu$ m-wide strips of C<sub>16</sub>SH onto the gold substrate, separated by 10- $\mu$ m-wide strips. Subsequently immersing the printed substrate into a solution of (C<sub>16</sub>)<sub>2</sub>DTPA for 15 minutes backfilled the unprinted strips with (C<sub>16</sub>)<sub>2</sub>DTPA SAM, producing a surface bearing alternating strips of C<sub>16</sub>SH and (C<sub>16</sub>)<sub>2</sub>DTPA SAMs. The 15 minute exposure time of the patterned C<sub>16</sub>SH SAM on gold to the (C<sub>16</sub>)<sub>2</sub>DTPA solution minimized the possibility of the exchange of (C<sub>16</sub>)<sub>2</sub>DTPA molecules in solution with the C<sub>16</sub>SH SAM while still producing (C<sub>16</sub>)<sub>2</sub>DTPA SAMs that exhibit head group binding modes and alkyl chain organization indistinguishable by XPS and RAIRS from (C<sub>16</sub>)<sub>2</sub>DTPA SAMs formed for 24 hours. Figure 5.4a shows LFM images of alternating strips of C<sub>16</sub>SH and (C<sub>16</sub>)<sub>2</sub>DTPA SAMs on As-Dep gold. In agreement with contact angle and RAIRS data, these SAMs are quite similar: Both exert low frictional force on the LFM tip, indicating that the surfaces of both SAMs consist of well-packed methyl groups. When these SAMs are formed on TS gold (Figure 5.4b), however, the contrast between the strips in the LFM image clearly highlights the difference between the organization of the alkyl chains in these SAMs. Here, the bright strips correspond to the higher frictional force exerted on the tip by the liquid-like (C<sub>16</sub>)<sub>2</sub>DTPA SAM relative to the low frictional force exerted by the C<sub>16</sub>SH SAM (dark strips).

**Scheme 5.2.** Process used to pattern alternating lines of  $(C_{16})_2DTPA$  and  $C_{16}SH$  SAMs on gold substrates.

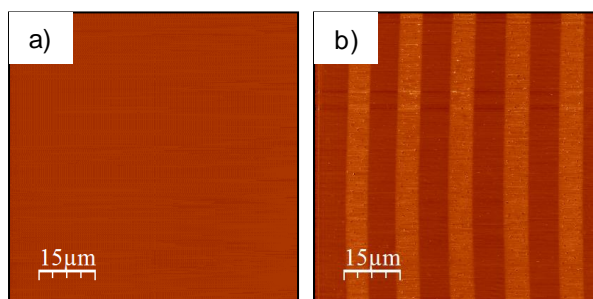
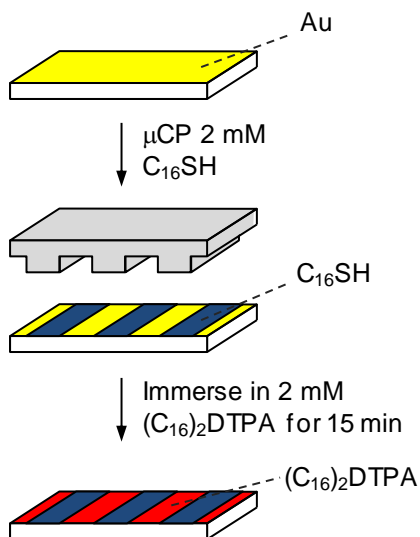


**Figure 5.4.** LFM images of alternating lines of  $C_{16}SH$  and  $(C_{16})_2DTPA$  SAMs patterned onto (a) As-Dep gold and (b) TS gold. Bright areas correspond to regions of higher friction. Z-scale is 250 mV for both images.

### *5.3.5. Electrochemical Barrier Properties of (C<sub>16</sub>)<sub>2</sub>DTPA SAMs on As-Dep and TS Gold*

We used EIS to investigate how the structural differences between (C<sub>16</sub>)<sub>2</sub>DTPA SAMs on As-Dep and TS gold affect the resistance of these SAMs to the diffusion of an ionic redox probe – aqueous solutions of K<sub>4</sub>Fe(CN)<sub>6</sub> and K<sub>3</sub>Fe(CN)<sub>6</sub> – to the underlying gold. In the EIS experiment, a sinusoidal ac perturbation is applied at frequencies ranging from 3.0 mHz to 100 kHz and the corresponding current response is used to measure the complex impedance of the SAM.<sup>43</sup> Impedance spectra in the form of Bode plots for (C<sub>16</sub>)<sub>2</sub>DTPA SAMs on As-Dep and TS gold are given in Figure 5.5. We used a simple circuit model (Figure 5.5, inset) – a Randles equivalent circuit commonly used for SAMs – to fit the impedance spectra, allowing us to determine the resistance (R<sub>SAM</sub>) and capacitance (C<sub>SAM</sub>) of the SAM.<sup>44</sup> R<sub>SAM</sub> indicates how well the SAM impedes electron transfer: A densely packed, crystalline SAM will have a higher resistance than a porous liquid-like SAM. C<sub>SAM</sub> is inversely proportional to the SAM thickness, which can be calculated using<sup>35</sup>

$$d = \frac{\varepsilon \cdot \varepsilon_0}{C} \quad [1]$$

where  $d$  is the SAM thickness in Angstroms,  $C$  is the capacitance per area in F m<sup>-2</sup>,  $\varepsilon$  is the dielectric constant of the SAM (measured for C<sub>*n*</sub>SH SAMs ( $n = 16, 18$ ) on gold using surface plasmon resonance (2.1)<sup>45</sup>), and  $\varepsilon_0$  is the permittivity of free space ( $8.54 \times 10^{-12}$  F m<sup>-1</sup>).

Values for R<sub>SAM</sub> and C<sub>SAM</sub>, along with calculated thickness values for (C<sub>16</sub>)<sub>2</sub>DTPA SAMs on As-Dep and TS gold are given in Table 5.3. The densely packed (C<sub>16</sub>)<sub>2</sub>DTPA SAM on As-Dep gold has a higher resistance (13.3 +/- 3.0 MΩ cm<sup>2</sup>) than the liquid-like SAM on TS gold (2.8 +/- 1.6 MΩ cm<sup>2</sup>), consistent with the SAM structure indicated by RAIRS and contact angle measurements. The resistance of the (C<sub>16</sub>)<sub>2</sub>DTPA SAM on As-Dep gold, however, is lower than that measured for C<sub>16</sub>SH SAMs on As-Dep gold (30.8 +/- 9.8 MΩ cm<sup>2</sup>), indicating that (C<sub>16</sub>)<sub>2</sub>DTPA SAMs are somewhat less densely packed

than C<sub>16</sub>SH SAMs. This distinction is consistent with the lower contact angle of HD on (C<sub>16</sub>)<sub>2</sub>DTPA SAMs on As-Dep gold compared to C<sub>16</sub>SH SAMs on As-Dep gold ( $\Delta\theta = 8^\circ$ ). The subtle difference in alkyl chain organization is only detected by methods that are sensitive to small structural differences such as EIS and contact angles of HD, whereas contact angles of water and the position of methylene C-H stretching modes in the RAIR spectra for these two SAMs are identical. The capacitance of the (C<sub>16</sub>)<sub>2</sub>DTPA SAM on As-Dep gold translates to a SAM thickness of 21.5 +/- 3.3 Å. This thickness is similar to the calculated thickness of the C<sub>16</sub>SH SAM on As-Dep gold (18.6 +/- 2.4 Å), suggesting that the DTPA alkyl chains are trans extended similar to C<sub>16</sub>SH SAMs. The capacitance of the (C<sub>16</sub>)<sub>2</sub>DTPA SAM on TS gold translates to a SAM that is 11.9 +/- 0.6 Å thick, significantly thinner than the (C<sub>16</sub>)<sub>2</sub>DTPA SAM on As-Dep Gold. This thickness is consistent with alkyl groups that are disordered and tilted from the surface normal at a larger angle on average than in the (C<sub>16</sub>)<sub>2</sub>DTPA SAM on As-Dep gold.

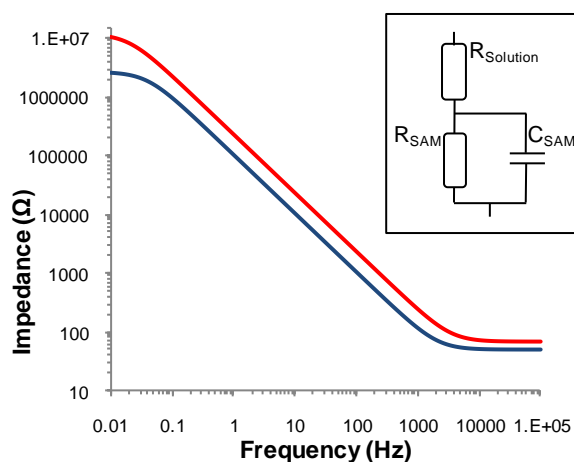


**Figure 5.5.** Bode plot of (C<sub>16</sub>)<sub>2</sub>DTPA SAMs formed on As-Dep gold (red) and TS gold (blue). Inset (upper right): Randles circuit model used to fit raw EIS data.

**Table 5.3.** Electrical parameters of (C<sub>16</sub>)<sub>2</sub>DTPA and C<sub>16</sub>SH SAMs formed on As-Dep gold and TS gold calculated by fitting raw EIS data using the Randles simple circuit model.

	(C <sub>16</sub> ) <sub>2</sub> DTPA SAM on As-Dep Gold	(C <sub>16</sub> ) <sub>2</sub> DTPA SAM on TS Gold	C <sub>16</sub> SH SAM on As-Dep Gold	C <sub>16</sub> SH SAM on TS Gold
Resistance (MΩ cm <sup>2</sup> )	13.3 +/- 3.0	2.8 +/- 1.6	30.8 +/- 9.8	89.9 +/- 34.2
Capacitance (μF cm <sup>-2</sup> )	0.85 +/- 0.13	1.51 +/- 0.8	0.97 +/- 0.1	1.03 +/- 0.03
Thickness (Å)	21.5 +/- 3.3	11.9 +/- 0.6	18.6 +/- 2.4	17.3 +/- 0.4

### 5.3.6. Thermal Stability

Thermal desorption experiments show that despite the alkyl chain crystallinity of (C<sub>16</sub>)<sub>2</sub>DTPA SAMs on As-Dep gold substrates, the presence of monodentate (C<sub>16</sub>)<sub>2</sub>DTPA molecules in these SAMs reduces the SAM thermal stability compared to (C<sub>16</sub>)<sub>2</sub>DTPA SAMs on TS gold substrates. It has previously been demonstrated that the desorption of alkanethiols from SAMs exposed to hot hydrocarbon solvents can be monitored using ellipsometry.<sup>46,47</sup> We monitored the desorption of (C<sub>16</sub>)<sub>2</sub>DTPA molecules by immersing SAM-coated substrates into decahydronaphthalene (decalin) heated to 70 °C and measuring the static contact angle of water after immersion times ranging from 30 seconds to 120 minutes. Unperturbed (C<sub>16</sub>)<sub>2</sub>DTPA and C<sub>16</sub>SH SAMs on both As-Dep and TS gold are hydrophobic; desorption of the molecules in hot decalin exposes the underlying gold and reduces the contact angle of water. After the contact angle of water has decreased to 45-55°, however, the contact angle plateaus and further desorption

cannot be detected. For C<sub>16</sub>SH SAMs on both As-Dep and TS gold, this plateau begins after the SAM has been exposed to the hot decalin for ~ 30 minutes. Previous desorption studies of C<sub>16</sub>SH SAMs using ellipsometry have shown that under the same conditions, ~ 90% of the SAM remains on the surface; after this time, further desorption can be detected by ellipsometry, but cannot be detected by changes in water contact angle. Despite the relatively limited sensitivity of contact angles to molecular desorption, plots of contact angles of water as a function of immersion time for (C<sub>16</sub>)<sub>2</sub>DTPA SAMs on As-Dep and TS gold substrates (Figure 5.6) clearly show the difference in thermal stability of these SAMs. The contact angle of water on (C<sub>16</sub>)<sub>2</sub>DTPA SAMs on As-Dep gold substrates rapidly decreases to the minimum measurable value after ~30 minutes. After reaching the minimum measurable value, molecular desorption likely continues but cannot be detected by contact angle changes. The contact angle of water on (C<sub>16</sub>)<sub>2</sub>DTPA SAMs on TS gold also rapidly decreases during the first 30 minutes, but the contact angle does not reach the minimum measurable value after this initial 30-minute period. Instead, the contact angle then gradually decreases, reaching the minimum measurable value after > 60 minutes. We attribute the difference in thermal stability of (C<sub>16</sub>)<sub>2</sub>DTPA SAMs on TS gold compared to (C<sub>16</sub>)<sub>2</sub>DTPA SAMs on As-Dep gold to the enhanced thermodynamic stability of the 100% bidentate adsorbates on TS gold. Desorption experiments using C<sub>16</sub>SH SAMs on As-Dep and TS gold substrates – in which there is no possible chelation to the gold substrate – support this idea. C<sub>16</sub>SH SAMs on both As-Dep and TS gold both show desorption behavior similar to that of (C<sub>16</sub>)<sub>2</sub>DTPA SAMs on As-Dep gold, and reach the minimum measurable contact angle after ~30 minutes.

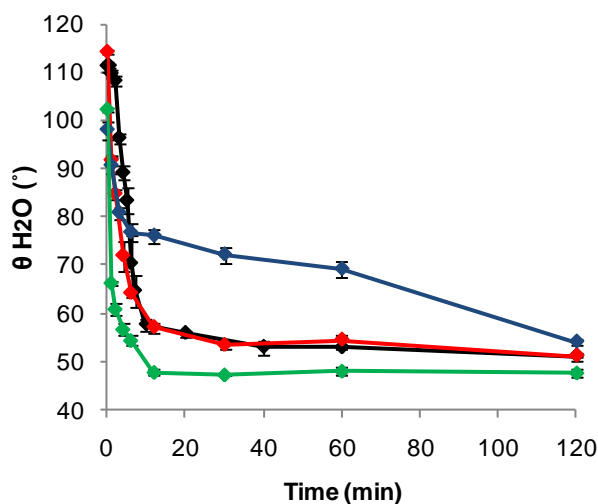


**Figure 5.6.** Thermal desorption of (C<sub>16</sub>)<sub>2</sub>DTPA SAMs on As-Dep gold (red) and TS gold (blue) plotted as the static contact angle of water as a function of immersion time in 70 °C decahydronaphthalene. Desorption of C<sub>16</sub>SH SAMs on As-Dep gold (black) and TS gold (green) is shown for reference.

## 5.4. Conclusions

(C<sub>16</sub>)<sub>2</sub>DTPA molecules adsorb on gold to form SAMs with properties that depend on whether the morphology of the underlying gold substrate permits the chelation of DTPA molecules to the gold surface, or disrupts chelation and causes monodentate binding. The shallow, large grains of TS gold permit chelation of (C<sub>16</sub>)<sub>2</sub>DTPA adsorbates; anchoring the adsorbates at two points produces SAMs with liquid-like alkyl chains. Although a consequence of this chelation is the inhibition of van der Waals interactions between alkyl chains, these SAMs are more stable to thermal desorption than linear C<sub>16</sub>SH SAMs due to the energetically favorable chelation of the head group. On the other hand, the numerous and deep grain boundaries of As-Dep gold disrupt chelation, producing SAMs in which 40% of the adsorbates are monodentate. The conformational freedom of monodentate adsorbates relative to bidentate adsorbates allows the alkyl chains to pack more densely in the SAM; van der Waals interactions between the chains are greater than in SAMs on TS gold and the alkyl chains are crystalline. However, van der Waals

*New Dialkyldithiophosphinic Acid Self Assembled Monolayers (SAMs):  
The Influence of Gold Substrate Morphology on Adsorbate Binding and SAM Structure*

interactions cannot compensate for the presence of monodentate adsorbates and SAMs on As-Dep gold are not as stable to thermal desorption as  $(C_{16})_2DTPA$  SAMs on TS gold.

Changing the morphology of the gold substrate produces  $(C_{16})_2DTPA$  SAMs that are chemically identical but possess distinctly different properties, and thus have different potential uses.  $(C_{16})_2DTPA$  SAMs on As-Dep gold have properties that are reasonably comparable to those of alkanethiolate SAMs on gold, although the lower electrochemical resistance of the  $(C_{16})_2DTPA$  SAM makes this system a less effective protective layer to the underlying gold substrate. The liquid-like alkyl layer of  $(C_{16})_2DTPA$  SAMs on TS gold imparts relatively poor electrochemical resistance, but the resonant bidentate structure exhibited by all  $(C_{16})_2DTPA$  adsorbates in this SAM make this system applicable to molecular electronic devices, particularly if conjugated substituents are combined with DTPA head groups.

## 5.5. References

- (1) Kim, D. S. *Bull. Korean Chem. Soc.* **1995**, *16*, 321-325.
- (2) Hope, G. A.; Woods, R.; Watling, K.; *Coll. Surf. A* **2003**, *214*, 87-97.
- (3) Hope, G. A.; Woods, R.; Boyd, S.; Watling, K.; *Coll. Surf. A* **2003**, *214*, 77-85.
- (4) Hope, G. A.; Woods, R.; Watling, K. *J. Appl. Electrochem.* **2001**, *31*, 1285-1291.
- (5) Love, J. C.; Estroff, L. A.; Kriebel, J. K.; Nuzzo, R. G.; Whitesides, G. M. *Chem. Rev.* **2005**, *105*, 1103-1169.
- (6) Trevor, D. J.; Chidsey, C. E. D.; Loiacono, D. N. *Phys. Rev. Lett.* **1989**, *62*, 929-932.
- (7) Wagner, P.; Hegner, M.; Guntherodt, H. -J.; Semenza, G. *Langmuir* **1995**, *11*, 3867-3875.
- (8) Weiss, E. A.; Kaufman, G. K.; Kriebel, J. K.; Li, Z.; Schalek, R.; Whitesides, G. M. *Langmuir* **2007**, *23*, 9686-9694.
- (9) Naumann, R.; Schiller, S. M.; Giess, F.; Grohe, B.; Hartman, K. B.; Karcher, I.; Koper, I.; Lubben, J.; Vasilev, K.; Knoll, W. *Langmuir* **2003**, *19*, 5435-5443.
- (10) Hegner, M.; Wagner, P.; Semenza, G. *Surface Science* **1993**, *291*, 39-46.
- (11) Wagner, P.; Zaugg, F.; Kern, P.; Hegner, M.; Semenza, G. *J. Vac. Sci. Technol. B* **1996**, *14*, 1466-1471.
- (12) Gupta, P.; Ulman, A.; Fanfan, S.; Korniyakov, A.; Loos, K. *J. Am. Chem. Soc.* **2005**, *127*, 4-5.
- (13) Gupta, P.; Loos, K.; Korniyakov, A.; Spagnoli, C.; Cowman, M.; Ulman, A. *Angew. Chem. Int. Ed.* **2004**, *43*, 520-523.
- (14) Weiss, E. A.; Chiechi, R. C.; Kaufman, G. K.; Kriebel, J. K.; Li, Z.; Duati, M.; Rampi, M. A.; Whitesides, G. M. *J. Am. Chem. Soc.* **2007**, *129*, 4336-4349.
- (15) Engelkes, V. B.; Beebe, J. M.; Frisbie, C. D. *J. Phys. Chem. B* **2005**, *109*, 16801-16810.

*New Dialkyldithiophosphinic Acid Self Assembled Monolayers (SAMs):  
The Influence of Gold Substrate Morphology on Adsorbate Binding and SAM Structure*

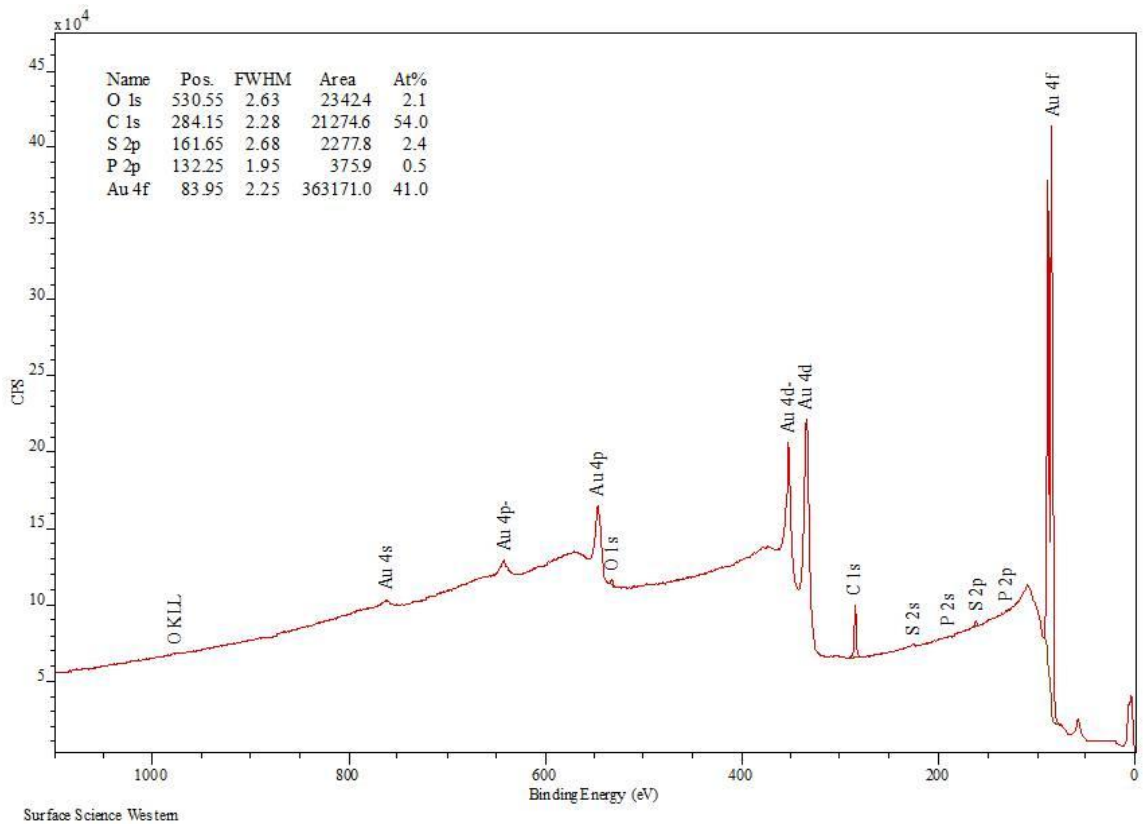
- (16) Von Wrochem, F.; Gao, D.; Scholz, F.; Nothofer, H. -G.; Nelles, G.; Wessels, J. M. *Nature Nanotech.* **2010**, *5*, 618-624.
- (17) Shon, Y. -S.; Colorado Jr., R.; Williams, C. T.; Bain, C. D.; Lee, T. R. *Langmuir* **2000**, *16*, 541-548.
- (18) Park, J. -S.; Smith, A. C.; Lee, T. R. *Langmuir* **2004**, *20*, 5829-5836.
- (19) Park, J. -S.; Vo, A. N.; Barriet, D.; Shon, Y. -S.; Lee, T. R. *Langmuir* **2005**, *21*, 2902-2911.
- (20) Weidner, T.; Kramer, A.; Bruhn, C.; Zharnikov, M.; Shaporenko, A.; Siemeling, U.; Trager, F. *Dalton Trans.* **2006**, 2767-2777.
- (21) Zhaom, Y.; Perez-Segarra, W.; Shi, Q.; Wei, A. *J. Am. Chem. Soc.* **2005**, *127*, 7328-7329.
- (22) Morf, P.; Raimondi, F.; Nothofer, H. -G.; Schnyder, B.; Yasuda, A.; Wessels, J. M.; Jung, T. A. *Langmuir* **2006**, *22*, 658-663.
- (23) Weinstein, R. D.; Richards, J.; Thai, S. D.; Omiatek, D. M.; Bessel, C. A.; Faulkner, C. J.; Othman, S.; Jennings, G. K. *Langmuir* **2007**, *23*, 2887-2891.
- (24) Lee, T. -C.; Hounihan, D. J.; Colorado Jr., R.; Park, J. -S.; Lee, T. R. *J. Phys. Chem. B* **2004**, *108*, 2648-2653.
- (25) Iha, A.; Uvdal, K.; Liedberg, B. *Langmuir* **1993**, *9*, 733-739.
- (26) Beattie, D. A.; Kempson, I. M.; Fan, L.-J.; Skinner, W. M. *Int. J. Miner. Process.* **2009**, *92*, 162-168.
- (27) Kumar, A.; Biebuyck, H. A.; Whitesides, G. M. *Langmuir* **1994**, *10*, 1498-1511.
- (28) I. Horcas, R. Fernandez, J.M. Gomez-Rodriguez, J. Colchero, J. Gomez-Herrero, and A.M. Baro *Review of Scientific Instruments* 2007, *78*, 013705.
- (29) Moulder, J. F.; Stickle, W. F.; Sobol, P. E.; Bomben, K. D. *Handbook of X-Ray Photoelectron Spectroscopy*; Physical Electronics: Eden Prairie, MN, 1995.
- (30) Guoxin, T.; Yongjun, Z.; Jingming, X. *Solvent Extr. Ion Exch.* **2001**, *19*, 993-1005.

*New Dialkyldithiophosphinic Acid Self Assembled Monolayers (SAMs):  
The Influence of Gold Substrate Morphology on Adsorbate Binding and SAM Structure*

- (31) Schoenfish, M. H.; Pemberton, J. E. *J. Am. Chem. Soc.* **1998**, *120*, 4502-4513.
- (32) Hutt, D. A.; Leggett, G. J. *J. Phys. Chem.* **1996**, *100*, 6657-6662.
- (33) Castner, D. G.; Hinds, K.; Grainger, D.W. *Langmuir* **1996**, *12*, 5083-5086.
- (34) Ishida, T.; Choi, N.; Mizutani, W.; Tokumoto, H.; Kojima, I.; Azebara, H.; Hokari, H.; Akiba, U.; Fujihira, M. *Langmuir* **1999**, *15*, 6799-6806.
- (35) Porter, M. D.; Bright, T. B.; Allara, D. L.; Chidsey, C. E. D. *J. Am. Chem. Soc.* **1987**, *109*, 3559-3568.
- (36) Bubert, H.; Jenett, H. *Surface and Thin Film Analysis*; Wiley-VCH: Weinham, 2002; p 250.
- (37) Yan, D.; Saunders, J. A.; Jennings, G. K. *Langmuir* **2000**, *16*, 7562-7565.
- (38) Adamson, A. W.; Gast, A. P. *Physical Chemistry of Surfaces*, 6<sup>th</sup> ed; Wiley & Sons: New York, 1997; p 358.
- (39) Ulman, A. *An Introduction to Ultrathin Organic Films*; Academic: Boston, 1991.
- (40) Tao, Y.-T. *J. Am. Chem. Soc.* **1993**, *115*, 4350.
- (41) Tao, Y.-T.; Lee, M.-T.; Chang, S.-C. *J. Am. Chem. Soc.* **1993**, *115*, 9547.
- (42) Lio, A.; Charych, D. H.; Salmeron, M. *J. Phys. Chem. B* **1997**, *101*, 3800-3805.
- (43) Barsoukov, E.; Macdonald, J. R. *Impedance Spectroscopy*, 2<sup>nd</sup> ed; Wiley & Sons: Hoboken, 2005.
- (44) Jennings, G. K.; Munro, J. C.; Yong, T.-H.; Laibinis, P.E. *Langmuir* **1998**, *14*, 6130-6139.
- (45) Peterlinz, K. A.; Georgiadis, R. *Langmuir* **1996**, *12*, 4731-4740.
- (46) Bain, C. D.; Troughton, E. B.; Tao, Y. -T.; Evall, J.; Whitesides, G. M.; Nuzzo, R. G. *J. Am. Chem. Soc.* **1989**, *111*, 321-335.
- (47) Shon, Y.-S.; Lee, T. R. *J. Phys. Chem. B* **2000**, *104*, 8192-8200

## 5.6. Supporting Information and Figures

a)



b)

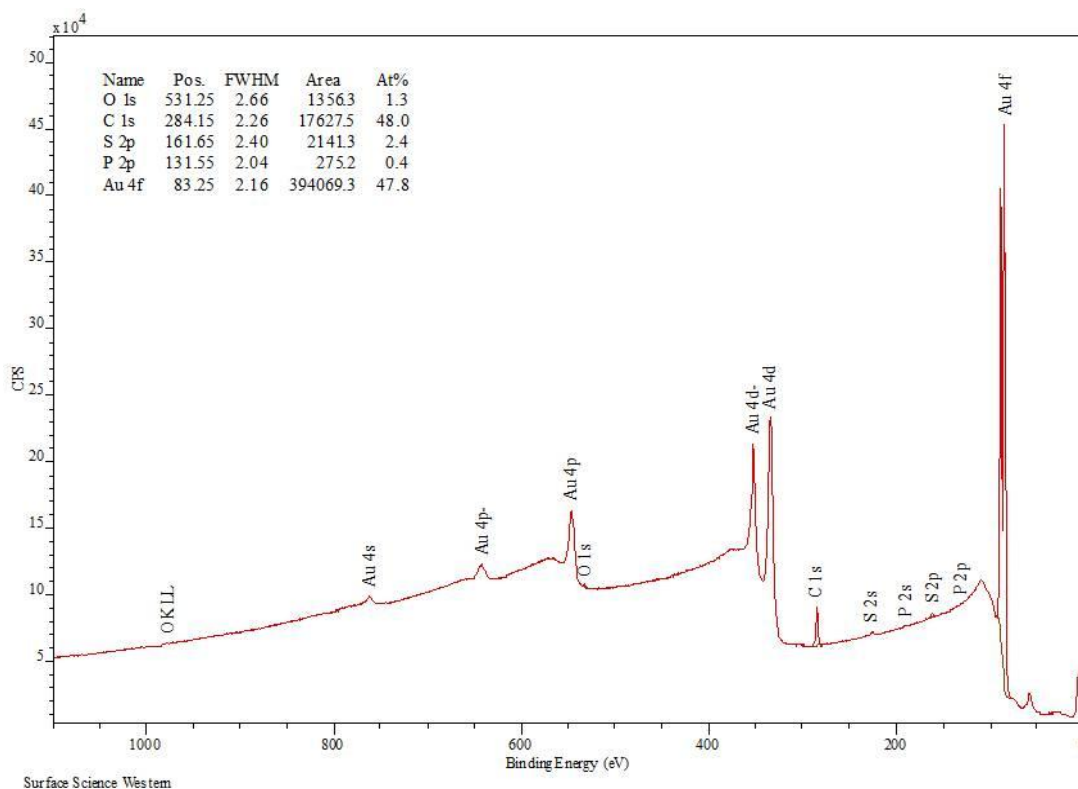
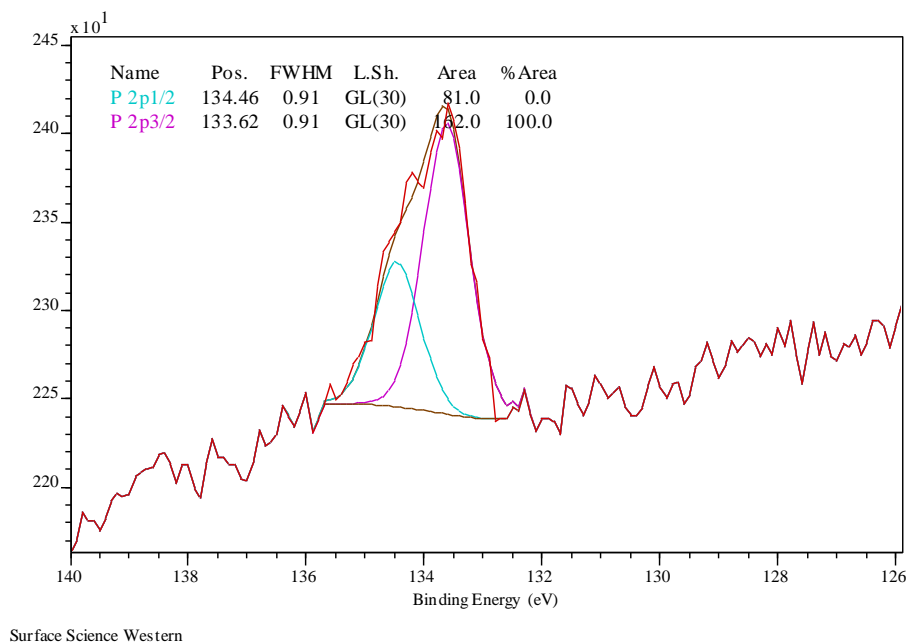


**Figure S5.1.** XPS survey spectra for  $(C_{16})_2DTPA$  SAMs formed for 24 hours on a) As-Dip gold and b) TS gold. Please note that when comparing the atomic percentages of sulphur and phosphorus that the phosphorus percentage is routinely lower than expected relative to sulphur. There are three reasons for this discrepancy: First, the phosphorus signal has a lower cross-section compared to sulphur (relative sensitivity factors of 0.486 and 0.668 respectively). Second, the P 2p peak is mixed in with the large inelastic background of the Au 4f peaks, which puts the peak on a slope that alters the applied Shirley background to give a smaller peak area than should be expected. Third, since we are at or near the detection limit for phosphorus any noise in the background strongly affects the amount of phosphorus reported. For these reasons, there is a significant amount of error (+/-) associated with the P numbers. Conversely, the sulfur peak is stronger due to its larger cross-section and the fact that there is more sulfur present, and it is not affected as greatly by the Au 4f background (much less slope). Therefore, much less error associated with it.

*New Dialkyldithiophosphinic Acid Self Assembled Monolayers (SAMs):  
The Influence of Gold Substrate Morphology on Adsorbate Binding and SAM Structure*

a)



b)

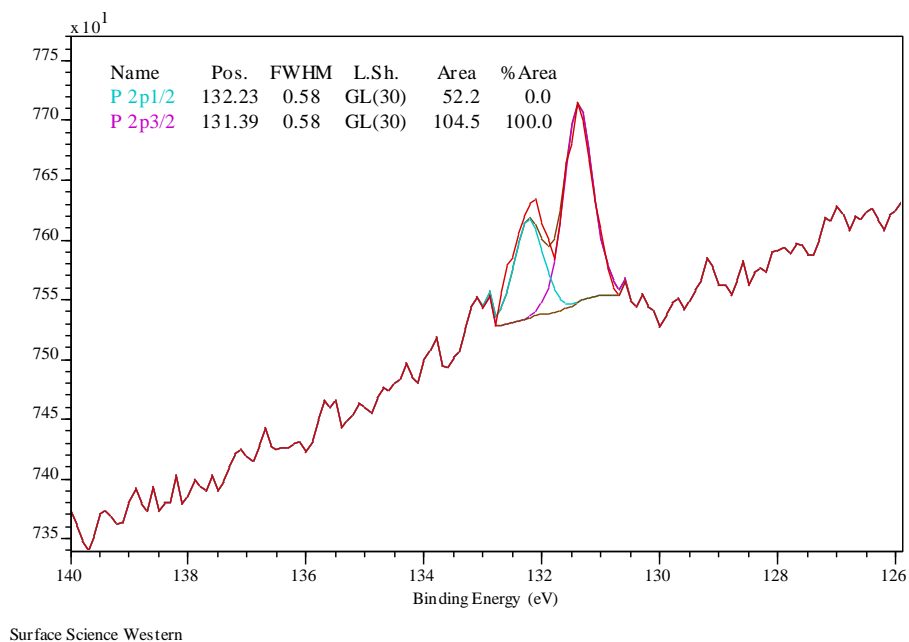


**Figure S5.2.** High resolution XPS spectra of the P 2p region for (C<sub>16</sub>)<sub>2</sub>DTPA SAMs formed for 24 hours on a) As-Dep gold and b) TS gold.

*New Dialkyldithiophosphinic Acid Self Assembled Monolayers (SAMs):  
The Influence of Gold Substrate Morphology on Adsorbate Binding and SAM Structure*

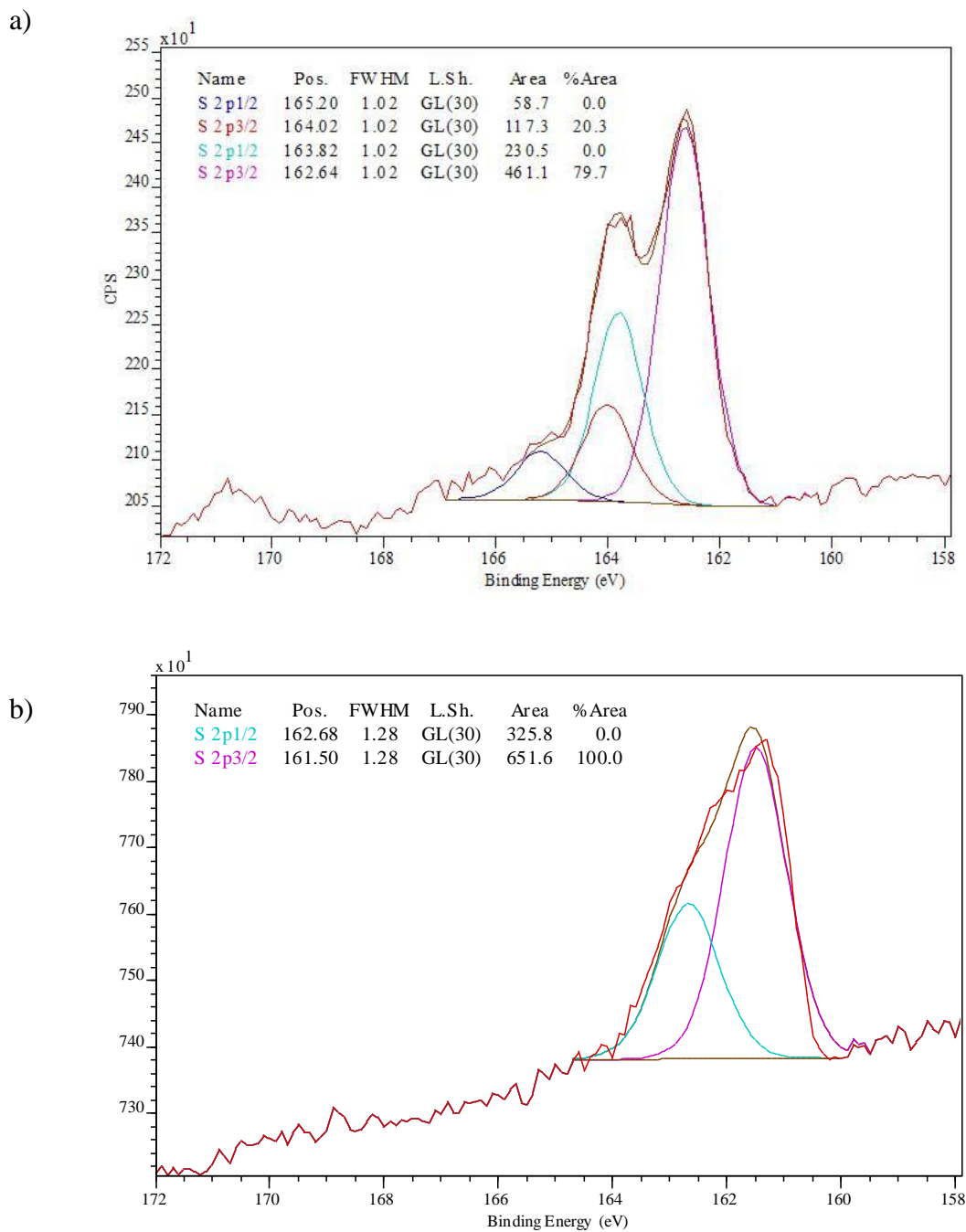


**Figure S5.3.** High resolution XPS spectra of the S 2p region for  $(C_{16})_2DTPA$  SAMs formed for 5 minutes on a) As-Dep gold and b) TS gold.

## **Chapter 6**

# **The Unusual Self-Organization of Dialkyldithiophosphinic Acid Self-Assembled Monolayers on UltrasMOOTH Gold**

## 6.1. Introduction

Forming self-assembled monolayers (SAMs) on surfaces is an exceptionally well-studied method to access a wide range of surface properties.<sup>1</sup> After 25 years of research, a vast number of SAMs have been reported that employ different substrates (metals, metal oxides, semiconductors) and different molecular adsorbates.<sup>2</sup> From these studies, it is generally accepted that two factors – the interaction between the adsorbate headgroup and the substrate, and lateral interactions between the organic portions of the adsorbates – determine the way in which adsorbates self-organize on surfaces to form SAMs. The interplay between these two factors determines structural features such as molecular packing density, molecular tilt, and crystallinity of the alkyl layer of the resulting SAM. These structural features have a practical importance because they contribute to the macroscopic surface properties of the SAM, such as wettability, frictional properties, and the ability of guest molecules to intercalate into the SAM. Predicting the details of SAM structure is fairly straightforward for adsorbates with simple structures, such as *n*-alkanethiolates. For example, adsorbate-substrate interactions and lateral van der Waals interactions between adsorbates are sufficient to explain the structures of *n*-alkanethiolate SAMs with different alkyl chain lengths on gold substrates.<sup>3,4</sup> The highly favorable Au-S adsorbate-substrate interaction stabilizes the SAM and determines the maximum packing density of the adsorbates. SAMs formed from *n*-alkanethiolates with short alkyl chains have liquid-like, disorganized alkyl groups because there are not enough van der Waals interactions possible between adjacent alkyl chains to stabilize a trans-extended, crystalline arrangement. As the number of methylene groups increases, however, the increasing number of van der Waals interactions between alkyl chains causes the progression from a liquid-like organization to one in which the alkyl chains are trans-extended and crystalline. Short-chain, liquid-like SAMs are wet by both water and hexadecane,<sup>4,5</sup> and exhibit higher frictional coefficients than long-chain crystalline SAMs.<sup>5-9</sup> Both properties have been attributed to gauche defects in the short alkyl chains, which expose methylene groups at the surface that contact probe liquids or AFM probe tips. In contrast, crystalline SAMs present a layer of well-packed methyl groups at the surface, causing higher water and hexadecane contact angles and lower frictional forces.

*The Unusual Self-Organization of Dialkyldithiophosphinic Acid  
Self-Assembled Monolayers on Ultrasoother Gold*

Although predicting the structure of a SAM is fairly straightforward for structurally simple adsorbates, a more rigorous understanding of the interplay between the factors affecting adsorbate self-organization will be necessary to develop design rules to enable the design of adsorbates that produce complex self-organized structures, and to predict structures of SAMs formed from structurally complex adsorbates. To fully elucidate these design rules, it is necessary to first deepen our understanding of the relationship between the adsorbate structure and the resulting SAM structure by studying SAMs formed from structurally complex adsorbates. A leading approach has been to vary the structure of the sulfur-containing headgroup. Studies of bidentate<sup>10-15</sup> and tridentate<sup>16-22</sup> thiols, dithiocarboxylic acids,<sup>23-25</sup> xanthic acids,<sup>26,27</sup> and dialkyldithiocarbamates<sup>28-33</sup> have all produced SAMs with structures that differ in some way from archetypical *n*-alkanethiolate SAMs. For example, Lee *et al.* have reported the use of bulky chelating spiroalkanedithiol and trithiol headgroups that enforce spacing between adjacent alkyl substituents.<sup>5,6,9,16,20,34-37</sup> The resulting SAMs exhibit alkyl group packing densities that depend on the combination of the chelating headgroup and pendant alkyl chain lengths. With such adsorbates, it is possible to form SAMs with loosely-packed alkyl groups even with long alkyl substituents;<sup>9,20,34</sup> furthermore, these SAMs exhibit enhanced stability to thermal<sup>16</sup> and electrochemical<sup>38</sup> desorption compared to *n*-alkanethiolate SAMs due to the chelate effect. Recent studies of xanthic acid and dithiocarboxylic acid adsorbates reveal subtle structural differences between these SAMs and analogous *n*-alkanethiolate SAMs, indicated by contact angles that exhibit a larger odd-even effect for the former SAMs.<sup>26,39</sup>

Our research group has explored the use of chelating dialkyldithiophosphinic acids [CH<sub>3</sub>(CH<sub>2</sub>)<sub>*n*</sub>]<sub>2</sub>P(S)SH (R<sub>2</sub>DTPA) to expand the understanding of the relationship between adsorbate structure and SAM structure, as well as to access SAMs with new structures and interfacial properties.<sup>40-43</sup> One might expect these SAMs to consist of DTPA head groups chelated to the gold substrate as shown in Scheme 6.1a, and the steric demands of the bulky DTPA headgroup to then space out the alkyl groups and produce SAMs with liquid-like, disorganized alkyl chains. However, a study of SAMs formed from R<sub>2</sub>DTPA adsorbates with *n* = 5, 9, 11, 13, 15 on gold films fabricated by electron beam evaporation

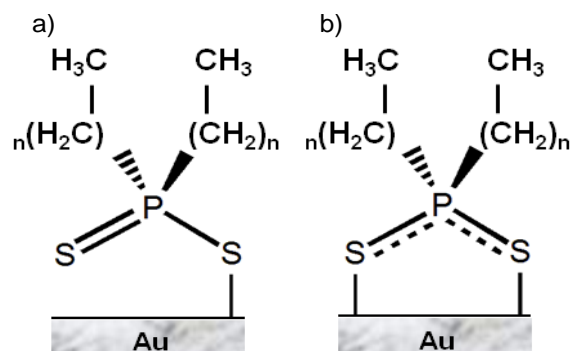
*The Unusual Self-Organization of Dialkyldithiophosphinic Acid  
Self-Assembled Monolayers on Ultrasoother Gold*

(As-Dep gold) showed that these SAMs consist of a 60:40 mixture of chelating and monodentate adsorbates (Scheme 6.1a and b) regardless of the length of the alkyl substituents, and the organization of the alkyl layer is very similar to that of RSH SAMs.<sup>41,43</sup> R<sub>2</sub>DTPA SAMs with short alkyl chains (n = 5, 9) have a liquid-like alkyl layer, and the chains become increasingly ordered and crystalline as the number of methylene groups increases. Through a combination of experimental<sup>41-43</sup> and computational<sup>42</sup> studies, we have determined that for these SAMs, the interplay between adsorbate-substrate interactions and intermolecular interactions in the SAM does not adequately account for the observed SAM structures. A third factor – the substrate morphology – is an important influence that affects how these adsorbates self-organize. The results of our studies can be summarized by three main points: First, computational studies using a model (<sup>n</sup>Bu)<sub>2</sub>DTPA adsorbate show that the energetic difference between monodentate binding and chelation is surprisingly small.<sup>42</sup> Second, even though monodentate binding may be accessible, experimental studies show that it occurs only when provoked by defect sites of the As-Dep gold substrate.<sup>43</sup> As-Dep gold films consist of small (~ 25 - 50 nm) grains separated by deep (~ 10 nm) grain boundaries, with a root-mean-squared (RMS) roughness of 2 - 4 nm.<sup>41,44-47</sup> The constrained spaces of these deep grain boundaries cause R<sub>2</sub>DTPA adsorbates to adopt monodentate binding, with chelation likely occurring on the small, atomically flat areas on the tops of the gold grains that measure ~50 nm across.<sup>41</sup> Support for this idea comes from a study of (C<sub>16</sub>)<sub>2</sub>DTPA SAMs formed on smooth, template-stripped (TS) gold surfaces, which consist of large, flat gold grains that measure ~200 - 500 nm across and are separated by shallow (~2 nm) grain boundaries.<sup>41,45-48</sup> On TS gold, all (C<sub>16</sub>)<sub>2</sub>DTPA adsorbates chelate to the surface. The adoption of monodentate binding at grain boundaries of As-Dep gold is believed to impart conformational flexibility to the head group, which is necessary for the molecules to bind in these constrained spaces by allowing rotation about the Au-S bond and small changes in the Au-S-P bond angle. Third, the adoption of monodentate binding over chelation is compensated energetically by favorable van der Waals interactions between alkyl groups in the SAM. The conformational flexibility of the monodentate adsorbates enables the alkyl groups to pack densely in R<sub>2</sub>DTPA SAMs on As-Dep gold.<sup>41,43</sup> The

*The Unusual Self-Organization of Dialkyldithiophosphinic Acid  
Self-Assembled Monolayers on Ultrasmooth Gold*

resulting van der Waals interactions between alkyl groups, which have been estimated at  $\sim 2 \text{ kcal mol}^{-1}$  per methylene unit, compensates for the small energy difference between monodentate binding and chelation, particularly for adsorbates with long alkyl chains. The outcome is that the alkyl layer of  $R_2\text{DTPA}$  SAMs formed on As-Dep gold becomes progressively more ordered and crystalline as the chain length increases due to the increased number of van der Waals interactions between the chains.<sup>43</sup> In contrast, the alkyl groups of the fully chelated  $(\text{C}_{16})_2\text{DTPA}$  SAM on TS gold are loosely packed and disorganized.<sup>41</sup> Having all of the adsorbates anchored to the gold surface at two points restricts the conformational freedom of the head group; consequently, the alkyl groups cannot pack together to stabilize a trans-extended, crystalline structure. The result is an alkyl layer that is disordered and liquid-like.

**Scheme 6.1.**  $R_2\text{DTPA}$  adsorbates bound to gold with (a) monodentate binding and (b) chelation.



Based on the study of  $(\text{C}_{16})_2\text{DTPA}$  SAMs on TS gold, it is reasonable to suggest that chelation, along with the steric demands of the DTPA head group, might limit the packing density in the SAM, and that reducing the length of the alkyl chain should merely result in a series of SAMs with liquid-like alkyl chains. Here, we present the series of  $[\text{CH}_3(\text{CH}_2)_n]_2\text{DTPA}$  ( $n = 5, 9, 11, 13, 15$ ) SAMs on TS gold and show that these SAMs possess structures that exhibit a most surprising trend in alkyl chain packing: SAMs formed from adsorbates with short alkyl chains ( $n = 5$ ) are ordered and crystalline, and the alkyl groups become increasingly disordered and liquid-like as the number of methylene units is increased. This trend is the opposite of the typical behavior exhibited

in *n*-alkanethiolate SAMs, and it illustrates that changes to the adsorbate structure can have profound and surprising effects on the self-organization of those adsorbates within SAMs. We rationalize the results presented here by considering not only the steric demands and chelation of the head group, but also the steric demands of the alkyl groups. To our knowledge, R<sub>2</sub>DTPA SAMs on TS gold are the first reported example of SAMs with alkyl groups that progress from crystalline to liquid-like as the chain length increases, as well as the first example of SAMs with short (*n* = 5) alkyl chains that are crystalline.

## 6.2. Experimental Section

All chemicals were purchased commercially and used as received. Anhydrous tetrahydrofuran (THF), diethyl ether, and toluene were obtained from an Innovative Technologies solvent purification system. All R<sub>2</sub>DTPA molecules were prepared according to published procedures.<sup>41,43</sup> PDMS stamps were prepared by casting PDMS prepolymer against photolithographic masters according to published procedures.<sup>49</sup>

### 6.2.1. Gold Substrate Preparation

As-Dep gold films were produced by depositing 2 nm titanium as an adhesion promoter followed by 200 nm gold onto silicon wafers using an e-beam evaporator. The gold films were used immediately after their fabrication to form SAMs to minimize surface contamination. TS gold films were prepared according to published procedures.<sup>46</sup> 400 nm of gold was deposited onto silicon wafers by e-beam evaporation, and then a small drop (10 μL) of Norland Optical Adhesive 83H was applied to the gold surface followed by a 2 cm x 2 cm glass substrate. After curing the adhesive using a UV lamp for 10 minutes, the glass slide was stripped from the silicon wafer using a scalpel. TS gold films were used immediately after their fabrication for SAM formation to minimize surface contamination.

### 6.2.2. SAM Formation

Approximately 2 cm x 2 cm As-Dep and TS gold substrates were immersed into a 1 mM R<sub>2</sub>DTPA solution in anhydrous toluene or a 1 mM solution of 1-hexadecanethiol in

anhydrous ethanol for 24 hours. Substrates were then removed from solution, rinsed with anhydrous toluene (for R<sub>2</sub>DTPA SAMs) or anhydrous ethanol (for 1-hexadecanethiolate SAMs), and dried under a stream of nitrogen.

### *6.2.3. Sample Preparation for Lateral Force Microscopy*

Microcontact printing of 1-hexadecanethiol onto As-Dep and TS gold substrates was carried out according to published procedures using a PDMS stamp bearing 10- $\mu$ m-wide raised lines separated by 10- $\mu$ m-wide recesses.<sup>49</sup> Printed gold substrates were rinsed with anhydrous ethanol, dried using a stream of nitrogen, and placed into a 2 mM toluene solution of R<sub>2</sub>DTPA for 15 minutes. Substrates were removed from the solution, rinsed with anhydrous toluene and anhydrous ethanol, and dried under a stream of nitrogen.

### *6.2.4. Atomic Force Microscopy (AFM) and Lateral Force Microscopy (LFM)*

AFM and LFM images were obtained using a Digital Instruments Multimode atomic force microscope run in contact mode. Veeco type SNL (Silicon-tip on Nitride Lever) cantilevers were used with a nominal tip radius of 2 nm and a nominal force constant of 0.12 N/m. The back side of the cantilever was coated with  $45 \pm 5$  nm of Ti/Au. LFM images were collected over a 75  $\mu$ m x 75  $\mu$ m scan area using a scan rate of 1.0 Hz, a scanning resolution of 512 samples/line, and a constant force estimated to be ~0.1 nN. AFM images were collected over a 1  $\mu$ m x 1  $\mu$ m scan area using a scan rate of 1.0 Hz and a scanning resolution of 512 samples / line. All images were collected using Nanoscope 6 software, and processed using WSxM 5.0 Develop 1.0 software.<sup>50</sup>

### *6.2.5. X-Ray Photoelectron Spectroscopy (XPS)*

XPS spectra were collected at Surface Science Western (London, Ontario, Canada) using a Kratos Axis Nova X-ray photoelectron spectrometer with a monochromatic Al K $\alpha$  source. The detection limit of the instrument is 0.1 – 0.5 atomic percent. Both survey scan and high resolution analyses were carried out over a 300  $\mu$ m x 700  $\mu$ m scan area. Survey scan analyses were carried out with a pass energy of 160 eV, and high resolution

analyses were carried out with a pass energy of 20 eV. Samples were analyzed at a 30 degree take-off angle (60 degree tilt). High resolution sulfur line shapes were fit using one pair of spin-orbit-split components (2  $p_{3/2}$  and 2  $p_{1/2}$ ) assuming a Gaussian:Lorentzian (70%:30%) line shape and a fixed splitting energy of 1.18 eV with a 2:1 area ratio.<sup>51</sup>

### *6.2.6. Infrared Spectroscopy*

Reflection-absorption infrared (RAIR) spectra were collected using a Bruker IFS 66/v spectrometer equipped with an MCT detector and Harrick Autoseagull accessory. The p-polarized light was incident at 85° from the surface normal; 1024 scans were collected at a resolution of 2  $\text{cm}^{-1}$ .

### *6.2.7. Contact Angle Measurements*

Water and hexadecane contact angles were measured using the sessile drop method on a Rame-Hart contact angle goniometer equipped with a microlitre syringe and a tilting stage. In each case, at least three drops from three samples (i.e., at least nine independent measurements) were averaged.

### *6.2.8. Electrochemical Impedance Spectroscopy (EIS)*

EIS spectra were collected using a BAS-Zahner IM6 ex impedance unit. A glass cell equipped with a calomel/saturated KCl reference electrode and a 1.0 mm Pt wire counter electrode was clamped to the working electrode, a 0.95- $\text{cm}^2$  area of the SAM on gold, and then filled with an aqueous solution of 1mM  $\text{K}_3\text{Fe}(\text{CN})_6$ , 1mM  $\text{K}_4\text{Fe}(\text{CN})_6 \cdot 3\text{H}_2\text{O}$  and 10 mM  $\text{Na}_2\text{SO}_4$ . The measurements were made at an open circuit potential set at 450 mV with a 5 mV ac perturbation that was controlled from  $5.0 \times 10^{-2}$  to  $2.0 \times 10^5$  Hz. SAM resistance and capacitance values were normalized to the area of the working electrode.

## **6.3. Results and Discussion**

### *6.3.1. Gold Substrate and $R_2\text{DTPA}$ Preparation*

We fabricated TS gold substrates by e-beam evaporation of 400 nm of gold onto a silicon wafer, followed by adhering a 2 cm x 2 cm glass slide on the surface using an

optical adhesive. After curing the adhesive, we removed the glass slide using a scalpel to expose the smooth underside of the film. These substrates consist of grains with sizes ranging from 200 – 500 nm with grain boundaries that are ~2 nm deep, and a root-mean-square roughness of 0.5 nm (Figure 6.1). We synthesized R<sub>2</sub>DTPA compounds according to published procedures,<sup>41,43</sup> and prepared SAMs by immersing TS gold substrates into 1 mM solutions of each adsorbate in toluene for 24 hours.

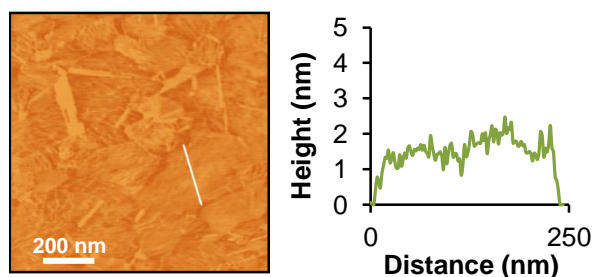


**Figure 6.1.** AFM topographic image recorded in contact mode of a typical TS gold film. The vertical scale is 20 nm. The white line shows the region that corresponds to the cross-sectional profile depicted beside the image.

### *6.3.2. Binding of the DTPA Head Group to the Gold Surface*

X-ray photoelectron spectroscopy (XPS) revealed that both sulfur atoms of R<sub>2</sub>DTPA adsorbates interact with the TS gold surface, indicating that the SAMs contain only chelating adsorbates regardless of the alkyl chain length. Survey scans of R<sub>2</sub>DTPA SAMs formed on TS gold (Figure S6.1) showed characteristic binding energies of gold, as well as the elements comprising the R<sub>2</sub>DTPA adsorbates (P, S, C). Survey scans also showed the presence of oxygen. We used high resolution XPS (HR-XPS) of the S 2p region to determine the binding state of the DTPA adsorbates to the gold surface. The electronic environment of the sulfur atom and the nature of the interaction between sulfur and gold surface atoms influence the S 2p binding energies. Previous HR-XPS studies of sulfur-containing SAMs on gold have established that the S 2p<sub>3/2</sub> peaks of sulfur atoms bound to gold appear at binding energies of ~161 - 162 eV, whereas sulfur atoms that are not interacting with the gold surface give S 2p<sub>3/2</sub> peaks at binding energies of ~163 - 165 eV, and oxidized sulfur species give S 2p<sub>3/2</sub> peaks at binding energies > 166 eV.<sup>52,53</sup> HR-

*The Unusual Self-Organization of Dialkyldithiophosphinic Acid  
Self-Assembled Monolayers on Ultrasmooth Gold*

XPS of the S 2p region of R<sub>2</sub>DTPA SAMs on TS gold (Figure 6.2) showed a simple line shape that we fit using one pair of spin-orbit-split components (S 2p<sub>3/2</sub> and S 2p<sub>1/2</sub>) by assuming a Gaussian/Lorentzian (70%:30%) line shape and a splitting energy fixed at 1.18 eV.<sup>51</sup> The fitted data show S 2p<sub>3/2</sub> peaks at binding energies ~ 161 - 162 eV (Table 6.1), which indicate that all sulfur atoms in these SAMs are bound to the gold substrate. Accordingly, all of the adsorbates are chelated to the gold surface, regardless of the alkyl chain length.

HR-XPS spectra of the S 2p region furthermore show that the oxygen detected in survey scans of R<sub>2</sub>DTPA SAMs on TS gold is likely due to the adsorption of adventitious oxygen-containing species rather than oxidation of the DTPA headgroup. The absence of peaks at binding energies > 168 eV, which correspond to oxidized sulfur species, is consistent with protection of the DTPA sulfur atoms from oxidation even for the shortest alkyl chain lengths studied. In contrast, XPS studies of R<sub>2</sub>DTPA SAMs on As-Dep gold with short alkyl chains (hexyl and decyl) show S 2p<sub>3/2</sub> peaks at binding energies > 168 eV.<sup>43</sup> In these SAMs, the hexyl and decyl chains are too short and disordered to prevent the penetration of oxygen through the SAM to the head group, resulting in DTPA oxidation. On TS gold, chelation of the headgroup and/or differences in alkyl group packing (*vide infra*) likely protect the head group from oxidation. Previously reported DTPA SAMs on As-Dep gold with long alkyl chains – R<sub>2</sub>DTPA SAMs ( $n = 11, 13, 15$ ) and R<sup>1</sup>R<sup>2</sup>DTPA SAMs (R<sup>1</sup> = hexyl, R<sup>2</sup> = decyl, hexadecyl) – do not show peaks in the HR-XPS spectra due to oxidized sulfur species, suggesting that the alkyl groups are long enough in these SAMs to protect the head group from oxidation.<sup>40,43</sup> However, survey scans of these SAMs do exhibit peaks due to oxygen, which have been attributed to the adsorption of adventitious species that contain oxygen. The presence of oxygen in the XPS survey scans of R<sub>2</sub>DTPA SAMs on TS gold suggests that these SAMs, like their long-chain counterparts on As-Dep gold, do not prevent adsorption of such oxygen containing species.

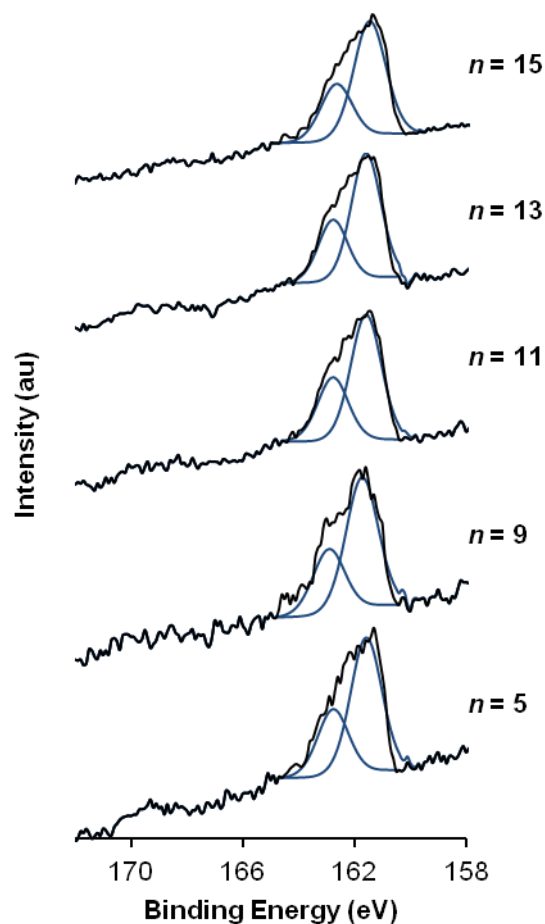


**Figure 6.2.** HR-XPS spectra of the S 2p region for  $[\text{CH}_3(\text{CH}_2)_n]_2\text{DTPA}$  SAMs on TS gold.

**Table 6.1.** S  $2p_{3/2}$  binding energies of  $[\text{CH}_3(\text{CH}_2)_n]_2\text{DTPA}$  SAMs on TS gold.

	[CH <sub>3</sub> (CH <sub>2</sub> ) <sub>n</sub> ] <sub>2</sub> DTPA SAM				
	<i>n</i> = 5	<i>n</i> = 9	<i>n</i> = 11	<i>n</i> = 13	<i>n</i> = 15
S $2p_{3/2}$ Binding Energy (eV)	161.6	161.7	161.6	161.6	161.5

### *6.3.3. Organization of the Alkyl Chains*

Reflection absorption infrared spectroscopy (RAIRS) revealed an unexpected trend in the organization of the alkyl layer of R<sub>2</sub>DTPA SAMs on TS gold: SAMs with short ( $n = 5$ ) alkyl chains are highly crystalline, and the layer becomes more disordered and liquid-like as the number of methylene units in the alkyl chain increases. This trend directly counters that of R<sub>2</sub>DTPA SAMs on As-Dep gold and RSH SAMs on coinage metals, which exhibit the typical trend of increasing alkyl group crystallinity as the number of methylene units in the chain increases.<sup>3,4,43</sup> The typical trend can be straightforwardly explained by the increasing number of van der Waals interactions between the chains as the chain length increases. We assessed the crystallinity of the alkyl layers of R<sub>2</sub>DTPA SAMs on TS gold by comparing the frequencies of the asymmetric and symmetric methylene C-H stretching modes to those of RSH SAMs and R<sub>2</sub>DTPA SAMs on As-Dep gold. RAIR spectra of the R<sub>2</sub>DTPA SAMs on TS gold are shown in Figure 6.3, along with dotted lines at 2918 cm<sup>-1</sup> and 2850 cm<sup>-1</sup> that correspond to the  $\nu_{as}(\text{CH}_2)$  and  $\nu_s(\text{CH}_2)$  stretching frequencies for the crystalline chains of C<sub>16</sub>SH SAMs on gold for comparison. The spectra show that, as expected, the intensities of the  $\nu_{as}(\text{CH}_2)$  and  $\nu_s(\text{CH}_2)$  peaks increase as the number of methylene groups increases. At the same time, the  $\nu_{as}(\text{CH}_2)$  and  $\nu_s(\text{CH}_2)$  peak frequencies also increase, which corresponds to a decrease in chain crystallinity. The SAM with the shortest alkyl chain length, (C<sub>6</sub>)<sub>2</sub>DTPA, exhibits the highest crystallinity, with  $\nu_{as}(\text{CH}_2)$  and  $\nu_s(\text{CH}_2)$  stretching frequencies of 2919 cm<sup>-1</sup> and 2850 cm<sup>-1</sup>, respectively, that are nearly identical to C<sub>16</sub>SH SAMs on gold and (C<sub>16</sub>)<sub>2</sub>DTPA SAMs on As-Dep gold (Table 6.2). The SAM with the longest chain length, (C<sub>16</sub>)<sub>2</sub>DTPA, exhibits the most disorder, with  $\nu_{as}(\text{CH}_2)$  and  $\nu_s(\text{CH}_2)$  stretching frequencies at 2925 cm<sup>-1</sup> and 2854 cm<sup>-1</sup>, indicative of a SAM in which the alkyl layer is more disordered and liquid-like than even C<sub>6</sub>SH SAMs on gold and (C<sub>6</sub>)<sub>2</sub>DTPA SAMs on As-Dep gold (Table 6.2).

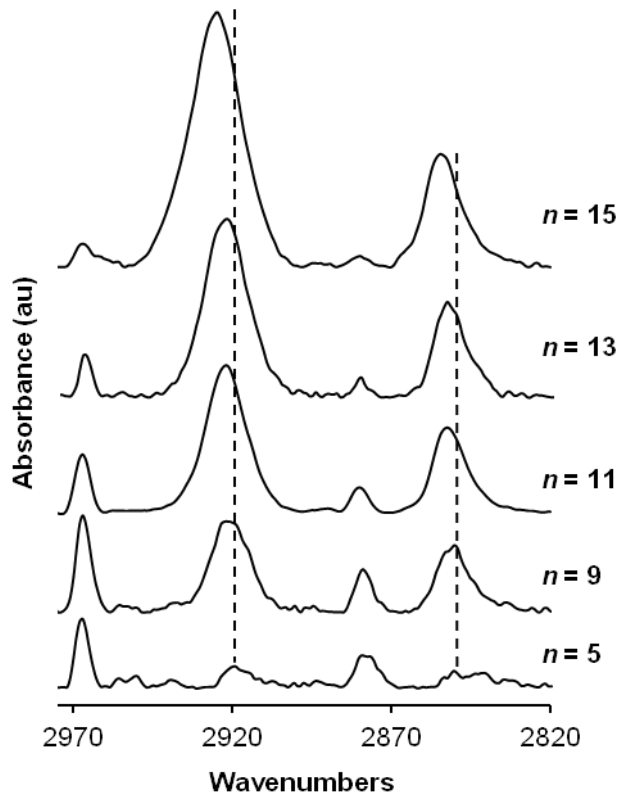


**Figure 6.3.** RAIR spectra (2970 - 2820 cm<sup>-1</sup>) of [CH<sub>3</sub>(CH<sub>2</sub>)<sub>n</sub>]<sub>2</sub>DTPA ( $n = 5, 9, 11, 13, 15$ ) SAMs formed on TS gold. Dashed lines correspond to symmetric (2850 cm<sup>-1</sup>) and asymmetric (2918 cm<sup>-1</sup>) methylene C-H stretches of C<sub>16</sub>SH SAMs formed on TS gold.

**Table 6.2.** Comparison of asymmetric and symmetric methylene C-H stretching frequencies for R<sub>2</sub>DTPA (n = 5, 15) SAMs on TS gold, RSH (n = 5, 15) SAMs on TS gold, and R<sub>2</sub>DTPA (n = 5, 15) SAMs on As-Dep gold.

SAM	Peak Positions (cm <sup>-1</sup> )			
	n = 5		n = 15	
	$\nu_{as}(\text{CH}_2)$	$\nu_s(\text{CH}_2)$	$\nu_{as}(\text{CH}_2)$	$\nu_s(\text{CH}_2)$
[CH <sub>3</sub> (CH <sub>2</sub> ) <sub>n</sub> ] <sub>2</sub> DTPA on TS Au	2919	2850	2925	2854
CH <sub>3</sub> (CH <sub>2</sub> ) <sub>n</sub> SH on TS Au	2921	2852	2917	2850
[CH <sub>3</sub> (CH <sub>2</sub> ) <sub>n</sub> ] <sub>2</sub> DTPA on As-Dep Au <sup>a</sup>	2922	2853	2918	2850

<sup>a</sup>Peak positions of R<sub>2</sub>DTPA SAMs on As-Dep gold obtained from reference 40.

As the alkyl chain length of R<sub>2</sub>DTPA SAMs on TS gold increases and the chains become more liquid-like, the orientation of the methyl groups also becomes more heterogeneous. Analysis of the asymmetric methyl C-H stretches at ~2967 cm<sup>-1</sup> indicates that these peaks become broader as the length of the alkyl chain increases (Figure 6.3). The uniformity of the orientation of the methyl groups influences the breadth of the asymmetric methyl stretch. Methyl groups of crystalline SAMs are tightly packed and uniformly oriented, which produces sharp  $\nu_{as}(\text{CH}_3)$  peaks, whereas the disordered methyl groups of liquid-like SAMs are heterogeneously oriented and produce broad  $\nu_{as}(\text{CH}_3)$  peaks.<sup>30</sup> As the alkyl chain length increases, the full width at half-maximum (FWHM) of the  $\nu_{as}(\text{CH}_3)$  peak of R<sub>2</sub>DTPA SAMs on TS gold increases from 5.0 cm<sup>-1</sup> for the (C<sub>6</sub>)<sub>2</sub>DTPA SAM to 6.5 cm<sup>-1</sup> for the (C<sub>16</sub>)<sub>2</sub>DTPA SAM (Table S6.1). The narrower width of the  $\nu_{as}(\text{CH}_3)$  peak of the (C<sub>6</sub>)<sub>2</sub>DTPA SAM compared to the (C<sub>16</sub>)<sub>2</sub>DTPA SAM is

consistent with crystalline, uniformly oriented alkyl chains in the former SAM and liquid-like, disorganized alkyl chains in the latter SAM.

To explain the unexpected trend in alkyl chain crystallinity observed for R<sub>2</sub>DTPA SAMs on TS gold, we must understand the factors that control how the adsorbates self-organize on the TS gold surface. We have previously reported that the packing density of the alkyl chains of (C<sub>16</sub>)<sub>2</sub>DTPA SAMs formed on As-Dep and TS gold depends how the adsorbates in the SAM bind to the gold substrate.<sup>41</sup> On As-Dep gold, the conformational flexibility of the monodentate (C<sub>16</sub>)<sub>2</sub>DTPA adsorbates enables dense packing of the alkyl groups, and consequently the interchain van der Waals interactions that stabilize a trans-extended, crystalline alkyl layer. In contrast, the liquid-like alkyl chains of (C<sub>16</sub>)<sub>2</sub>DTPA SAMs on TS gold indicates that there is a difference in how these adsorbates pack in the SAM. Based on this study, we concluded that because all adsorbates chelate on TS gold, the inflexibility of the chelated head groups, along with the steric demands of the bulky DTPA head group, likely reduce the packing density of these adsorbates on the surface compared to (C<sub>16</sub>)<sub>2</sub>DTPA SAMs on As-Dep gold. Reduced adsorbate packing density consequently limits the interchain van der Waals interactions necessary to stabilize trans-extended and crystalline alkyl groups, and instead leads to a disordered alkyl layer. The present study shows that this conclusion is only part of the picture: Reducing the steric demands of the alkyl groups by shortening the chain length profoundly changes the structures of R<sub>2</sub>DTPA SAMs on TS gold. The alkyl layer becomes increasingly crystalline as the steric demands of the alkyl group are decreased, which may signify that the packing density of the adsorbates in the SAM also increases. When the chain length is shortened to hexyl groups, the packing density may be high enough to enable the interchain van der Waals interactions necessary to stabilize a crystalline alkyl layer. Although our interpretation of the RAIRS data is consistent with differences in packing density as a function of alkyl chain length, obtaining direct evidence of differences in adsorbate packing density by comparing the intensities of the  $\nu_s(\text{CH}_3)$  and  $\nu_{as}(\text{CH}_3)$  peaks in the RAIRS spectra is unfortunately complicated by the surface selection rule.<sup>54</sup> SAMs with densely packed adsorbates will produce more intense  $\nu_s(\text{CH}_3)$  and  $\nu_{as}(\text{CH}_3)$  peaks than those with a low packing density. At the same time, however, the tilt of the methyl

*The Unusual Self-Organization of Dialkyldithiophosphinic Acid  
Self-Assembled Monolayers on Ultrasmooth Gold*

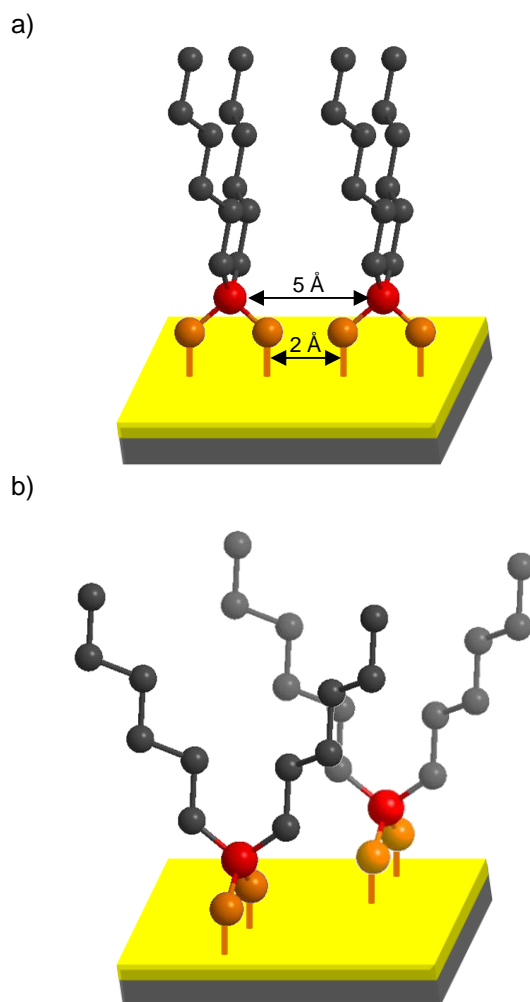
groups relative to the surface normal affects the intensities of the  $\nu_s(\text{CH}_3)$  and  $\nu_{as}(\text{CH}_3)$  peaks according to the surface selection rule. As the length of the alkyl chain in  $\text{R}_2\text{DTPA}$  SAMs on TS gold increases from hexyl to hexadecyl, both the  $\nu_s(\text{CH}_3)$  and  $\nu_{as}(\text{CH}_3)$  peaks decrease in intensity. The intensities of both the  $\nu_{as}(\text{CH}_3)$  and  $\nu_s(\text{CH}_3)$  peaks of the  $(\text{C}_6)_2\text{DTPA}$  SAM are 2.2 times higher than those of the  $(\text{C}_{16})_2\text{DTPA}$  SAM. Although the higher intensity of the methyl C-H stretching peaks in the  $(\text{C}_6)_2\text{DTPA}$  SAM may be due to a higher density of methyl groups on the surface, a different average tilt angle of these adsorbates may also contribute to the observed differences in intensity.

For  $\text{R}_2\text{DTPA}$  SAMs on TS gold with short alkyl chains, one important question is *how* the molecules can self-organize on the surface to produce alkyl chains that are crystalline. Although a definitive answer to this question is beyond the scope of this work and will likely require careful study using scanning tunneling microscopy, we present a plausible scenario based on the van der Waals distances between alkyl chains necessary to stabilize a trans-extended, crystalline arrangement along with the geometric parameters previously calculated for a model  $(^n\text{Bu})_2\text{DTPA}$  adsorbate.<sup>42</sup> In RSH SAMs on gold, the S...S distance between adjacent adsorbates (4.97 Å) is too large to allow van der Waals interactions between adjacent alkyl groups; consequently, the adsorbates tilt about 30° to reduce the distance between adjacent methylene groups to 4.2 Å, which enables interchain van der Waals interactions and produces a crystalline alkyl layer.<sup>1</sup> The alkyl groups of adjacent DTPA adsorbates from the viewpoint in Scheme 6.2a are also too far apart to stabilize crystalline chains. In Scheme 6.2a, we consider the distance between the C-P-C planes of adjacent adsorbates. Even when the adsorbates are brought unrealistically close (making the S...S distance 2 Å, which corresponds to the S-S bond length in a dialkyldisulfide),<sup>55</sup> the distance between adjacent C-P-C planes is 5 Å.<sup>56</sup> On the other hand, we can also consider adjacent DTPA adsorbates from the viewpoint depicted in Scheme 6.2b, in which the alkyl chains are directed toward one another. These chains can interact with one another if they interdigitate, which may enable sufficient interchain van der Waals interactions to stabilize chain crystallinity and also will increase the packing density of adsorbates on the surface. Since one driving force for monolayer self-assembly is the formation of highly favorable Au-S bonds, it is

*The Unusual Self-Organization of Dialkyldithiophosphinic Acid  
Self-Assembled Monolayers on Ultrasmooth Gold*

reasonable to propose a self-organization process that increases the density of Au-S bonds. Therefore, we propose that a reasonable model for R<sub>2</sub>DTPA SAMs with short alkyl chains consists of adsorbates that self-organize on the TS gold surface with interdigitated chains, which maximizes both interchain van der Waals forces *and* the number of Au-S bonds that form during self-assembly. As the chain length increases, however, the increased space necessary for trans-extended, interdigitated alkyl chains will begin to reduce the packing density of adsorbates in the SAM. At this point, the two processes that stabilize the SAM – the formation of favorable Au-S bonds and interchain van der Waals forces via interdigitation – will be at odds with each other. We propose that at this point it is energetically more favorable to sacrifice interchain van der Waals interactions in favor of increasing the number of Au-S bonds. The outcome is that R<sub>2</sub>DTPA SAMs with long alkyl chains have adsorbates that pack as densely as possible, with a disorganized and liquid-like alkyl layer.

**Scheme 6.2.** Diagrams depicting two possibilities for the self-organization of  $(C_6)_2DTPA$  adsorbates in SAMs on TS gold. a)  $(C_6)_2DTPA$  adsorbates aligned laterally. b)  $(C_6)_2DTPA$  adsorbates oriented to enable interdigitation of the alkyl chains.



Contact angles of hexadecane (HD) on  $R_2DTPA$  SAMs on TS gold are consistent with the proposed model. The contact angle data of  $R_2DTPA$  SAMs on TS gold are plotted as a function of the number of methylene groups in the alkyl chains in Figure 6.4a and tabulated in Table S6.3. We also include contact angle data of  $R_2DTPA$  SAMs on As-Dep gold as a comparison system that follows the typical trend of increasing alkyl chain

*The Unusual Self-Organization of Dialkyldithiophosphinic Acid  
Self-Assembled Monolayers on UltrasMOOTH Gold*

crystallinity as a function of chain length. HD is a low surface tension liquid that is sensitive to the structure and density of the alkyl chains of SAMs.<sup>4,57,58</sup> HD contact angles are typically low on SAMs with liquid-like alkyl groups due to interactions with exposed methylene groups. On SAMs formed from adsorbates with short alkyl chains, such as C<sub>6</sub>SH, low HD contact angles can also be caused by interactions between HD and the underlying gold.<sup>4</sup> In contrast, SAMs with long crystalline alkyl chains, such as SAMs of C<sub>16</sub>SH, have a densely packed methyl surface that generates HD contact angles of > 40°. HD wets the surfaces of (C<sub>6</sub>)<sub>2</sub>DTPA and (C<sub>10</sub>)<sub>2</sub>DTPA SAMs on both TS gold and As-Dep gold (contact angle < 15°). Although RAIRS data indicates that the alkyl chains are crystalline on the former substrate and liquid-like on the latter (Table S6.1 and S6.2), these SAMs may be too thin to prevent HD from sensing the underlying gold. In addition, both SAMs may expose methylene groups at the surface, either due to the liquid-like, disorganized chains in the SAMs on As-Dep gold or to the interdigitated alkyl groups proposed for SAMs on TS gold. The HD contact angle increases to ~32° on both TS and As-Dep gold when the length of the alkyl chain is increased to (C<sub>12</sub>)<sub>2</sub>DTPA, suggesting that the alkyl layers of these SAMs are thick enough to screen the underlying gold surface from the HD drop. On both substrates, the contact angles of < 40° indicate that the HD drop interacts with methylene units of the alkyl chains, which is consistent with the liquid-like alkyl chains indicated by the  $\nu_{as}(\text{CH}_2)$  and  $\nu_s(\text{CH}_2)$  stretching frequencies from RAIRS spectra of (C<sub>12</sub>)<sub>2</sub>DTPA SAMs on both As-Dep and TS gold (Table S6.2 and S6.3). On As-Dep gold, the dodecyl chains are not yet long enough to stabilize crystalline packing via interchain van der Waals interactions. On TS gold, conversely, the dodecyl chains are likely too long to permit the interdigitated packing proposed for alkyl chain crystallinity. As the alkyl chain length is increased further, the HD contact angles sharply diverge: On As-Dep gold, the HD contact angle continues to increase due to the increasing number of interchain van der Waals interactions that impart crystallinity to the alkyl layer, ultimately leading to a well-packed methyl surface. In contrast, on TS gold the HD contact angle decreases to 17° for (C<sub>14</sub>)<sub>2</sub>DTPA SAM and then wets the surface of the (C<sub>16</sub>)<sub>2</sub>DTPA SAM. This progression in HD contact angles follows the trend indicated by RAIRS analysis: As the alkyl chain length is increased,

*The Unusual Self-Organization of Dialkyldithiophosphinic Acid  
Self-Assembled Monolayers on Ultrasmooth Gold*

the alkyl layer becomes increasingly disordered, exposing more methylene groups that interact with the HD probe liquid and lower the contact angle.

Water contact angle measurements are less sensitive than HD to subtle structural differences between SAMs, such as disorder in the alkyl layer; however, the higher surface tension of water can also yield measurable contact angles on SAMs that are simply wet by HD to provide additional insight into the SAM structure. The water contact angles of (C<sub>10</sub>)<sub>2</sub>-, (C<sub>12</sub>)<sub>2</sub>-, (C<sub>14</sub>)<sub>2</sub>- and (C<sub>16</sub>)<sub>2</sub>DTPA SAMs on both TS and As-Dep gold fall within a fairly narrow range (97 – 103°) (Figure 6.3b). On these SAMs, the water drop does not distinguish the structural differences implied by RAIRS and HD contact angle measurements. The water contact angles of (C<sub>6</sub>)<sub>2</sub>DTPA SAMs on TS and As-Dep gold, however, are more informative: On TS gold,  $\theta_a(\text{H}_2\text{O})$  is 80°, whereas on As-Dep gold the value is 93°. This marked difference in water contact angles must stem from the structural differences between (C<sub>6</sub>)<sub>2</sub>DTPA SAMs on TS and As-Dep gold indicated by RAIRS. On As-Dep gold, the water contact angle is similar to that of a C<sub>6</sub>SH SAM on gold and is consistent with the short, liquid-like alkyl chains of both SAMs. On TS gold, however, the alkyl chains are crystalline, and yet the contact angle is 13° lower. Generally, SAMs with crystalline alkyl chains present well-packed methyl surfaces that produce water contact angles > 100°. The incongruity between chain crystallinity and water contact angle in the (C<sub>6</sub>)<sub>2</sub>DTPA SAM on TS gold can be rationalized by considering the proposed model for this SAM, in which the crystallinity of the alkyl chains is stabilized by an interdigitated arrangement of alkyl chains. It is possible that interdigitation leads to a porous (but crystalline) alkyl layer that presents a higher density of exposed methylene units than the liquid-like alkyl chains of the (C<sub>6</sub>)<sub>2</sub>DTPA SAM on As-Dep gold. A porous alkyl layer may also allow water to penetrate the SAM and interact with the underlying gold substrate.

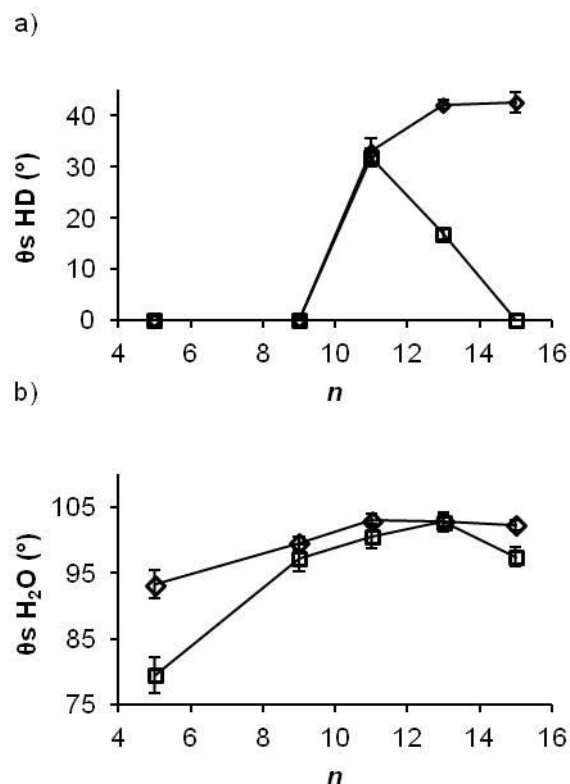


**Figure 6.4.** Hexadecane (a) and water (b) contact angles of  $R_2$ DTPA ( $n = 5, 9, 11, 13, 15$ ) SAMs on TS gold (squares) and As-Dep gold (diamonds) plotted as a function of the number of methylene groups in the alkyl chains.

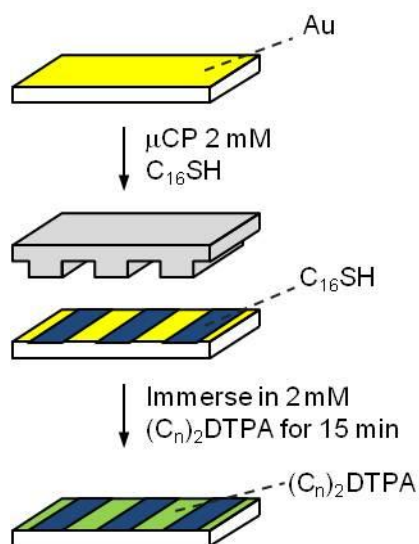
#### *6.3.4. Frictional Properties*

We used lateral force microscopy (LFM) to probe the outermost surface of  $R_2$ DTPA SAMs on TS gold to add to our understanding of the unusual trend in crystallinity as a function of the alkyl chain length indicated by RAIRS and contact angle measurements. LFM records frictional forces between the tip and the sample as the tip is raster scanned across the surface. Due to the lower frictional forces of methyl groups compared to methylene groups, this technique can distinguish between densely packed methyl surfaces, which are typical of SAMs comprised of ordered and crystalline alkyl groups, and SAM surfaces with exposed methylene groups due to disordered, liquid-like alkyl chains.<sup>8</sup> We characterized the frictional properties of the series of  $R_2$ DTPA SAMs on both TS and As-Dep gold using a  $C_{16}SH$  SAM as a standard, well-packed methyl surface

*The Unusual Self-Organization of Dialkyldithiophosphinic Acid  
Self-Assembled Monolayers on Ultrasmooth Gold*

*in situ* by preparing the samples according to Scheme 6.3. We first used microcontact printing<sup>49</sup> to pattern 10- $\mu\text{m}$ -wide lines of a  $\text{C}_{16}\text{SH}$  SAM onto the gold substrate, and then immersed the substrate into a 2 mM solution of  $\text{R}_2\text{DTPA}$  in anhydrous toluene for 15 minutes to form a SAM in the 10- $\mu\text{m}$ -wide spaces between the lines of the  $\text{C}_{16}\text{SH}$  SAM. The 15 minute exposure time minimizes exchange between  $\text{R}_2\text{DTPA}$  and  $\text{C}_{16}\text{SH}$  molecules, and produces  $\text{R}_2\text{DTPA}$  SAMs that are indistinguishable by RAIRS and XPS from  $\text{R}_2\text{DTPA}$  SAMs formed for 24 hours.<sup>41</sup>

**Scheme 6.3.** Process used to pattern alternating lines of  $\text{R}_2\text{DTPA}$  and  $\text{C}_{16}\text{SH}$  SAMs on TS and As-Dep gold substrates.



LFM images of alternating lines of  $\text{C}_{16}\text{SH}$  and  $\text{R}_2\text{DTPA}$  SAMs on both TS and As-Dep gold are shown in Figure 6.5. We used a minimal force ( $\sim 0.1$  nN) between the tip and the surface in order to limit penetration of the tip into the SAM. In the resulting LFM images, dark areas correspond to methyl groups (low friction), and bright areas correspond to methylene groups (high friction). LFM images of both patterned substrates show a set of lines that are consistently dark, which are due to the well-packed methyl surface of the  $\text{C}_{16}\text{SH}$  SAM. On As-Dep gold, the frictional forces between the tip and the

*The Unusual Self-Organization of Dialkyldithiophosphinic Acid  
Self-Assembled Monolayers on UltrasMOOTH Gold*

R<sub>2</sub>DTPA SAM follow the typical trend: As the alkyl chain length increases, the frictional forces decrease, corresponding to an increase in alkyl group crystallinity and methyl group packing density at the surface. Upon reaching the hexadecyl chain length, the surface of the (C<sub>16</sub>)<sub>2</sub>DTPA SAM on As-Dep gold is indistinguishable from that of the C<sub>16</sub>SH SAM. In contrast, the LFM images of patterned R<sub>2</sub>DTPA SAMs on TS gold show that the frictional forces between the tip and the R<sub>2</sub>DTPA SAM increase as the alkyl chain length increases, which is consistent with the increasing alkyl group disorder indicated by RAIRS and contact angle measurements. The surface of the (C<sub>16</sub>)<sub>2</sub>DTPA SAM exhibits the highest difference in friction compared to the C<sub>16</sub>SH SAM; not surprisingly, this SAM has the most liquid-like and disorganized alkyl layer of the series according to RAIRS and contact angle data. It is interesting, however, that the frictional forces of the (C<sub>10</sub>)<sub>2</sub>DTPA SAM are the lowest (i.e., the most similar to the C<sub>16</sub>SH SAM) of the series on TS gold, even though RAIRS data indicates that the alkyl chains of the (C<sub>10</sub>)<sub>2</sub>DTPA SAM are less crystalline than those of the (C<sub>6</sub>)<sub>2</sub>DTPA SAM (Table S6.1). At the same time, however, the water contact angle of the (C<sub>6</sub>)<sub>2</sub>DTPA SAM is 17° lower than that of the (C<sub>10</sub>)<sub>2</sub>DTPA SAM. We interpret the markedly low water contact angle of the (C<sub>6</sub>)<sub>2</sub>DTPA SAM and the slightly higher frictional forces as an outcome of the interdigitated alkyl chains proposed for this SAM: Trans-extended, interdigitated alkyl groups may produce a rather porous structure that exposes methylene units to both the water drop and the AFM tip. Increasing the alkyl chain length by four methylene units in the (C<sub>10</sub>)<sub>2</sub>DTPA SAM results in an alkyl layer with slightly more disordered chains due to the increased steric demands of these alkyl groups, but the water contact angle increases and the frictional forces are lower. The methylene groups are evidently screened by the methyl surface in this SAM, which indicates that the structure of this SAM is less porous than that of the (C<sub>6</sub>)<sub>2</sub>DTPA SAM.

*The Unusual Self-Organization of Dialkyldithiophosphinic Acid  
Self-Assembled Monolayers on Ultrasmooth Gold*

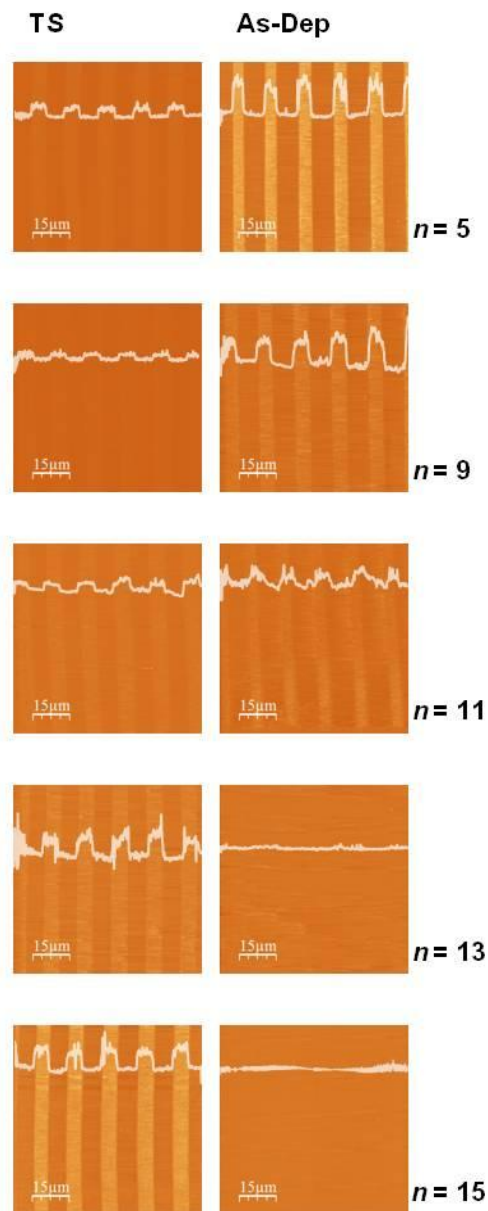


**Figure 6.5.** LFM images of alternating lines of  $C_{16}SH$  and  $R_2DTPA$  ( $n = 5, 9, 11, 13, 15$ ) SAMs patterned on TS gold (left) and As-Dep gold (right). Bright areas correspond to regions of higher friction. White lines correspond to representative profile measurements depicting the change in friction across the image. Z-scale is 250 mV for all images.

### 6.3.5. Electrochemical Barrier Properties

We used electrochemical impedance spectroscopy (EIS) to further characterize the structures of R<sub>2</sub>DTPA SAMs on TS gold. In the EIS experiment, we apply a small sinusoidal ac perturbation at frequencies ranging from 50 mHz to 20 kHz to the SAM in the presence of an aqueous K<sub>4</sub>Fe(CN)<sub>6</sub> / K<sub>3</sub>Fe(CN)<sub>6</sub> redox probe.<sup>59</sup> Measuring the corresponding current response yields the complex impedance of the SAM, which is presented as a Bode magnitude plot for each R<sub>2</sub>DTPA SAM on TS gold in Figure 6.6. We fit the impedance data using a Randles equivalent circuit to determine values of resistance and capacitance for each SAM. The simple circuit model in Figure 6.7a was appropriate to model the EIS data of R<sub>2</sub>DTPA SAMs with alkyl chain lengths ranging from decyl to hexadecyl. This circuit model consists of a solution resistance in series with a parallel Faradaic impedance (R<sub>SAM</sub>) and coating capacitance (C<sub>SAM</sub>). The Nyquist plot of the (C<sub>6</sub>)<sub>2</sub>DTPA SAM (Figure S6.2), however, exhibited a 45° Warburg line on the low frequency side, which indicates that this SAM permits the diffusion of the redox probe molecule through the SAM to the underlying gold.<sup>60</sup> Accordingly, we used the Randles equivalent circuit in Figure 6.7b to model this data. This circuit model includes a Warburg element to model the linear diffusion.

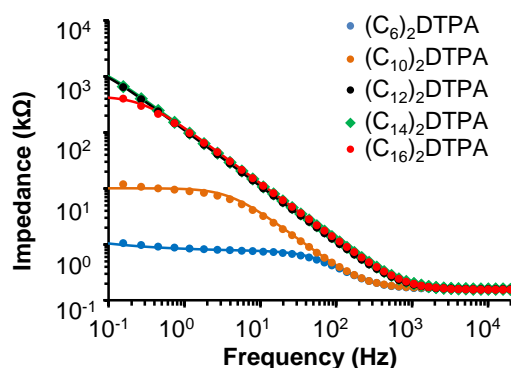


**Figure 6.6.** Bode magnitude plots for R<sub>2</sub>DTPA SAMs formed on TS gold showing the raw data (dotted lines) and data derived from circuit modeling (solid lines).

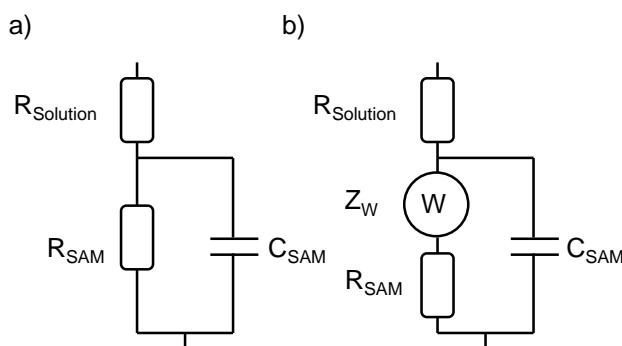


**Figure 6.7.** Randles circuit models used to fit raw EIS data of R<sub>2</sub>DTPA SAMs on TS gold. a) Circuit model used to model impedance data of R<sub>2</sub>DTPA SAMs with  $n = 9, 11, 13, 15$ . b) Circuit model used to model impedance data of (C<sub>6</sub>)<sub>2</sub>DTPA SAMs.

The resistances of R<sub>2</sub>DTPA SAMs derived from circuit modeling are plotted in Figure 6.8a as a function of the number of methylene units in the adsorbate. We used the capacitance values (plotted in Figure 6.8b) from circuit modeling to calculate SAM thicknesses using the following relation:<sup>3</sup>

$$d = \frac{\varepsilon \cdot \varepsilon_0}{C} \quad [1]$$

where  $d$  is the SAM thickness in Angstroms,  $C$  is the capacitance per area in  $\text{F m}^{-2}$ ,  $\varepsilon$  is the dielectric constant of the SAM (measured for C<sub>*n*</sub>SH SAMs ( $n = 16, 18$ ) on gold using surface plasmon resonance to be 2.1)<sup>61</sup> and  $\varepsilon_0$  is the permittivity of free space ( $8.854 \times 10^{-12} \text{ F m}^{-1}$ ). Capacitances and calculated thickness values of R<sub>2</sub>DTPA SAMs are plotted as a function of the number of methylene groups in Figures 8b and 8c. Resistance values, capacitances, and calculated thicknesses are tabulated in Table S6.4. Among the series of R<sub>2</sub>DTPA SAMs studied, the (C<sub>6</sub>)<sub>2</sub>DTPA SAM is unique: Despite having alkyl chains with the highest crystallinity, it exhibits the lowest resistance to charge transfer, it is the thinnest SAM, and it is the only one that permits diffusion of the redox probe through the SAM to the gold surface. We have proposed a model for this SAM based on RAIRS,

*The Unusual Self-Organization of Dialkyldithiophosphinic Acid  
Self-Assembled Monolayers on Ultrasmooth Gold*

contact angle, and LFM results in which the alkyl layer is porous due to an interdigitated arrangement of crystalline alkyl chains. The barrier properties are consistent with this model, and indicate that the alkyl layer is porous enough to permit diffusion of the redox probe through the SAM. Increasing the chain length to decyl increases the resistance of the SAM by an order of magnitude and reduces diffusion of the redox probe molecule through the SAM, which indicates that this SAM is less porous than the (C<sub>6</sub>)<sub>2</sub>DTPA SAM. Considering these barrier properties along with our interpretation of RAIRS and contact angle data, we conclude that the decyl chains are too long to support the interdigitated, crystalline arrangement proposed for the (C<sub>6</sub>)<sub>2</sub>DTPA SAM; consequently, the decyl chains become disordered, which lowers the porosity of the alkyl layer and thus prevents diffusion of the redox probe molecule. Despite the addition of four methylene units, the (C<sub>10</sub>)<sub>2</sub>DTPA SAM is only ~1 Å thicker than the (C<sub>6</sub>)<sub>2</sub>DTPA SAM, which may be due to the change from trans-extended alkyl chains in the (C<sub>6</sub>)<sub>2</sub>DTPA SAM to disordered and liquid-like alkyl chains in the (C<sub>10</sub>)<sub>2</sub>DTPA SAM. Increasing the alkyl chain length to dodecyl chains increases the resistance and thickness of the SAM, as expected; however, both of these properties remain relatively constant as the chain length is increased further to tetradecyl and hexadecyl. We believe that this result not only supports the model we have proposed for long-chain R<sub>2</sub>DTPA SAMs on TS gold, it also adds to our understanding: We have proposed that the alkyl layer becomes increasingly liquid-like due to the steric demands of the alkyl groups, which prevent the chains from adopting the trans-extended, interdigitated arrangement proposed for the (C<sub>6</sub>)<sub>2</sub>DTPA SAM. For the SAM thickness and resistance to remain relatively unchanged in SAMs with dodecyl to hexadecyl chains, however, there must be a gradual decrease in adsorbate packing density that allows the alkyl groups fill the space between adsorbates. The reduction in packing density is likely caused by the increased steric demands of the alkyl groups. It is important to note that we have not directly determined the adsorbate packing densities of these SAMs; nonetheless, RAIRS  $\nu_{as}(\text{CH}_3)$  intensities and EIS data both support the idea that adsorbate packing densities decrease as the steric demands of the alkyl groups increase.

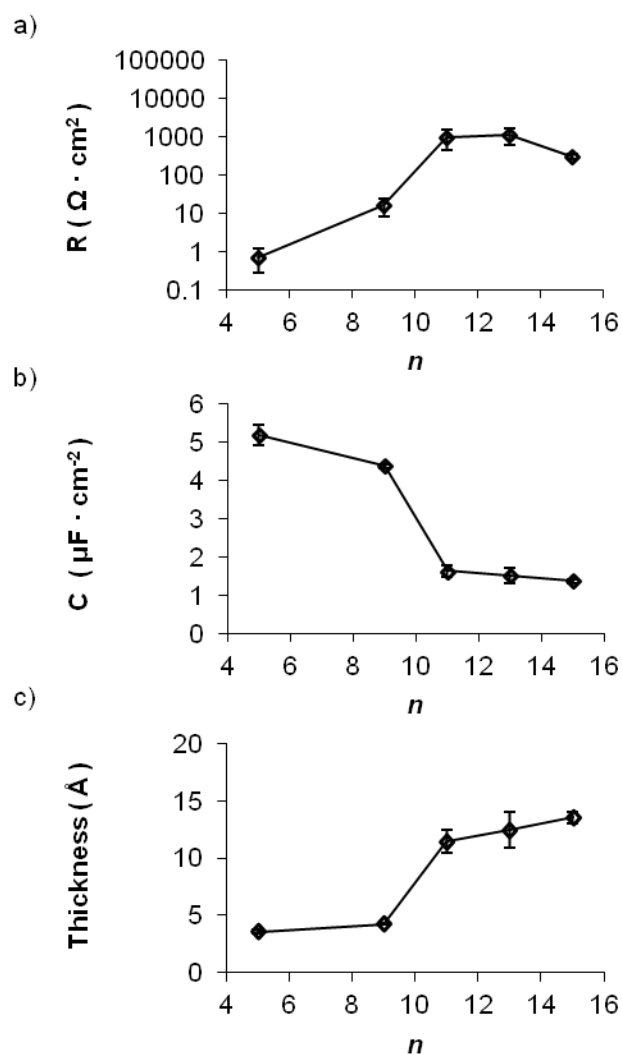


**Figure 6.8.** EIS parameters calculated from fitting raw impedance data to the appropriate Randles equivalent circuit model for  $\text{R}_2\text{DTPA}$  ( $n = 5, 9, 11, 13, 15$ ) SAMs on TS gold. (a) Resistance, (b) capacitance, and (c) effective thickness plotted as a function of the number of methylene groups in the alkyl chains.

## 6.4. Conclusions

Identifying the factors that influence the self-assembly of adsorbates on surfaces, and understanding the interplay between them, is essential for the development of design rules to permit the design of adsorbates to produce complex self-organized structures on surfaces. For example, effective design rules may permit the design of adsorbates to produce SAMs with specific adsorbates packing densities, wettabilities, and frictional properties. Surfaces might be custom designed to permit intercalation of specific guest molecules. Our work on SAMs formed from DTPA adsorbates demonstrates that the simplistic picture invoked for *n*-alkanethiolate SAMs on gold, in which adsorbate-substrate interactions and intermolecular van der Waals interactions govern SAM structure, is not sufficient to explain the self-organization of these complex adsorbates on surfaces. The study presented here reveals that the structures of R<sub>2</sub>DTPA SAMs on TS gold are determined by the interplay of four factors: (i) adsorbate-substrate interactions; (ii) gold substrate morphology; (iii) lateral van der Waals interactions between alkyl groups; and (iv) steric demands of the alkyl groups. The first two factors operate independently of the alkyl chain length. Regardless of the choice of alkyl substituent, highly favorable the Au-S interactions between the R<sub>2</sub>DTPA adsorbates and gold substrate are a driving force for the formation of the SAMs, and the smooth morphology of the TS gold surface is necessary to enable chelation of the adsorbate headgroups. The establishment of favorable van der Waals interactions between alkyl chains drives R<sub>2</sub>DTPA adsorbates with hexyl substituents to self-assemble in an arrangement that likely features interdigitation of the alkyl groups, leading to a crystalline and ordered alkyl layer. As the chain length is increased, however, the final factor – steric demands of the alkyl groups – comes into play. As the steric demands increase, the alkyl chains become increasingly liquid-like and disorganized, and the packing density of adsorbates likely decreases on the surface.

## 6.5. References

- (1) Love, C. J.; Estroff, L. A.; Kriebel, J. K.; Nuzzo, R. G.; Whitesides, G. M. *Chem. Rev.* **2005**, *105*, 1103.
- (2) Ulman, A. *Chem. Rev.* **1996**, *96*, 1533.
- (3) Porter, M. D.; Bright, T. B.; Allara, D. L.; Chidsey, C. E. D. *J. Amer. Chem. Soc.* **1987**, *109*, 3559.
- (4) Bain, C. D.; Troughton, E. B.; Tao, Y. T.; Evall, J.; Whitesides, G. M.; Nuzzo, R. G. *J. Am. Chem. Soc.* **1989**, *111*, 321.
- (5) Shon, Y. S.; Lee, S.; Colorado, R.; Perry, S. S.; Lee, T. R. *J. Am. Chem. Soc.* **2000**, *122*, 7556.
- (6) Shon, Y. S.; Lee, S.; Perry, S. S.; Lee, T. R. *J. Am. Chem. Soc.* **2000**, *122*, 1278.
- (7) Xiao, X.; Hu, J.; Charych, D. H.; Salmeron, M. *Langmuir* **1996**, *12*, 235.
- (8) Lio, A.; Charych, D. H.; Salmeron, M. *J. Phys. Chem. B* **1997**, *101*, 3800.
- (9) Lee, S.; Shon, Y. S.; Colorado, R.; Guenard, R. L.; Lee, T. R.; Perry, S. S. *Langmuir* **2000**, *16*, 2220.
- (10) Lee, Y. J.; Jeon, T. C.; Paik, W. K.; Kim, K. *Langmuir* **1996**, *12*, 5830.
- (11) Garg, N.; Lee, T. R. *Langmuir* **1998**, *14*, 3815.
- (12) Kim, C. H.; Han, S. W.; Ha, T. H.; Kim, K. *Langmuir* **1999**, *15*, 8399.
- (13) Lim, J. K.; Kim, Y.; Kwon, O.; Joo, S. W. *Chem. Phys. Chem.* **2008**, *9*, 1781.
- (14) Lim, J. K.; Kwon, O.; Joo, S. W. *J. Phys. Chem. C* **2008**, *112*, 6816.
- (15) Bruno, G.; Babudri, F.; Operamolla, A.; Bianco, G. V.; Losurdo, M.; Giangregorio, M. M.; Omar, O. H.; Mavelli, F.; Farinola, G. M.; Capezzuto, P.; Naso, F. *Langmuir* **2010**, *26*, 8430.
- (16) Srisombat, L. O.; Zhang, S. S.; Lee, T. R. *Langmuir* **2010**, *26*, 41.
- (17) Fox, M. A.; Whitesell, J. K.; McKerrow, A. J. *Langmuir* **1998**, *14*, 816.

*The Unusual Self-Organization of Dialkyldithiophosphinic Acid  
Self-Assembled Monolayers on Ultrasoother Gold*

- (18) Kittredge, K. R.; Minton, M. A.; Fox, M. A.; Whitesell, J. K. *Helv. Chim. Acta* **2002**, *85*, 788.
- (19) Yam, C. M.; Cho, J.; Cai, C. Z. *Langmuir* **2003**, *19*, 6862.
- (20) Park, J. S.; Vo, A. N.; Barriet, D.; Shon, Y. S.; Lee, T. R. *Langmuir* **2005**, *21*, 2902.
- (21) Kitagawa, T.; Idomoto, Y.; Matsubara, H.; Hobara, D.; Kakiuchi, T.; Okazaki, T.; Komatsu, K. *J. Org. Chem.* **2006**, *71*, 1362.
- (22) Katano, S.; Kim, Y.; Matsubara, H.; Kitagawa, T.; Kawai, M. *J. Am. Chem. Soc.* **2007**, *129*, 2511.
- (23) Colorado, R.; Villazana, R. J.; Lee, T. R. *Langmuir* **1998**, *14*, 6337.
- (24) Lee, T. C.; Hounihan, D. J.; Colorado, R.; Park, J. S.; Lee, T. R. *J. Phys. Chem. B* **2004**, *108*, 2648.
- (25) Lee, T. C.; Chen, P. C.; Lai, T. Y.; Tuntiwechapikul, W.; Kim, J. H.; Lee, T. R. *Appl. Surf. Sci.* **2008**, *254*, 7064.
- (26) Moore, H. J.; Colorado, R.; Lee, H. J.; Jamison, A. C.; Lee, T. R. *Langmuir* **2013**, *29*, 10674.
- (27) Gothelf, K. V. *J. Electroanal Chem.* **2000**, *494*, 147.
- (28) Zhao, Y.; Perez-Segarra, W.; Shi, Q. C.; Wei, A. *J. Am. Chem. Soc.* **2005**, *127*, 7328.
- (29) Morf, P.; Raimondi, F.; Nothofer, H. G.; Schnyder, B.; Yasuda, A.; Wessels, J. M.; Jung, T. A. *Langmuir* **2006**, *22*, 658.
- (30) Weinstein, R. D.; Richards, J.; Thai, S. D.; Omiatek, D. M.; Bessel, C. A.; Faulkner, C. J.; Othman, S.; Jennings, G. K. *Langmuir* **2007**, *23*, 2887.
- (31) Zhu, H.; Coleman, D. M.; Dehen, C. J.; Geisler, I. M.; Zemlyanov, D.; Chmielewski, J.; Simpson, G. J.; Wei, A. *Langmuir* **2008**, *24*, 8660.
- (32) von Wrochem, F.; Gao, D.; Scholz, F.; Nothofer, H.-G.; Nelles, G.; Wessels, J. *M. Nat. Nanotechnol.* **2010**, *5*, 618.

*The Unusual Self-Organization of Dialkyldithiophosphinic Acid  
Self-Assembled Monolayers on Ultrasoother Gold*

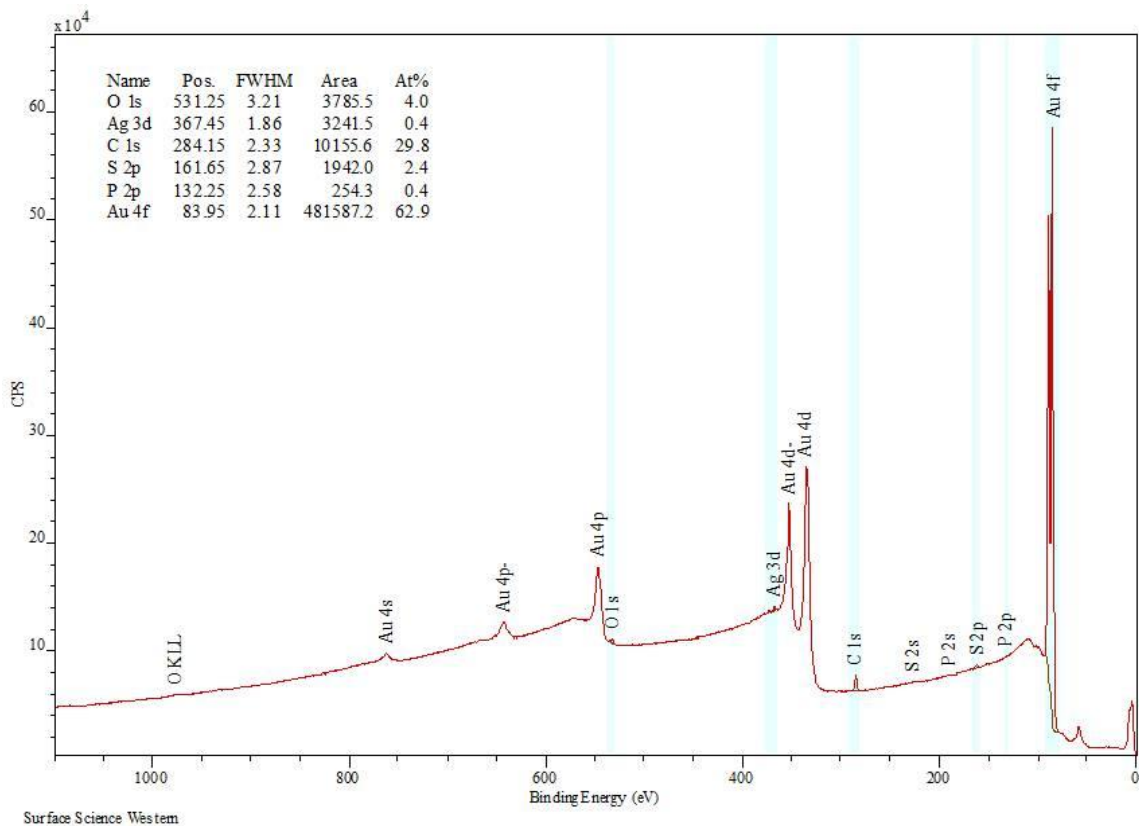
- (33) Gao, D. Q.; Scholz, F.; Nothofer, H. G.; Ford, W. E.; Scherf, U.; Wessels, J. M.; Yasuda, A.; von Wrochem, F. *J. Am. Chem. Soc.* **2011**, *133*, 5921.
- (34) Shon, Y. S.; Lee, T. R. *Langmuir* **1999**, *15*, 1136.
- (35) Shon, Y. S.; Lee, T. R. *J. Phys. Chem. B* **2000**, *104*, 8192.
- (36) Shon, Y. S.; Colorado, R.; Williams, C. T.; Bain, C. D.; Lee, T. R. *Langmuir* **2000**, *16*, 541.
- (37) Park, J. S.; Smith, A. C.; Lee, T. R. *Langmuir* **2004**, *20*, 5829.
- (38) Wang, W.; Zhang, S.; Chinwangso, P.; Advincula, R. C.; Lee, T. R. *J. Phys. Chem. C* **2009**, *113*, 3717.
- (39) Colorado, R., Jr.; Villazana, R. J. L., T. Randall *Langmuir* **1998**, *14*, 6337.
- (40) Juan, R. R. S.; Carmichael, T. B. *Langmuir* **2012**, *28*, 17701.
- (41) Miller, M. S.; Juan, R. R. S.; Ferrato, M.-A.; Carmichael, T. B. *Langmuir* **2011**, *27*, 10019.
- (42) San Juan, R. R.; Allan, C. J.; Iqbal, M.; Eichhorn, S. H.; Macdonald, C. L. B.; Carmichael, T. B. *J. Am. Chem. Soc.* **2013**, *135*, 15784.
- (43) San Juan, R. R.; Miller, M. S.; Ferrato, M. A.; Carmichael, T. B. *Langmuir* **2012**, *28*, 13253.
- (44) Trevor, D. J.; Chidsey, C. E. D.; Loiacono, D. N. *Phys. Rev. Lett.* **1989**, *62*, 929.
- (45) Wagner, P.; Hegner, M.; Guntherodt, H. J.; Semenza, G. *Langmuir* **1995**, *11*, 3867.
- (46) Weiss, E. A.; Kaufman, G. K.; Kriebel, J. K.; Li, Z.; Schalek, R.; Whitesides, G. M. *Langmuir* **2007**, *23*, 9686.
- (47) Naumann, R.; Schiller, S. M.; Giess, F.; Grohe, B.; Hartman, K. B.; Karcher, I.; Koper, I.; Lubben, J.; Vasilev, K.; Knoll, W. *Langmuir* **2003**, *19*, 5435.
- (48) Hegner, M.; Wagner, P.; Semenza, G. *Surf. Sci.* **1993**, *291*, 39.
- (49) Kumar, A.; Biebuyck, H. A.; Whitesides, G. M. *Langmuir* **1994**, *10*, 1498.

*The Unusual Self-Organization of Dialkyldithiophosphinic Acid  
Self-Assembled Monolayers on Ultrasoother Gold*

- (50) Horcas, I.; Fernandez, R.; Gomez-Rodriguez, J. M.; Colchero, J.; Gomez-Herrero, J.; Baro, A. M. *Rev. Sci. Instrum.* **2007**, *78*.
- (51) Moulder, J. F.; Stickle, W. F.; Sobol, P. E.; Bomben, K. D. *Handbook of X-Ray Photoelectron Spectroscopy* Eden Prairie, MN, 1995.
- (52) Castner, D. G.; Hinds, K.; Grainger, D. W. *Langmuir* **1996**, *12*, 5083.
- (53) Ishida, T.; Choi, N.; Mizutani, W.; Tokumoto, H.; Kojima, I.; Azehara, H.; Hokari, H.; Akiba, U.; Fujihira, M. *Langmuir* **1999**, *15*, 6799.
- (54) Bubert, H.; Jenett, H. *Surface and Thin Film Analysis*; Wiley-VCH: Weinham, 2002.
- (55) Koval, I. V. *Russ. Chem. Rev.* **1994**, *63*, 735.
- (56) The distance between adjacent C-P-C planes was calculated assuming a separation distance of 2 Å between the sulfur atoms of nearest neighbour DTPA molecules, and an intramolecular DTPA S-S distance of 3 Å which was calculated for <sup>n</sup>Bu<sub>2</sub>DTPA in reference 42.
- (57) Ulman, A. *Ultrathin Organic Films*; Academic Press: San Diego, 1991.
- (58) Bain, C. D.; Whitesides, G. M. *J. Am. Chem. Soc.* **1989**, *111*, 7164.
- (59) Barsoukov, E.; Macdonald, J. R. *Impedance Spectroscopy*; 2nd ed.; Wiley and Sons: Hoboken, NJ, 2005.
- (60) Diao, P.; Guo, M.; Tong, R. T. *J. Electroanal. Chem.* **2001**, *495*, 98.
- (61) Peterlinz, K. A.; Georgiadis, R. *Langmuir* **1996**, *12*, 4731.

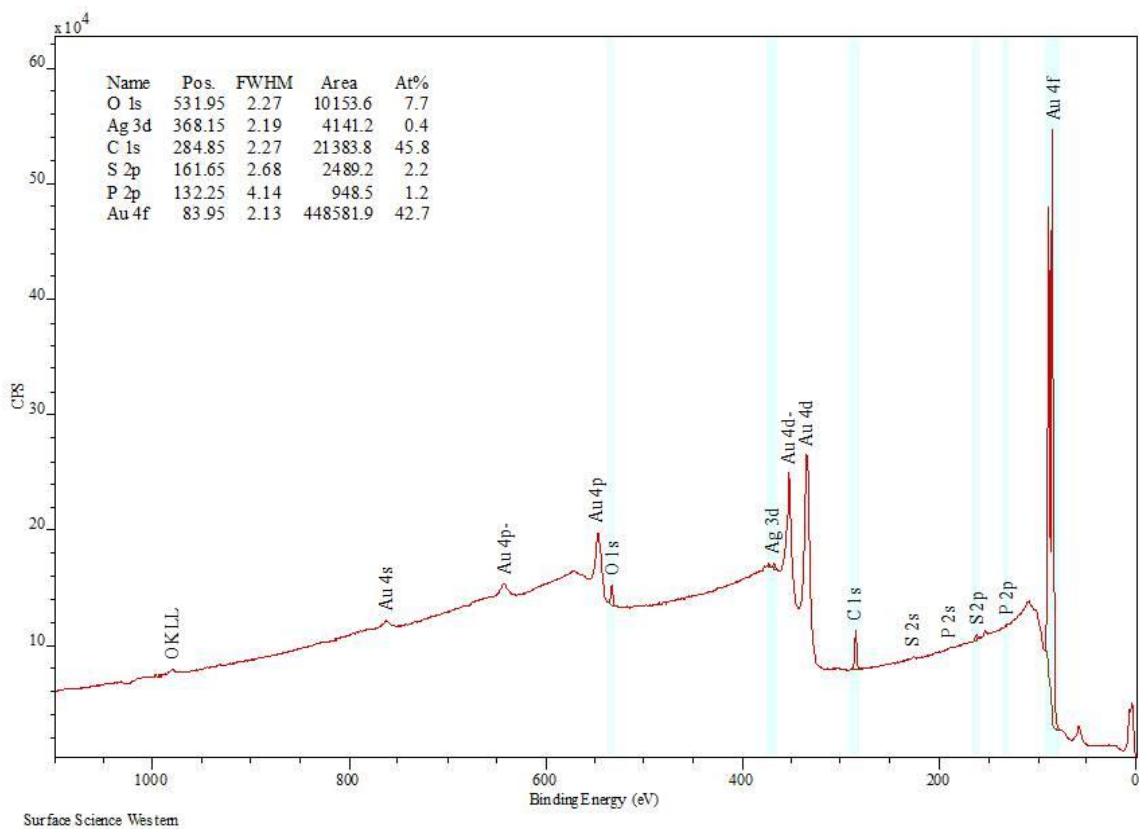
## 6.6. Supporting Information and Figures

a)



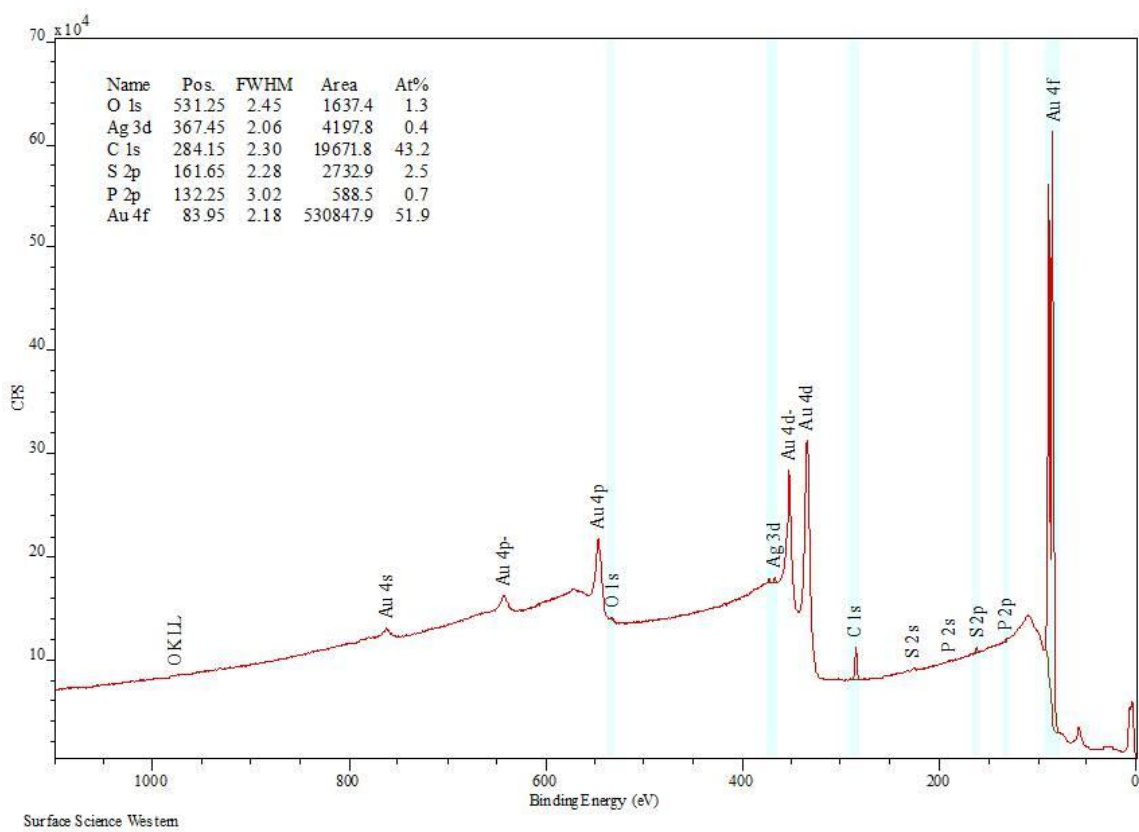
*The Unusual Self-Organization of Dialkyldithiophosphinic Acid  
Self-Assembled Monolayers on Ultrasmooth Gold*

b)



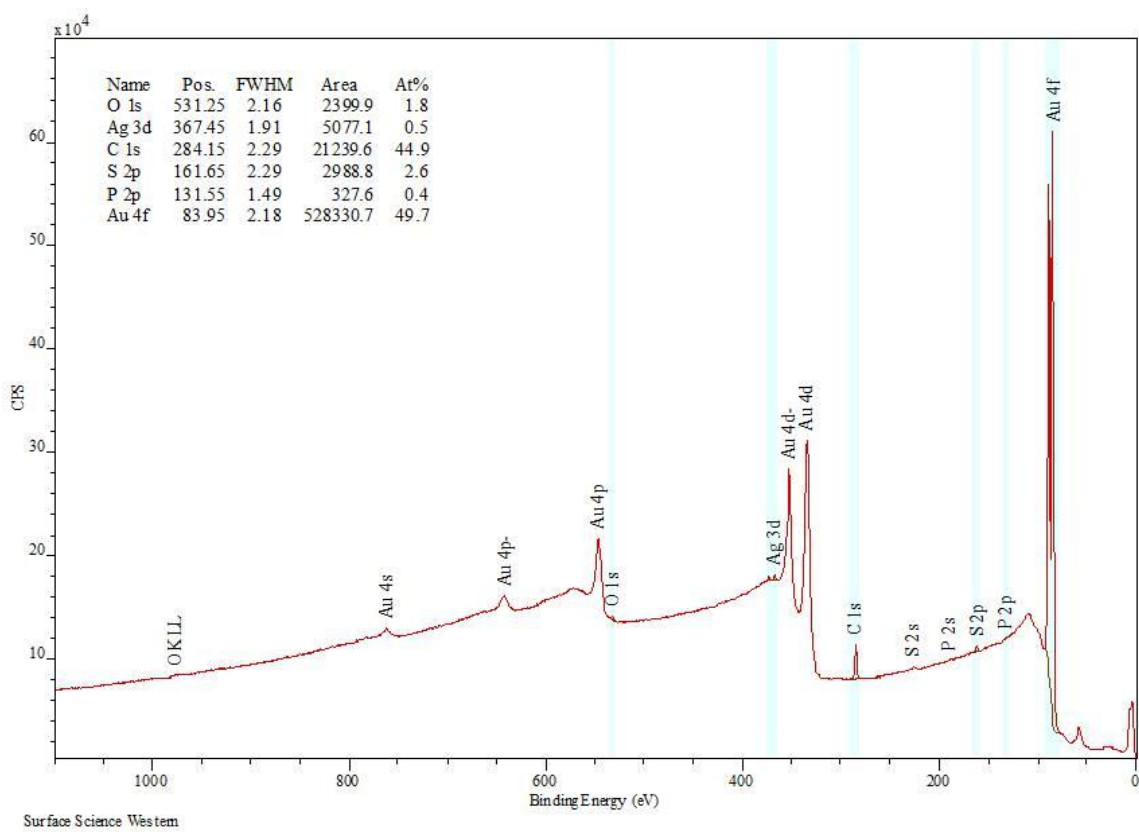
*The Unusual Self-Organization of Dialkyldithiophosphinic Acid  
Self-Assembled Monolayers on Ultrasmooth Gold*

c)



*The Unusual Self-Organization of Dialkyldithiophosphinic Acid  
Self-Assembled Monolayers on Ultrasmooth Gold*

d)



e)

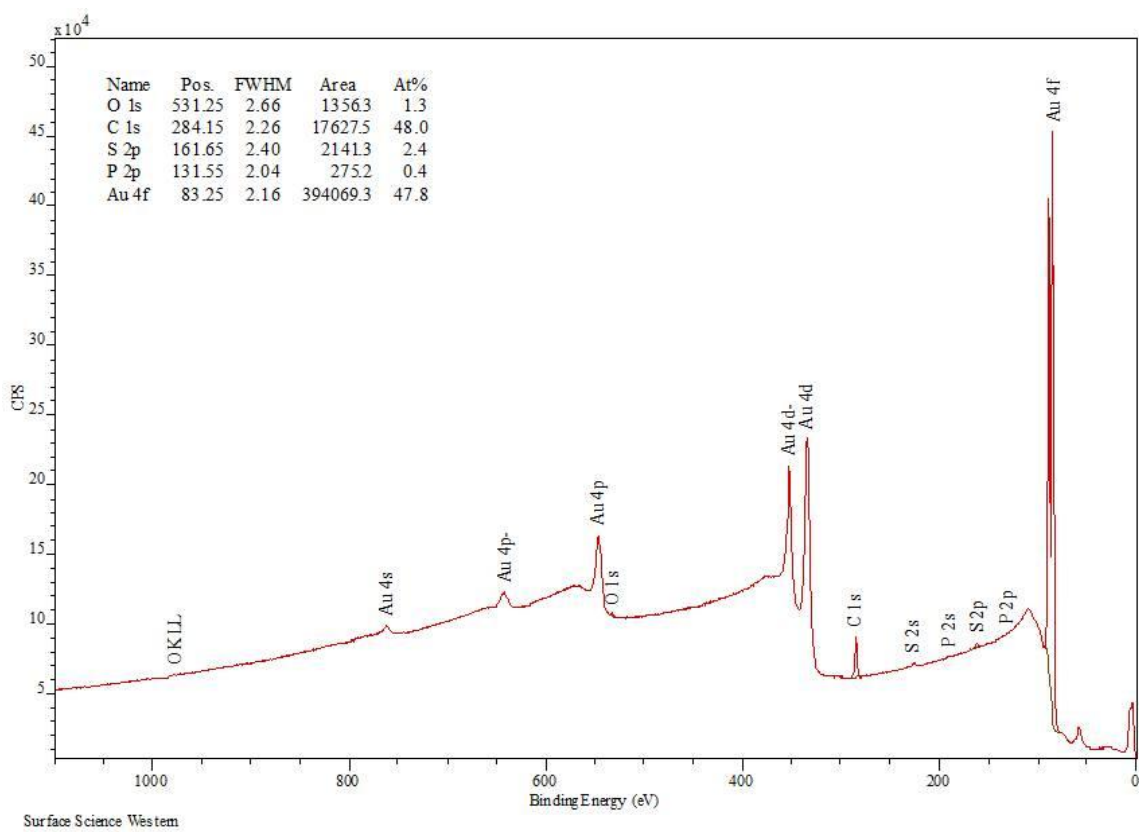


**Figure S6.1.** XPS survey scans for SAMs formed from a)  $(C_6)_2DTPA$ , b)  $(C_{10})_2DTPA$ , c)  $(C_{12})_2DTPA$ , d)  $(C_{14})_2DTPA$ , and e)  $(C_{16})_2DTPA$  on TS gold.

*The Unusual Self-Organization of Dialkyldithiophosphinic Acid  
Self-Assembled Monolayers on Ultrasmooth Gold*

**Table S6.1.** Position and intensity of methyl and methylene C-H stretches of R<sub>2</sub>DTPA SAMs on TS gold as determined by RAIRS.

	(C <sub>6</sub> ) <sub>2</sub> DTPA	(C <sub>10</sub> ) <sub>2</sub> DTPA	(C <sub>12</sub> ) <sub>2</sub> DTPA	(C <sub>14</sub> ) <sub>2</sub> DTPA	(C <sub>16</sub> ) <sub>2</sub> DTPA
$\nu_{\text{as}}(\text{CH}_3)$ (cm <sup>-1</sup> )	2967	2967	2967	2967	2967
FWHM (cm <sup>-1</sup> )	5.0	5.4	5.5	4.6	6.5
Intensity (au)	0.00039	0.00062	0.00037	0.00027	0.00018
$\nu_{\text{as}}(\text{CH}_2)$ (cm <sup>-1</sup> )	2919	2922	2922	2923	2925
Intensity (au)	0.00012	0.00059	0.00095	0.00115	0.00195
$\nu_{\text{s}}(\text{CH}_3)$ (cm <sup>-1</sup> )	2878	2879	2880	2880	2880
Intensity (au)	0.00018	0.00028	0.00016	0.000121	0.00008
$\nu_{\text{s}}(\text{CH}_2)$ (cm <sup>-1</sup> )	2850	2851	2852	2853	2854
Intensity (au)	0.000093	0.00043	0.00054	0.00061	0.00087

*The Unusual Self-Organization of Dialkyldithiophosphinic Acid  
Self-Assembled Monolayers on Ultrasmooth Gold*

**Table S6.2.** Position of methylene C-H stretches of R<sub>2</sub>DTPA SAMs on As-Dep gold as determined by RAIRS.<sup>43</sup>

	peak positions (cm <sup>-1</sup> )				
	(C <sub>6</sub> ) <sub>2</sub> DTPA	(C <sub>10</sub> ) <sub>2</sub> DTPA	(C <sub>12</sub> ) <sub>2</sub> DTPA	(C <sub>14</sub> ) <sub>2</sub> DTPA	(C <sub>16</sub> ) <sub>2</sub> DTPA
$\nu_{\text{as}}(\text{CH}_2)$ (cm <sup>-1</sup> )	2922	2922	2921	2921	2918
$\nu_{\text{s}}(\text{CH}_2)$ (cm <sup>-1</sup> )	2853	2853	2852	2851	2850

**Table S6.3.** Static water and hexadecane contact angles of R<sub>2</sub>DTPA SAMs on As-Dep and TS gold.

	As-Dep Gold		TS Gold	
	$\theta_{\text{s}}(\text{H}_2\text{O})$ (°)	$\theta_{\text{s}}(\text{HD})$ (°)	$\theta_{\text{s}}(\text{H}_2\text{O})$ (°)	$\theta_{\text{s}}(\text{HD})$ (°)
(C <sub>6</sub> ) <sub>2</sub> DTPA	93.3 +/- 2.2	<15	79.5 +/- 2.8	<15
(C <sub>10</sub> ) <sub>2</sub> DTPA	99.6 +/- 1.0	<15	97.3 +/- 2.1	<15
(C <sub>12</sub> ) <sub>2</sub> DTPA	103 +/- 1.0	33.2 +/- 2.3	100.6 +/- 1.8	31.9 +/- 1.8
(C <sub>14</sub> ) <sub>2</sub> DTPA	102.9 +/- 0.9	42.4 +/- 0.8	102.8 +/- 1.4	17.0 +/- 1.1
(C <sub>16</sub> ) <sub>2</sub> DTPA	102.3 +/- 0.7	42.6 +/- 1.9	97.5 +/- 1.5	<15

*The Unusual Self-Organization of Dialkyldithiophosphinic Acid  
Self-Assembled Monolayers on Ultrasmooth Gold*

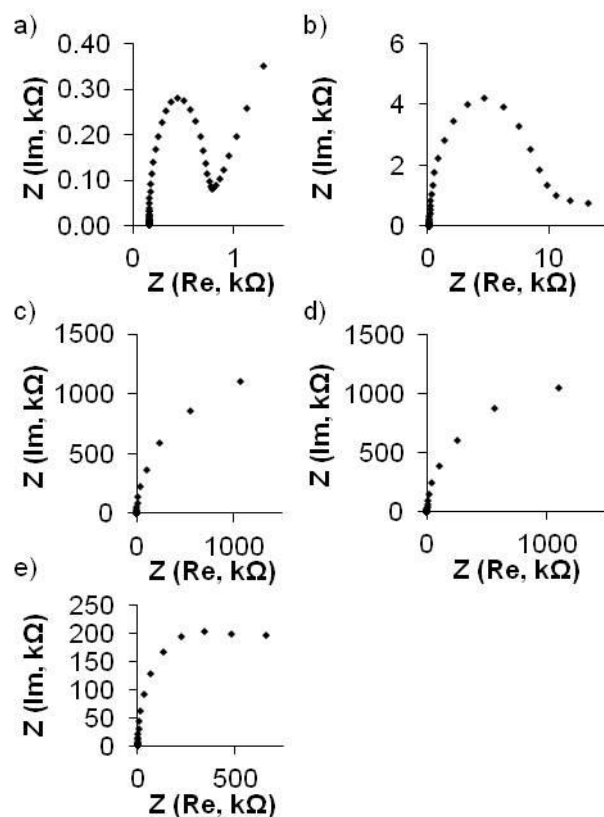


**Figure S6.2** Nyquist plots of  $R_2$ DTPA SAMs on TS gold for  $n =$  a) 5 b) 9 c) 11 d) 13 e) 15.

**Table S6.4.** Resistance, capacitance, and thickness values of  $R_2$ DTPA SAMs on TS gold calculated from Randles equivalent circuit analysis.

	R ( $k\Omega \cdot cm^2$ )	C ( $\mu F \cdot cm^2$ )	T ( $\text{\AA}$ )
$(C_6)_2$ DTPA	0.7 +/- 0.4	5.18 +/- 0.27	3.59 +/- 0.18
$(C_{10})_2$ DTPA	16.4 +/- 7.8	4.38 +/- 0.05	4.24 +/- 0.05
$(C_{12})_2$ DTPA	1000 +/- 545	1.63 +/- 0.15	11.44 +/- 0.98
$(C_{14})_2$ DTPA	1156 +/- 544	1.51 +/- 0.20	12.46 +/- 1.55
$(C_{16})_2$ DTPA	317 +/- 51	1.37 +/- 0.05	13.55 +/- 0.49

## **Chapter 7**

# **Ultra Smooth Gold Substrates Prepared by Chemical Mechanical Polishing: A New Substrate for Measuring Charge Transport in Metal-SAM//Ga<sub>2</sub>O<sub>3</sub>/EGaIn Junctions**

## 7.1. Introduction

This chapter describes the preparation and structural characterization of ultra smooth gold substrates fabricated using chemical mechanical polishing (CMP). We demonstrate CMP – a well established semiconductor fabrication technique – is capable of producing gold substrates with root mean squared (RMS) surface roughness values of 3 – 5 Å over the full surface area of a 75 mm diameter silicon wafer. In addition, this process is fast (< 5 minutes), and produces extremely uniform surfaces; wafer-to-wafer and within-wafer roughness non-uniformities are < 17%. We show that polished gold (Au<sup>CMP</sup>) substrates are ideal candidates for bottom electrodes in metal-SAM//Ga<sub>2</sub>O<sub>3</sub>/EGaIn molecular junctions by measuring the charge transport properties of a series of *n*-alkanethiolate self assembled monolayers (SAMs) (*n* = 9 – 16). We compare *n*-alkanethiolate SAMs formed on Au<sup>CMP</sup> substrates to those formed on template-stripped gold (Au<sup>TS</sup>) substrates – the most commonly used ultra smooth substrate for SAM based junctions – and show that the charge transport properties are statistically indistinguishable, furthermore, junctions formed using Au<sup>CMP</sup> substrates had a significantly higher working junction yield.

The integration of individual molecules as the active or passive components in electronic devices (now known as ‘molecular electronics’) has been the subject of a great research effort in recent years.<sup>1-10</sup> Moore’s law states that the number of electrical components (transistors) that fit onto a conventional integrated circuit (IC) chip grows exponentially, doubling about every two years.<sup>7,11</sup> In order for this trend to continue past the capabilities of current complementary metal-oxide semiconductor (CMOS) fabrication methods, the size of the components that make up these devices must shrink accordingly, with some estimates predicting a need for molecular scale components in the very near future.<sup>7</sup> Molecules are a promising candidate to fulfill this need owing to their small size and easily tunable electronic properties.<sup>6</sup>

Measuring the charge transport properties of molecules requires sandwiching them in between two conductive electrodes to form a ‘molecular junction’.<sup>3</sup> SAMs provide an excellent platform for studying charge transport properties owing to the fact that molecules in the SAM are already supported by a coinage metal (silver, gold) substrate which serves as the bottom electrode in a molecular junction.<sup>12</sup> A variety of structures

have been studied as the top electrode in molecular junctions, including scanning tunneling microscopy (STM) and conductive atomic force microscopy (AFM) probes,<sup>13-30</sup> conductive polymers,<sup>31</sup> mercury liquid metal drops,<sup>32-42</sup> and more recently, EGaIn (a liquid eutectic alloy, 75.5 wt % Ga and 24.5 wt % In),<sup>43-55</sup> to name a few.

It is widely accepted that charge transport through insulating SAMs, such as those formed from *n*-alkanethiolates, occurs via non-resonant, coherent tunneling and adheres to an approximation of the Simmons equation:<sup>56,57</sup>

$$J = J_0 e^{-\beta d}$$

In this model, the current density through the SAM,  $J$ , is exponentially dependent upon the thickness of the tunneling barrier,  $d$ . The parameter  $\beta$  governs the relationship between the exponential decay of current density as the thickness of the tunneling barrier is increased. In principle,  $\beta$  depends only on the molecular orbitals of the molecules comprising the SAM, and should be independent of the top and bottom contacts used to assemble the junction.<sup>3</sup> The pre-exponential factor,  $J_0$ , describes the resistance of the top and bottom contact of the junction, and depends on position of the molecular orbitals of the molecules comprising the SAM with respect to the Fermi energy levels of the top and bottom electrode.<sup>6</sup> Top and bottom contacts that are highly conductive will lead to high values of  $J_0$ , while resistive contacts will lead to low values of  $J_0$ . In order to determine  $\beta$  and  $J_0$  for a given system, current densities must be measured through a series of molecules while varying the length of the tunneling barrier, which is often accomplished by increasing the molecular length by a discrete amount (i.e. one methylene unit). One inherent assumption of using the Simmons equation to describe charge transport through SAMs is that the molecular orbitals, and consequently  $\beta$ , are independent of the molecular length.

Despite a plethora of test structures available for measuring charge transport through SAMs, and suitable physics to model and describe the mechanism of transport, data that are ambiguous, inconsistent, and irreproducible have stymied progress in this field. The origins of these problems can be traced to two major contributing factors: experimental design and statistical analysis.<sup>5,46</sup>

*Ultra Smooth Gold Substrates Prepared by Chemical Mechanical Polishing: A New Substrate for Measuring Charge Transport in Metal-SAM//Ga<sub>2</sub>O<sub>3</sub>/EGaIn Junctions*

Recently, a large research effort has been put forth to develop a set of reliable protocols for measuring and analyzing charge transport through SAMs.<sup>46,55,58</sup> and references therein In a system pioneered by the Whitesides group, many researchers are now measuring charge transport through SAMs using a metal-SAM//Ga<sub>2</sub>O<sub>3</sub>/EGaIn junction. EGaIn is used as a top contact for several reasons: First, EGaIn is a liquid eutectic alloy that makes conformal, non-damaging contact to the surface of the SAM.<sup>54</sup> Second, the surface of EGaIn readily oxidizes in ambient conditions to form a self-limiting ‘skin’ of Ga<sub>2</sub>O<sub>3</sub>.<sup>55</sup> This skin not only provides a barrier between the SAM and the EGaIn metal, increasing the junction yield, but also imparts non-Newtonian properties to the liquid eutectic which allows it to be formed into a conical shaped tip. The EGaIn tip can be made sharp, with radii as small as 25 microns, reducing the effect of ensemble measurements seen in large area soft-contact top electrode junctions. Finally, the EGaIn tip electrode requires no specialized equipment, and allows for numerous (> 500) measurements in a day, providing a large pool of data from which meaningful statistics can be drawn.<sup>54</sup>

The development of the EGaIn tip electrode and a set of statistical tools for proper data analysis have aided the ability of researchers to produce meaningful measurements of charge transport through SAMs. However, structural defects inherent to SAMs will always be a major contributing factor to variability in the data.<sup>36</sup> Current density is exponentially dependent on the thickness of the tunneling barrier; defects in the SAM that lead to ‘thin’ or ‘thick’ areas will cause variation in the measured values of  $J$ .<sup>46</sup> While ‘thick’ areas of the SAM are usually caused the adsorption of adventitious organics on the surface of either the SAM or the Ga<sub>2</sub>O<sub>3</sub> skin and are unavoidable in ambient conditions,<sup>55</sup> ‘thin’ areas of the SAM can be caused by local disorder due to the roughness and grain structure of the underlying metal substrate.<sup>20,36</sup>

Scanning probe methods have shown that polycrystalline coinage metal films produced by electron beam evaporation (As-Deposited, or As-Dep films) are rough (RMS roughness values of 30 – 80 Å),<sup>59-61</sup> and have a surface morphology comprised of small grains which are separated by deep grain boundaries.<sup>59-62</sup> Although the tops of these grains are atomically flat, the grain boundaries are made up of several atomic steps, which can cause misalignment between neighbouring molecules leading to a disruption of intermolecular van der Waals interactions.<sup>12</sup> For *n*-alkanethiolate SAMs, this

disruption of van der Waals interactions between neighbouring alkyl chains can lead to various types of defects in the monolayer.

In an effort to minimize the number of substrate induced defects in SAMs – and consequently the statistical variation in measurements of current density – researchers now fabricate junctions using ultra smooth coinage metal substrates as the SAM-bearing bottom electrode. These substrates are produced using a process known as ‘template stripping’ in which the coinage metal film is evaporated onto an ultra smooth ‘template’ substrate, and subsequently stripped away to reveal the smooth underside of the film.<sup>60,61,63,64</sup> Template stripped (TS) metal substrates are smooth (RMS roughness values of 2 – 10 Å), and have a surface comprised of large (50 – 500 nm), atomically flat terraces that vary by only a few atomic steps in height.<sup>60</sup> Contact angle hysteresis measurements of *n*-alkanethiolate SAMs formed on TS metal substrates demonstrate that the low density of atomic steps at the metal surface leads to better alignment of neighbouring alkyl chains through increased van der Waals interaction.<sup>65,66</sup>

Molecular tunnel junctions formed from *n*-alkanethiolate SAMs on TS metal substrates have a lower statistical variance in the measured current densities, as well as a decreased number of failed junctions compared to those formed using As-Dep substrates.<sup>20,36</sup> A comparison of molecular tunnel junctions formed from *n*-alkanethiolate (*n* = 10, 12, 14) SAMs formed on both TS silver (Ag<sup>TS</sup>) and As-Dep silver (Ag<sup>As-Dep</sup>) substrates using the hanging Hg drop electrode show that SAMs formed on Ag<sup>TS</sup> substrates have a statistical variance in current density several order of magnitudes lower than for those formed on Ag<sup>As-Dep</sup> substrates, with greatly improved junction yields.<sup>36</sup> A similar study comparing molecular tunnel junctions formed from 1-decanethiolate SAMs formed on both Au<sup>TS</sup> substrates and Au<sup>As-Dep</sup> substrates using a conductive probe AFM top electrode also revealed a decrease in the statistical variance of the measured current densities for SAMs formed on Au<sup>TS</sup> substrates.<sup>20</sup> These two studies are important because they demonstrate that substrate morphology has a profound influence on the measurement of current density through SAMs, and that this influence is independent of the nature of the top contact (hard vs. soft), the area of measurement (several nanometers vs. several micrometers), and the metal used as the bottom electrode (Ag vs. Au).

TS metal substrates have proven to be a reliable platform for the formation and electrical characterization of *n*-alkanethiolate SAMs; however, several limitations, owing to the fabrication procedure, may inhibit their use in more complicated systems. First, the fabrication of TS metal substrates leads to an excess of wasted material; a sacrificial ultra smooth substrate (usually a silicon wafer<sup>60</sup> or freshly cleaved mica<sup>63</sup>) is needed to template the growth of the film, and the evaporated metal films must be very thick (up to 600 nm) to avoid pinhole defects.<sup>60</sup> Second, template stripping requires that a secondary substrate – usually glass – be adhered to the top, rough side of the evaporated metal film using an optical adhesive which is cured using UV light. Immersing adhesive backed substrates into solvent during SAM formation may lead to unintended contamination. The adhesives commonly used for template stripping contain thiol precursors which may act as competitive adsorbates on coinage metal surfaces if cross-linking is not 100% complete prior to immersion.<sup>67</sup> Consequently, it is common practice amongst researchers to allow TS metal substrates to cure in ambient conditions for over a week after the initial prescribed UV cure time to ensure complete cross-linking. Furthermore, although these adhesives are compatible with the ethanolic solutions required for *n*-alkanethiolate SAMs, more complicated molecules may require strong organic or chlorinated solvents, which can cause swelling and dissolution of the film.<sup>68</sup> Finally, template stripping requires that the material to be deposited does not adhere to the smooth template surface. Coinage metals do not adhere to silicon or mica, making them ideal candidates for template stripping; however, the study of molecules with different head group binding chemistry will require ultra smooth substrates of different materials. If these new materials adhere to silicon or mica, new template substrates or template surface modification will be required to inhibit adhesion.

This work details the fabrication of ultra smooth gold substrates for use as bottom electrodes in SAM-based molecular tunnel junctions that retain the benefits of Au<sup>TS</sup>, while eliminating the shortcomings. We fabricate ultra smooth gold substrates using chemical mechanical polishing, a well known fabrication method in the semiconductor manufacturing industry. CMP is widely regarded as the foremost technology for planarization in silicon integrated circuit fabrication.<sup>69</sup> The two most common applications of CMP include the planarization of dielectric and metallic films during the

fabrication of multilevel interconnects, and the fabrication of microstructures through shallow trench isolation or the damascene/dual damascene processes.<sup>69</sup> During the CMP process, the wafer to be polished is mounted onto a wafer carrier, or jig, which is held in forced contact with a polishing pad that has been adhered to a stainless steel platen. An aqueous slurry containing abrasive particles and/or chemical etchants is continuously dripped onto the polishing pad while the wafer is moved linearly and rotationally relative to the pad, causing removal of material at the wafer surface. The polishing pad and the jig are rotated in the same direction about their own independent axes while the jig is swept linearly across the pad to improve processing uniformity.

Although CMP has traditionally been applied to planarization processes, it can also be used to remove surface defects such as scratches and roughness.<sup>69</sup> In metal-CMP processes, chemical etchants in the slurry oxidize the metal surface to produce a layer that is either soluble in aqueous media, or a layer that is soft and porous which can subsequently be removed by the mechanical force of the abrasive and polishing pad. The addition of organic complexing agents can improve the metal-CMP process by lowering the surface free energy of metal ions produced at the surface of the film and promoting dissolution.<sup>69</sup> Without dissolution of surface metal ions, re-deposition and material buildup can cause surface damage. Another important parameter in the metal-CMP process is the pH of the aqueous slurry; both the oxidation potential of the metal and the ability of the organic additive to complex with the free metal ions are dependent upon pH.<sup>69</sup>

Gold CMP processes have previously been developed for solder bump planarization,<sup>70</sup> damascene processes,<sup>71</sup> and nanochannel fabrication,<sup>72</sup> but there has yet to be a process developed specifically for fabricating ultra smooth gold surfaces for use as substrates in SAM formation. Williams et al. have demonstrated that, using CMP, As-Dep platinum (Pt<sup>As-Dep</sup>) surfaces on 100 mm diameter silicon wafers can be polished to produce RMS surface roughness values as low as 1 Å, and that these substrates can serve as bottom electrodes in molecular electronic devices.<sup>73</sup> Langmuir Blodgett monolayers of alkoxy-naphthalenethiol formed on polished Pt (Pt<sup>CMP</sup>) electrodes with a evaporated metal top electrodes showed an impressive 100% device yield, while SAMs of alkoxy-naphthalenethiol showed a 35% device yield. Apart from this isolated study, we

*Ultra Smooth Gold Substrates Prepared by Chemical Mechanical Polishing: A New Substrate for Measuring Charge Transport in Metal-SAM//Ga<sub>2</sub>O<sub>3</sub>/EGaIn Junctions*

are unaware of other attempts to characterize the electrical properties of SAMs on polished metal electrodes, particularly the most common metals used in SAM formation, gold and silver.

We used a fast (< 5 min) CMP process to fabricate gold substrates that are (i) ultra smooth, with an average RMS surface roughness value of 3.8 Å, (ii) uniform over the full area of a 75 mm silicon wafer, having within-wafer and wafer-to-wafer surface roughness non-uniformities < 17%, (iii) free from optical adhesive and compatible with all common organic solvents, (iv) free from wasted materials – the entire area of a polished silicon wafer can be used for SAM characterization, and the thickness of the deposited metal film need only be 50 nm – and (v) ideal as substrates for measuring charge transport through *n*-alkanethiolate SAMs using Au<sup>CMP</sup>-SAM//Ga<sub>2</sub>O<sub>3</sub>/EGaIn junctions. We studied a series of *n*-alkanethiolate SAMs with different chain lengths (*n* = 9 – 16) formed on Au<sup>CMP</sup> substrates, and demonstrate that the measured values of  $\beta$  and  $J_0$  are indistinguishable from SAMs formed on Au<sup>TS</sup> substrates, and that the working junction yield is significantly higher on Au<sup>CMP</sup>.

## 7.2. Experimental Section

All chemicals were purchased commercially and used as received unless otherwise specified. Nuclear magnetic resonance (NMR) spectroscopic data were obtained and recorded on a Bruker Ultrashield 300 MHz spectrometer at room temperature, and shifts are reported in parts per million (ppm). <sup>1</sup>H NMR spectra were referenced to residual proton peaks of CDCl<sub>3</sub> ( $\delta = 7.27$  ppm). 1-tridecanethiol was synthesized according to published procedures.<sup>58</sup> The synthetic procedure and NMR spectroscopic data are available in the supporting information. *n*-alkanethiols (synthesized and commercially received) were purified by silica gel column chromatography using gravity elution with 100% hexanes. Sample spectra of purified thiols are available in the supporting information.

### 7.2.1. Preparation of CMP Polishing Slurry

CMP polishing slurry was prepared by adding 5 g of hydrophilic fumed silica (Aerosil 200), 0.03 g of I<sub>2</sub>, 0.3 g of KI, 4.1 g of citric acid, and 0.925 g of trisodium citrate to a flask containing 500 mL of deionized water. The aqueous mixture was simultaneously sonicated (Branson model 3500) and bubbled with dry nitrogen for one hour and then poured into a PM5 Syton feed unit (Logitech Ltd.) prior to polishing.

### 7.2.2. CMP of Gold Substrates

Au<sup>As-Dep</sup> substrates were fabricated by evaporating 2 nm of titanium as an adhesion promoter onto 75 mm diameter silicon wafers, followed by 50 nm of gold using an e-beam evaporator. Prior to polishing, Au<sup>As-Dep</sup> substrates were bonded to a 75 mm diameter glass carrier disc (Logitech Ltd.) using low melting quartz wax (South Bay Technologies Inc.) at 100 °C on a hot plate. The glass carrier disc bearing the Au<sup>As-Dep</sup> substrate was held in vacuum contact with the chuckface of a PP5 polishing jig (Logitech Ltd., UK). A 12 inch diameter polyurethane polishing cloth (Chemcloth, Logitech Ltd.) was adhered to the 12 inch diameter stainless steel platen of a PM5 lapping and polishing system (Logitech Ltd). The polishing cloth was cleaned by first soaking with deionized water for 5 minutes, followed by removal of the water using a glass microscope slide (VWR). The cleaning procedure was repeated three times. After cleaning, polishing

slurry was dripped onto the polishing cloth from the PM5 Syton feed unit and allowed to soak for 15 minutes before being removed with a glass microscope slide. Fresh polishing slurry was dripped onto the polishing cloth until a thin film covered the entire area of the cloth, at which point the polishing jig bearing the Au<sup>As-Dep</sup> substrate was placed face down onto the polishing cloth with minimal down force (< 1 psi). Au<sup>As-Dep</sup> substrates were polished for four minutes with a platen rotational speed of 25 rpm and a jig head sweep speed of 5 mm / sec. During polishing, fresh slurry was dripped onto the polishing pad at a rate of 2 – 3 drops per second from the PM5 Syton feed unit. Polishing slurry in the PM5 Syton feed unit underwent constant stirring throughout the duration of the polish using a stir bar and stir plate. After polishing, the glass carrier disc bearing the Au<sup>As-Dep</sup> substrate was removed from the PP5 jig chuck face and immediately rinsed with deionized water to remove residual slurry, followed by drying under a stream of dry nitrogen.

### *7.2.3. Cleaning of Au<sup>CMP</sup> Substrates*

Au<sup>CMP</sup> substrates were removed from the glass carrier disc after heating to 100 °C on a hot plate for 5 minutes to melt the bonding wax. Residual wax on the backside of the polished gold wafers was removed using a cloth soaked with toluene, followed by rinsing with toluene and drying under a stream of dry nitrogen. Polished gold wafers were sonicated for 15 minutes in deionized water at 75 °C to which 5 g of detergent (Sparkleen, Fisher Scientific) had been added. Polished gold wafers were then rinsed successively with deionized water and methanol, dried under a stream of dry nitrogen, and stored in a polystyrene Petri dish at ambient conditions prior to use.

### *7.2.4. Preparation of Au<sup>TS</sup> Substrates*

Au<sup>TS</sup> substrates were fabricated according to published procedures.<sup>60</sup> 500 nm of gold was deposited onto a 75 mm diameter silicon wafer using an e-beam evaporator, then a small drop (5 µL) of UV curable adhesive (NOA 83H, Norland Optical) was applied to the gold surface followed by a 1 cm x 1 cm glass substrate. After curing the adhesive using a 100 W UV lamp for 15 minutes, the glass slide was stripped from the silicon

wafer using a scalpel. Au<sup>TS</sup> substrates were used immediately after stripping for SAM formation to minimize surface contamination.

### *7.2.5. Atomic Force Microscopy and Uniformity Study*

AFM images were obtained using a Digital Instruments Multimode atomic force microscope run in contact mode. Veeco type SNL (silicon tip on nitride lever) cantilevers were used with a nominal tip radius of 2 nm and a nominal force constant of 0.12 N/m. AFM images were collected over a 1 μm x 1 μm scan area using a scan rate of 2.0 Hz and a scanning resolution of 512 samples/line. Images were collected using Nanoscope 6 software and processed using WSxM 5.0 Develop 1.0 software.<sup>74</sup> The uniformity of polished gold substrates was assessed by collecting AFM images and measuring the RMS surface roughness of three randomly selected 1 μm x 1 μm areas from 1 cm x 1 cm Au<sup>CMP</sup> substrates. These 1 cm x 1 cm polished gold substrates were cut from four different geometric locations (~ 15 mm, 30 mm, 45 mm, and 60 mm from the wafer flat) of five different Au<sup>CMP</sup> wafers to make a total sample size of 20 substrates, and 60 AFM images.

### *7.2.6. Substrate Characterization*

Optical inspection was performed using an Olympus BX51 microscope equipped with an Olympus Q-Color3 camera. SEM images were collected with a LEO (Zeiss) 1540XB SEM (Western Nanofabrication Facility, London, ON, Canada).

### *7.2.7. Formation of Dihexadecyldithiophosphinic acid SAMs on*

#### *Au<sup>CMP</sup> Substrates*

1 cm x 1 cm Au<sup>CMP</sup> substrates were cut from a 75 mm diameter Au<sup>CMP</sup> wafer and sonicated in anhydrous ethanol for 5 minutes to remove residual organics. The cleaned Au<sup>CMP</sup> substrates were submerged into a 1 mM solution of dihexadecyldithiophosphinic acid (synthesized according to published procedures) in toluene and allowed to incubate under a N<sub>2</sub> atmosphere for 12 hours at room temperature. Prior to XPS analysis, Au<sup>CMP</sup> substrates were removed from solution, immersed into 100 mL of fresh toluene (to remove residual organics) and dried under a stream of dry N<sub>2</sub>.

### *7.2.8. Formation of *n*-Alkanethiolate SAMs on Au<sup>CMP</sup> Substrates*

1 cm x 1 cm Au<sup>CMP</sup> substrates were cut from a 75 mm diameter Au<sup>CMP</sup> wafer and sonicated in anhydrous ethanol for 5 minutes to remove residual organics. The cleaned Au<sup>CMP</sup> substrates were submerged into a 1 mM solution of the appropriate *n*-alkanethiol in ethanol and allowed to incubate under a N<sub>2</sub> atmosphere for 12 hours at room temperature. Prior to electrical characterization, SAM-bearing Au<sup>CMP</sup> substrates were removed from solution, immersed successively into three vials containing 10 mL of fresh anhydrous ethanol (to remove residual organics), and dried under a gentle stream of dry nitrogen.

### *7.2.9. Formation of *n*-Alkanethiolate SAMs on Au<sup>TS</sup> Substrates*

1 cm x 1 cm Au<sup>TS</sup> substrates were stripped from a silicon wafer and immediately submerged into a 3 mM solution of the appropriate *n*-alkanethiol in ethanol and allowed to incubate under an N<sub>2</sub> atmosphere for 3 hours at room temperature. Prior to electrical characterization, SAM bearing Au<sup>TS</sup> substrates were removed from solution, immersed successively into three vials containing 10 mL of fresh anhydrous ethanol (to remove residual organics), and dried under a gentle stream of dry nitrogen.

### *7.2.10. X-Ray Photoelectron Spectroscopy (XPS)*

XPS spectra were collected at Surface Science Western (London, Ontario, Canada) using a Kratos Axis Ultra X-ray photoelectron spectrometer with a monochromatic Al K $\alpha$  source. The detection limit of the instrument is 0.1 - 0.5 at. %. Analyses were carried out over a 300  $\mu$ m x 700  $\mu$ m scan area. Survey scan analyses were carried out with a pass energy of 160 eV. High resolution analyses were carried out with a pass energy of 20 eV. Samples were analyzed at a 30° takeoff angle (60° tilt). High resolution sulfur line shapes were fit using one pair of spin-orbit-split components (2p<sub>3/2</sub> and 2p<sub>1/2</sub>) assuming a Gaussian:Lorentzian (70%:30%) line shape and a fixed splitting energy of 1.18 eV with a 2:1 area ratio.<sup>75</sup> Thickogram calculations<sup>76</sup> were also carried out at Surface Science Western.

### *7.2.11. Electrical Measurements of *n*-Alkanethiolate SAMs on Gold*

Electrical characterization was performed using a home-made molecular tunnel junction characterization system. The conical shaped EGaIn (Aldrich) top electrode was fabricated by extruding a small drop (~ 0.5  $\mu$ L) of EGaIn from a 10  $\mu$ L gas tight syringe (Hamilton Scientific LLC), bringing the drop into contact with a sacrificial Au<sup>TS</sup> substrate using a micropositioner (Newport Corp.), and bifurcating the EGaIn drop into a conical shape by slowly removing the syringe from the sacrificial substrate. A test lead equipped with a micro hook (E-Z Hook) was used to make electrical connection to the syringe needle bearing the conical EGaIn tip. The gold substrate served as the ground electrode by means of a second micro hook test lead that penetrated the SAM and contacted the gold directly. A triaxial cable connected both electrodes to an external amplifier, which was connected to a Keithley 6430 source meter. Molecular tunnel junctions were formed by slowly bringing the conical EGaIn tip into gentle contact with its own reflection in the SAM bearing gold substrate as imaged by a high resolution analytical CCD camera (Edmund Optics). The source meter applied a bias across the molecular tunnel junction and measured the resulting current, with a single scan being defined as a bias sweep from 0 V  $\rightarrow$  -0.5 V  $\rightarrow$  +0.5 V  $\rightarrow$  0 V. Current densities were calculated assuming a circular contact area, with the diameter of the junction measured using the high magnification CCD camera. After establishing contact between the EGaIn top electrode and the SAM, the presence of a molecular tunnel junction was confirmed by measuring a single J(V) trace. A working junction was defined as a sigmoidally shaped J(V) trace, while a short circuit was defined as a straight line in which the current reached the compliance of the source meter (105 mA). After establishing a working tunnel junction with the first J(V) trace, 20 subsequent J(V) traces were measured from the same area. A minimum of 13 randomly sampled tunnel junctions totalling a minimum of 260 J(V) traces were measured for each *n*-alkanethiolate SAM on both Au<sup>TS</sup> and Au<sup>CMP</sup> substrates. The non-shortening junction yield is defined as the number of junctions that short circuit divided by the total number of junctions sampled, after the first working junction (21 J(V) traces) of that particular sample has been established.

### *7.2.12. Solvent Compatibility Study*

1 cm x 1 cm Au<sup>TS</sup> and Au<sup>CMP</sup> substrates were immersed into separate vials containing 5 mL of various solvents (ethanol, toluene, chloroform, and dichloromethane). Optical micrographs were collected before immersion and after removing the substrates from solvent at various time intervals (1 hour, 3 hours, 24 hours). After optical inspection, the substrates were immediately placed back into solution.

## **7.3. Results and Discussion**

### *7.3.1. Ultrasmooth Gold Films Fabricated using CMP*

We prepared Au<sup>As-Dep</sup> and Au<sup>TS</sup> gold substrates according to published procedures.<sup>60</sup> We prepared Au<sup>As-Dep</sup> films by evaporating 2 nm of titanium as an adhesion promoter onto a 75 mm diameter silicon (100) wafer followed by 50 nm of gold using an electron beam evaporator. We prepared template-stripped gold films by first evaporating 500 nm of gold onto a 75 mm diameter silicon (100) wafer. We then placed a small drop (~ 5  $\mu$ l) of optical adhesive NOA 83H onto the gold surface followed by a 1 cm x 1 cm glass substrate. We cured the adhesive using a 100 W UV lamp and stripped the glass substrate away from the silicon wafer using a scalpel immediately prior to SAM formation.

Au<sup>As-Dep</sup> films produced by electron beam evaporation have a rough (RMS roughness ~30 – 80 Å) surface comprised of small grains separated by deep grain boundaries.<sup>59-62</sup> Our CMP process is designed to polish these grains down to the base of the grain boundaries to reduce the number of atomic steps and, consequently, the surface roughness. We chose gentle CMP processing conditions, with minimal substrate downforce and low etchant concentration, for two reasons. First, gold is extremely soft and prone to scratching; scratches in the gold surface will cause defects in any adsorbed SAMs and reduce working junction yields. Minimizing substrate downforce reduces the pressure exerted on the gold surface by the abrasive silica particles and prevents scratches. Second, polishing to the base of the Au<sup>As-Dep</sup> grain boundaries only requires the removal of ~5 nm of metal; low etchant concentrations and minimal downforce permit a low material removal rate. A low material removal rate allows for fine control over the final thickness of the polished gold film; higher rates would make it difficult to remove

the required amount of gold without polishing through the film down to the underlying substrate.

The aqueous CMP slurry used in this study comprises three components: an abrasive, a chemical etchant, and an organic acid. The abrasive consists of 5 wt.% hydrophilic fumed silica with a mean primary particle size of 12 nm. We chose a small particle size to avoid surface defects and scratching which are often associated with large particles.<sup>69</sup> Although these particles have a primary size of 12 nm, they are prone to forming aggregates in solution that can be as large as several hundred nanometers.<sup>77</sup> To reduce the number of aggregates in solution, we sonicated the aqueous slurry for a minimum of 1 hour prior to polishing; this has previously been shown to reduce the average aggregate size to ~25 nm.<sup>77,78</sup> We used a common gold etchant, triiodide, to oxidize the outermost layer of the gold film during the CMP process. A mixture of potassium iodide and iodine in aqueous solution produces triiodide, which reacts with gold to produce a surface comprised of gold (I) iodide (AuI).<sup>79</sup> We chose triiodide as the chemical etchant for this CMP process because it allows for fine control over the etch rate by simply changing the concentration of the constituents. Standard triiodide etchants (1.5 M I<sub>2</sub> / 2.5 M KI) can have static material removal rates as high as several hundred nanometers per minute.<sup>79</sup> We reduced the concentration of the triiodide etchant (0.5 mM I<sub>2</sub> / 3.5 mM KI) to achieve removal rates compatible with thin (50 nm) Au<sup>As-Dep</sup> films. We added a citric acid/trisodium citrate buffer (50 mM, pH = 3) to our slurry for two reasons. First, the oxidation potential of metals is sensitive to the environmental pH; buffering the solution provided a stable pH throughout the dynamic CMP process.<sup>69</sup> Second, citric acid can stabilize gold ions at the surface of the film during polishing, improving solubility and preventing re-deposition.<sup>69</sup>

During the CMP process, a polishing jig held the Au<sup>As-Dep</sup> wafer in contact with a grooved polyurethane polishing pad that had been soaked with slurry. We chose a minimal (< 1 psi) downforce on the wafer to keep removal rates low as well as prevent a high density of nanoscratches. We polished Au<sup>As-Dep</sup> wafers for 4 minutes with a platen rotational speed of 25 rpm, a linear jig sweep speed of 5 mm/s, and a slurry drip rate of 2 – 3 drops per second to produce ultra smooth gold films. After polishing, we immediately

*Ultra Smooth Gold Substrates Prepared by Chemical Mechanical Polishing: A New Substrate for Measuring Charge Transport in Metal-SAM//Ga<sub>2</sub>O<sub>3</sub>/EGaIn Junctions*

cleaned the polished gold wafers to remove residual slurry using a post-CMP cleaning process (see experimental for details).

SEM (Figure 7.1e) and AFM (Figure 7.1b) images clearly depict a Au<sup>CMP</sup> surface that is ultra smooth (RMS roughness = 3.4 Å) and comprised of small grains that have been polished flat. A line scan taken from the AFM image (Figure 7.1d) shows that while the grains that comprise the film are flat, shallow (~1 nm) pits are visible at the grain intersection points. A line scan taken from the Au<sup>As-Dep</sup> AFM image (Figure 7.1a,c) shows the presence of a similar density of pits that are ~ 5 – 6 nm deep prior to polishing, suggesting that the CMP process has removed ~5 nm of material. The presence of these pits may be unavoidable due to the growth kinetics of the gold film during evaporation that leads to incomplete coalescence of the individual grains.

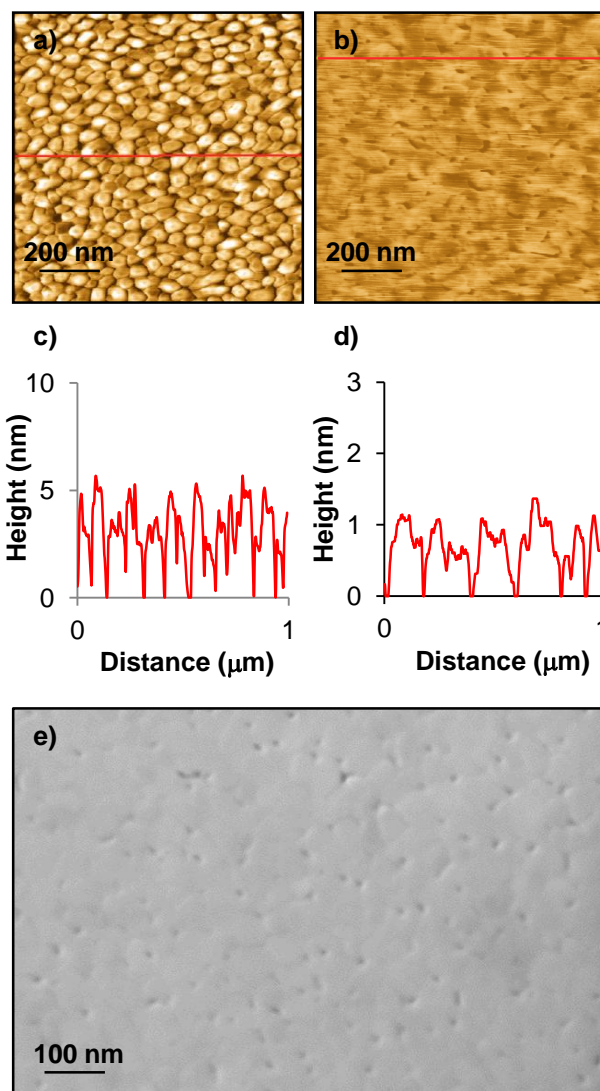


**Figure 7.1.** a-b) AFM topographic images of an Au<sup>As-Dep</sup> and Au<sup>CMP</sup> gold film with corresponding line scan profiles shown below (c-d). e) SEM image of a Au<sup>CMP</sup> film. The z-scale for the AFM images is 20 nm.

Three dimensional AFM micrographs and corresponding profile measurements reveal the differences between Au<sup>CMP</sup> (Figure 7.2a), and Au<sup>TS</sup> (Figure 7.2b) substrates. Au<sup>CMP</sup> and Au<sup>TS</sup> substrates are both ultra smooth, having RMS surface roughness values of 3.4 Å and 4.4 Å, respectively; however, the grain structure comprising the two films are markedly different. Au<sup>CMP</sup> films are comprised of small (20 – 50 nm) grains that have been polished flat by the CMP process, and contain shallow (~1 nm) pits at the grain intersection points. In contrast, Au<sup>TS</sup> films are comprised of large (200 – 500 nm), flat grains that have been templated against a smooth silicon wafer; the size and shape of

*Ultra Smooth Gold Substrates Prepared by Chemical Mechanical Polishing: A New Substrate for Measuring Charge Transport in Metal-SAM//Ga<sub>2</sub>O<sub>3</sub>/EGaIn Junctions*

these grains are also more heterogeneous than those that comprise Au<sup>CMP</sup> films. Au<sup>TS</sup> gold films also exhibit ~1 nm deep grain intersection points; however, these points are found in decreased density compared to Au<sup>CMP</sup> films owing to the larger grain size of the former substrate.

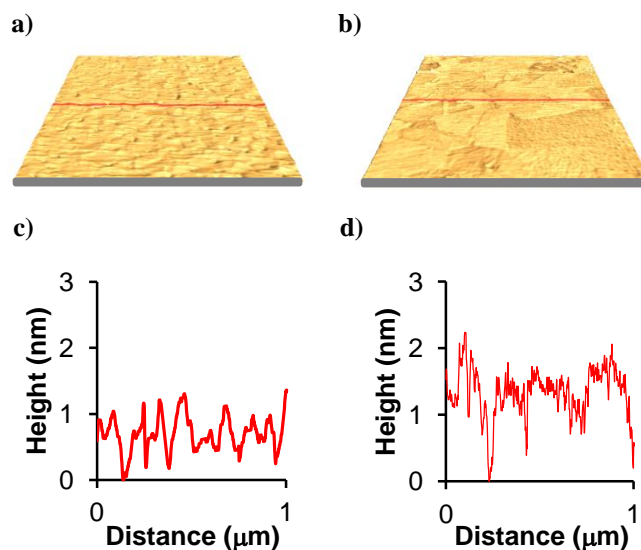


**Figure 7.2.** Three dimensional 1  $\mu\text{m}$  x 1  $\mu\text{m}$  AFM images (a – b) and corresponding height profile measurements (c – d) of Au<sup>CMP</sup> and Au<sup>TS</sup> films, respectively. The z-scale in the AFM images is 20 nm.

### 7.3.2. Uniformity of Au<sup>CMP</sup> Substrates

The CMP process produces gold films with uniform surface roughness across an entire 75 mm diameter silicon wafer, and the process is reproducible when polishing several different wafers. Uniformity is important for any CMP process, particularly for electrical characterization of SAMs where even slight variations in substrate morphology can have profound implications for the measured current densities. To assess uniformity, we measured the RMS surface roughness of 60 randomly sampled 1  $\mu\text{m}$  x 1  $\mu\text{m}$  areas from four different geometric locations (~ 15 mm, 30 mm, 45 mm, and 60 mm from the wafer flat) that have been cut from a total of five Au<sup>CMP</sup> wafers. The results of the uniformity study, summarized in Table 7.1 and Figure 7.3, show that the Au<sup>CMP</sup> substrates have an average RMS surface roughness value of 3.80 +/- 0.45 Å. A histogram representing all 60 RMS roughness values (Figure 7.3) shows a Gaussian-type distribution with all values

*Ultra Smooth Gold Substrates Prepared by Chemical Mechanical Polishing: A New Substrate for Measuring Charge Transport in Metal-SAM//Ga<sub>2</sub>O<sub>3</sub>/EGaIn Junctions*

falling between 2.8 Å and 5.2 Å. The overall non-uniformity of the process, a measure of the standard deviation of all 60 surface roughness values expressed as a percentage, was 12%. Within-wafer non-uniformity, a measure of the deviation of surface roughness within each of the five 75 mm diameter silicon wafers (12 scans each), was less than 15% in all cases. Wafer-to-wafer non-uniformity, calculated by averaging the 5 mean surface roughness values of the individual wafers and expressing the deviation as a percentage, was 17%.

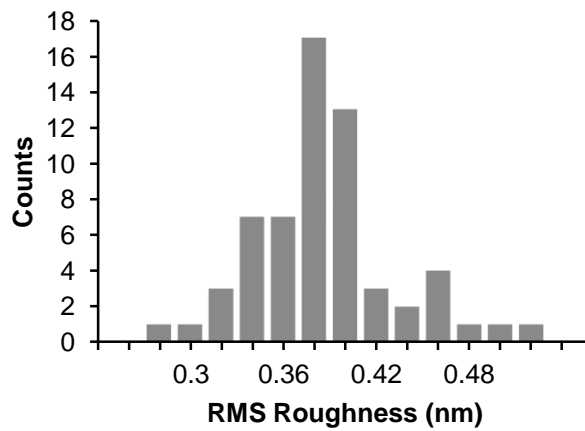


**Figure 7.3.** Histogram detailing the RMS surface roughness values of Au<sup>CMP</sup> substrates collected from 60 1 μm x 1 μm AFM images.

**Table 7.1.** Summary of the Au<sup>CMP</sup> surface roughness uniformity study

Wafer	$\mu R_{\text{RMS}}$ (Å)	$\sigma R_{\text{RMS}}$ (Å)	Non-Uniformity (+/- %)	Wafer-to-Wafer Non-Uniformity (+/- %)
1	4.10	0.33	8	-
2	3.98	0.61	15	-
3	3.84	0.34	9	-
4	3.50	0.36	10	-
5	3.58	0.24	7	-
All 60 Scans	3.80	0.45	12	17

### 7.3.3. Composition of the Au<sup>CMP</sup> surface

It is important that the Au<sup>CMP</sup> surface is free of defects including not only surface roughness and scratches, but also contamination that can interfere with SAM formation. X-Ray photoelectron spectroscopy (XPS) survey scan analysis of a Au<sup>CMP</sup> film (Figure 7.4) shows elements consistent with a gold surface, as well as an overlayer of adsorbed adventitious organics (carbon, oxygen, sulfur). Adsorption of organic molecules found in ambient laboratory conditions is unavoidable due to the high surface free energy of gold. XPS analysis also reveals the presence 0.4 at.% iodine, which we attribute to residual AuI formed at the gold surface during the CMP process; post-CMP water/methanol rinsing should have removed any unbound iodine or potassium iodide from the surface (KI is known to be soluble in water and I<sub>2</sub> is known to be soluble in simple alcohols). We attempted to calculate the thickness of the AuI layer using a thickogram calculation.<sup>76</sup> The thickogram calculation is a graphical method for measuring overlayer thicknesses where the overlayer has a different elemental chemistry than the substrate. Thickogram

calculations (Figure 7.5, details in the supporting information) estimate the thickness of the AuI overlayer to be  $< 0.1 \text{ \AA}$ , suggesting surface coverage far less than that of a monolayer (The bond length of AuI is  $\sim 2.5 \text{ \AA}$ <sup>80</sup>). *n*-Alkanethiolates are known to displace unwanted contaminants at the gold surface due to the high affinity of the sulfur atom for gold. We formed a 1-hexadecanethiolate SAM on the surface of a Au<sup>CMP</sup> substrate to determine if displacement of both the adventitious organic layer as well as the AuI overlayer would occur. XPS survey scan analysis (Figure 7.6) shows elements consistent with the formation of an *n*-alkanethiolate SAM on a gold surface (gold, sulfur, carbon). After SAM formation, the amount of carbon present in the spectrum increased from 38.6 at.% to 67.1 at.% and the amount of gold decreased from 51.8 at.% to 30.2 at.%, consistent with attenuation of the gold signal due to the presence of the monolayer. The amount of sulfur present in the spectrum decreased from 2.7 at.% to 1.8 at.% after SAM formation, suggesting that either the unintended contamination present prior to SAM formation had sulfur containing species in greater than monolayer coverage, or that the sulfur signal in the SAM is attenuated by the hexadecyl chains. The presence of the O 1s line in the survey scan suggests that the SAM did not entirely prevent the adsorption of adventitious oxygen-containing organics; however, the amount of oxygen present in the spectrum is far lower (0.6 at.%) than the amount present prior to SAM formation (6.5 at.%). The survey scan shows the presence of identical amounts (0.4 at. %) of iodine in the SAM-bearing Au<sup>CMP</sup> film as the neat Au<sup>CMP</sup> film, with an identical thickness estimation of  $0.1 \text{ \AA}$ . The lack of iodine displacement after SAM formation is consistent with a chemisorbed iodine species at the surface of the polished gold film, likely in the form of AuI. Although the AuI layer could be removed either electrochemically,<sup>81</sup> or by employing a two-stage polish in which the second step contains no etchant,<sup>69</sup> we speculate that AuI on the polished gold surface is present in trace amounts and does not disrupt formation of *n*-alkanethiolate SAMs.

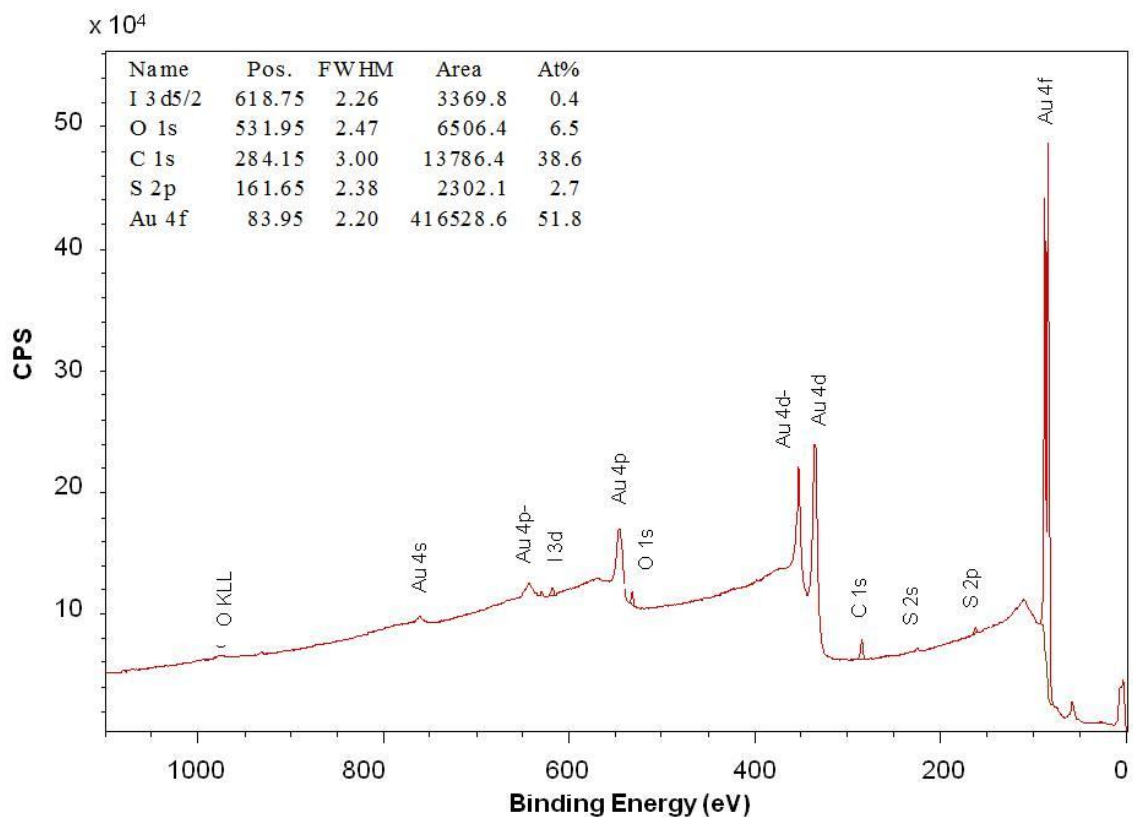


**Figure 7.4.** XPS survey scan of a Au<sup>CMP</sup> substrate.

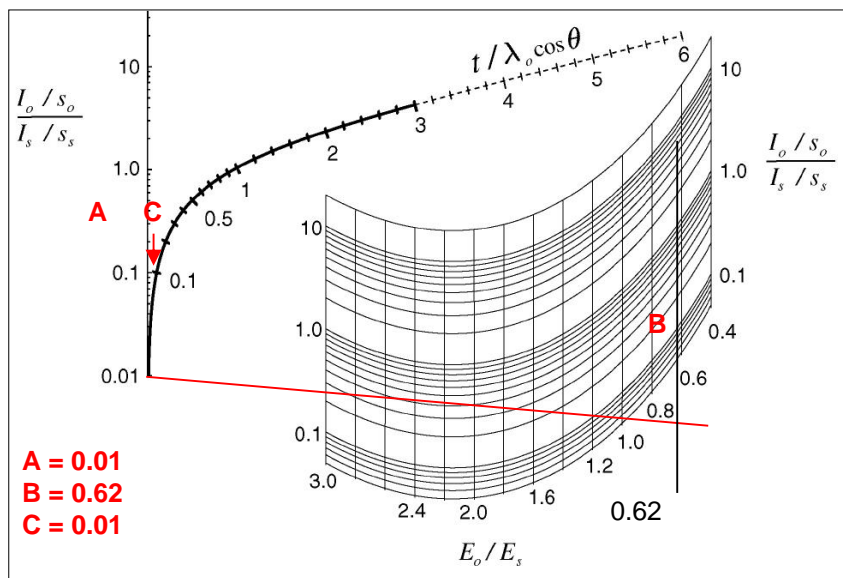


**Figure 7.5.** Graphical representation of the thickogram calculation used to determine the thickness of the AuI overlayer on a Au<sup>CMP</sup> substrate. Details of the thickogram calculation are available in the supporting information.

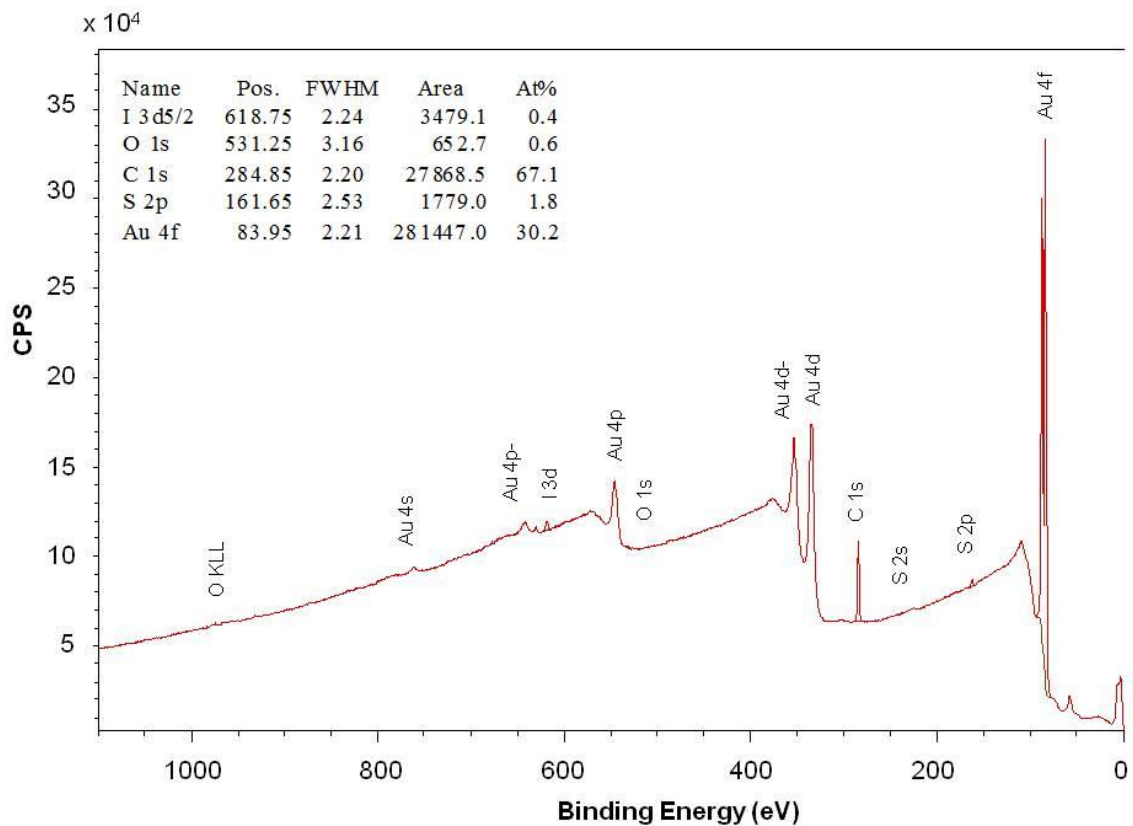


**Figure 7.6.** XPS survey scan of a Au<sup>CMP</sup> substrate after the formation of a 1-hexadecanethiolate SAM.

#### **7.3.4. Binding of (C<sub>16</sub>)<sub>2</sub>DTPA SAMs on Polished Gold Substrates**

We have previously reported a class of SAMs on gold in which the binding of the adsorbate head group is extremely sensitive to changes in substrate morphology.<sup>82</sup> Dihexadecyldithiophosphinic acid ((C<sub>16</sub>)<sub>2</sub>DTPA) SAMs on Au<sup>As-Dep</sup> have a binding motif in which 60% of the adsorbate molecules are chelated to the surface, while 40% of the molecules are monodentate. On Au<sup>TS</sup> however, 100% of the adsorbate molecules are chelated. The atomic steps present in the Au<sup>As-Dep</sup> surface disrupt chelation of the adsorbate head group at the grain boundaries; the reduced density and depth of atomic steps in the Au<sup>TS</sup> surface permits chelation. We formed (C<sub>16</sub>)<sub>2</sub>DTPA SAMs on Au<sup>CMP</sup> substrates to determine if the grain boundaries, and consequently the density of atomic steps, have been polished down to a level that is competitive with Au<sup>TS</sup>. High resolution XPS analysis of the S 2p region of a (C<sub>16</sub>)<sub>2</sub>DTPA SAM formed on a Au<sup>CMP</sup> substrate (Figure 7.7) shows a simple line shape that we fit using a pair of spin orbit-split components (S 2p<sub>3/2</sub> and S 2p<sub>1/2</sub>) assuming a Gaussian/Lorentzian (70%:30%) line shape and a fixed splitting energy at 1.18 eV. Based on previous studies,<sup>83,84</sup> we assign the S 2p<sub>3/2</sub> peak at 161.9 eV to a sulfur atom that is bound to the gold surface. The lack of a S 2p<sub>3/2</sub> peak appearing at binding energies > 163 eV confirms that there are no unbound sulfur atoms, and the lack of a peak at binding energies > 168 eV confirms that there are no oxidized sulfur atoms. The presence of a single, bound sulfur atom confirms that all (C<sub>16</sub>)<sub>2</sub>DTPA adsorbate molecules in the SAM are chelated to the Au<sup>CMP</sup> surface. Chelation of the (C<sub>16</sub>)<sub>2</sub>DTPA adsorbate molecules indicates that the number of atomic steps in the Au<sup>CMP</sup> surface has been reduced to a level that is indeed competitive with Au<sup>TS</sup>.

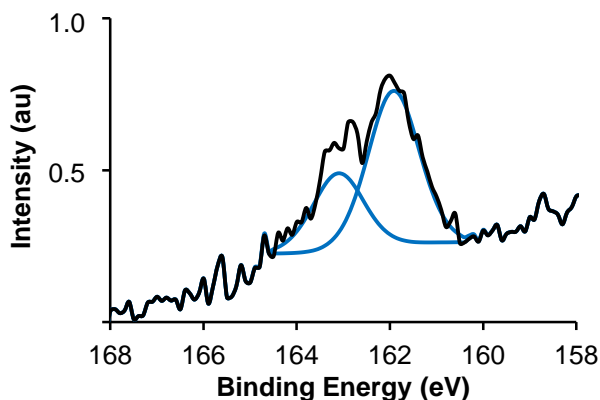


**Figure 7.7.** HR-XPS spectrum of the S 2p region of a (C<sub>16</sub>)<sub>2</sub>DTPA SAM formed on a Au<sup>CMP</sup> substrate.

### 7.3.5. Electrical Characterization of *n*-Alkanethiolate SAMs on Au<sup>TS</sup> and Au<sup>CMP</sup> Substrates

#### 7.3.5.1. Forming Au-SAM//Ga<sub>2</sub>O<sub>3</sub>/EGaIn junctions

We formed *n*-alkanethiolate SAMs on gold substrates by immersing them into degassed 1 mM ethanolic solutions for 12 hours (Au<sup>CMP</sup>) or degassed 3 mM ethanolic solutions for 3 hours (Au<sup>TS</sup>). It is well known that the properties (wettability, coverage, and alkyl chain organization) of *n*-alkanethiolate SAMs on gold do not change beyond 12-18 hours of immersion into 1 mM solutions.<sup>12</sup> The reduced immersion time and increased thiol concentration for Au<sup>TS</sup> compared to Au<sup>CMP</sup> was chosen to minimize the time spent in solution by the optical adhesive, and is in line with procedures performed by others in the field.<sup>44</sup>

We formed Au-SAM//Ga<sub>2</sub>O<sub>3</sub>/EGaIn junctions according to previously published procedures.<sup>54</sup> We brought a conical EGaIn tip into contact with the top surface of the SAM-bearing substrate and measured the contact area, assumed to be circular, using a high magnification camera. We measured 315 – 483 *J(V)* traces for every *n*-alkanethiolate SAM formed on Au<sup>CMP</sup> substrates, and 260 – 265 *J(V)* traces for every *n*-alkanethiolate SAM formed on Au<sup>TS</sup> substrates. We sampled these *J(V)* traces from a minimum of 13 junctions chosen from random areas of the SAM-bearing Au<sup>CMP</sup> and

Au<sup>TS</sup> gold surfaces. We measured a maximum of 5 junctions before fabricating a new EGaIn tip. We collected a maximum of 21  $J(V)$  traces for each junction using a source meter, with each trace being defined as a voltage bias sweep from 0 V  $\rightarrow$  -0.5 V  $\rightarrow$  +0.5 V  $\rightarrow$  0 V. We converted the currents measured by the source meter to current densities using the contact area measured for each individual junction. We define a failed junction or 'short' as a current measurement that reaches the compliance of the source meter (105 mA) due to penetration of the EGaIn tip through the SAM to the underlying gold substrate. We define the non-shortening yield as the percentage of working junctions after formation of the first junction capable of producing 21  $J(V)$  traces without a short. Current density measurements of  $n$ -alkanethiolate SAMs are known to be log-normally distributed; we performed all statistical analysis using  $\log J$  rather than  $J$ , as is common amongst researchers in this field. As a convention, we report all measurements of  $\log J$  at a bias of -0.5 V to provide comparison to previously published literature; however, we note that all measured biases for a given  $n$ -alkanethiolate SAM were log-normally distributed, fit with a unimodal Gaussian distribution, and had similar standard deviation ( $\sigma_{\log}$ ). Charge transport data for  $n$ -alkanethiolate SAMs formed on Au<sup>CMP</sup> and Au<sup>TS</sup> substrates are summarized in Table 7.2 and Table 7.3, respectively. Average  $J(V)$  traces, beta plots, and histograms of charge transport measurements for  $n$ -alkanethiolate SAMs on Au<sup>CMP</sup> and Au<sup>TS</sup> substrates are shown in Figure 7.8 and Figure 7.9, respectively.

*7.3.5.2. Non-shortening yields of  $n$ -alkanethiolate SAMs are higher on Au<sup>CMP</sup> substrates than on Au<sup>TS</sup> substrates*

Table 7.2 and Table 7.3 show non-shortening yields that are higher for  $n$ -alkanethiolate SAMs formed on Au<sup>CMP</sup> substrates (90 – 100%) compared to Au<sup>TS</sup> substrates (72 – 95%). A student's  $t$ -test performed on the two data sets confirms that the difference in yield between the two systems is statistically significant (> 99% confidence,  $p$  value = 0.0002). We speculate that this difference in yield is due to the fact that Au<sup>TS</sup> substrates have a layer of optical adhesive which can leach contaminants into the solution during SAM formation; Au<sup>CMP</sup> substrates are adhesive-free. The optical adhesives commonly used for Au<sup>TS</sup> substrate fabrication are known to contain thiols which may act as competitive adsorbates during SAM formation, leading to defects in the layer.<sup>68</sup> Defects in the SAM can lead to pathways for electrical shorts by allowing the EGaIn tip to directly contact the

underlying metal surface. We note that previous studies have shown high non-shortening yields (> 90%) for *n*-alkanethiolate SAMs formed on Ag<sup>TS</sup> substrates;<sup>44</sup> however, we suspect the junction yield of SAMs formed on gold are more sensitive to contamination due to a well known decrease in molecular packing density.<sup>78,85</sup> The higher molecular packing density of *n*-alkanethiolates on silver compared to gold prevent competitive adsorbates from disrupting the SAM. It is also possible the longer immersion times used for forming SAMs on Au<sup>CMP</sup> compared to Au<sup>TS</sup> are responsible for the increased yield. The short immersion time for SAMs formed on Au<sup>TS</sup> is explicitly chosen to minimize the exposure of the solution to the optical adhesive; increasing immersion times may introduce more defects in the SAM. We believe both factors – the lack of optical adhesive, and the resulting freedom to increase immersion times – contribute to fewer defects in SAMs formed on Au<sup>CMP</sup> substrates compared to Au<sup>TS</sup> substrates.

*7.3.5.3. Tunneling is the primary charge transport mechanism for n-alkanethiolate SAMs formed on Au<sup>CMP</sup> and Au<sup>TS</sup> substrates*

Average  $J(V)$  traces of *n*-alkanethiolate SAMs formed on both Au<sup>CMP</sup> and Au<sup>TS</sup> substrates (Figure 7.8a and Figure 7.9a) show a sigmoidal line shape (half sigmoidal line shape for absolute  $J(V)$  traces), consistent with a coherent non-resonant tunneling charge transport mechanism. Within the series of *n*-alkanethiolate SAMs on Au<sup>CMP</sup> and Au<sup>TS</sup> (Figure 7.8b and 7.9b),  $\log J$  decreases exponentially as the tunneling distance – determined by the number of carbons in the methylene chain – is increased, consistent with the simplified Simmons equation. We note the appearance of the ‘odd-even’ effect – previously reported for a series of *n*-alkanethiolate SAMs formed on Ag<sup>TS</sup> – in which the values of  $\log J$  for *n*-alkanethiols with an even number of carbons can be treated as a statistically independent series from those with an odd number of carbons.<sup>44</sup> To illustrate the odd-even effect, we have labeled the data series (Figure 7.8b and Figure 7.9b) corresponding to *n*-alkanethiol SAMs with an even number of carbons red, and those with an odd number of carbons black. Though we highlight the presence of the ‘odd-even’ effect, we do not observe a statistically significant difference between the two data sets in this study; values of  $\beta$  and  $J_0$  for the series of *n*-alkanethiolate SAMs formed on Au<sup>CMP</sup> and Au<sup>TS</sup> were calculated by treating all chain lengths as a single dataset. Histograms plotting the distribution of  $\log J$  (Figure 7.8c and Figure 7.9c) show a normal

distribution that can be fit with a unimodal Gaussian curve, with nearly all of the measured values falling within the fit. The normal distribution of  $\log J$  has previously been attributed to a variety of defects in the SAM (thin area and thick area) that lead to a normally distributed variation in the SAM thickness, and consequently, the tunneling barrier thickness. A normally distributed tunneling thickness will cause log-normally distributed values of  $J$  based on the Simmons equation.<sup>56</sup> We extracted the mean and standard deviation of  $\log J$  ( $\mu_{\log}$  and  $\sigma_{\log}$ ) from the Gaussian fits according to published procedures detailing best practices for handling this type of data.<sup>46</sup>

*7.3.5.4.  $\mu_{\log}$ ,  $\sigma_{\log}$ ,  $\beta$ , and  $\log J_0$  for  $n$ -alkanethiolate SAMs formed on Au<sup>CMP</sup> substrates and Au<sup>TS</sup> substrates are statistically indistinguishable.*

Table 7.2 and Table 7.3 express  $\mu_{\log}$  and  $\sigma_{\log}$  for  $n$ -alkanethiolate SAMs formed on Au<sup>CMP</sup> and Au<sup>TS</sup> substrates, respectively. For all chain lengths studied (C<sub>9</sub>SH – C<sub>16</sub>SH),  $\mu_{\log}$  for SAMs formed on Au<sup>CMP</sup> substrates were within +/- 1  $\sigma_{\log}$  of SAMs formed on Au<sup>TS</sup> substrates, making the values statistically indistinguishable. The range of  $\sigma_{\log}$ , a measure of the magnitude of the variance in the data, was nearly identical for SAMs formed on Au<sup>CMP</sup> substrates (0.13 – 0.53) compared to SAMs formed on Au<sup>TS</sup> substrates (0.21 – 0.59), suggesting that both substrates have a similar density of normally distributed defects in the SAM, and consequently, the tunneling barrier thickness. Not surprisingly, beta plots for SAMs formed on Au<sup>CMP</sup> and Au<sup>TS</sup> substrates (Figure 7.8b and Figure 7.9b) show values of  $\beta$  and  $\log J_0$  that are also statistically indistinguishable.  $\beta$  values calculated for  $n$ -alkanethiolate SAMs formed on Au<sup>CMP</sup> and Au<sup>TS</sup> substrates were 1.08 +/- 0.18 C<sup>-1</sup> and 0.99 +/- 0.08 C<sup>-1</sup>, respectively, and are in good agreement with the widely accepted value of ~ 1.0 C<sup>-1</sup> for SAMs containing trans-extended methylene chains.<sup>58</sup>  $\log J_0$  values calculated for  $n$ -alkanethiolate SAMs formed on Au<sup>CMP</sup> and Au<sup>TS</sup> substrates were 1.55 +/- 0.65 and 1.05 +/- 0.45, respectively. These values of  $\log J_0$  are approximately one log unit lower than what was previously reported for a series of  $n$ -alkanethiolate SAMs on Ag<sup>TS</sup> measured using the EGaIn top contact, which can be attributed to either the increased number of molecules per unit area in SAMs on silver compared to gold,<sup>78,85,86</sup> or the different hybridization of the bound sulfur atom on silver compared to gold (sp vs sp<sup>3</sup>).<sup>87</sup> Electrical characterization suggests that  $n$ -alkanethiolate

*Ultra Smooth Gold Substrates Prepared by Chemical Mechanical Polishing: A New Substrate for Measuring Charge Transport in Metal-SAM//Ga<sub>2</sub>O<sub>3</sub>/EGaIn Junctions*

SAMs formed on Au<sup>CMP</sup> and Au<sup>TS</sup> substrates are structurally indistinguishable. The only clear difference between SAMs formed on these two substrates is an increase in the number of large defects for Au<sup>TS</sup> that can cause catastrophic disorder in the layer, resulting in electrical short circuits.

**Table 7.2.** Summary of charge transport measurements of *n*-alkanethiolate SAMs formed on Au<sup>CMP</sup> substrates.

<i>n</i>	$\mu_{\log}$	$\sigma_{\log}$	# of Junctions	Scans	Shorts	Yield (%)
9	-2.46	0.37	20	378	2	90
10	-3.51	0.53	24	483	1	96
11	-3.26	0.23	16	315	1	94
12	-4.38	0.37	16	315	1	94
13	-4.43	0.45	16	315	1	94
14	-5.26	0.27	16	315	1	94
15	-5.08	0.32	16	315	1	94
16	-6.10	0.13	15	315	0	100

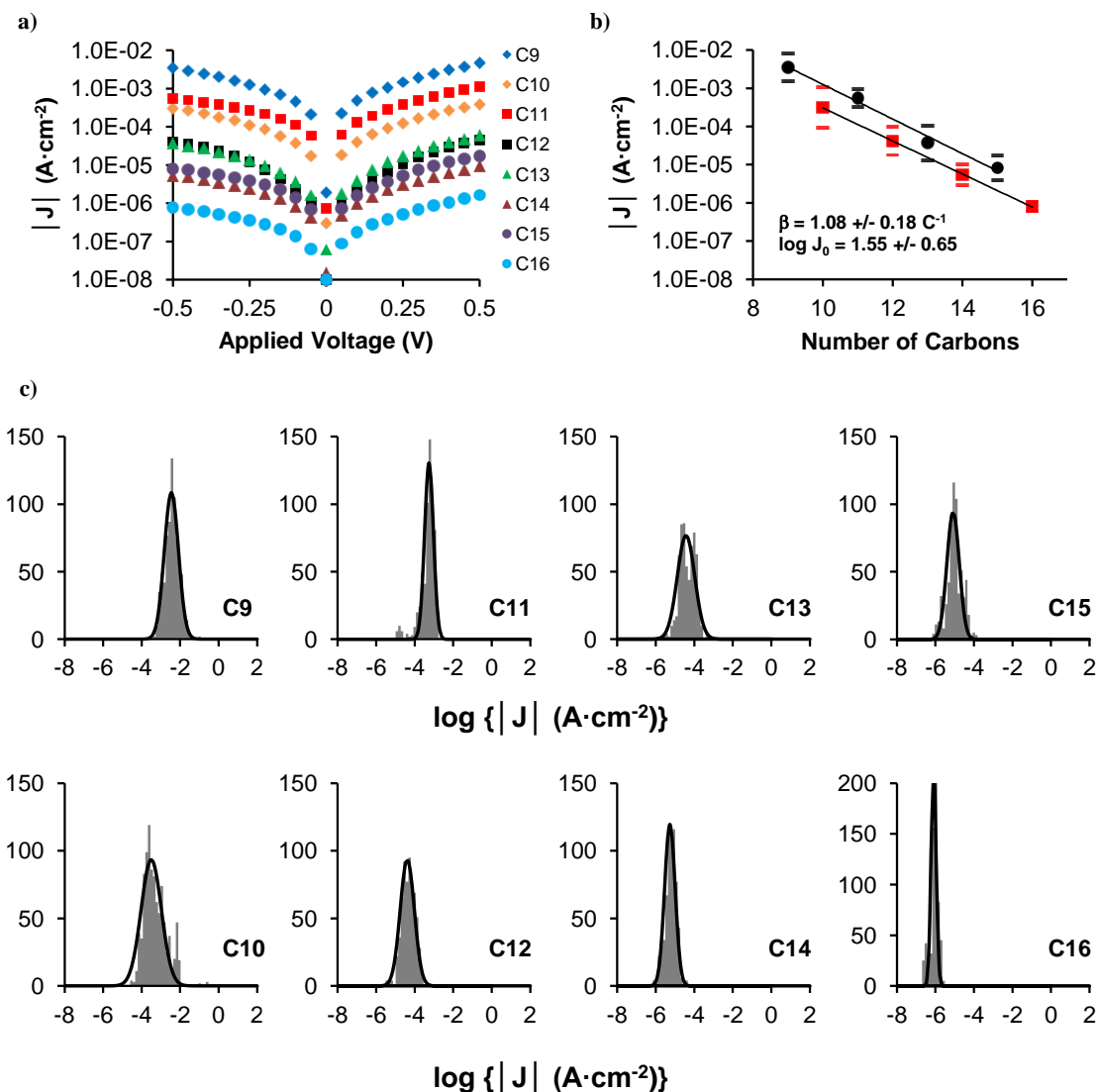


**Figure 7.8.** Average traces (a), beta plot (b) and histograms with unimodal Gaussian fit (c) of  $\log J$  for *n*-alkanethiolate SAMs formed on Au<sup>CMP</sup> substrates. Beta plot and histograms are shown for a bias of -0.5 V. Trendlines in the beta plot for *n*-alkanethiolate SAMs with even (red) and odd (black) number of carbons have been separated to illustrate the odd-even effect. Beta and  $\log J_0$  values are calculated by treating all chain lengths as a single series. The y-axis of the Gaussian distributions corresponds to the number of counts for a given statistical bin.

**Table 7.3.** Summary of charge transport measurements of *n*-alkanethiolate SAMs formed on Au<sup>TS</sup> substrates.

<i>n</i>	$\mu_{\log}$	$\sigma_{\log}$	# of Junctions	Scans	Shorts	Yield (%)
9	-2.76	0.35	18	260	5	72
10	-3.26	0.50	16	260	3	81
11	-3.65	0.37	18	260	5	72
12	-4.24	0.38	17	260	4	76
13	-4.45	0.21	18	265	5	72
14	-5.38	0.59	14	260	1	95
15	-5.06	0.49	20	260	6	70
16	-5.87	0.34	15	264	2	87

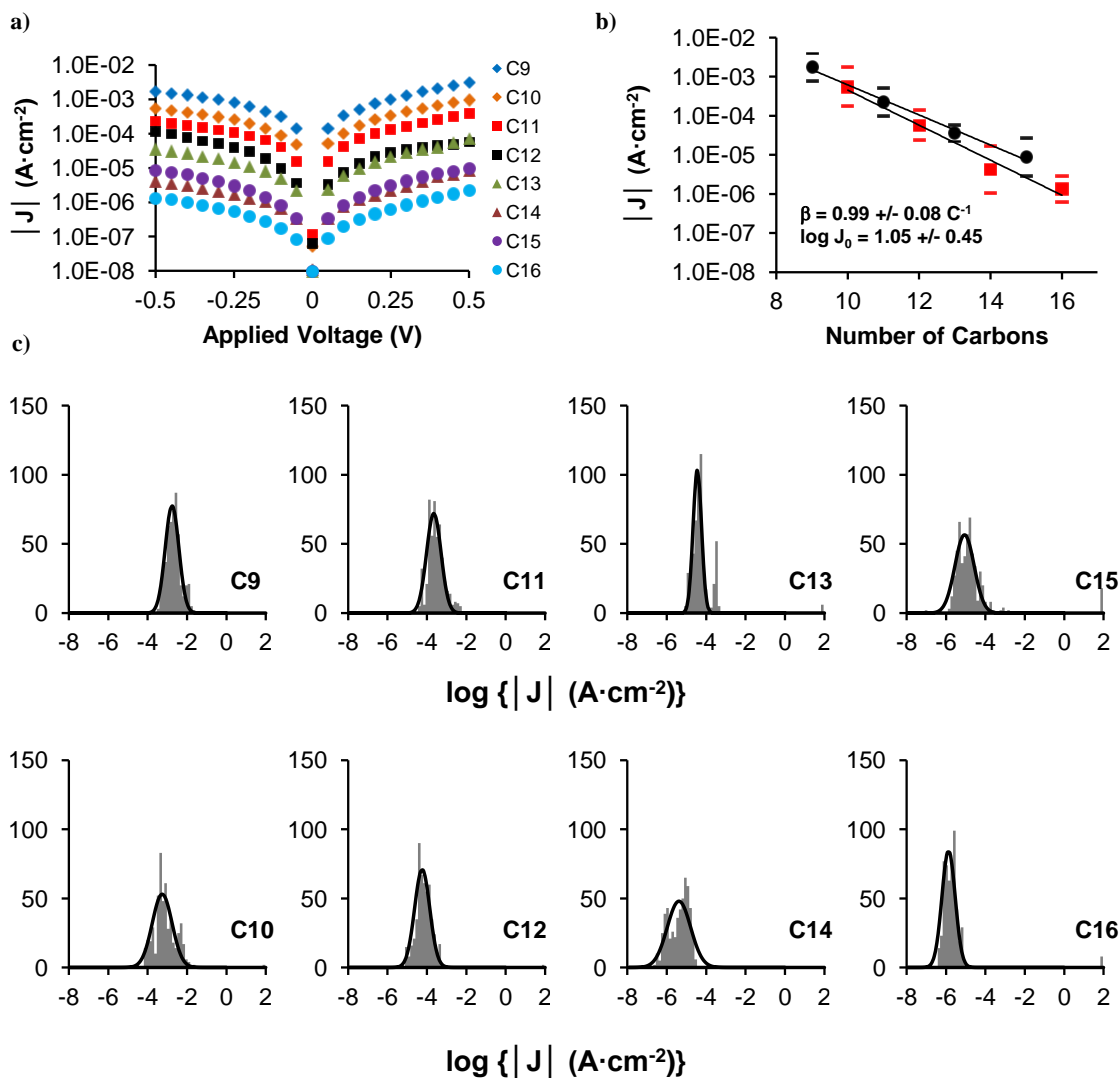


**Figure 7.9.** Average traces (a), beta plot (b) and histograms with unimodal Gaussian fit (c) of  $\log J$  for *n*-alkanethiolate SAMs formed on Au<sup>TS</sup> substrates. Beta plot and histograms are shown for a bias of -0.5 V. Trendlines in the beta plot for *n*-alkanethiolate SAMs with even (red) and odd (black) number of carbons have been separated to illustrate the odd-even effect. Beta and  $\log J_0$  values are calculated by treating all chain lengths as a single series. The y-axis of the Gaussian distributions corresponds to the number of counts for a given statistical bin.

### *7.3.6. Solvent Compatibility of Au<sup>CMP</sup> and Au<sup>TS</sup> Substrates*

An important characteristic of Au<sup>CMP</sup> substrates is that they are free from adhesive, making them compatible with most any common laboratory solvent; Au<sup>TS</sup> substrates are only compatible with those solvents that do not swell or dissolve the underlying adhesive film. We immersed both Au<sup>CMP</sup> and Au<sup>TS</sup> substrates into various common laboratory solvents (ethanol, toluene, chloroform, dichloromethane) for 24 hours to assess their compatibility. Optical micrographs of the Au<sup>CMP</sup> substrates (Figure 7.10a) show no damage to the gold surface after 24 hours of immersion in any of the solvents that were tested. In contrast, the surface of Au<sup>TS</sup> substrates (Figure 7.10b) were damaged by all of the chosen solvents, including the two most common solvents used to form SAMs – ethanol and toluene. Au<sup>TS</sup> substrates were completely incompatible with chlorinated solvents, as evidenced by complete delamination of the gold film after only 1 hour in dichloromethane, or 3 hours in chloroform. Although ethanol and toluene did not delaminate the gold films, evidence of blister formation due to swelling of the underlying adhesive is present after 24 hours. We note that nanoscale changes to the gold surface morphology may occur sooner than the aforementioned immersion times required to cause blistering/delamination of the film, however a more in-depth AFM study is required to probe these effects in detail.

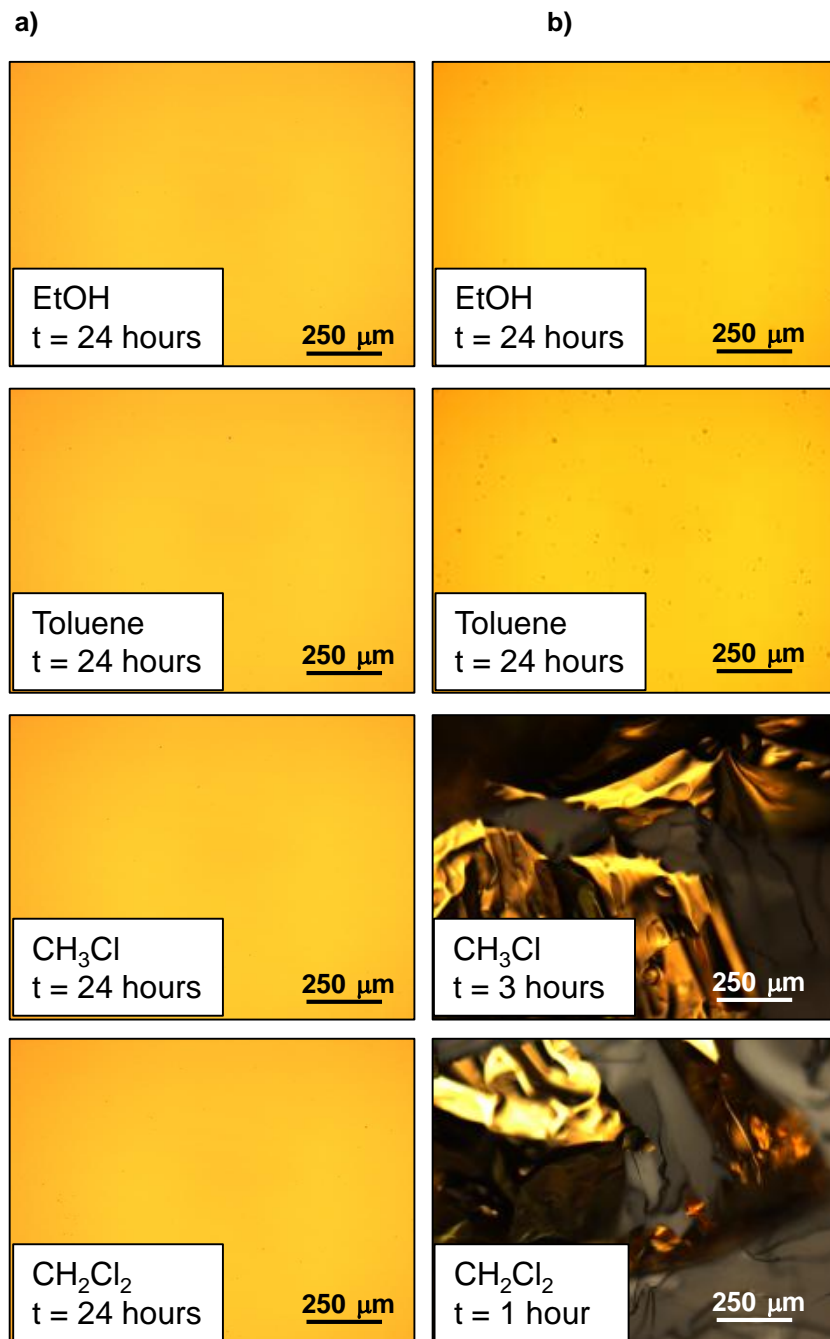


**Figure 7.10.** Optical micrographs of Au<sup>CMP</sup> (a) and Au<sup>TS</sup> (b) substrates after immersion in ethanol, toluene, chloroform, and dichloromethane for various time intervals.

The incompatibility of Au<sup>TS</sup> substrates with common laboratory solvents limits their use as bottom electrodes in SAM-based molecular junctions; immersion times must be kept short to minimize blistering of the gold surface (which can in turn cause defects in the SAM), and molecules that may only be soluble in chlorinated solvents cannot be studied. The future of molecular electronics does not likely lie in the study of simple *n*-alkanethiolate SAMs, but rather more interesting adsorbate molecules that may require the use of stronger solvents. In this regard, Au<sup>CMP</sup> substrates are far superior to Au<sup>TS</sup> substrates as bottom electrodes for SAM-based molecular junctions.

## 7.4. Conclusions

Using CMP, we have produced Au<sup>CMP</sup> substrates that retain all the beneficial characteristics of Au<sup>TS</sup> substrates while eliminating the shortcomings. Throughout this study, we have shown Au<sup>CMP</sup> substrates to be i) ultrasmooth – with an average RMS surface roughness value of 3.8 Å, ii) uniform – having within-wafer and wafer-to-wafer non-uniformities of 10% and 17%, respectively, iii) adhesive free – making these substrates compatible with common organic solvents, iv) suitable for the study of SAMs that are sensitive to the morphology of the substrate, such as (C<sub>16</sub>)<sub>2</sub>DTPA, v) ideal as substrates for measuring the electrical properties of SAMs – all parameters that describe the charge transport process of Au-SAM//Ga<sub>2</sub>O<sub>3</sub>/EGaIn Junctions ( $\mu_{\log}$ ,  $\sigma_{\log}$ ,  $\beta$ ,  $\log J_0$ ) are statistically indistinguishable for *n*-alkanethiolate SAMs formed on Au<sup>CMP</sup> substrates compared to SAMs formed on Au<sup>TS</sup> substrates. The working junction yield was significantly higher for SAMs formed on Au<sup>CMP</sup> substrates compared to Au<sup>TS</sup> substrates, which we attribute to the elimination of optical adhesive in the former substrate.

We note that our CMP process left trace amounts of iodine at the surface, which we believe to be in the form of AuI. Though this trace contaminant is undesirable, thickogram calculations suggest a very low surface coverage, consistent with the fact that Au<sup>CMP</sup> substrates performed as well, or better, than Au<sup>TS</sup> substrates as bottom electrodes in Au-SAM//Ga<sub>2</sub>O<sub>3</sub>/EGaIn junctions.

*Ultra Smooth Gold Substrates Prepared by Chemical Mechanical Polishing: A New Substrate for Measuring Charge Transport in Metal-SAM//Ga<sub>2</sub>O<sub>3</sub>/EGaIn Junctions*

We believe CMP to be an extremely versatile technique for controlling the surface morphology of thin films, particularly for reducing roughness to provide ultra smooth substrates for SAM formation. The number of process variables (downforce, abrasive, etchant, complexing agent, pH, etc.) allows the process to be extended to a variety of materials including metals, oxides, and dielectrics. CMP is also a much more practical technology than template-stripping; it is fast, produces less wasted material, is easily scalable, and is already integrated within the semiconductor manufacturing industry. We are currently exploring the use of CMP to produce ultra smooth films of different metals which can also serve as bottom electrodes within SAM-based molecular junctions.

## 7.5. References

- (1) McCreery, R. L.; Yan, H. J.; Bergren, A. J. *Physical Chemistry Chemical Physics* **2013**, *15*, 1065.
- (2) McCreery, R. L.; Bergren, A. J. *Advanced Materials* **2009**, *21*, 4303.
- (3) McCreery, R. L. *Chemistry of Materials* **2004**, *16*, 4477.
- (4) Salomon, A.; Cahen, D.; Lindsay, S.; Tomfohr, J.; Engelkes, V. B.; Frisbie, C. D. *Advanced Materials* **2003**, *15*, 1881.
- (5) Heath, J. R. In *Annual Review of Materials Research* 2009; Vol. 39, p 1.
- (6) Erbe, A.; Verleger, S. *Acta Physica Polonica A* **2009**, *115*, 455.
- (7) Joachim, C. G., J. K. Aviram, A. *Nature* **2000**, *408*, 541.
- (8) Del Nero, J.; de Souza, F. M.; Capaz, R. B. *Journal of Computational and Theoretical Nanoscience* **2010**, *7*, 503.
- (9) Song, H.; Reed, M. A.; Lee, T. *Advanced Materials* **2011**, *23*, 1583.
- (10) Tsutsui, M.; Taniguchi, M. *Sensors* **2012**, *12*, 7259.
- (11) Moore, G. E. In *Electroncis Magazine* 1965; Vol. 38.
- (12) Love, J. C.; Estroff, L. A.; Kriebel, J. K.; Nuzzo, R. G.; Whitesides, G. M. *Chemical Reviews* **2005**, *105*, 1103.
- (13) Lindsay, S. M. *Japanese Journal of Applied Physics Part 1-Regular Papers Short Notes & Review Papers* **2002**, *41*, 4867.
- (14) Wang, G.; Yoo, H.; Na, S.-I.; Kim, T.-W.; Cho, B.; Kim, D.-Y.; Lee, T. *Thin Solid Films* **2009**, *518*, 824.
- (15) Wang, G.; Kim, T.-W.; Jang, Y. H.; Lee, T. *Journal of Physical Chemistry C* **2008**, *112*, 13010.
- (16) He, J.; Forzani, E. S.; Nagahara, L. A.; Tao, N.; Lindsay, S. *J. Phys.-Condes. Matter* **2008**, *20*.
- (17) Cui, X. D.; Primak, A.; Zarate, X.; Tomfohr, J.; Sankey, O. F.; Moore, A. L.; Moore, T. A.; Gust, D.; Harris, G.; Lindsay, S. M. *Science* **2001**, *294*, 571.

*Ultra Smooth Gold Substrates Prepared by Chemical Mechanical Polishing: A New Substrate for Measuring Charge Transport in Metal-SAM//Ga<sub>2</sub>O<sub>3</sub>/EGaIn Junctions*

- (18) Cui, X. D.; Zarate, X.; Tomfohr, J.; Sankey, O. F.; Primak, A.; Moore, A. L.; Moore, T. A.; Gust, D.; Harris, G.; Lindsay, S. M. *Nanotechnology* **2002**, *13*, 5.
- (19) Kim, B.; Beebe, J. M.; Jun, Y.; Zhu, X. Y.; Frisbie, C. D. *Journal of the American Chemical Society* **2006**, *128*, 4970.
- (20) Engelkes, V. B.; Beebe, J. M.; Frisbie, C. D. *Journal of Physical Chemistry B* **2005**, *109*, 16801.
- (21) Beebe, J. M.; Kim, B.; Gadzuk, J. W.; Frisbie, C. D.; Kushmerick, J. G. *Physical Review Letters* **2006**, 97.
- (22) Engelkes, V. B.; Frisbie, C. D. *Journal of Physical Chemistry B* **2006**, *110*, 10011.
- (23) Wold, D. J.; Frisbie, C. D. *Journal of the American Chemical Society* **2001**, *123*, 5549.
- (24) Song, H.; Lee, H.; Lee, T. *Ultramicroscopy* **2008**, *108*, 1196.
- (25) Yoo, H.; Choi, J.; Wang, G.; Kim, T.-W.; Noh, J.; Lee, T. *J. Nanosci. Nanotechnol.* **2009**, *9*, 7012.
- (26) Kim, Y.; Song, H.; Kim, D.; Lee, T.; Jeong, H. *ACS Nano* **2010**, *4*, 4426.
- (27) Venkataraman, B.; Breen, J. J.; Flynn, G. W. *SCANNING TUNNELING MICROSCOPY STUDIES OF ALCOHOL ALKANE MIXTURES ADSORBED ON GRAPHITE SURFACES*, 1994.
- (28) Venkataraman, B.; Breen, J. J.; Flynn, G. W. *Journal of Physical Chemistry* **1995**, *99*, 6608.
- (29) Venkataraman, B.; Flynn, G. W.; Wilbur, J. L.; Folkers, J. P.; Whitesides, G. M. *Journal of Physical Chemistry* **1995**, *99*, 8684.
- (30) Bumm, L. A.; Arnold, J. J.; Cygan, M. T.; Dunbar, T. D.; Burgin, T. P.; Jones, L.; Allara, D. L.; Tour, J. M.; Weiss, P. S. *Science* **1996**, *271*, 1705.
- (31) Akkerman, H. B.; Blom, P. W. M.; de Leeuw, D. M.; de Boer, B. *Nature* **2006**, *441*, 69.
- (32) Slowinski, K.; Majda, M. *Journal of Electroanalytical Chemistry* **2000**, *491*, 139.

*Ultra Smooth Gold Substrates Prepared by Chemical Mechanical Polishing: A New Substrate for Measuring Charge Transport in Metal-SAM//Ga<sub>2</sub>O<sub>3</sub>/EGaIn Junctions*

- (33) Slowinski, K.; Fong, H. K. Y.; Majda, M. *Journal of the American Chemical Society* **1999**, *121*, 7257.
- (34) Slowinski, K.; Chamberlain, R. V.; Miller, C. J.; Majda, M. *Journal of the American Chemical Society* **1997**, *119*, 11910.
- (35) Slowinski, K.; Chamberlain, R. V.; Bilewicz, R.; Majda, M. *Journal of the American Chemical Society* **1996**, *118*, 4709.
- (36) Weiss, E. A.; Chiechi, R. C.; Kaufman, G. K.; Kriebel, J. K.; Li, Z. F.; Duati, M.; Rampi, M. A.; Whitesides, G. M. *Journal of the American Chemical Society* **2007**, *129*, 4336.
- (37) Ashwell, G. J.; Mohib, A.; Miller, J. R. *Journal of Materials Chemistry* **2005**, *15*, 1160.
- (38) Tran, E.; Rampi, M. A.; Whitesides, G. M. *Angewandte Chemie-International Edition* **2004**, *43*, 3835.
- (39) York, R. L.; Slowinski, K. *Journal of Electroanalytical Chemistry* **2003**, *550*, 327.
- (40) Chabinyk, M. L.; Holmlin, R. E.; Haag, R.; Chen, X. X.; Ismagilov, R. F.; Rampi, M. A.; Whitesides, G. M. In *Molecules as Components of Electronic Devices*; Lieberman, M., Ed.; Amer Chemical Soc: Washington, 2003; Vol. 844, p 16.
- (41) Anariba, F.; McCreery, R. L. *Journal of Physical Chemistry B* **2002**, *106*, 10355.
- (42) Mann, B.; Kuhn, H. *Journal of Applied Physics* **1971**, *42*, 4398.
- (43) Thuo, M. M.; Reus, W. F.; Simeone, F. C.; Kim, C.; Schulz, M. D.; Yoon, H. J.; Whitesides, G. M. *Journal of the American Chemical Society* **2012**, *134*, 10876.
- (44) Thuo, M. M.; Reus, W. F.; Nijhuis, C. A.; Barber, J. R.; Kim, C.; Schulz, M. D.; Whitesides, G. M. *Journal of the American Chemical Society* **2011**, *133*, 2962.
- (45) Ricoeur, G.; Lenfant, S.; Guerin, D.; Vuillaume, D. *Journal of Physical Chemistry C* **2012**, *116*, 20722.
- (46) Reus, W. F.; Nijhuis, C. A.; Barber, J. R.; Thuo, M. M.; Tricard, S.; Whitesides, G. M. *Journal of Physical Chemistry C* **2012**, *116*, 6714.

*Ultra Smooth Gold Substrates Prepared by Chemical Mechanical Polishing: A New Substrate for Measuring Charge Transport in Metal-SAM//Ga<sub>2</sub>O<sub>3</sub>/EGaIn Junctions*

- (47) Nijhuis, C. A.; Reus, W. F.; Whitesides, G. M. *Journal of the American Chemical Society* **2010**, *132*, 18386.
- (48) Nijhuis, C. A.; Reus, W. F.; Whitesides, G. M. *Journal of the American Chemical Society* **2009**, *131*, 17814.
- (49) Nijhuis, C. A.; Reus, W. F.; Siegel, A. C.; Whitesides, G. M. *Journal of the American Chemical Society* **2011**, *133*, 15397.
- (50) Nijhuis, C. A.; Reus, W. F.; Barber, J. R.; Whitesides, G. M. *Journal of Physical Chemistry C* **2012**, *116*, 14139.
- (51) Nijhuis, C. A.; Reus, W. F.; Barber, J. R.; Dickey, M. D.; Whitesides, G. M. *Nano Letters* **2010**, *10*, 3611.
- (52) Fracasso, D.; Valkenier, H.; Hummelen, J. C.; Solomon, G. C.; Chiechi, R. C. *Journal of the American Chemical Society* **2011**, *133*, 9556.
- (53) Fracasso, D.; Muglali, M. I.; Rohwerder, M.; Terfort, A.; Chiechi, R. C. *Journal of Physical Chemistry C* **2013**, *117*, 11367.
- (54) Chiechi, R. C.; Weiss, E. A.; Dickey, M. D.; Whitesides, G. M. *Angewandte Chemie* **2008**, *120*, 148.
- (55) Cademartiri, L.; Thuo, M. M.; Nijhuis, C. A.; Reus, W. F.; Tricard, S.; Barber, J. R.; Sodhi, R. N. S.; Brodersen, P.; Kim, C.; Chiechi, R. C.; Whitesides, G. M. *Journal of Physical Chemistry C* **2012**, *116*, 10848.
- (56) Simmons, J. G. *Conduction in Thin Films*; Mills and Boon Ltd.: London, 1971.
- (57) Lamb, D. R. *Electrical Conduction Measurements in Thin Insulating Films*; Methuen and Co.: London, 1968.
- (58) Thuo, M. M.; Reus, W. F.; Nijhuis, C. A.; Barber, J. R.; Kim, C.; Schulz, M. D.; Whitesides, G. M. *Journal of the American Chemical Society* **2011**, *133*, 2962.
- (59) Wagner, P.; Hegner, M.; Guntherodt, H. J.; Semenza, G. *Langmuir* **1995**, *11*, 3867.
- (60) Weiss, E. A.; Kaufman, G. K.; Kriebel, J. K.; Li, Z.; Schalek, R.; Whitesides, G. M. *Langmuir* **2007**, *23*, 9686.

*Ultra Smooth Gold Substrates Prepared by Chemical Mechanical Polishing: A New Substrate for Measuring Charge Transport in Metal-SAM//Ga<sub>2</sub>O<sub>3</sub>/EGaIn Junctions*

- (61) Naumann, R.; Schiller, S. M.; Giess, F.; Grohe, B.; Hartman, K. B.; Karcher, I.; Koper, I.; Lubben, J.; Vasilev, K.; Knoll, W. *Langmuir* **2003**, *19*, 5435.
- (62) Trevor, D. J.; Chidsey, C. E. D.; Loiacono, D. N. *Physical Review Letters* **1989**, *62*, 929.
- (63) Hegner, M.; Wagner, P.; Semenza, G. *Surface Science* **1993**, *291*, 39.
- (64) Wagner, P.; Zaugg, F.; Kernen, P.; Hegner, M.; Semenza, G. *Journal of Vacuum Science & Technology B* **1996**, *14*, 1466.
- (65) Gupta, P.; Ulman, A.; Fanfan, S.; Korniaikov, A.; Loos, K. *Journal of the American Chemical Society* **2005**, *127*, 4.
- (66) Gupta, P.; Loos, K.; Korniaikov, A.; Spagnoli, C.; Cowman, M.; Ulman, A. *Angewandte Chemie-International Edition* **2004**, *43*, 520.
- (67) Silvestrini, S.; Ferraro, D.; Toth, T.; Pierno, M.; Carofiglio, T.; Mistura, G.; Maggini, M. *Lab on a Chip* **2012**, *12*, 4041.
- (68) Products, N.; Vol. 2013.
- (69) *Microelectronic Applications of Chemical Mechanical Planarization*; LI, Y., Ed.; John Wiley & Sons Inc.: Hoboken, 2007.
- (70) Huang, J. T.; Chao, P. S.; Hsu, H. J.; Shih, S. H. *A novel polishing mechanism used in manufacturing ultra-high uniformity gold solder bump*; Ieee: New York, 2005.
- (71) Ishii, H.; Yagi, S.; Minotani, T.; Royter, Y.; Kudou, K.; Yano, M.; Nagatsuma, T.; Machida, K.; Kyuragi, H. In *Micromachining and Microfabrication Process Technology Vii*; Karam, J. M., Yasaitis, J., Eds.; Spie-Int Soc Optical Engineering: Bellingham, 2001; Vol. 4557, p 210.
- (72) Lee, C.; Yang, E. H.; Myung, N. V.; George, T.; Ieee *A nanochannel fabrication technique using chemical-mechanical polishing (CMP) and thermal oxidation*; Ieee: New York, 2003.

*Ultra Smooth Gold Substrates Prepared by Chemical Mechanical Polishing: A New Substrate for Measuring Charge Transport in Metal-SAM//Ga<sub>2</sub>O<sub>3</sub>/EGaIn Junctions*

- (73) Islam, M. S.; Jung, G. Y.; Ha, T.; Stewart, D. R.; Chen, Y.; Wang, S. Y.; Williams, R. S. *Applied Physics a-Materials Science & Processing* **2005**, *80*, 1385.
- (74) Horcas, I.; Fernandez, R.; Gomez-Rodriguez, J. M.; Colchero, J.; Gomez-Herrero, J.; Baro, A. M. *Review of Scientific Instruments* **2007**, *78*.
- (75) Moulder, J. F.; Stickle, W. F.; Sobol, P. E.; Bomben, K. D. *Handbook of X-Ray Photoelectron Spectroscopy* Eden Prairie, MN, 1995.
- (76) Cumpson, P. J. *Surf. Interface Anal.* **2000**, *29*, 403.
- (77) Streng, K.; Pilgrim, H. *Colloid and Polymer Science* **1983**, *261*, 855.
- (79) *CRC Handbook of Metal Etchants*; Walker, P.; Tarn, W. H., Eds.; CRC Press: Boca Raton, Florida, 2010.
- (80) Ahrland, S.; Noren, B.; Oskarsson, A. *Inorganic Chemistry* **1985**, *24*, 1330.
- (81) Rodriguez, J. F.; Soriaga, M. P. *Journal of the Electrochemical Society* **1988**, *135*, 616.
- (82) Miller, M. S.; Juan, R. R. S.; Ferrato, M.-A.; Carmichael, T. B. *Langmuir* **2011**, *27*, 10019.
- (83) Castner, D. G.; Hinds, K.; Grainger, D. W. *Langmuir* **1996**, *12*, 5083.
- (84) Ishida, T.; Choi, N.; Mizutani, W.; Tokumoto, H.; Kojima, I.; Azebara, H.; Hokari, H.; Akiba, U.; Fujihira, M. *Langmuir* **1999**, *15*, 6799.
- (85) Sellers, H.; Ulman, A.; Shnidman, Y.; Eilers, J. E. *Journal of the American Chemical Society* **1993**, *115*, 9389.
- (86) Schlenoff, J. B.; Li, M.; Ly, H. *Journal of the American Chemical Society* **1995**, *117*, 12528.
- (87) Ulman, A. *Chemical Reviews* **1996**, *96*, 1533.

## 7.6. Supporting Information

### 7.6.1. Thickogram Calculation

Thickogram calculations were performed by Dr. Mark Biesinger (Surface Science Western, London, ON). The AuI band gap was estimated to be 0.5 – 1 eV, and the inelastic mean free path was used as an estimate for the attenuation length.

$$\text{Thickness (nm)} = C \cdot \lambda \cdot \cos\theta$$

	Au <sup>CMP</sup>	Au <sup>CMP</sup> – C <sub>16</sub> SH
I <sub>0</sub> – Intensity of AuI peak	3369.8	3479.1
I <sub>s</sub> – Intensity of Au peak	416528.6	281447
S <sub>0</sub> – RSF of AuI peak	6.205	6.205
S <sub>s</sub> – RSF of Au peak	6.25	6.25
E <sub>0</sub> – K.E. of AuI peak	868.5	868.5
E <sub>s</sub> – K.E. of Au peak	1403.3	1403.3
Theta	60	60
Cos Theta	0.5	0.5
λ (attenuation length of photoelectrons from AuI) (nm)	1.7	1.7
I <sub>0</sub> /S <sub>0</sub> / I <sub>s</sub> /S <sub>s</sub> ( <b>A</b> )	0.01	0.01
E <sub>0</sub> / E <sub>s</sub> ( <b>B</b> )	0.62	0.62
Measured from thickogram ( <b>C</b> )	0.01	0.01
AuI thickness (nm)	< 0.01	< 0.01

### 7.6.2. Synthesis of 1-tridecanethiol

We added 50 mL of anhydrous ethanol to a 250 mL round bottom flask containing 1-bromotridecane (1.0 g, 3.6 mmol), followed by thiourea (0.36 g, 4.7 mmol) dissolved in 50 mL of anhydrous ethanol. The mixture was heated to reflux and stirred for 12 hours. We removed the solvent *in vacuo* to give a residual oil. We added NaOH (0.5 g, 12.5 mmol) in 50 mL of deionized water and heated the mixture to reflux for 1 hour. We cooled the reaction to room temperature and extracted three times with 30 mL of diethyl ether. We dried the ethereal extracts over Na<sub>2</sub>SO<sub>4</sub> and removed the solvent *in vacuo*. The compound was purified by passing through a silica gel column, eluting with 100% *n*-hexanes. After purification, the product was stored in a refrigerator at < 5°C. The <sup>1</sup>H NMR data (Figure S7.5) matched literature values. <sup>1</sup>H NMR (CDCl<sub>3</sub>): δ 0.8698 (t, 3H, *J* = 7.0 Hz), 1.2466 (m, 20H), 1.5972 (m, 2H), 2.5240 (q, 2H, *J* = 7.2 Hz).

### 7.6.3. <sup>1</sup>H NMR spectra of Purified *n*-alkanethiols

Figures S7.1 – S7.8 show <sup>1</sup>H NMR spectra of 1-nonanethiol, 1-decanethiol, 1-undecanethiol, 1-dodecanethiol, 1-tridecanethiol, 1-tetradecanethiol, 1-pentadecanethiol, and 1-hexadecanethiol after purification using silica gel column chromatography, eluting with 100% *n*-hexanes. We assign and label <sup>1</sup>H NMR peaks as follows:

**a** :  $\delta = \sim 2.5$  ppm, quartet, 2 H,  $J = \sim 7.2$  Hz.

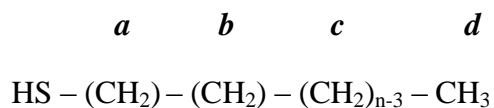
**b** :  $\delta = \sim 1.6$  ppm, multiplet, 2H.

**c** :  $\delta = \sim 1.3$  ppm, multiplet,  $2n - 6$  H.

**d** :  $\delta = \sim 0.9$  ppm, triplet, 3H,  $J = \sim 7.0$  Hz.

**e** :  $\delta = \sim 1.5$  ppm, H<sub>2</sub>O

**e** :  $\delta = 7.27$  ppm, CDCl<sub>3</sub>



*Ultra Smooth Gold Substrates Prepared by Chemical Mechanical Polishing: A New Substrate for Measuring Charge Transport in Metal-SAM//Ga<sub>2</sub>O<sub>3</sub>/EGaIn Junctions*

1-nonanethiol (purified)

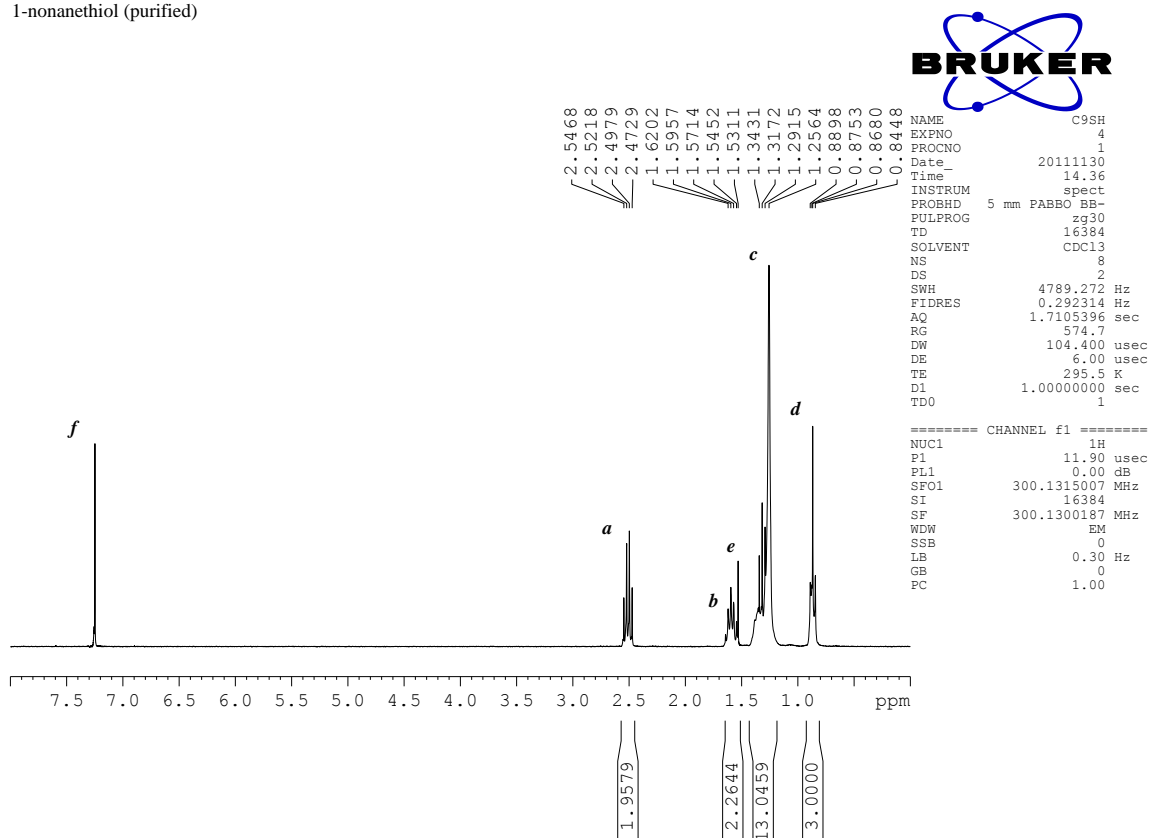


**Figure S7.1.** <sup>1</sup>H NMR spectrum of 1-nonanethiol after purification by column chromatography.

*Ultra Smooth Gold Substrates Prepared by Chemical Mechanical Polishing: A New Substrate for Measuring Charge Transport in Metal-SAM//Ga<sub>2</sub>O<sub>3</sub>/EGaIn Junctions*

1-decanethiol (purified)

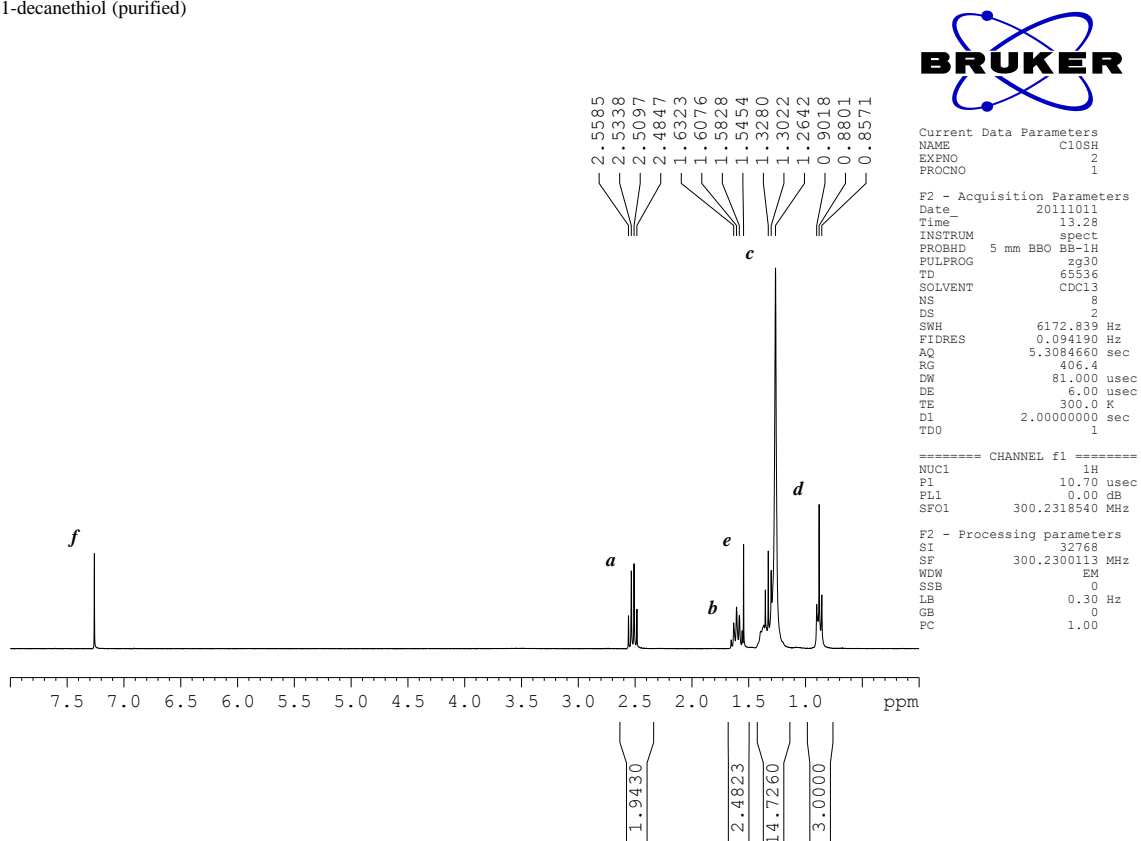


**Figure S7.2.** <sup>1</sup>H NMR spectrum of 1-decanethiol after purification by column chromatography.

*Ultra Smooth Gold Substrates Prepared by Chemical Mechanical Polishing: A New Substrate for Measuring Charge Transport in Metal-SAM//Ga<sub>2</sub>O<sub>3</sub>/EGaIn Junctions*

1-undecanethiol (purified)

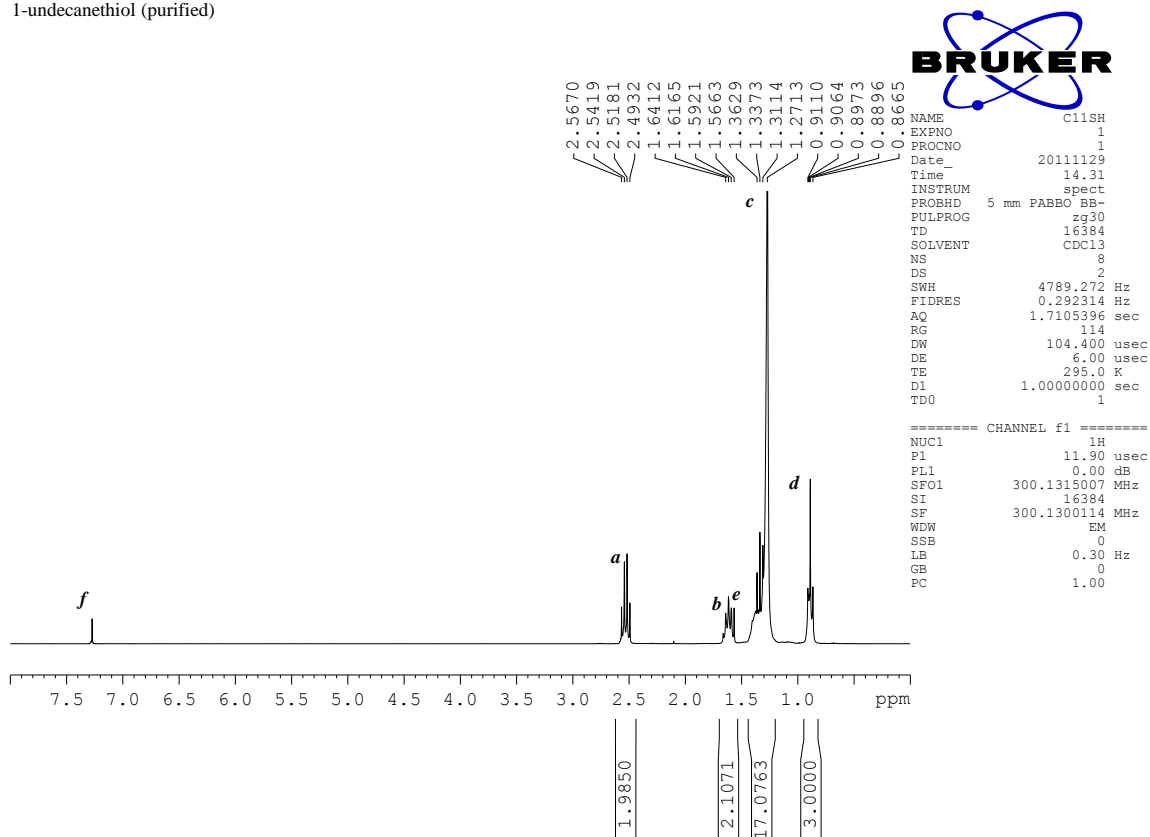


**Figure S7.3.** <sup>1</sup>H NMR spectrum of 1-undecanethiol after purification by column chromatography.

*Ultra Smooth Gold Substrates Prepared by Chemical Mechanical Polishing: A New Substrate for Measuring Charge Transport in Metal-SAM//Ga<sub>2</sub>O<sub>3</sub>/EGaIn Junctions*

1-dodecanethiol (purified)

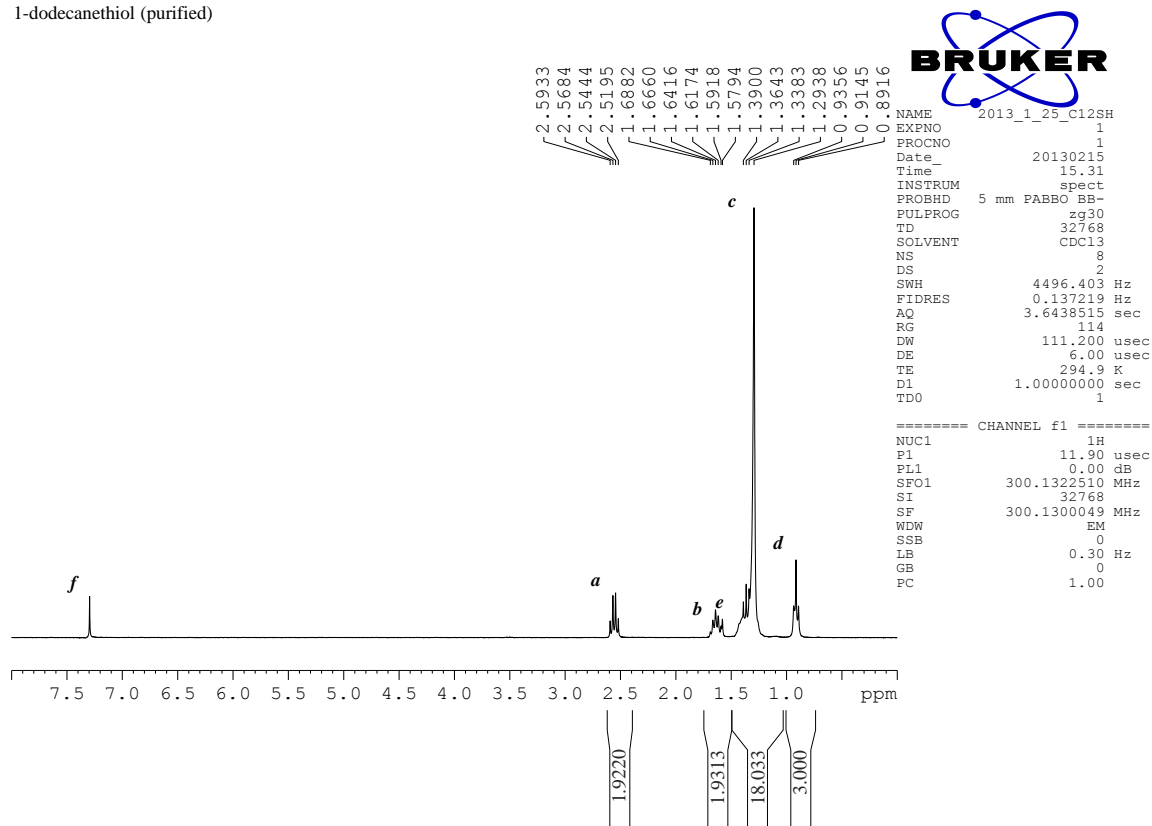


**Figure S7.4.** <sup>1</sup>H NMR spectrum of 1-dodecanethiol after purification by column chromatography.

*Ultra Smooth Gold Substrates Prepared by Chemical Mechanical Polishing: A New Substrate for Measuring Charge Transport in Metal-SAM//Ga<sub>2</sub>O<sub>3</sub>/EGaIn Junctions*

1-tridecanethiol (purified)

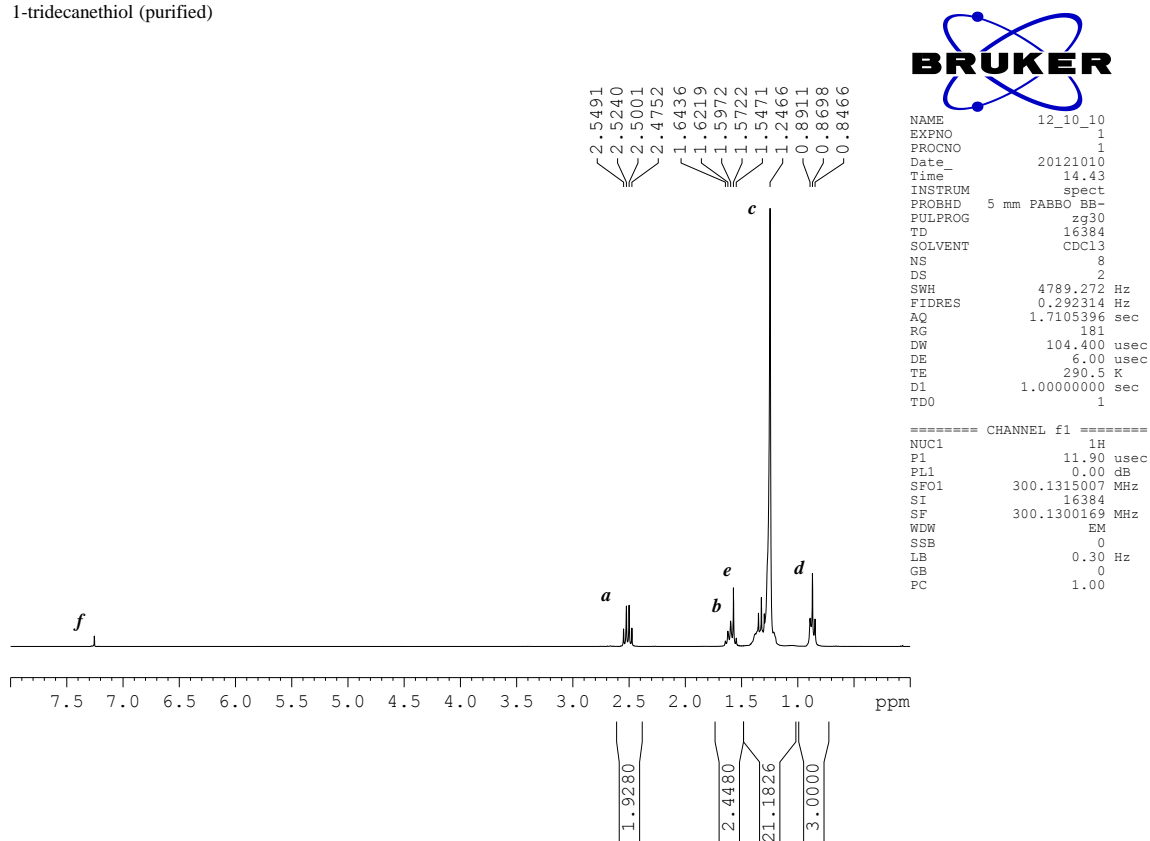


**Figure S7.5.** <sup>1</sup>H NMR spectrum of 1-tridecanethiol after purification by column chromatography.

*Ultra Smooth Gold Substrates Prepared by Chemical Mechanical Polishing: A New Substrate for Measuring Charge Transport in Metal-SAM//Ga<sub>2</sub>O<sub>3</sub>/EGaIn Junctions*

1-tetradecanethiol (purified)

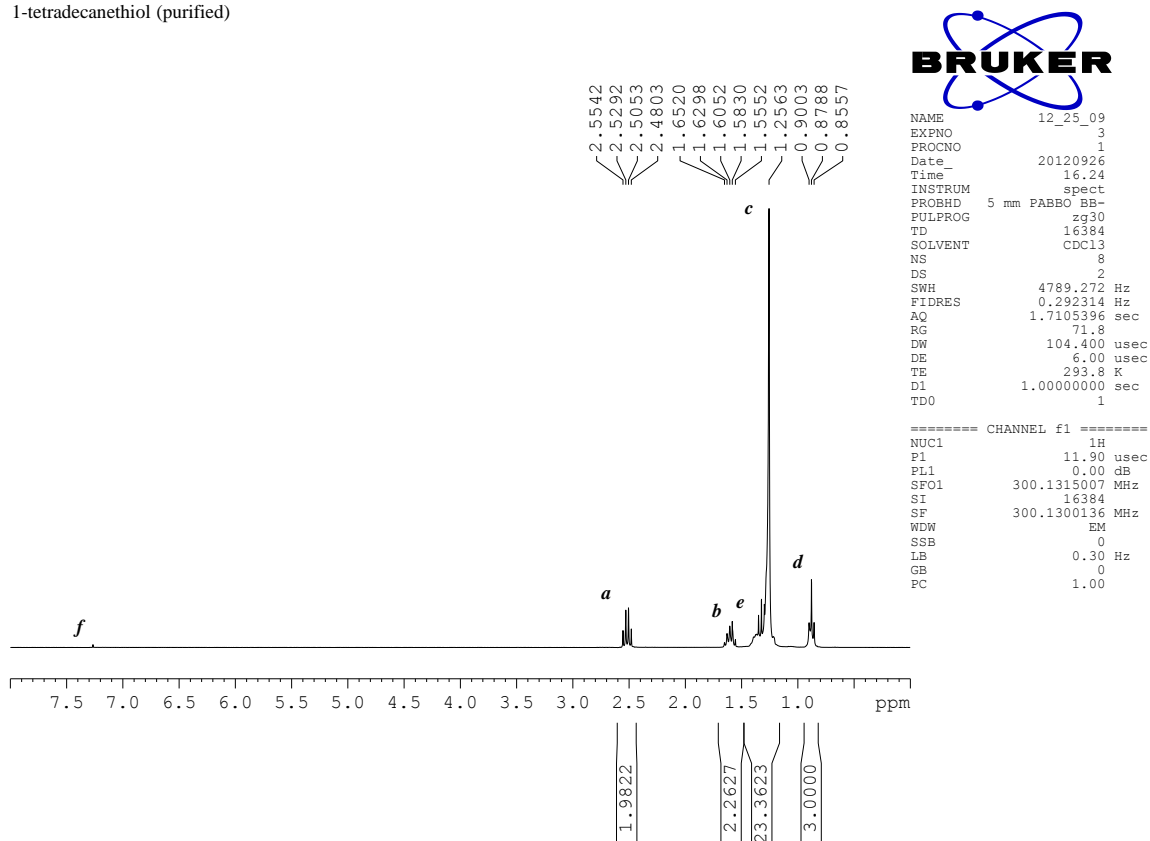


**Figure S7.6.** <sup>1</sup>H NMR spectrum of 1-tetradecanethiol after purification by column chromatography.

*Ultra Smooth Gold Substrates Prepared by Chemical Mechanical Polishing: A New Substrate for Measuring Charge Transport in Metal-SAM//Ga<sub>2</sub>O<sub>3</sub>/EGaIn Junctions*

1-pentadecanethiol (purified)

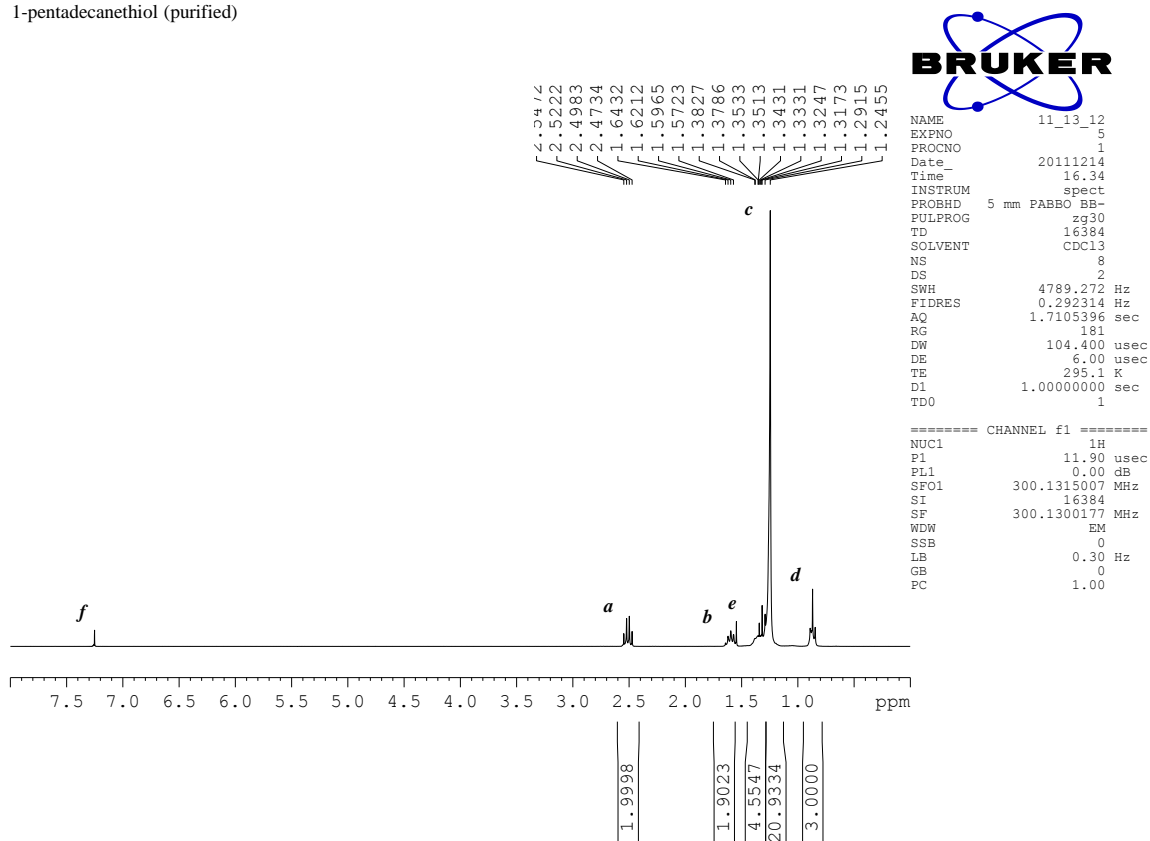


**Figure S7.7.** <sup>1</sup>H NMR spectrum of 1-pentadecanethiol after purification by column chromatography.

*Ultra Smooth Gold Substrates Prepared by Chemical Mechanical Polishing: A New Substrate for Measuring Charge Transport in Metal-SAM//Ga<sub>2</sub>O<sub>3</sub>/EGaIn Junctions*

1-hexadecanethiol (purified)

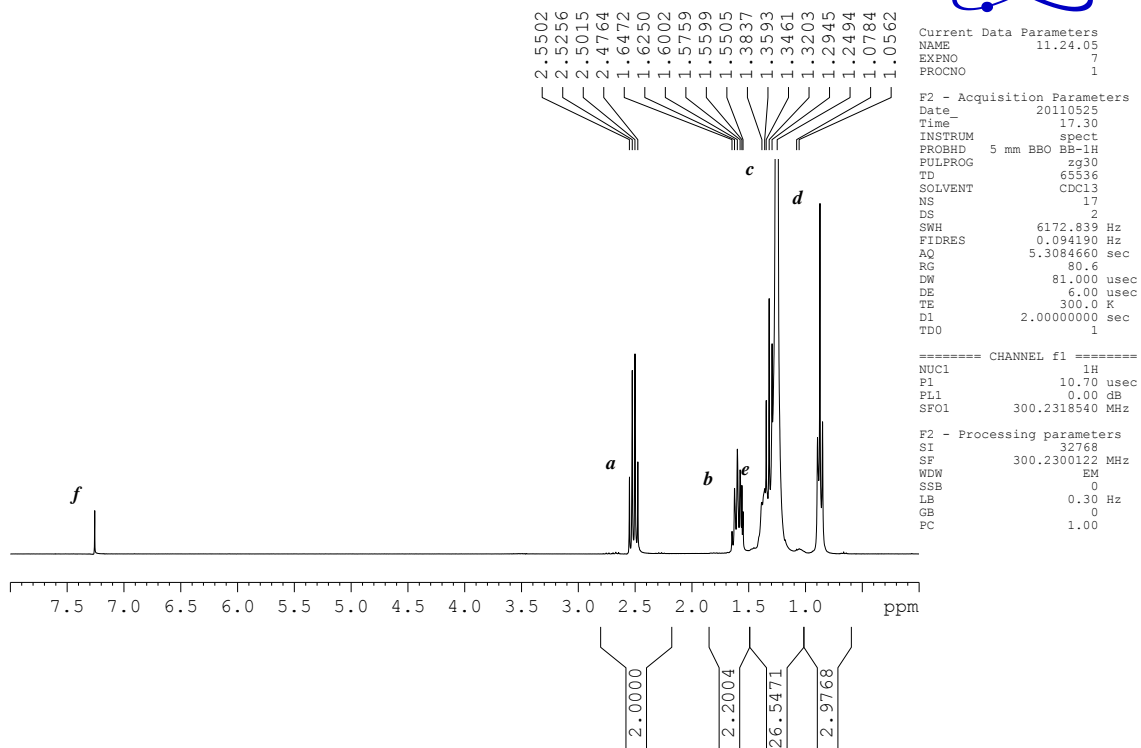


**Figure S7.8.** <sup>1</sup>H NMR spectrum of 1-hexadecanethiol after purification by column chromatography.

## **Chapter 8**

# **Electronic Properties of Diphenyldithiophosphinic Acid Self- Assembled Monolayers**

## 8.1. Introduction

This work presents the formation and characterization of new self-assembled monolayers (SAMs) on gold formed from diphenyldithiophosphinic acid ( $\text{Ph}_2\text{DTPA}$ ) adsorbate molecules (Scheme 8.1a). We have previously reported the detailed characterization of dialkyl-DTPA SAMs on gold, with particular focus on the influence on substrate morphology on head group binding and alkyl chain organization.<sup>1,2</sup> In this work, we shift focus to study the electrical properties of  $\text{Ph}_2\text{DTPA}$  SAMs within metal-SAM// $\text{Ga}_2\text{O}_3$ /EGaIn molecular tunnel junctions. Specifically, we assess the influence of DTPA head group chelation on charge transport properties of the SAM by measuring the current densities through  $\text{Ph}_2\text{DTPA}$  SAMs and comparing them to those of SAMs formed from a monodentate analogue, thiophenol ( $\text{PhSH}$ , Scheme 8.1b).

Research in the field of SAM-based molecular electronics has grown drastically over the past 10 years, with much of the research effort focusing on the development of reliable protocols for fabricating and characterizing molecular junctions using simple model systems.<sup>3-5</sup> *n*-Alkanethiolate SAMs have emerged as an ideal candidate for these model systems due to the extensive literature detailing their formation, structure, and kinetic and thermodynamic properties.<sup>6</sup> Although *n*-alkanethiolate SAMs are well understood systems that are appropriate for fundamental molecular electronics research, their potential inclusion into real devices is severely inhibited by two major factors associated with the metal-thiolate bond: First, the sulfur 3p orbitals involved in the metal-thiolate bond are localized, restricting charge transport through the molecule.<sup>7,8</sup> Second, a low energy barrier to molecular diffusion and desorption causes poor stability and could limit the lifetime of such a device.

Owing to the aforementioned limitations of *n*-alkanethiolates, many researchers have begun exploring alternative adsorbate molecules for use in SAM-based molecular junctions. Adsorbates that chelate to the gold surface are particularly interesting candidates for molecular junctions due to the increased thermal and chemical stability associated with multi-dentate binding, as well as the potential for these head groups to strongly couple to the electrode surface through delocalized bonding motifs.<sup>9</sup> A study by

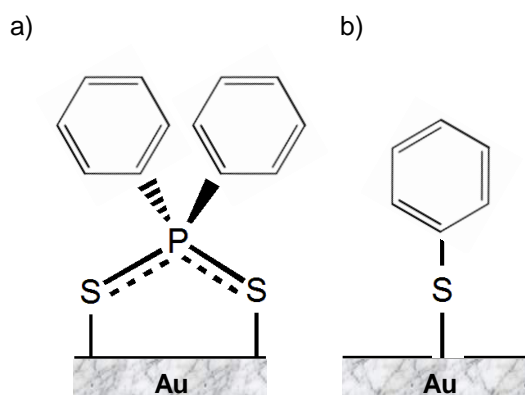
von Wrochem et al. investigated the use of a dithiocarbamate (DTC) head group within a SAM-based molecular junction.<sup>9</sup> SAMs formed from terphenyl-DTC adsorbate molecules exhibited chelation of the head group to the gold surface, improving thermal stability, as well as strong coupling between the metal electrode and the delocalized terphenyl backbone, resulting in a high density of states near the Fermi level of the metal. Within a Hg drop molecular junction, the strong coupling of the metal surface to the terphenyl-DTC adsorbate molecule led to current densities that were  $\sim 2$  orders of magnitude higher than a non-chelating analogue (terphenylthiol). Similar studies, both experimental and theoretical in nature, also show that chelation of conjugated dithiocarboxylic acid (DTCA) adsorbate molecules to the gold surface improves metal-molecule coupling and reduces the charge injection barrier compared to non-chelating analogues within a molecular junction.<sup>10,11</sup>

Our recent work has focused on SAMs on gold formed from another class of chelating adsorbate molecules, dithiophosphinic acids (DTPAs).<sup>1,2,12,13</sup> DTPAs exhibit a unique substrate morphology-dependant head group binding: SAMs formed on rough, As-Deposited (As-Dep) gold demonstrate a mixture of monodentate and bidentate binding modes, while SAMs formed on smooth template-stripped (TS) gold exhibit strictly bidentate binding. DTPAs are interesting candidates for use in SAM-based molecular electronics for two reasons: First, chelation of the DTPA head group has been shown to increase SAM stability, and may also improve the coupling of the adsorbate molecules to the underlying gold surface. Second, the DTPA synthetic pathway allows for the introduction of various pendant groups which may be used to control the charge transport properties of the resulting SAM-based molecular junctions.

This work presents the first study detailing the electrical properties of SAMs on gold formed from DTPA adsorbate molecules. We chose to study SAMs formed from a DTPA derivative with two phenyl groups, Ph<sub>2</sub>DTPA, to allow us to determine the ability of the head group to act as an electronic coupling agent between the gold surface and the pendant groups of the molecule. We show that Ph<sub>2</sub>DTPA adsorbate molecules form stable SAMs on TS gold, exhibit a completely bidentate binding motif, have phenyl group organization similar to SAMs formed from analogous monodentate adsorbate molecules

(PhSH), and provide little resistance to the diffusion of an ionic redox probe – aqueous solutions of  $K_4Fe(CN)_6$  and  $K_3Fe(CN)_6$  – to the underlying gold substrate. Furthermore, we show that within a metal-SAM// $Ga_2O_3$ /EGaIn molecular tunnel junction, current densities through  $Ph_2DTPA$  SAMs are, unexpectedly,  $\sim 3$  orders of magnitude lower than through SAMs formed from analogous monodentate adsorbate molecules (PhSH). We present a computational investigation which suggests that the phosphorus atom present in the DTPA head group decouples the aromatic pendant groups from the gold substrate, resulting in the lower than expected current densities.

**Scheme 8.1.**  $Ph_2DTPA$  (a) and PhSH (b) adsorbate molecules shown bound to a gold surface.



## 8.2. Experimental Section

All chemicals were purchased commercially and used as received. Nuclear magnetic resonance (NMR) spectroscopic data were obtained and recorded on a Bruker Avance 300 MHz Ultrashield spectrometer at room temperature and reported in ppm.  $^{31}P$  NMR spectra were referenced externally to 85%  $H_3PO_4$  ( $\delta = 0$  ppm).  $^1H$  NMR spectra were referenced to residual proton peaks of  $CDCl_3$  ( $\delta = 7.27$  ppm). Diphenyldithiophosphinic acid ( $Ph_2DTPA$ ) (Alfa Aesar) was purified by recrystallization from anhydrous ethanol prior to use, and purity was periodically checked by  $^1H$  and  $^{31}P$  NMR.

### *8.2.1. Gold Substrate Preparation*

Template-stripped gold films were prepared according to published procedures.<sup>14</sup> 400 nm of gold was deposited onto silicon wafers, then a small drop (5 - 10  $\mu$ L) of Norland Optical Adhesive 83-H was applied to the gold surface followed by a 1 cm x 1 cm glass substrate. After curing the adhesive using a 100 W UV lamp for 10 minutes the glass slide was stripped from the silicon wafer using a scalpel. Template-stripped gold films were used immediately after their fabrication to form SAMs to minimize surface contamination.

### *8.2.2. SAM Formation*

Prior to SAM formation, diphenyldithiophosphinic acid (Alfa Aesar) was purified by recrystallization from ethanol. Thiophenol (Sigma Aldrich, > 99% purity) was used as received. 1 cm x 1 cm TS gold substrates were immersed into a 1 mM Ph<sub>2</sub>DTPA or PhSH solution in anhydrous toluene for 3 hours. Substrates were then removed from solution, rinsed with anhydrous toluene and dried under a stream of nitrogen prior to use.

### *8.2.3. X-Ray Photoelectron Spectroscopy (XPS)*

XPS spectra were collected at Surface Science Western (London, Ontario, Canada) using a Kratos Axis Nova X-ray photoelectron spectrometer with a monochromatic Al K $\alpha$  source. The detection limit of the instrument is 0.1 – 0.5 atomic percent. Both survey scan and high resolution analyses were carried out over a 300  $\mu$ m x 700  $\mu$ m scan area. Survey scan analyses were carried out with a pass energy of 160 eV, and high resolution analyses were carried out with a pass energy of 20 eV. Samples were analyzed at a 30 degree take-off angle (60 degree tilt). High resolution sulfur line shapes were fit using one pair of spin-orbit-split components (2p<sub>3/2</sub> and 2p<sub>1/2</sub>) assuming a Gaussian:Lorentzian (70%:30%) line shape and a fixed splitting energy of 1.18 eV with a 2:1 area ratio.<sup>15</sup>

#### *8.2.4. Contact Angle Goniometry*

Advancing water contact angles of Ph<sub>2</sub>DTPA SAMs were measured with a Ramé-Hart contact angle goniometer equipped with a microlitre syringe and a tilting stage. At least three drops from each of three samples were averaged.

#### *8.2.5. Electrochemical Impedance Spectroscopy (EIS)*

EIS spectra were collected using a BAS-Zahner IM6 ex impedance unit. A glass cell equipped with a calomel/saturated KCl reference electrode and a 1.0 mm Pt wire counter electrode was clamped to the working electrode, a 0.95-cm<sup>2</sup> area of the SAM on gold, and then filled with an aqueous solution of 1mM K<sub>3</sub>Fe(CN)<sub>6</sub>, 1mM K<sub>4</sub>Fe(CN)<sub>6</sub>·3H<sub>2</sub>O and 10 mM Na<sub>2</sub>SO<sub>4</sub>. The measurements were made at an open circuit potential set at 450 mV with a 5 mV ac perturbation that was controlled from 5.0×10<sup>-2</sup> to 2.0×10<sup>5</sup> Hz. SAM resistance and capacitance values were normalized to the area of the working electrode.

#### *8.2.6. Electrical Characterization of Ph<sub>2</sub>DTPA SAMs*

Electrical characterization was performed using a home-made molecular tunnel junction characterization system. The conical shaped EGaIn (Aldrich) top electrode was fabricated by extruding a small drop (~ 0.5 μL) of EGaIn from a 10 μL gas tight syringe (Hamilton Scientific LLC), bringing the drop into contact with a sacrificial Au<sup>TS</sup> substrate using a micropositioner (Newport Corp.), and bifurcating the EGaIn drop into a conical shape by slowly removing the syringe from the sacrificial substrate. A test lead equipped with a micro hook (E-Z Hook) was used to make electrical connection to the syringe needle bearing the conical EGaIn tip. The gold substrate served as the ground electrode by means of a second micro hook test lead that penetrated the SAM and contacted the gold directly. A triaxial cable connected both electrodes to an external amplifier, which was connected to a Keithley 6430 source meter. Molecular tunnel junctions were formed by slowly bringing the conical EGaIn tip into gentle contact with its own reflection in the SAM bearing gold substrate as imaged by a high resolution analytical CCD camera (Edmund Optics). The source meter applied a bias across the molecular tunnel junction

and measured the resulting current, with a single scan being defined as a bias sweep from 0 V  $\rightarrow$  -0.5 V  $\rightarrow$  +0.5 V  $\rightarrow$  0 V. Current densities were calculated assuming a circular contact area, with the diameter of the junction measured using the high magnification CCD camera. After establishing contact between the EGaIn top electrode and the SAM, the presence of a molecular tunnel junction was confirmed by measuring a single J(V) trace. A working junction was defined as a sigmoidally shaped J(V) trace, while a short circuit was defined as a straight line in which the current reached the compliance of the source meter (105 mA). After establishing a working tunnel junction with the first J(V) trace, 20 subsequent J(V) traces were measured from the same area. 25 randomly sampled tunnel junctions totaling 525 J(V) traces were measured for both PhSH and Ph<sub>2</sub>DTPA SAMs. The non-shortening junction yield is defined as the number of junctions that short circuit divided by the total number of junctions sampled, after the first working junction (21 J(V) traces) of that particular sample has been established.

### *8.2.7. Density Functional Theory (DFT) Calculations*

All density functional theory (DFT) calculations were performed using the B3PW91 method implemented in the Gaussian 09 program suite<sup>16</sup> using the SHARCNET high-performance computing network ([www.sharcnet.ca](http://www.sharcnet.ca)). Where applicable, the Stuttgart group (SDD) effective core potentials<sup>17,18</sup> (ECP) and corresponding basis sets were used for gold atoms and the 6-31+G(d) basis set was used for all lighter atoms in all calculations. Natural bond order (NBO) analyses to determine orbital contributions,<sup>19</sup> Wiberg Bond Indices and HOMO/LUMO energies were obtained using the NBO routine included in the Gaussian distributions. All stationary points were confirmed to be minima exhibiting no imaginary frequencies. Molecular orbital pictures and electrostatic potential plots were calculated using Molden.<sup>20</sup> Molecular orbital diagrams were generated using POV-Ray for Windows.<sup>21</sup>

## 8.3. Results and Discussion

### *8.3.1. Gold Substrate Fabrication and SAM Formation*

We fabricated TS gold substrates by e-beam evaporation of 400 nm of gold onto a silicon wafer followed by adhering of a 1 cm x 1 cm glass slide using an optical adhesive.<sup>14</sup> Upon curing the adhesive, we removed the glass slide using a scalpel to expose the smooth underside of the film. We formed SAMs of Ph<sub>2</sub>DTPA and PhSH by immersing 1 cm x 1 cm TS gold substrates into a 1 mM solution of these adsorbates in toluene for 24 hours (for XPS, contact angle, and EIS) or 3 hours (for electrical characterization). We used a shorter immersion time to form SAMs for use in electrical characterization to minimize exposure of the optical adhesive to toluene, which could potentially lead to swelling of the film and leaching of unwanted contaminants into solution.

### *8.3.2. Ph<sub>2</sub>DTPA Head Group Binding*

X-ray photoelectron spectroscopy (XPS) confirmed the presence of elements consistent with Ph<sub>2</sub>DTPA SAM formation, and high resolution XPS (HR-XPS) of the sulfur 2p region (Figure 8.1) confirmed that the DTPA head group of all Ph<sub>2</sub>DTPA adsorbates is chelated to the gold surface. XPS survey scans of Ph<sub>2</sub>DTPA SAMs formed on TS gold (Figure S8.1) showed characteristic binding energies of gold, as well as the elements comprising the Ph<sub>2</sub>DTPA adsorbates (P, S, C). Survey scans also showed the presence of oxygen.

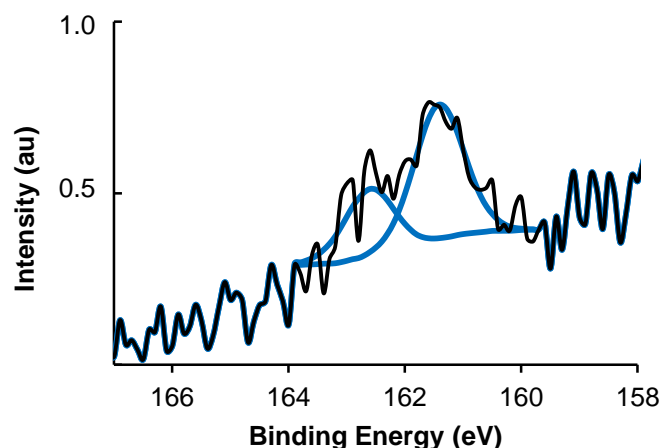


**Figure 8.1.** HR-XPS spectra of the S 2p region of a Ph<sub>2</sub>DTPA SAM formed on TS gold.

HR-XPS of the S 2p region of a Ph<sub>2</sub>DTPA SAM formed on TS gold exhibited a simple line shape that we fit using one pair of spin-orbit-split components (S 2p<sub>3/2</sub> and S 2p<sub>1/2</sub>) by assuming a Gaussian/Lorentzian (70%:30%) line shape and a splitting energy fixed at 1.18 eV.<sup>15</sup> The fitted data show a single S 2p<sub>3/2</sub> peak appearing at a binding energy of 161.4 eV, indicating that the sulfur atoms in the Ph<sub>2</sub>DTPA SAM are bound to the gold substrate.<sup>22,23</sup> There were no peaks at binding energies of 163 - 164 eV, which would indicate the presence of sulfur atoms not interacting with gold, or at binding energies >168 eV, which correspond to oxidized sulfur species.<sup>22,23</sup> HR-XPS thus confirms that Ph<sub>2</sub>DTPA SAMs on TS gold consist of solely bidentate adsorbates, consistent with our previous studies of dialkyl-DTPA SAMs formed on TS gold.<sup>1</sup>

### 8.3.3. Contact Angle Measurements

We used contact angle goniometry to probe the wettability of Ph<sub>2</sub>DTPA SAMs on TS gold. Contact angles of short chain aromatic SAMs on gold depend on surface composition, structure, and coverage, and therefore can be used to probe the overall quality of the SAM.<sup>24-26</sup> Well-ordered SAMs with a high packing density, such as long chain *n*-alkanethiolates, prevent the probe liquid from sensing the underlying gold surface resulting in high contact angles ( $\theta_{\text{H}_2\text{O}} > 100^\circ$ ); porous or liquid-like SAMs, such as short

chain *n*-alkanethiolates, present low contact angles.<sup>26</sup> Contact angles of SAMs formed from aromatic adsorbates also depend upon the orientation of the tail group; the proportion of face-exposed aromatic rings at the surface strongly influences wettability.<sup>27</sup> The simplest short-chain aromatic SAM, thiophenol (PhSH), has previously been shown to have a contact angle that is strongly dependent upon the quality of the SAM; densely packed PhSH SAMs prevent the probe liquid from sensing the underlying gold, leading to increased contact angles compared to more disordered SAMs.<sup>27</sup> Previous work has concluded that an advancing water contact angle of  $\sim 80^\circ$  is indicative of a PhSH SAM of the highest quality.<sup>27,28</sup> We note that SAMs formed from adsorbate molecules with a long alkyl spacer and a phenyl tail group have much higher contact angles ( $> 90^\circ$ ), however this is most likely due to the separation of the probe liquid from the underlying gold substrate rather than increased packing density of the surface phenyl groups.<sup>29</sup>

Advancing water contact angles of Ph<sub>2</sub>DTPA SAMs on TS gold ( $76 \pm 2^\circ$ ) are slightly lower than the accepted value for densely packed PhSH SAMs formed on As-Deposited (As-Dep) gold ( $80^\circ$ ).<sup>27</sup> Several possible reasons could explain the lower contact angle of Ph<sub>2</sub>DTPA SAMs on TS gold: First, the probe liquid could be sensing the underlying gold substrate. Although Ph<sub>2</sub>DTPA SAMs and PhSH SAMs have a very similar thickness (*vide infra*), a higher porosity of the Ph<sub>2</sub>DTPA SAM – possibly owing to the large size and bidentate binding motif of the DTPA head group on the gold surface – compared to the PhSH SAM could account for this behavior. Second, the tetrahedral geometry at the phosphorus atom of Ph<sub>2</sub>DTPA SAMs could lead to an increased proportion of face-exposed phenyl rings at the surface compared to PhSH SAMs. Finally, SAMs formed on TS gold have previously been shown to exhibit decreased contact angle hysteresis compared to those formed on As-Dep gold, lowering the advancing contact angle and increasing the receding contact angle.<sup>30</sup> Contact angle hysteresis of Ph<sub>2</sub>DTPA SAMs on TS gold ( $12^\circ$ ) is lower than the literature values of PhSH SAMs on As-Dep gold ( $\sim 20^\circ$ ),<sup>28</sup> suggesting that the change in substrate morphology between the two systems may be the cause of the variation in contact angle.

### 8.3.4. Electrochemical Barrier Properties

We used EIS to investigate the resistance of Ph<sub>2</sub>DTPA SAMs to the diffusion of an ionic redox probe – aqueous solutions of K<sub>4</sub>Fe(CN)<sub>6</sub> and K<sub>3</sub>Fe(CN)<sub>6</sub> – to the underlying gold. Applying a small sinusoidal ac perturbation at frequencies ranging from 50 mHz to 20 kHz and measuring the corresponding current response yields the complex impedance of the SAM.<sup>31</sup> The data are represented as Bode magnitude plots (Figure 8.2 a) and Nyquist plots (Figure 8.2b). We used a Randles equivalent circuit model – shown in Figure 8.2a (inset) – to fit the impedance spectra, allowing us to determine the resistance ( $R_{\text{SAM}}$ ) and capacitance ( $C_{\text{SAM}}$ ) of the SAM (Table 8.1). We included a Warburg impedance element ( $Z_{\text{W}}$ ) in the equivalent circuit to model any diffusion controlled charge transfer processes. Fitting errors were less than 1% in all cases.  $R_{\text{SAM}}$  indicates how well the SAM impedes charge transfer.  $C_{\text{SAM}}$  is inversely proportional to the SAM thickness, which can be calculated using<sup>32</sup>

$$d = \frac{\epsilon \cdot \epsilon_0}{C} \quad [1]$$

where  $d$  is the SAM thickness in Angstroms,  $C$  is the capacitance per area in F m<sup>-2</sup>,  $\epsilon$  is the dielectric constant of the SAM (measured for C<sub>*n*</sub>SH SAMs ( $n = 16, 18$ ) on gold using surface plasmon resonance (2.1)<sup>33</sup>), and  $\epsilon_0$  is the permittivity of free space ( $8.54 \times 10^{-12}$  F m<sup>-1</sup>). We note that assuming the dielectric constant of Ph<sub>2</sub>DTPA SAMs to be the same as long-chain alkanethiolate SAMs may be a gross oversimplification; however, the value chosen (2.1) falls within the range of dielectric constants reported for SAMs formed from thiophenol (0.52), biphenylmercaptan (4.5), and terphenyl mercaptan (4.2).<sup>27</sup> Ellipsometric thickness measurements are required to verify the calculated thickness values and choice of dielectric constant.

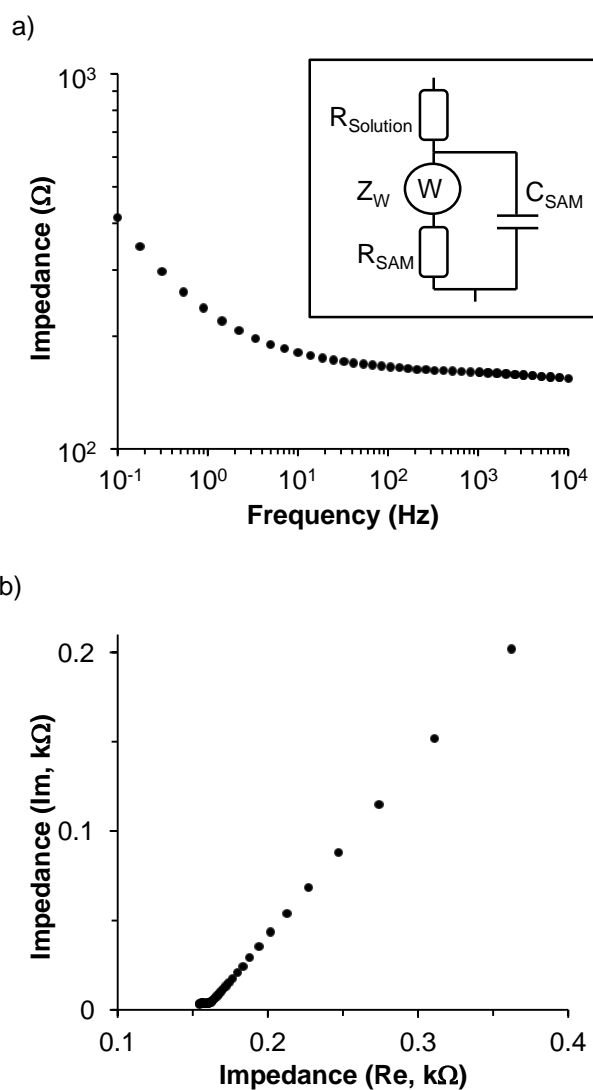


**Figure 8.2.** Bode magnitude plots (a) and Nyquist plots (b) of Ph<sub>2</sub>DTPA SAMs on TS gold. 8.2a inset: Randles circuit model used to fit raw EIS data.

**Table 8.1.** Electrochemical barrier parameters of Ph<sub>2</sub>DTPA SAMs on TS gold calculated by fitting raw EIS data using the Randles simple circuit model.

	Resistance ( $\Omega \cdot \text{cm}^2$ )	Capacitance ( $\mu\text{F} \cdot \text{cm}^{-2}$ )	Thickness ( $\text{\AA}$ )
Ph <sub>2</sub> DTPA SAM	7.9	3.7	5.1
on TS Gold	+/- 2.1	+/- 0.4	+/- 0.5

The Nyquist plot (Figure 8.2b) shows the presence of very small diameter semi-circle on the high frequency side – indicating a very low resistance to charge transfer – and a 45° straight line on the low frequency side, suggesting that charge transfer is primarily a diffusion controlled process. The calculated value of  $R_{\text{SAM}}$  ( $7.9 \Omega \cdot \text{cm}^2$ ) of Ph<sub>2</sub>DTPA SAMs on TS gold is 1-2 orders of magnitude lower than the literature value for PhSH SAMs on gold ( $360 \Omega \cdot \text{cm}^2$ ).<sup>34</sup> Furthermore, the mechanism of charge transport for Ph<sub>2</sub>DTPA SAMs (diffusion dominated) is different than PhSH SAMs (barrier dominated). Increased porosity of the Ph<sub>2</sub>DTPA SAM compared to the PhSH SAM – a possible consequence of head group chelation and molecular shape/size supported by water contact angle measurements – could lead to diffusion controlled charge transfer directly between the redox probe and the underlying gold surface, resulting in very poor barrier properties.

Capacitance values indicate that Ph<sub>2</sub>DTPA SAMs on TS gold are  $\sim 5 \text{\AA}$  thick, similar to previously reported ellipsometric thicknesses of PhSH SAMs on gold ( $4 - 6 \text{\AA}$ ).<sup>28</sup> Although the molecular structure indicates that Ph<sub>2</sub>DTPA SAMs should be thicker than PhSH SAMs, the discrepancy can be explained in one of three ways: First, the phenyl pendant groups of Ph<sub>2</sub>DTPA SAMs could be more tilted with respect to the surface normal than those of PhSH SAMs, though this is unlikely due to the rigid tetrahedral geometry at the phosphorus atom and the restriction of freedom enforced by head group

chelation. Second, the dielectric constant chosen to calculate the thickness of Ph<sub>2</sub>DTPA SAMs (2.1) could be lower than the true value. Finally, the SAM thickness is calculated as an average value measured over the entire area of the working electrode; a lower surface coverage of the Ph<sub>2</sub>DTPA SAM compared to the PhSH SAM could result in an artificially low average value.

### *8.3.5. Electrical Properties of Ph<sub>2</sub>DTPA SAMs on TS Gold*

We measured the electrical properties of Ph<sub>2</sub>DTPA SAMs within a metal-SAM//Ga<sub>2</sub>O<sub>3</sub>/EGaIn molecular tunnel junction. We have speculated in previous work that the chelation of the DTPA head group to the TS gold surface would improve the metal-molecule coupling, leading to a decreased barrier to charge transport.<sup>1</sup> Here, we directly assess this behavior by comparing the current density through Ph<sub>2</sub>DTPA SAMs on TS gold SAMs formed from thiophenol adsorbate molecules – a monodentate analogue.

We formed Au-SAM//Ga<sub>2</sub>O<sub>3</sub>/EGaIn junctions according to previously published procedures.<sup>3</sup> We brought a conical-shaped EGaIn tip into contact with the surface of the SAM-bearing gold substrate and measured the contact area using a high magnification analytical CCD camera. We measured 525  $J(V)$  traces for both Ph<sub>2</sub>DTPA and PhSH SAMs on TS gold. We randomly sampled these  $J(V)$  traces from a minimum of 25 junctions on the SAM-bearing substrate. We measured a maximum of 5 junctions before fabricating a new EGaIn tip. We collected a maximum of 21  $J(V)$  traces for each junction using a source meter, with each trace being defined as a voltage bias sweep from 0 V  $\rightarrow$  -0.5 V  $\rightarrow$  +0.5 V  $\rightarrow$  0 V. We normalized the current measured by the source meter to the area of the junction as measured by the CCD camera. We define a failed junction or ‘short’ as a current measurement that reaches the compliance of the source meter (105 mA) due to penetration of the EGaIn tip through the SAM to the underlying gold substrate. We define the non-shortening yield as the percentage of working junctions after formation of the first stable junction (21  $J(V)$  traces without a short). Current densities of SAM based molecular tunnel junctions are known to be log-normally distributed.<sup>5</sup> As such, we performed all statistical analysis using  $\log J$  rather than  $J$ . As a convention, we report all measurements of  $\log J$  at a bias of -0.5 V to provide comparison to previously

published literature; however, we note that current densities measured at all biases could be fit with a unimodal Gaussian distribution, and had similar standard deviation ( $\sigma_{\log}$ ). Charge transport data for Ph<sub>2</sub>DTPA and PhSH SAMs on TS gold are summarized in Table 8.2. Average  $J(V)$  traces and histograms of charge transport measurements for Ph<sub>2</sub>DTPA and PhSH SAMs on TS gold are shown in Figure 8.3 and Figure 8.4, respectively.

**Table 8.2.** Charge transport data of PhSH and Ph<sub>2</sub>DTPA SAMs on TS gold.

SAM	$\mu_{\log}$	$\sigma_{\log}$	Junctions	Scans	Shorts	Yield (%)
PhSH	0.35	0.43	32	525	7	78
(Ph) <sub>2</sub> DTPA	-3.16	0.37	33	525	8	76

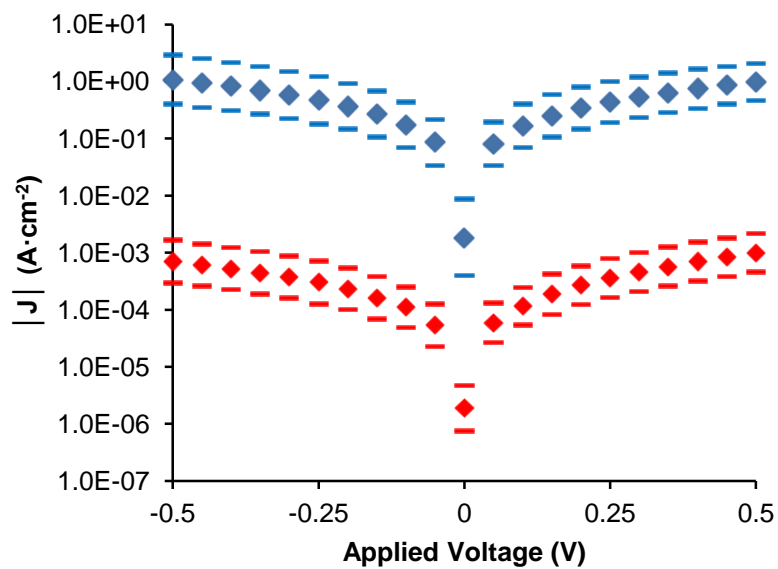


**Figure 8.3.** Average  $J(V)$  traces of PhSH SAMs (blue) and Ph<sub>2</sub>DTPA SAMs (red) on TS gold.

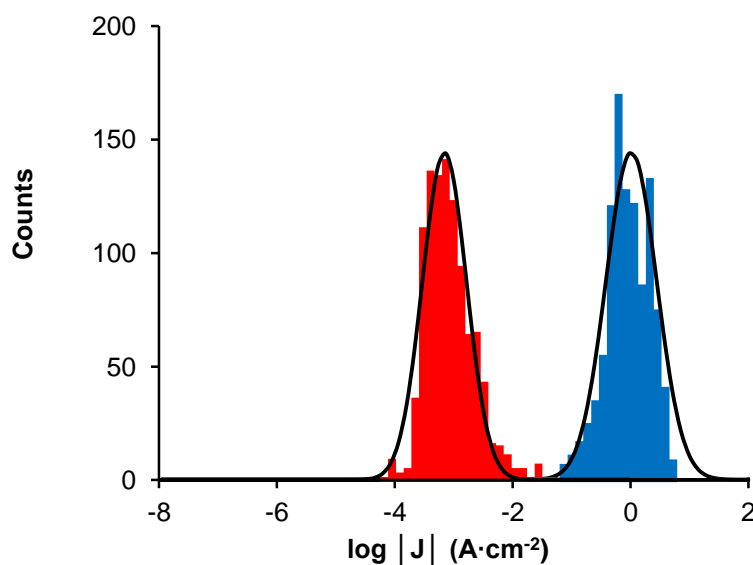


**Figure 8.4.** Histograms and corresponding Gaussian fit of PhSH SAMs (blue) and Ph<sub>2</sub>DTPA SAMs (blue) on TS gold.

Both PhSH and Ph<sub>2</sub>DTPA SAMs formed stable molecular tunnel junctions with non-shortening yields similar to our previously reported values for *n*-alkanethiolate SAMs on TS gold. High yields indicate that both PhSH and Ph<sub>2</sub>DTPA SAMs have a high surface coverage, preventing the EGaIn tip from directly contacting the underlying gold surface. PhSH and Ph<sub>2</sub>DTPA SAMs demonstrated a log-normal distribution of current densities which were fit with a unimodal Gaussian curve. From these distributions, we extracted the parameters  $\mu_{\log}$  – the mean of all measured values of  $\log J$  after excluding shorts – and  $\sigma_{\log}$  – the standard deviation of all measured values of  $\log J$  after excluding shorts (Table 8.2). The value of  $\sigma_{\log}$  for PhSH SAMs (0.43) was similar to Ph<sub>2</sub>DTPA SAMs (0.37), suggesting that both SAMs have a similar density of normally distributed structural irregularities that manifest as log-normally distributed current densities. For *n*-alkanethiolate SAMs, in which the charge transport mechanism is assumed to be strictly non-resonant hole tunneling, normally distributed variations in the thickness of the SAM cause changes in the tunneling barrier thickness, leading to log-normally distributed values of  $J$  according to the Simmons equation.<sup>35</sup> For aromatic systems, such as the PhSH and Ph<sub>2</sub>DTPA SAMs in this study, the charge transport mechanism is likely a

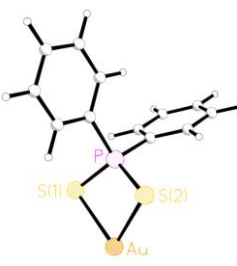
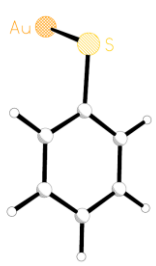
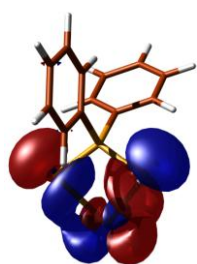
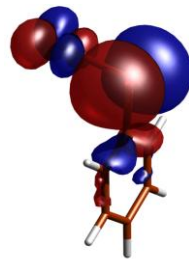
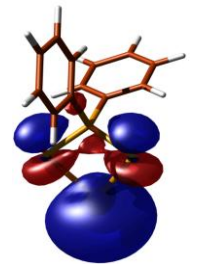
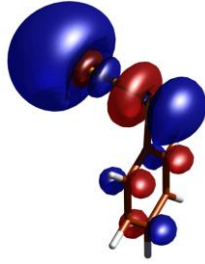
combination of coherent tunneling and activated transport,<sup>36</sup> making it difficult to assess the cause of the distribution of current densities within the molecular junction.

Much to our surprise, current densities through Ph<sub>2</sub>DTPA SAMs were, on average, three orders of magnitude lower than those measured for PhSH SAMs.  $\mu_{\log}$  for Ph<sub>2</sub>DTPA SAMs on TS gold (-3.16) are much lower than what was expected for a short-chain, aromatic SAM,<sup>11</sup> and are comparable to our previously measured values for a 1-decanethiolate SAM on TS gold (-3.26). Unlike previous work describing molecular junctions formed from dithiocarbamate<sup>9</sup> and dithiocarboxylic acid<sup>10,11</sup> SAMs, chelation of the DTPA head group to the gold surface did not decrease the barrier to charge transport compared to a monodentate analogue with identical pendant groups (PhSH). We propose two possible explanations for the low current densities through Ph<sub>2</sub>DTPA SAMs compared to PhSH SAMs: First, the molecular packing density of Ph<sub>2</sub>DTPA SAMs may be lower than PhSH SAMs, leading to a fewer charge transport pathways and a consequent decrease in measured current densities. We have previously shown that chelation of the DTPA head group for dialkyl-DTPA SAMs on TS gold leads to a decreased molecular packing density compared to SAMs with monodentate adsorbates.<sup>1</sup> It is unlikely that this behavior accounts for the three orders of magnitude decrease in average current densities of Ph<sub>2</sub>DTPA SAMs compared to PhSH SAMs, supported by the fact that contact angle measurements and the non-shortening junction yield suggest a high molecular packing density for both of these systems. Second, the electronic structure of Ph<sub>2</sub>DTPA SAM based junctions may lead to an increased barrier to charge transport compared to PhSH SAM based junctions. For SAM based molecular junctions, three parameters can influence the electronic contribution to the charge transport properties: The thickness of the tunneling barrier – determined by the length of the molecule separating the two electrodes, the height of the tunneling barrier – determined by the relative positions of the HOMO and LUMO energy levels with respect to the Fermi level of the two metal electrodes, and finally, the HOMO-LUMO gap of the adsorbate molecule within the SAM.<sup>36,37</sup> Electrochemical thickness measurements indicate that Ph<sub>2</sub>DTPA SAMs and PhSH SAMs on TS gold present a similar tunneling barrier

thickness within a molecular junction, reducing the likelihood that this is the reason for the lower current densities through Ph<sub>2</sub>DTPA SAMs.

We performed a computational investigation to assess the HOMO-LUMO gap and the relative positions of the HOMO and LUMO energy levels compared to the Fermi level of the two metal electrodes for Ph<sub>2</sub>DTPA and PhSH SAMs on gold. We used individual molecules bound to a single gold atom (bidentate binding for Ph<sub>2</sub>DTPA molecules and monodentate binding for PhSH molecules) as a model system for the SAMs on gold. The structures were optimized using the B3PW91 density functional theory (DFT) method with the basis sets specified in the Experimental section; pertinent information about the structures is presented in Table 8.3. The relative positions of the HOMO and LUMO energy levels of the Ph<sub>2</sub>DTPA and PhSH model systems with respect to the work function (used as an estimate for the Fermi energy levels) of the metal electrodes are shown in Figure 8.5.

**Table 8.3.** Calculated electronic properties of Ph<sub>2</sub>DTPA and PhSH model systems.

	Ph <sub>2</sub> DTPA	PhSH
Optimized Structures		
HOMO		
LUMO		
HOMO (eV)	-5.70	-6.36
LUMO (eV)	-2.91	-3.33
H-L Gap (eV)	2.80	3.03

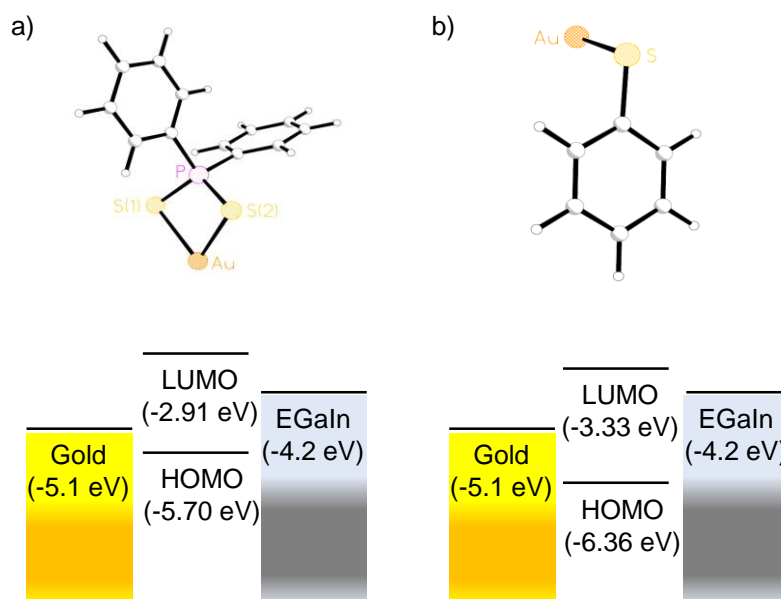


**Figure 8.5.** Illustration of the HOMO and LUMO energy levels of the Ph<sub>2</sub>DTPA (a) and PhSH (b) model systems with respect to the work function of the metal electrodes.

Results of the computational investigation provide important insight into the electronic nature of Ph<sub>2</sub>DTPA and PhSH based molecular junctions. First, the HOMO-LUMO gap of the Ph<sub>2</sub>DTPA (2.80 eV) and PhSH (3.03 eV) model systems are very similar, differing by only 0.23 eV, and are both much lower than previously reported values for *n*-alkanethiolate SAMs on gold (8 – 10 eV). Small HOMO-LUMO energy gaps suggest delocalization within the system and favor activated transport mechanisms over non-resonant, coherent tunneling. Second, the position of the HOMO and LUMO energy levels with respect to the work functions of the metal electrodes are different for the two systems. For the Ph<sub>2</sub>DTPA system, the work functions of the metal electrodes reside more closely to the HOMO (energy gaps of 0.6 eV and 1.5 eV for gold and EGaIn, respectively) than the LUMO (energy gaps of 2.19 eV and 1.29 eV for gold and EGaIn, respectively), suggesting that hole transport is the more likely charge transfer mechanism. For the PhSH system, the work functions of the metal electrodes reside more closely to the LUMO (energy gaps of 1.77 eV and 0.87 eV for gold and EGaIn, respectively) than the HOMO (energy gaps of 1.26 eV and 2.16 eV for gold and EGaIn, respectively), suggesting that electron transport is the more likely charge transfer mechanism. The

barriers to hole transport for the Ph<sub>2</sub>DTPA system are slightly lower than the barriers to electron transport for the PhSH system, suggesting that the probability of charge transport should be greater for Ph<sub>2</sub>DTPA SAMs. This result indicates that the position of the HOMO and LUMO energy levels are not responsible for the observed decrease in current densities through Ph<sub>2</sub>DTPA SAMs compared to PhSH SAMs. It is important to note that these barriers to charge transport are calculated assuming that the work function of the gold electrode is not affected by the formation of the SAM, which is very unlikely. Due to this uncertainty, the effect of the relative energy level positions on the charge transport properties of the SAMs should be considered estimates at best. Finally, the contribution from the aromatic pendant groups to the frontier orbitals of each system are very different. The Ph<sub>2</sub>DTPA model shows almost no contribution from the phenyl groups to the HOMO and LUMO energy levels of the system – indicating that they are decoupled from the gold surface – while the PhSH system shows significant contribution from the phenyl group to both the HOMO and LUMO energy levels of the system – indicating strong coupling to the gold surface. These results are consistent with previous work by Kornilovitch et al that presented a theoretical study of the distance through which an aromatic ring can remain coupled to a metal surface through a thiolate bond; strong coupling is observed when the thiol group is attached directly to the benzene ring (as is the case for PhSH) due to overlap between the lone pair of electrons in the sulfur p orbital and the pi electrons of the phenyl ring.<sup>38</sup> However, introducing a two-carbon methylene spacer between the thiol group and the phenyl ring provides enough separation to prevent this overlap, resulting in a drastic decrease in the observed coupling. We speculate that the phosphorus atom present in the DTPA head group acts as a spacer which decouples the phenyl rings from the gold-thiolate interface.

Taken together, these results indicate that charge transport for the PhSH system occurs via electron transfer from one metal electrode to the other through resonant charge hopping across the LUMO of the molecule. Resonant charge hopping is a much more favorable process than non-resonant tunneling, resulting in high current densities through PhSH SAMs. Charge transport for the Ph<sub>2</sub>DTPA system occurs via hole transfer from one metal electrode to the other through the HOMO of the molecule; however, the phenyl

groups do not contribute to the HOMO, resulting in the formation of a non-resonant tunneling barrier between the DTPA head group and the EGaIn top electrode. The presence of a non-resonant tunneling barrier decreases the likelihood of charge transport, resulting in low current densities through Ph<sub>2</sub>DTPA SAMs. In summary, coupling of the aromatic pendant group to the electrode surface leads to high current densities through PhSH SAMs on gold, while decoupling of the aromatic pendant groups from the electrode surface leads to low current densities through Ph<sub>2</sub>DTPA SAMs on gold.

## 8.4. Conclusions

The work presents the formation and characterization of SAMs on gold formed from Ph<sub>2</sub>DTPA adsorbate molecules. These adsorbate molecules chelate to the underlying gold surface, and contact angle results suggest that the orientation and packing density of the phenyl groups are similar to SAMs formed from a monodentate analogue, PhSH. Despite these similarities, Ph<sub>2</sub>DTPA and PhSH SAMs have very different electrical properties within a molecular junction; current densities through PhSH SAMs are ~3 orders of magnitude higher than those through Ph<sub>2</sub>DTPA SAMs. A computational study suggests that the presence of the phosphorus atom in the DTPA head group decouples the phenyl pendant groups from the substrate surface in Ph<sub>2</sub>DTPA SAMs, resulting in a higher barrier to charge transport compared to PhSH SAMs.

Although this computational study suggests a possible explanation for the much lower current densities through Ph<sub>2</sub>DTPA SAMs on gold compared to PhSH SAMs on gold, several assumptions and simplifications may cause error in the calculated parameters. First, the models used in the calculation are isolated systems and ignore the contribution of neighboring molecules to molecular geometry. Second, a single gold atom is used to represent the gold (111) surface and may not accurately reflect the contribution of the substrate to the electronic and geometric properties of the bound molecule. Third, choosing to represent the Fermi energy levels of the metal electrodes with the corresponding work functions ignores any change in work function caused by formation of the SAM. Finally, it is assumed that charge transport occurs only through the frontier

orbitals (HOMO and LUMO), ignoring potential contribution from other orbitals in the system.

This study could be improved by incorporating the use of ultraviolet photoelectron spectroscopy (UPS)<sup>39</sup> and Kelvin probe microscopy<sup>40</sup> to directly measure the position of the frontier orbital energy levels and the work function of the SAM-coated electrode, respectively. A more in-depth computational study in which the systems are expanded to include multiple adsorbate molecules and multiple gold atoms to represent the gold (111) surface would provide a more accurate representation of the electronic nature of these molecular junctions.<sup>9</sup> Comparing the density of states of the adsorbate molecules to those of the underlying gold substrate would include the contribution of all orbitals to the charge transfer process, rather than strictly the frontier orbitals.<sup>9</sup> We are currently pursuing many of these options to verify the proposed model explaining the electronic properties of Ph<sub>2</sub>DTPA SAMs.

## 8.5. References

- (1) Miller, M. S.; Juan, R. R. S.; Ferrato, M.-A.; Carmichael, T. B. *Langmuir* **2011**, *27*, 10019.
- (2) San Juan, R. R.; Miller, M. S.; Ferrato, M. A.; Carmichael, T. B. *Langmuir* **2012**, *28*, 13253.
- (3) Chiechi, R. C.; Weiss, E. A.; Dickey, M. D.; Whitesides, G. M. *Angew. Chem.* **2008**, *120*, 148.
- (4) Thuo, M. M.; Reus, W. F.; Nijhuis, C. A.; Barber, J. R.; Kim, C.; Schulz, M. D.; Whitesides, G. M. *J. Am. Chem. Soc.* **2011**, *133*, 2962.
- (5) Reus, W. F.; Nijhuis, C. A.; Barber, J. R.; Thuo, M. M.; Tricard, S.; Whitesides, G. M. *J. Phys. Chem. C* **2012**, *116*, 6714.
- (6) Love, C. J. E., Lara A.; Kriebel, J. K. N., Ralph G.; Whitesides, G. M. *Chem. Rev.* **2005**, *105*, 1103.
- (7) Nitzan, A.; Ratner, M. A. *Science* **2003**, *300*, 1384.
- (8) Xue, Y. Q.; Datta, S.; Ratner, M. A. *J. Chem. Phys.* **2001**, *115*, 4292.
- (9) von Wrochem, F.; Gao, D.; Scholz, F.; Nothofer, H.-G.; Nelles, G.; Wessels, J. M. *Nat. Nanotechnol.* **2010**, *5*, 618.
- (10) Xing, Y.; Park, T.-H.; Venkatramani, R.; Keinan, S.; Beratan, D. N.; Therien, M. J.; Borguet, E. *J. Am. Chem. Soc.* **2010**, *132*, 7946.
- (11) Tivanski, A. V.; He, Y. F.; Borguet, E.; Liu, H. Y.; Walker, G. C.; Waldeck, D. H. *J. Phys. Chem. B* **2005**, *109*, 5398.
- (12) Juan, R. R. S.; Carmichael, T. B. *Langmuir* **2012**, *28*, 17701.
- (13) San Juan, R. R.; Allan, C. J.; Iqbal, M.; Eichhorn, S. H.; Macdonald, C. L. B.; Carmichael, T. B. *J. Am. Chem. Soc.* **2013**, *135*, 15784.

- (14) Weiss, E. A.; Kaufman, G. K.; Kriebel, J. K.; Li, Z.; Schalek, R.; Whitesides, G. M. *Langmuir* **2007**, *23*, 9686.
- (15) Moulder, J. F.; Stickle, W. F.; Sobol, P. E.; Bomben, K. D. *Handbook of X-Ray Photoelectron Spectroscopy* Eden Prairie, MN, 1995.
- (16) Frisch, M. J.; Trucks, G. W.; Schlegel, H. B.; Scuseria, G. E.; Robb, M. A.; Cheeseman, J. R.; Scalmani, G.; Barone, V.; Mennucci, B.; Petersson, G. A.; Nakatsuji, H.; Caricato, M.; Li, X.; Hratchian, H. P.; Izmaylov, A. F.; Bloino, J.; Zheng, G.; Sonnenberg, J. L.; Hada, M.; Ehara, M.; Toyota, K.; Fukuda, R.; Hasegawa, J.; Ishida, M.; Nakajima, T.; Honda, Y.; Kitao, O.; Nakai, H.; Vreven, T.; Montgomery, J. A., Jr.; Peralta, J. E.; Ogliaro, F.; Bearpark, M.; Heyd, J. J.; Brothers, E.; Kudin, K. N.; Staroverov, V. N.; Kobayashi, R.; Normand, J.; Raghavachari, K.; Rendell, A.; Burant, J. C.; Iyengar, S. S.; Tomasi, J.; Cossi, M.; Rega, N.; Millam, N. J.; Klene, M.; Knox, J. E.; Cross, J. B.; Bakken, V.; Adamo, C.; Jaramillo, J.; Gomperts, R.; Stratmann, R. E.; Yazyev, O.; Austin, A. J.; Cammi, R.; Pomelli, C.; Ochterski, J. W.; Martin, R. L.; Morokuma, K.; Zakrzewski, V. G.; Voth, G. A.; Salvador, P.; Dannenberg, J. J.; Dapprich, S.; Daniels, A. D.; Farkas, Ö.; Foresman, J. B.; Ortiz, J. V.; Cioslowski, J.; Fox, D. J. *Gaussian 09*, C.1, Gaussian, Inc.: Wallingford, CT, 2009
- (17) Dolg, M.; Wedig, U.; Stoll, H.; Preuss, H. *J. Chem. Phys.* **1987**, *86*, 866.
- (18) Schwerdtfeger, P.; Dolg, M.; Schwartz, W. H. E.; Bowmaker, G. A.; Boyd, P. D. *W. J. Chem. Phys.* **1989**, *91*, 1762.
- (19) Reed, A. E.; Curtiss, L. A.; Weinhold, F. *Chem. Rev.* **1988**, *88*, 899.
- (20) Schaftenaar, G.; Noordik, J. H. *J. Comput.-Aided Mol. Des.* **2000**, *14*, 123.
- (21) Cason, C.; Froehlich, T.; Kopp, N.; Parker, R. Persistence of Vision Raytracer (POV-Ray) for Windows, 3.6; Persistence of Vision Raytracer Pty .Ltd.: Victoria, Australia, 2009

- (22) Ishida, T.; Choi, N.; Mizutani, W.; Tokumoto, H.; Kojima, I.; Azehara, H.; Hokari, H.; Akiba, U.; Fujihira, M. *Langmuir* **1999**, *15*, 6799.
- (23) Castner, D. G.; Hinds, K.; Grainger, D. W. *Langmuir* **1996**, *12*, 5083.
- (24) Ulman, A. *Ultrathin Organic Films*; Academic Press: San Diego, 1991.
- (25) Allara, D. L.; Nuzzo, R. G. *Langmuir* **1985**, *1*, 45.
- (26) Bain, C. D.; Troughton, E. B.; Tao, Y. T.; Evall, J.; Whitesides, G. M.; Nuzzo, R. G. *J. Am. Chem. Soc.* **1989**, *111*, 321.
- (27) Sabatani, E.; Cohen-Boulakia, J.; Bruening, M.; Rubinstein, I. *Langmuir* **1993**, *9*, 2974.
- (28) Barriet, D.; Yam, C. M.; Shmakova, O. E.; Jamison, A. C.; Lee, T. R. *Langmuir* **2007**, *23*, 8866.
- (29) Lee, S.; Puck, A.; Graupe, M.; Colorado, R.; Shon, Y.-S.; Lee, T. R.; Perry, S. S. *Langmuir* **2001**, *17*, 7364.
- (30) Gupta, P.; Ulman, A.; Fanfan, S.; Korniaikov, A.; Loos, K. *J. Am. Chem. Soc.* **2005**, *127*, 4.
- (31) Barsoukov, E.; Macdonald, J. R. *Impedance Spectroscopy*; 2nd ed.; Wiley and Sons: Hoboken, NJ, 2005.
- (32) Porter, M. D.; Bright, T. B.; Allara, D. L.; Chidsey, C. E. D. *J. Am. Chem. Soc.* **1987**, *109*, 3559.
- (33) Peterlinz, K. A.; Georgiadis, R. *Langmuir* **1996**, *12*, 4731.
- (34) Ganesh, V.; Pandey, R. R.; Malhotra, B. D.; Lakshminarayanan, V. *J. Electroanal. Chem.* **2008**, *619–620*, 87.
- (35) Simmons, J. G. *Conduction in Thin Films*; Mills and Boon Ltd.: London, 1971.
- (36) McCreery, R. L. *Chem. Mat.* **2004**, *16*, 4477.

- (37) McCreery, R. L.; Yan, H. J.; Bergren, A. J. *Phys. Chem. Chem. Phys.* **2013**, *15*, 1065.
- (38) Kornilovitch, P. E.; Bratkovsky, A. M.; Stanley Williams, R. *Physical Review B* **2002**, *66*, 165436.
- (39) Duwez, A. S.; Ghijsen, J.; Riga, J.; Deleuze, M.; Delhalle, J. *J. Phys. Chem. B* **1997**, *101*, 884.
- (40) Nonnenmacher, M.; O'Boyle, M. P.; Wickramasinghe, H. K. *Appl. Phys. Lett.* **1991**, *58*, 2921.

## 8.6. Supporting Information

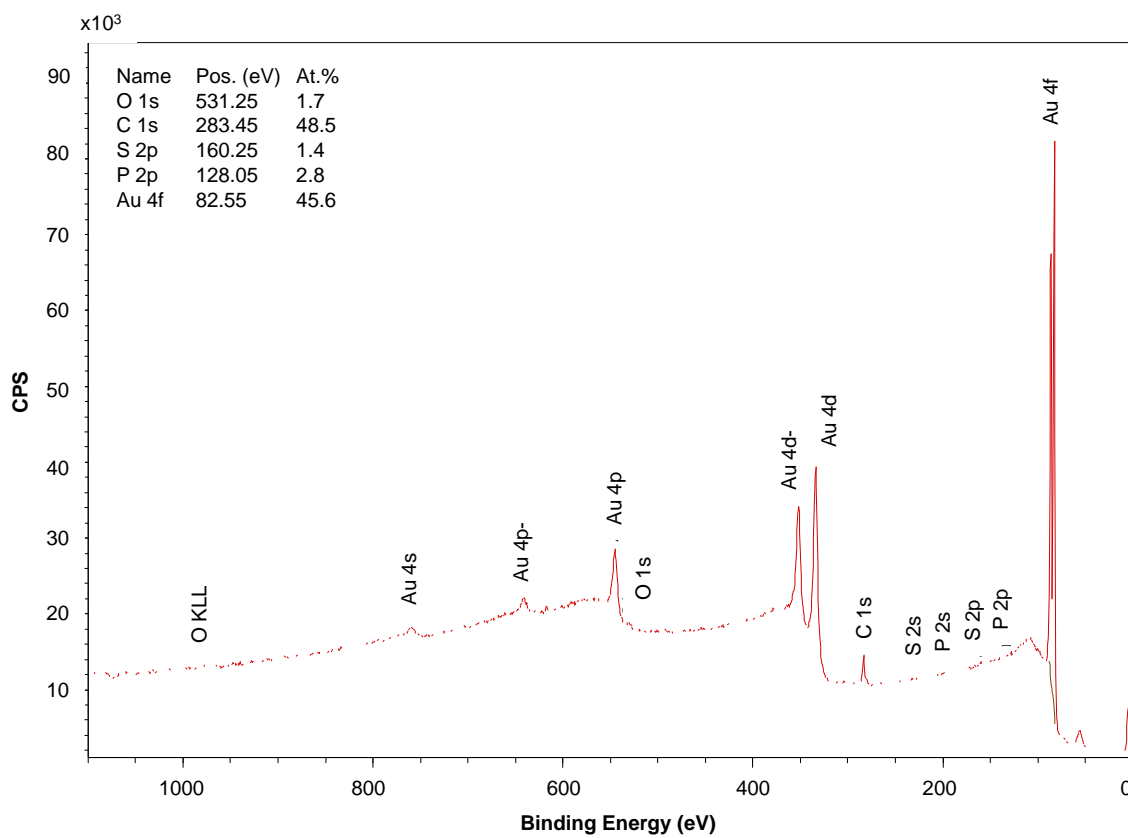


**Figure S8.1.** XPS survey scan of a Ph<sub>2</sub>DTPA SAM formed on TS gold.

## **Chapter 9**

# **Conclusions and Outlook**

## 9.1. Conclusions

The research described throughout this dissertation spans across several fields of study, with one unifying theme: Many materials science problems can be solved by the careful manipulation of surfaces and interfaces. Though many of the challenges addressed in this dissertation may be seemingly unrelated, solving these problems was always done by asking the same questions: What is the nature of the surface, and how can it be manipulated to provide a solution? With this logic in mind, any new or exciting materials science challenge that arose was accepted, regardless of whether or not it fit into a pre-existing framework. Outlined below for each chapter is a summary of the challenges that emerged over the course of this research, and the solutions that make up this dissertation.

The notion of low-cost, polymer and organic based electronic devices is exciting for a variety of reasons. These devices can be made to be light-weight, portable, and more compatible with the human body; polymers and organic materials can be made flexible or stretchable, providing a much more intimate form factor. Another advantage of these types of devices is that they are comprised of materials that are far less expensive than their inorganic counterparts. Despite the availability of low-cost materials, many researchers continue to integrate high-cost deposition and patterning techniques into device fabrication. Realizing practical, low-cost polymer based electronics requires finding alternatives to these techniques that are both economical, and compatible with the flexible and stretchable nature of polymer substrates. Our research group has been interested in developing low-cost device fabrication alternatives for the past five years. In 2008, we published a manuscript detailing a procedure for the selective electroless metallization of the most commonly used elastomer, polydimethylsiloxane (PDMS).<sup>1</sup> This work specifically focused on modifying the surface chemistry of PDMS to enable metallization and patterning of copper on the polymer substrate. Our metallization scheme was very successful in generating stretchable metal circuitry onto PDMS substrates, however we soon began brainstorming a more general scheme that could be applied to all of the polymer substrates that are commonly used for electronic devices. Although each of these polymers has a different chemical structure, simple surface oxidation provided a common platform upon which we could work. This common surface

chemistry provided a route for selective electroless metallization through the binding of an aluminum (III) porphyrin complex. Patterning this complex onto the polymer surface using microcontact printing activated those areas for selective metal deposition, leading to highly resilient copper circuitry that can be deposited onto numerous polymer substrates. This process is fast, low-cost, and compatible with roll-to-roll processing, all of which are appealing characteristics for flexible electronic device fabrication. This work was presented in Chapter 2.

Optoelectronic devices, such as displays and solar cells, are also being made using organic materials and polymeric substrates. As we began navigating this vast field of research, it quickly became apparent that biggest hurdle to realizing flexible or stretchable optoelectronic devices may be the requirement of a transparent conductive electrode (TCE) that can withstand large degrees of tensile and compressive strain. Despite the development of active components that can tolerate strain, most flexible electronic devices continued to use tin-doped indium oxide (ITO) as the TCE. ITO is brittle by its very nature, and fails under even moderate ( $\sim 2\%$ ) tensile strain,<sup>2,3</sup> making it incompatible with flexible electronic devices. We quickly recognized the need for a drop-in replacement for ITO that has the following characteristics: low sheet resistance, high transparency, low surface roughness, high durability, high resilience to strain, and a method for applying such a coating to various polymer substrates. In Chapter 3, we combine all of the advantageous characteristics of silver nanowire films (highly conductive and transparent) with template-stripping – a technique we commonly use to fabricate ultra smooth metal surfaces – to produce TCEs that fulfill all of the aforementioned needs. The silver nanowire network is highly conductive and transparent, while the template-stripping method produced films that are embedded into a polymer surface; embedding the network makes these films smooth, durable, and resilient to strain. These high performance silver nanowire TCEs are simple to fabricate and can be applied to various polymer substrates, making them an attractive test structure for many researchers in the field of flexible electronics. In this work, we have highlighted the functionality of the silver nanowire films as anodes within flexible light-emitting electrochemical cells.

From its onset, our research group was particularly interested in the process of self-assembly. As was detailed in the introduction to this dissertation, the process of self-assembly finds roots in all areas of science and nature;<sup>4</sup> understanding such a process provides a great toolset for solving a myriad of different problems. Of specific interest to us was the application of self-assembly to the fabrication of microelectronic devices; the Moore's law predictions – which have emerged as a driving factor for much of the work presented in this dissertation – requires the fabrication of very small electronic components, which may not be compatible with traditional serial assembly methods.<sup>5,6</sup> We were troubled by the fact that most of the self-assembly methods developed to solve these problems involved immersing the entire system in solvent, usually water; electronics are not compatible with water by their very nature. We approached this problem by taking a well-understood assembly method – templated assembly – and modified the surface properties of the template to create a system that operated under dry conditions. This work, presented in Chapter 4, not only eliminated the need for solvent, but also opened the door to multi-component assembly and fine control over the geometry and spacing of the assembled structures.

Another area of significant interest within our research group is the study of new self-assembled monolayers (SAMs) with application in materials science. My colleague, Dr. Ronan San Juan, has undertaken an impressive and comprehensive study of a new class of adsorbate molecules which bear a dithiophosphinic acid (DTPA) head group.<sup>7,8</sup> This molecule was of particular interest to us because of the potential for the head group to chelate to a gold surface; chelation not only opens the door to loosely-packed SAMs, but the resonance generated between the sulfur atoms also makes this molecule a candidate for use in molecular electronic devices. After preliminary analysis, we were surprised to find that dialkyl-DTPA molecules did not always chelate; 40% of adsorbate molecules in the SAM were bound to the surface in a monodentate fashion. Exhaustive investigation led us to the hypothesis that the disruption of chelation was a result of the roughness and morphology of the underlying As-Deposited (As-Dep) gold substrate; atomic step-edges associated with the grain boundaries typical of polycrystalline gold films could prevent both sulfur atoms from binding to the surface. Chapter 5 details this investigation, with particular focus on the role of substrate morphology in controlling the binding of

dihexadecyl-DTPA molecules, and the subsequent impact on the SAM structure. In summary, we were able to enforce chelation by modifying the morphology of the gold substrate; eliminating step-edge defects by using ultra smooth template-stripped gold films for SAM formation resulted in 100% bidentate binding of the DTPA molecules. Changing the way in which the DTPA head group binds to the gold surface also had significant impact on the structure of the SAM. On As-Dep gold, the freedom of the monodentate adsorbates permits extensive van der Waals interactions between neighbouring chains, resulting in a highly ordered alkyl layer. On template-stripped gold however, the restriction on the DTPA head group enforced by chelation prevents van der Waals interactions between chains, leading to an alkyl layer that is disordered and liquid-like. Our interest in this class of molecules grew upon the realization that it is the only known class of SAM in which the binding of the head group can be controlled by manipulating the morphology of the underlying substrate.

In Chapter 6, we continued our investigation into the influence of chelation on the binding and structure of dialkyl-DTPA SAMs. After confirming that substrate morphology was the primary influence on the ability of dihexadecyl-DTPA molecules to chelate to the gold surface, we set out to determine if this head group binding phenomenon was consistent across DTPA adsorbates with different alkyl chain lengths. We formed and characterized dialkyl-DTPA SAMs with different alkyl chain lengths (hexyl, decyl, dodecyl, tetradecyl, hexadecyl) on template-stripped gold and determined that these adsorbate molecules chelate to the gold surface independently of steric effects. More interestingly, we were surprised to find that the relationship between SAM structure and alkyl chain length for these molecules is quite unusual compared to well known *n*-alkanethiolate SAMs, and dialkyl-DTPA SAMs on As-Dep gold; SAMs formed from short chain DTPA adsorbates have a high molecular packing density and crystalline organic layer, while SAMs formed from long chain adsorbates have a low molecular packing density and liquid-like organic layer. The work presented in Chapter 5 and Chapter 6 reveals that four primary factors determine the structure of dialkyl-DTPA SAMs formed on TS gold: (i) adsorbate-substrate interactions; (ii) gold substrate morphology; (iii) lateral van der Waals interactions between alkyl groups; and (iv) steric demands of the alkyl groups; the first two factors are independent of the length of the

alkyl chain. Importantly, this work highlights the fact that the simple model used to describe the structure of *n*-alkanethiolate SAMs – which considers only the adsorbate-substrate interaction and intermolecular van der Waals interaction – does not apply to systems which bear more complex adsorbate molecules. There is currently a shift in focus amongst researchers in this field away from simple *n*-alkanethiolates towards more complex systems with exciting applications and possibilities; our work is a reminder that these systems will require a deep understanding of the factors influencing self-organization before new design rules can be developed and implemented.

The work presented in Chapter 7 began with a simple objective: to fabricate ultra smooth gold substrates using chemical mechanical polishing (CMP) – a well known semiconductor fabrication method. Although developing a process capable of achieving this goal took a significant amount of time and effort, the number of applications for these substrates grew alongside the evolution of our research. Our interest in SAM-based molecular electronics was the key motivating factor for developing new, ultra smooth gold substrates. Gold substrate morphology plays a key role in any SAM-based molecular junction; rough surfaces cause misalignment between neighbouring molecules that can lead to a high degree of variability in the measured charge transport properties.<sup>9,10</sup> Not surprisingly, the nature of molecular electronic devices make them very sensitive to environmental conditions, which is why we were surprised to learn that the substrates most commonly used to form molecular junctions contain contaminants that could potentially interfere with SAM formation. Template-stripped metal films – the same ultra smooth substrates used in our study of DTPA molecules – are fabricated using photocurable adhesives that contain thiol precursors; any unreacted thiol in the adhesive can act as a competitive adsorbate during SAM formation. Furthermore, these adhesives are often incompatible with common laboratory solvents, severely limiting the versatility of template-stripped films in studying new classes of molecules. After learning of these limitations, we began realizing that CMP could be used to fabricate ultra smooth gold substrates that have all the beneficial characteristics of template-stripped films, while eliminating all of the drawbacks. We fabricated polished gold films that are i) ultra smooth, with an average root mean squared (RMS) surface roughness value of 3.8 Å, ii) uniform, having within-wafer and wafer-to-wafer non-uniformities < 17%, and iii) free

from adhesive. We showcased these substrates by forming and measuring a series of *n*-alkanethiolate SAM-based molecular junctions on polished gold surfaces. The charge transport properties of these systems were indistinguishable from those formed on template-stripped gold, however eliminating the adhesive significantly increased junction yields. By removing the limitations imposed by using template-stripped substrates, this work opens the door to the study of new SAM-based molecular electronic systems. This work has provided the materials science community with a new type of ultra smooth gold substrate; the number of potential applications for these substrates will continue to grow as more light is shed on the importance of substrate morphology in all areas of nanoscience.

The work presented in Chapter 8 provides a first look into the charge transport properties of SAMs formed from DTPA adsorbate molecules. Throughout our research on dialkyl-DTPA SAMs, we have suggested that chelation of the DTPA head group to the underlying gold substrate should present a resonant, low-barrier pathway for charge transport within SAM-based molecular junctions. We tested this hypothesis by forming and characterizing new SAMs formed from diphenyl-DTPA ( $\text{Ph}_2\text{DTPA}$ ) adsorbate molecules and measuring the charge transport properties within metal-SAM// $\text{Ga}_2\text{O}_3$ /EGaIn molecular tunnel junctions. To our surprise, current densities through  $\text{Ph}_2\text{DTPA}$  SAMs on template-stripped gold were three orders of magnitude lower than SAMs formed from monodentate adsorbate analogue thiophenol ( $\text{PhSH}$ ). A computational study revealed the origins of the unexpected discrepancy in charge transport properties between these two systems: the phosphorus atom, present in the DTPA head group and not the analogous thiol, decouples the phenyl pendant groups from the underlying gold for  $\text{Ph}_2\text{DTPA}$  SAMs, presenting a resistive, non-resonant tunneling barrier. Although we believe that more in-depth calculations and experimentation will be required to confirm our hypothesis, this work again cautions against applying structural and electronic design rules across systems with different classes of adsorbate molecules.

## 9.2. Outlook

As is often the case, much of the work described throughout this dissertation has raised as many questions as it has answered. Many of these projects have now evolved beyond their initial objectives into new and exciting areas of research, a few of which are briefly outlined below:

### *9.2.1. Stretchable Electronics*

Much of the work described in Chapters 2 and 3 of this dissertation focused on developing low-cost methods for fabricating metal circuitry and transparent conductive electrodes for flexible electronic devices. A question that remains unanswered is whether or not the processes we used to develop flexible electronic components can also produce stretchable electronic components. Stretchable electronics is currently one of the most popular fields of study in materials science, with many researchers racing to fabricate displays, solar cells, and sensors that can conform to the contours of the human body. A current focus in our research group is applying the knowledge and insight gained during our previous studies on flexible substrates to our new work on stretchable substrates. Although this often involves incorporating new materials into the stretchable components, many of the same ideas and processes still apply.

### *9.2.2. Molecular Junctions Formed from DTPA SAMs*

The work presented in this dissertation has comprehensively detailed the factors that influence the structure and self-organization of dialkyl-DTPA SAMs on template-stripped gold. The focus of this work is now shifting away from structural characterization, and towards electronic characterization of these SAMs. Although Chapter 9 provided initial insight into the electronic properties of the DTPA head group, we have now begun a more exhaustive study detailing the charge transport properties of DTPA SAMs formed from adsorbates with a variety of different pendant groups including symmetrical alkyl chains, unsymmetrical alkyl chains, and unsymmetrical alkyl/aromatic groups. We plan to use a new toolset – including in-depth computational studies, Kelvin probe microscopy, and ultraviolet photoelectron spectroscopy – to further our understanding of these complex

electronic systems. We believe these studies will contribute to the growing body of fundamental research in the field of SAM-based molecular electronics.

### *9.2.3. New Applications of CMP*

CMP has proven to be an invaluable tool for fabricating adhesive-free, ultra smooth gold substrates. We intend to explore other non-obvious materials science applications of CMP including: 1) The fabrication of continuous, ultra thin metal films for use as transparent conductive electrodes. Thin metal films have previously been studied as TCEs, however they suffer from poor transparency due to limitations imposed by physical vapour deposition.<sup>11</sup> During the evaporation process, coalescence of the individual grains to form a continuous, conductive film doesn't occur until a substantial amount of material has been deposited, reducing the transparency. We intend to use CMP to polish these thick, continuous films down a level at which they become highly transparent, yet remain highly conductive. 2) Creating ultra smooth metal films that bear an overlayer with a different elemental chemistry; changing the elemental composition at the outermost layer of the surface opens the door to new surface modification chemistry, while maintaining all of the bulk properties of underlying metal film. In practice, this would permit the formation of SAMs formed from new types of adsorbate molecules (non thiol-based) onto coinage metal substrates, with potential implications in molecular electronics.

### 9.3. References

- (1) Miller, M. S.; Davidson, G. J. E.; Sahli, B. J.; Mailloux, C. M.; Carmichael, T. B. *Adv. Mater.* **2008**, *20*, 59.
- (2) Lewis, J. *Mater. Today* **2006**, *9*, 38.
- (3) Yu, Z. B.; Zhang, Q. W.; Li, L.; Chen, Q.; Niu, X. F.; Liu, J.; Pei, Q. B. *Adv. Mater.* **2011**, *23*, 664.
- (4) Whitesides, G. M. *Sci. Am.* **1995**, *273*, 146.
- (5) Moore, G. E. In *Electronics Magazine* 1965; Vol. 38.
- (6) Cohn, M. B.; Bohringer, K. F.; Noworolski, J. M.; Singh, A.; Keller, C. G.; Goldberg, K. Y.; Howe, R. T. In *Materials and Device Characterization in Micromachining*; Friedrich, C. R., Vladimirsky, Y., Eds.; Spie-Int Soc Optical Engineering: Bellingham, 1998; Vol. 3512, p 2.
- (7) San Juan, R. R.; Miller, M. S.; Ferrato, M. A.; Carmichael, T. B. *Langmuir* **2012**, *28*, 13253.
- (8) Juan, R. R. S.; Carmichael, T. B. *Langmuir* **2012**, *28*, 17701.
- (9) Engelkes, V. B.; Beebe, J. M.; Frisbie, C. D. *J. Phys. Chem. B* **2005**, *109*, 16801.
- (10) Weiss, E. A.; Chiechi, R. C.; Kaufman, G. K.; Kriebel, J. K.; Li, Z. F.; Duati, M.; Rampi, M. A.; Whitesides, G. M. *J. Am. Chem. Soc.* **2007**, *129*, 4336.
- (11) Stec, H. M.; Williams, R. J.; Jones, T. S.; Hatton, R. A. *Adv. Funct. Mater.* **2011**, *21*, 1709.

## **Appendices**

## **Copyright Permissions**

I hereby declare that I have contacted, and received permission from IOP publishing to include the following copyright protected material in this dissertation, as outlined in the following correspondence:

From: Michael S. Miller (mille2h@uwindsor.ca)

Hello.

I respectfully ask permission to include the following figures/tables in my dissertation entitled:

"New Materials, Methods, and Molecules for Microelectronic and Molecular Electronic Devices"

This dissertation is being completed in partial fulfillment of the degree of Doctor of Philosophy (Chemistry and Biochemistry) at the University of Windsor in Windsor, Ontario, Canada.

#1.

Title: Control of molecule-based transport for future molecular electronic devices

Author: Karthaus, Silvia

Citation: 2011 J. Phys.: Condens. Matter 23 013001

I ask for permission to include Table 2 in my dissertation

#2

Title: Transferable self-welding nanowire network as high performance transparent flexible electrode

Author: Zhu, Siwei; Gao, Yuan; Hu, Bin; Li, Jia; Su, Jun; Fan, Zhiyong; Zhou, Jun.

Citation: 2013 Nanotechnology 24 335202

I ask for permission to include Figure 1 and Figure 4 in my dissertation

I would like to include these figures/tables as part of my introductory chapter to provide examples of exceptional work being done in the field.

This is strictly for academic, non-profit use.

I appreciate your consideration,  
Michael S. Miller  
University of Windsor

Response:

“Dear Michael Miller,

Thank you for your request to reproduce IOP Publishing material.

We are happy to grant permission for the use you request on the terms set out below.

If you have any questions, please feel free to contact our Permissions team at [permissions@iop.org](mailto:permissions@iop.org).

I should be grateful if you would acknowledge receipt of this email.

Kind regards,

Sarah Ryder

Publishing Administrator

Email: [permissions@iop.org](mailto:permissions@iop.org)

Conditions

Non-exclusive, non-transferrable, revocable, worldwide, permission to use the material in print and electronic form will be granted subject to the following conditions:

- Permission will be cancelled without notice if you fail to fulfil any of the conditions of this letter.
- You will make reasonable efforts to contact the author(s) to seek consent for your intended use. Contacting one author acting expressly as authorised agent for their co-authors is acceptable.
- You will reproduce the following prominently alongside the material:
  - o the source of the material, including author, article title, title of journal, volume number, issue number (if relevant), page range (or first page if this is the only information available) and date of first publication
  - o for material being published electronically, a link back to the article (via DOI)
  - o if practical and IN ALL CASES for works published under any of the Creative Commons licences the words “© IOP Publishing. Reproduced by permission of IOP Publishing. All rights reserved”
- The material will not, without the express permission of the author(s), be used in any way which, in the opinion of IOP Publishing, could distort or alter the author(s)’ original intention(s) and meaning, be prejudicial to the honour or reputation of the author(s) and/or imply endorsement by the author(s) and/or IOP Publishing.
- Payment of £0 is received in full by IOP Publishing prior to use.

Please note: IOP does not usually provide signed permission forms as a separate attachment. Please print this email and provide it to your publisher as proof of permission.

**RightsLink**®[Home](#)[Account Info](#)[Help](#)**ACS Publications**  
High quality. High impact.**Title:** Molecular Electronic Junctions**Author:** Richard L. McCreery\***Publication:** Chemistry of Materials**Publisher:** American Chemical Society**Date:** Nov 1, 2004

Copyright © 2004, American Chemical Society

Logged in as:

Michael Miller

[LOGOUT](#)**PERMISSION/LICENSE IS GRANTED FOR YOUR ORDER AT NO CHARGE**

This type of permission/license, instead of the standard Terms & Conditions, is sent to you because no fee is being charged for your order. Please note the following:

- Permission is granted for your request in both print and electronic formats, and translations.
- If figures and/or tables were requested, they may be adapted or used in part.
- Please print this page for your records and send a copy of it to your publisher/graduate school.
- Appropriate credit for the requested material should be given as follows: "Reprinted (adapted) with permission from (COMPLETE REFERENCE CITATION). Copyright (YEAR) American Chemical Society." Insert appropriate information in place of the capitalized words.
- One-time permission is granted only for the use specified in your request. No additional uses are granted (such as derivative works or other editions). For any other uses, please submit a new request.

If credit is given to another source for the material you requested, permission must be obtained from that source.

[BACK](#)[CLOSE WINDOW](#)

Copyright © 2013 [Copyright Clearance Center, Inc.](#) All Rights Reserved. [Privacy statement.](#)  
Comments? We would like to hear from you. E-mail us at [customer@copyright.com](mailto:customer@copyright.com)



RightsLink®

[Home](#)[Account Info](#)[Help](#)ACS Publications  
High quality. High impact.**Title:** Self-Assembly of 10- $\mu$ m-Sized Objects into Ordered Three-Dimensional ArraysLogged in as:  
Michael Miller**Author:** Thomas D. Clark et al.[LOGOUT](#)**Publication:** Journal of the American Chemical Society**Publisher:** American Chemical Society**Date:** Aug 1, 2001

Copyright © 2001, American Chemical Society

**PERMISSION/LICENSE IS GRANTED FOR YOUR ORDER AT NO CHARGE**

This type of permission/license, instead of the standard Terms & Conditions, is sent to you because no fee is being charged for your order. Please note the following:

- Permission is granted for your request in both print and electronic formats, and translations.
- If figures and/or tables were requested, they may be adapted or used in part.
- Please print this page for your records and send a copy of it to your publisher/graduate school.
- Appropriate credit for the requested material should be given as follows: "Reprinted (adapted) with permission from (COMPLETE REFERENCE CITATION). Copyright (YEAR) American Chemical Society." Insert appropriate information in place of the capitalized words.
- One-time permission is granted only for the use specified in your request. No additional uses are granted (such as derivative works or other editions). For any other uses, please submit a new request.

If credit is given to another source for the material you requested, permission must be obtained from that source.

[BACK](#)[CLOSE WINDOW](#)

Copyright © 2013 [Copyright Clearance Center, Inc.](#) All Rights Reserved. [Privacy statement.](#)  
Comments? We would like to hear from you. E-mail us at [customercare@copyright.com](mailto:customercare@copyright.com)

**RightsLink**®[Home](#)[Account Info](#)[Help](#)**ACS Publications**  
High quality. High impact.**Title:** Mesoscopic, Templated Self-Assembly at the Fluid–Fluid InterfaceLogged in as:  
Michael Miller**Author:** Insung S. Choi et al.[LOGOUT](#)**Publication:** Langmuir**Publisher:** American Chemical Society**Date:** Apr 1, 2000

Copyright © 2000, American Chemical Society

**PERMISSION/LICENSE IS GRANTED FOR YOUR ORDER AT NO CHARGE**

This type of permission/license, instead of the standard Terms & Conditions, is sent to you because no fee is being charged for your order. Please note the following:

- Permission is granted for your request in both print and electronic formats, and translations.
- If figures and/or tables were requested, they may be adapted or used in part.
- Please print this page for your records and send a copy of it to your publisher/graduate school.
- Appropriate credit for the requested material should be given as follows: "Reprinted (adapted) with permission from (COMPLETE REFERENCE CITATION). Copyright (YEAR) American Chemical Society." Insert appropriate information in place of the capitalized words.
- One-time permission is granted only for the use specified in your request. No additional uses are granted (such as derivative works or other editions). For any other uses, please submit a new request.

If credit is given to another source for the material you requested, permission must be obtained from that source.

[BACK](#)[CLOSE WINDOW](#)

Copyright © 2013 [Copyright Clearance Center, Inc.](#) All Rights Reserved. [Privacy statement.](#)  
Comments? We would like to hear from you. E-mail us at [customercare@copyright.com](mailto:customercare@copyright.com)

**RightsLink®**[Home](#)[Account Info](#)[Help](#)**ACS Publications**  
High quality. High impact.**Title:** Three-Dimensional Mesoscale Self-Assembly**Author:** Wilhelm T. S. Huck, Joe Tien, and, and George M. Whitesides\***Publication:** Journal of the American Chemical Society**Publisher:** American Chemical Society**Date:** Aug 1, 1998

Copyright © 1998, American Chemical Society

Logged in as:  
Michael Miller[LOGOUT](#)**PERMISSION/LICENSE IS GRANTED FOR YOUR ORDER AT NO CHARGE**

This type of permission/license, instead of the standard Terms & Conditions, is sent to you because no fee is being charged for your order. Please note the following:

- Permission is granted for your request in both print and electronic formats, and translations.
- If figures and/or tables were requested, they may be adapted or used in part.
- Please print this page for your records and send a copy of it to your publisher/graduate school.
- Appropriate credit for the requested material should be given as follows: "Reprinted (adapted) with permission from (COMPLETE REFERENCE CITATION). Copyright (YEAR) American Chemical Society." Insert appropriate information in place of the capitalized words.
- One-time permission is granted only for the use specified in your request. No additional uses are granted (such as derivative works or other editions). For any other uses, please submit a new request.

If credit is given to another source for the material you requested, permission must be obtained from that source.

[BACK](#)[CLOSE WINDOW](#)

Copyright © 2013 [Copyright Clearance Center, Inc.](#) All Rights Reserved. [Privacy statement.](#)  
Comments? We would like to hear from you. E-mail us at [customer@copyright.com](mailto:customer@copyright.com)



RightsLink®

[Home](#)[Account Info](#)[Help](#)ACS Publications  
High quality. High impact.**Title:** Design of Three-Dimensional,  
Millimeter-Scale Models for  
Molecular FoldingLogged in as:  
Michael Miller**Author:** Thomas D. Clark et al.[LOGOUT](#)**Publication:** Journal of the American  
Chemical Society**Publisher:** American Chemical Society**Date:** Jan 1, 2002

Copyright © 2002, American Chemical Society

**PERMISSION/LICENSE IS GRANTED FOR YOUR ORDER AT NO CHARGE**

This type of permission/license, instead of the standard Terms & Conditions, is sent to you because no fee is being charged for your order. Please note the following:

- Permission is granted for your request in both print and electronic formats, and translations.
- If figures and/or tables were requested, they may be adapted or used in part.
- Please print this page for your records and send a copy of it to your publisher/graduate school.
- Appropriate credit for the requested material should be given as follows: "Reprinted (adapted) with permission from (COMPLETE REFERENCE CITATION). Copyright (YEAR) American Chemical Society." Insert appropriate information in place of the capitalized words.
- One-time permission is granted only for the use specified in your request. No additional uses are granted (such as derivative works or other editions). For any other uses, please submit a new request.

If credit is given to another source for the material you requested, permission must be obtained from that source.

[BACK](#)[CLOSE WINDOW](#)

Copyright © 2013 [Copyright Clearance Center, Inc.](#) All Rights Reserved. [Privacy statement.](#)  
Comments? We would like to hear from you. E-mail us at [customercare@copyright.com](mailto:customercare@copyright.com)



RightsLink®

[Home](#)[Account Info](#)[Help](#)ACS Publications  
High quality. High impact.

**Title:** Templated Self-Assembly of Glass Microspheres into Ordered Two-Dimensional Arrays under Dry Conditions

**Author:** Michael S. Miller, Gregory J. E. Davidson, and Tricia Breen Carmichael

Logged in as:  
Michael Miller

[LOGOUT](#)

**Publication:** Langmuir  
**Publisher:** American Chemical Society  
**Date:** Apr 1, 2010  
Copyright © 2010, American Chemical Society

**PERMISSION/LICENSE IS GRANTED FOR YOUR ORDER AT NO CHARGE**

This type of permission/license, instead of the standard Terms & Conditions, is sent to you because no fee is being charged for your order. Please note the following:

- Permission is granted for your request in both print and electronic formats, and translations.
- If figures and/or tables were requested, they may be adapted or used in part.
- Please print this page for your records and send a copy of it to your publisher/graduate school.
- Appropriate credit for the requested material should be given as follows: "Reprinted (adapted) with permission from (COMPLETE REFERENCE CITATION). Copyright (YEAR) American Chemical Society." Insert appropriate information in place of the capitalized words.
- One-time permission is granted only for the use specified in your request. No additional uses are granted (such as derivative works or other editions). For any other uses, please submit a new request.

[BACK](#)[CLOSE WINDOW](#)

Copyright © 2013 [Copyright Clearance Center, Inc.](#) All Rights Reserved. [Privacy statement.](#)  
Comments? We would like to hear from you. E-mail us at [customer care@copyright.com](mailto:customer care@copyright.com)

**RightsLink®**[Home](#)[Account Info](#)[Help](#)**ACS Publications**  
High quality. High impact.**Title:** Selectively Metallized Polymeric Substrates by Microcontact Printing an Aluminum(III) Porphyrin ComplexLogged in as:  
Michael Miller[LOGOUT](#)**Author:** Michael S. Miller, Heather L. Filiatrault, Gregory J. E. Davidson, Minmin Luo, and Tricia Breen Carmichael**Publication:** Journal of the American Chemical Society**Publisher:** American Chemical Society**Date:** Jan 1, 2010

Copyright © 2010, American Chemical Society

**PERMISSION/LICENSE IS GRANTED FOR YOUR ORDER AT NO CHARGE**

This type of permission/license, instead of the standard Terms & Conditions, is sent to you because no fee is being charged for your order. Please note the following:

- Permission is granted for your request in both print and electronic formats, and translations.
- If figures and/or tables were requested, they may be adapted or used in part.
- Please print this page for your records and send a copy of it to your publisher/graduate school.
- Appropriate credit for the requested material should be given as follows: "Reprinted (adapted) with permission from (COMPLETE REFERENCE CITATION). Copyright (YEAR) American Chemical Society." Insert appropriate information in place of the capitalized words.
- One-time permission is granted only for the use specified in your request. No additional uses are granted (such as derivative works or other editions). For any other uses, please submit a new request.

[BACK](#)[CLOSE WINDOW](#)

Copyright © 2013 [Copyright Clearance Center, Inc.](#) All Rights Reserved. [Privacy statement.](#) Comments? We would like to hear from you. E-mail us at [customerca@copyright.com](mailto:customerca@copyright.com)



RightsLink®

[Home](#)[Account Info](#)[Help](#)ACS Publications  
High quality. High impact.**Title:** New Dialkyldithiophosphinic Acid Self-Assembled Monolayers (SAMs): Influence of Gold Substrate Morphology on Adsorbate Binding and SAM StructureLogged in as:  
Michael Miller[LOGOUT](#)**Author:** Michael S. Miller, Ronan R. San Juan, Michael-Anthony Ferrato, and Tricia Breen Carmichael**Publication:** Langmuir**Publisher:** American Chemical Society**Date:** Aug 1, 2011

Copyright © 2011, American Chemical Society

**PERMISSION/LICENSE IS GRANTED FOR YOUR ORDER AT NO CHARGE**

This type of permission/license, instead of the standard Terms & Conditions, is sent to you because no fee is being charged for your order. Please note the following:

- Permission is granted for your request in both print and electronic formats, and translations.
- If figures and/or tables were requested, they may be adapted or used in part.
- Please print this page for your records and send a copy of it to your publisher/graduate school.
- Appropriate credit for the requested material should be given as follows: "Reprinted (adapted) with permission from (COMPLETE REFERENCE CITATION). Copyright (YEAR) American Chemical Society." Insert appropriate information in place of the capitalized words.
- One-time permission is granted only for the use specified in your request. No additional uses are granted (such as derivative works or other editions). For any other uses, please submit a new request.

[BACK](#)[CLOSE WINDOW](#)

Copyright © 2013 [Copyright Clearance Center, Inc.](#) All Rights Reserved. [Privacy statement.](#) Comments? We would like to hear from you. E-mail us at [customer@copyright.com](mailto:customer@copyright.com)



RightsLink®

[Home](#)[Account Info](#)[Help](#)ACS Publications  
High quality. High impact.**Title:** Comparison of SAM-Based Junctions with Ga<sub>2</sub>O<sub>3</sub>/EGaIn Top Electrodes to Other Large-Area Tunneling Junctions**Author:** Christian A. Nijhuis, William F. Reus, Jabulani R. Barber, and George M. Whitesides**Publication:** The Journal of Physical Chemistry C**Publisher:** American Chemical Society**Date:** Jul 1, 2012

Copyright © 2012, American Chemical Society

Logged in as:  
Michael Miller[LOGOUT](#)**PERMISSION/LICENSE IS GRANTED FOR YOUR ORDER AT NO CHARGE**

This type of permission/license, instead of the standard Terms & Conditions, is sent to you because no fee is being charged for your order. Please note the following:

- Permission is granted for your request in both print and electronic formats, and translations.
- If figures and/or tables were requested, they may be adapted or used in part.
- Please print this page for your records and send a copy of it to your publisher/graduate school.
- Appropriate credit for the requested material should be given as follows: "Reprinted (adapted) with permission from (COMPLETE REFERENCE CITATION). Copyright (YEAR) American Chemical Society." Insert appropriate information in place of the capitalized words.
- One-time permission is granted only for the use specified in your request. No additional uses are granted (such as derivative works or other editions). For any other uses, please submit a new request.

If credit is given to another source for the material you requested, permission must be obtained from that source.

[BACK](#)[CLOSE WINDOW](#)

Copyright © 2013 [Copyright Clearance Center, Inc.](#) All Rights Reserved. [Privacy statement.](#)  
Comments? We would like to hear from you. E-mail us at [customerca@copyright.com](mailto:customerca@copyright.com)

**RightsLink®**[Home](#)[Account Info](#)[Help](#)**ACS Publications**  
High quality. High impact.**Title:** Influence of Defects on the Electrical Characteristics of Mercury-Drop Junctions: Self-Assembled Monolayers of n-Alkanethiolates on Rough and Smooth SilverLogged in as:  
Michael Miller[LOGOUT](#)**Author:** Emily A. Weiss et al.  
**Publication:** Journal of the American Chemical Society  
**Publisher:** American Chemical Society  
**Date:** Apr 1, 2007

Copyright © 2007, American Chemical Society

**PERMISSION/LICENSE IS GRANTED FOR YOUR ORDER AT NO CHARGE**

This type of permission/license, instead of the standard Terms & Conditions, is sent to you because no fee is being charged for your order. Please note the following:

- Permission is granted for your request in both print and electronic formats, and translations.
- If figures and/or tables were requested, they may be adapted or used in part.
- Please print this page for your records and send a copy of it to your publisher/graduate school.
- Appropriate credit for the requested material should be given as follows: "Reprinted (adapted) with permission from (COMPLETE REFERENCE CITATION). Copyright (YEAR) American Chemical Society." Insert appropriate information in place of the capitalized words.
- One-time permission is granted only for the use specified in your request. No additional uses are granted (such as derivative works or other editions). For any other uses, please submit a new request.

If credit is given to another source for the material you requested, permission must be obtained from that source.

[BACK](#)[CLOSE WINDOW](#)

Copyright © 2013 [Copyright Clearance Center, Inc.](#) All Rights Reserved. [Privacy statement.](#)  
Comments? We would like to hear from you. E-mail us at [customercafe@copyright.com](mailto:customercafe@copyright.com)



RightsLink®

[Home](#)[Account Info](#)[Help](#)ACS Publications  
High quality. High impact.**Title:** Three-Dimensional and Multilayer Nanostructures Formed by Nanotransfer Printing**Author:** Jana Zaumseil et al.**Publication:** Nano Letters**Publisher:** American Chemical Society**Date:** Sep 1, 2003

Copyright © 2003, American Chemical Society

Logged in as:

Michael Miller

Account #:

3000686749

[LOGOUT](#)**PERMISSION/LICENSE IS GRANTED FOR YOUR ORDER AT NO CHARGE**

This type of permission/license, instead of the standard Terms & Conditions, is sent to you because no fee is being charged for your order. Please note the following:

- Permission is granted for your request in both print and electronic formats, and translations.
- If figures and/or tables were requested, they may be adapted or used in part.
- Please print this page for your records and send a copy of it to your publisher/graduate school.
- Appropriate credit for the requested material should be given as follows: "Reprinted (adapted) with permission from (COMPLETE REFERENCE CITATION). Copyright (YEAR) American Chemical Society." Insert appropriate information in place of the capitalized words.
- One-time permission is granted only for the use specified in your request. No additional uses are granted (such as derivative works or other editions). For any other uses, please submit a new request.

If credit is given to another source for the material you requested, permission must be obtained from that source.

[BACK](#)[CLOSE WINDOW](#)

Copyright © 2013 [Copyright Clearance Center, Inc.](#) All Rights Reserved. [Privacy statement.](#)  
Comments? We would like to hear from you. E-mail us at [customercare@copyright.com](mailto:customercare@copyright.com)



RightsLink®

[Home](#)[Account Info](#)[Help](#)ACS Publications  
High quality. High impact.**Title:** Influence of Alkyl Chain Length on the Structure of Dialkyldithiophosphinic Acid Self-Assembled Monolayers on GoldLogged in as:  
Michael Miller  
Account #:  
3000686749**Author:** Ronan R. San Juan, Michael S. Miller, Michael-Anthony Ferrato, and Tricia Breen Carmichael[LOGOUT](#)**Publication:** Langmuir**Publisher:** American Chemical Society**Date:** Sep 1, 2012

Copyright © 2012, American Chemical Society

**PERMISSION/LICENSE IS GRANTED FOR YOUR ORDER AT NO CHARGE**

This type of permission/license, instead of the standard Terms & Conditions, is sent to you because no fee is being charged for your order. Please note the following:

- Permission is granted for your request in both print and electronic formats, and translations.
- If figures and/or tables were requested, they may be adapted or used in part.
- Please print this page for your records and send a copy of it to your publisher/graduate school.
- Appropriate credit for the requested material should be given as follows: "Reprinted (adapted) with permission from (COMPLETE REFERENCE CITATION). Copyright (YEAR) American Chemical Society." Insert appropriate information in place of the capitalized words.
- One-time permission is granted only for the use specified in your request. No additional uses are granted (such as derivative works or other editions). For any other uses, please submit a new request.

[BACK](#)[CLOSE WINDOW](#)

Copyright © 2013 [Copyright Clearance Center, Inc.](#) All Rights Reserved. [Privacy statement.](#)  
Comments? We would like to hear from you. E-mail us at [customercare@copyright.com](mailto:customercare@copyright.com)



RightsLink®

Home

Account  
Info

Help

ACS Publications  
High quality. High impact.

**Title:** Molecule/Electrode Interface Energetics in Molecular Junction: A "Transition Voltage Spectroscopy" Study

**Author:** Guillaume Ricœur, Stéphane Lenfant, David Guérin, and Dominique Vuillaume

**Publication:** The Journal of Physical Chemistry C

**Publisher:** American Chemical Society

**Date:** Oct 1, 2012

Logged in as:  
Michael Miller

LOGOUT

Copyright © 2012, American Chemical Society

**PERMISSION/LICENSE IS GRANTED FOR YOUR ORDER AT NO CHARGE**

This type of permission/license, instead of the standard Terms & Conditions, is sent to you because no fee is being charged for your order. Please note the following:

- Permission is granted for your request in both print and electronic formats, and translations.
- If figures and/or tables were requested, they may be adapted or used in part.
- Please print this page for your records and send a copy of it to your publisher/graduate school.
- Appropriate credit for the requested material should be given as follows: "Reprinted (adapted) with permission from (COMPLETE REFERENCE CITATION). Copyright (YEAR) American Chemical Society." Insert appropriate information in place of the capitalized words.
- One-time permission is granted only for the use specified in your request. No additional uses are granted (such as derivative works or other editions). For any other uses, please submit a new request.

If credit is given to another source for the material you requested, permission must be obtained from that source.

BACK

CLOSE WINDOW

Copyright © 2013 [Copyright Clearance Center, Inc.](#) All Rights Reserved. [Privacy statement.](#)  
Comments? We would like to hear from you. E-mail us at [customerca@copyright.com](mailto:customerca@copyright.com)

**RightsLink**®[Home](#)[Account Info](#)[Help](#)**ACS Publications**  
High quality. High impact.**Title:** Self-Assembled Monolayers of Thiolates on Metals as a Form of NanotechnologyLogged in as:  
Michael Miller**Author:** J. Christopher Love et al.[LOGOUT](#)**Publication:** Chemical Reviews**Publisher:** American Chemical Society**Date:** Apr 1, 2005

Copyright © 2005, American Chemical Society

**PERMISSION/LICENSE IS GRANTED FOR YOUR ORDER AT NO CHARGE**

This type of permission/license, instead of the standard Terms & Conditions, is sent to you because no fee is being charged for your order. Please note the following:

- Permission is granted for your request in both print and electronic formats, and translations.
- If figures and/or tables were requested, they may be adapted or used in part.
- Please print this page for your records and send a copy of it to your publisher/graduate school.
- Appropriate credit for the requested material should be given as follows: "Reprinted (adapted) with permission from (COMPLETE REFERENCE CITATION). Copyright (YEAR) American Chemical Society." Insert appropriate information in place of the capitalized words.
- One-time permission is granted only for the use specified in your request. No additional uses are granted (such as derivative works or other editions). For any other uses, please submit a new request.

If credit is given to another source for the material you requested, permission must be obtained from that source.

[BACK](#)[CLOSE WINDOW](#)

Copyright © 2013 [Copyright Clearance Center, Inc.](#) All Rights Reserved. [Privacy statement.](#)  
Comments? We would like to hear from you. E-mail us at [customercare@copyright.com](mailto:customercare@copyright.com)

**JOHN WILEY AND SONS LICENSE  
TERMS AND CONDITIONS**

Aug 17, 2013

This is a License Agreement between Michael S Miller ("You") and John Wiley and Sons ("John Wiley and Sons") provided by Copyright Clearance Center ("CCC"). The license consists of your order details, the terms and conditions provided by John Wiley and Sons, and the payment terms and conditions.

**All payments must be made in full to CCC. For payment instructions, please see information listed at the bottom of this form.**

License Number	3211621115225
License date	Aug 17, 2013
Licensed content publisher	John Wiley and Sons
Licensed content publication	Angewandte Chemie International Edition
Licensed content title	Eutectic Gallium-Indium (EGaIn): A Moldable Liquid Metal for Electrical Characterization of Self-Assembled Monolayers
Licensed copyright line	Copyright © 2008 WILEY-VCH Verlag GmbH & Co. KGaA, Weinheim
Licensed content author	Ryan C. Chiechi, Emily A. Weiss, Michael D. Dickey, George M. Whitesides
Licensed content date	Nov 23, 2007
Start page	142
End page	144
Type of use	Dissertation/Thesis
Requestor type	University/Academic
Format	Print and electronic
Portion	Figure/table
Number of figures/tables	1
Original Wiley figure/table number(s)	Figure 1
Will you be translating?	No
Total	0.00 USD
Terms and Conditions	

**TERMS AND CONDITIONS**

This copyrighted material is owned by or exclusively licensed to John Wiley & Sons, Inc. or one of its group companies (each a "Wiley Company") or a society for whom a Wiley Company has exclusive publishing rights in relation to a particular journal (collectively "WILEY"). By clicking

<https://s100.copyright.com/AppDispatchServlet>

**THE AMERICAN ASSOCIATION FOR THE ADVANCEMENT OF SCIENCE LICENSE  
TERMS AND CONDITIONS**

Aug 17, 2013

This is a License Agreement between Michael S Miller ("You") and The American Association for the Advancement of Science ("The American Association for the Advancement of Science") provided by Copyright Clearance Center ("CCC"). The license consists of your order details, the terms and conditions provided by The American Association for the Advancement of Science, and the payment terms and conditions.

**All payments must be made in full to CCC. For payment instructions, please see information listed at the bottom of this form.**

License Number	3211631387626
License date	Aug 17, 2013
Licensed content publisher	The American Association for the Advancement of Science
Licensed content publication	Science
Licensed content title	Self-Assembly of Mesoscale Objects into Ordered Two-Dimensional Arrays
Licensed content author	Ned Bowden, Andreas Terfort, Jeff Carbeck, George M. Whitesides
Licensed content date	Apr 11, 1997
Volume number	276
Issue number	5310
Type of Use	Thesis / Dissertation
Requestor type	Scientist/individual at a research institution
Format	Print and electronic
Portion	Figure
Number of figures/tables	1
Order reference number	
Title of your thesis / dissertation	New Materials, Methods, and Molecules for Microelectronic and Molecular Electronic Devices
Expected completion date	Sep 2013
Estimated size(pages)	300
Total	0.00 USD

**Terms and Conditions**

**American Association for the Advancement of Science TERMS AND CONDITIONS**

Regarding your request, we are pleased to grant you non-exclusive, non-transferable permission, to republish the AAAS material identified above in your work identified above, subject to the terms

**THE AMERICAN ASSOCIATION FOR THE ADVANCEMENT OF SCIENCE LICENSE  
TERMS AND CONDITIONS**

Aug 17, 2013

This is a License Agreement between Michael S Miller ("You") and The American Association for the Advancement of Science ("The American Association for the Advancement of Science") provided by Copyright Clearance Center ("CCC"). The license consists of your order details, the terms and conditions provided by The American Association for the Advancement of Science, and the payment terms and conditions.

**All payments must be made in full to CCC. For payment instructions, please see information listed at the bottom of this form.**

License Number	3211640400036
License date	Aug 17, 2013
Licensed content publisher	The American Association for the Advancement of Science
Licensed content publication	Science
Licensed content title	Forming Electrical Networks in Three Dimensions by Self-Assembly
Licensed content author	David H. Gracias, Joe Tien, Tricia L. Breen, Carey Hsu, George M. Whitesides
Licensed content date	Aug 18, 2000
Volume number	289
Issue number	5482
Type of Use	Thesis / Dissertation
Requestor type	Scientist/individual at a research institution
Format	Print and electronic
Portion	Figure
Number of figures/tables	1
Order reference number	
Title of your thesis / dissertation	New Materials, Methods, and Molecules for Microelectronic and Molecular Electronic Devices
Expected completion date	Sep 2013
Estimated size(pages)	300
Total	0.00 USD

**Terms and Conditions**

**American Association for the Advancement of Science TERMS AND CONDITIONS**

Regarding your request, we are pleased to grant you non-exclusive, non-transferable permission, to republish the AAAS material identified above in your work identified above, subject to the terms

**THE AMERICAN ASSOCIATION FOR THE ADVANCEMENT OF SCIENCE LICENSE  
TERMS AND CONDITIONS**

Aug 17, 2013

---

This is a License Agreement between Michael S Miller ("You") and The American Association for the Advancement of Science ("The American Association for the Advancement of Science") provided by Copyright Clearance Center ("CCC"). The license consists of your order details, the terms and conditions provided by The American Association for the Advancement of Science, and the payment terms and conditions.

**All payments must be made in full to CCC. For payment instructions, please see information listed at the bottom of this form.**

License Number	3211700682376
License date	Aug 17, 2013
Licensed content publisher	The American Association for the Advancement of Science
Licensed content publication	Science
Licensed content title	Fabrication of a Cylindrical Display by Patterned Assembly
Licensed content author	Heiko O. Jacobs, Andrea R. Tao, Alexander Schwartz, David H. Gracias, George M. Whitesides

[Print This Page](#)

**NATURE PUBLISHING GROUP LICENSE  
TERMS AND CONDITIONS**

Aug 17, 2013

This is a License Agreement between Michael S Miller ("You") and Nature Publishing Group ("Nature Publishing Group") provided by Copyright Clearance Center ("CCC"). The license consists of your order details, the terms and conditions provided by Nature Publishing Group, and the payment terms and conditions.

**All payments must be made in full to CCC. For payment instructions, please see information listed at the bottom of this form.**

License Number	3211620964800
License date	Aug 17, 2013
Licensed content publisher	Nature Publishing Group
Licensed content publication	Nature Nanotechnology
Licensed content title	Efficient electronic coupling and improved stability with dithiocarbamate-based molecular junctions
Licensed content author	Florian von Wrochem, Deqing Gao, Frank Scholz, Heinz-Georg Nothofer, Gabriele Nelles, Jurina M. Wessels
Licensed content date	Jun 20, 2010
Volume number	5
Issue number	8
Type of Use	reuse in a thesis/dissertation
Requestor type	academic/educational
Format	print and electronic
Portion	figures/tables/illustrations
Number of figures/tables/illustrations	2
High-res required	no
Figures	Figure 1 Figure 2
Author of this NPG article	no
Your reference number	
Title of your thesis / dissertation	New Materials, Methods, and Molecules for Microelectronic and Molecular Electronic Devices
Expected completion date	Sep 2013
Estimated size (number of pages)	300
Total	0.00 USD

Terms and Conditions

<https://s100.copyright.com/AppDispatchServlet>

**JOHN WILEY AND SONS LICENSE  
TERMS AND CONDITIONS**

Aug 17, 2013

This is a License Agreement between Michael S Miller ("You") and John Wiley and Sons ("John Wiley and Sons") provided by Copyright Clearance Center ("CCC"). The license consists of your order details, the terms and conditions provided by John Wiley and Sons, and the payment terms and conditions.

**All payments must be made in full to CCC. For payment instructions, please see information listed at the bottom of this form.**

License Number	3211600949015
License date	Aug 17, 2013
Licensed content publisher	John Wiley and Sons
Licensed content publication	Advanced Materials
Licensed content title	Single Molecule Electronic Devices
Licensed copyright line	Copyright © 2011 WILEY-VCH Verlag GmbH & Co. KGaA, Weinheim
Licensed content author	Hyunwook Song, Mark A. Reed, Takhee Lee
Licensed content date	Feb 2, 2011
Start page	1583
End page	1608
Type of use	Dissertation/Thesis
Requestor type	University/Academic
Format	Print and electronic
Portion	Figure/table
Number of figures/tables	1
Original Wiley figure/table number(s)	Figure 1
Will you be translating?	No
Total	0.00 USD
Terms and Conditions	

**TERMS AND CONDITIONS**

This copyrighted material is owned by or exclusively licensed to John Wiley & Sons, Inc. or one of its group companies (each a "Wiley Company") or a society for whom a Wiley Company has exclusive publishing rights in relation to a particular journal (collectively "WILEY"). By clicking "accept" in connection with completing this licensing transaction, you agree that the following terms and conditions apply to this transaction (along with the billing and payment terms and conditions

<https://s100.copyright.com/AppDispatchServlet>

**JOHN WILEY AND SONS LICENSE  
TERMS AND CONDITIONS**

Aug 17, 2013

---

This is a License Agreement between Michael S Miller ("You") and John Wiley and Sons ("John Wiley and Sons") provided by Copyright Clearance Center ("CCC"). The license consists of your order details, the terms and conditions provided by John Wiley and Sons, and the payment terms and conditions.

**All payments must be made in full to CCC. For payment instructions, please see information listed at the bottom of this form.**

License Number	3211630883782
License date	Aug 17, 2013
Licensed content publisher	John Wiley and Sons
Licensed content publication	Advanced Functional Materials
Licensed content title	Uniformly Interconnected Silver-Nanowire Networks for Transparent Film Heaters
Licensed copyright line	Copyright © 2013 WILEY-VCH Verlag GmbH & Co. KGaA, Weinheim

[Print This Page](#)

ACS Publications  
High quality. High impact.

**Title:** Silver Nanowire/Optical Adhesive Coatings as Transparent Electrodes for Flexible Electronics

**Author:** Michael S. Miller, Jessica C. O'Kane, Adrian Niec, R. Stephen Carmichael, and Tricia Breen Carmichael

**Publication:** Applied Materials

**Publisher:** American Chemical Society

**Date:** Oct 1, 2013

Copyright © 2013, American Chemical Society

User ID
<input type="text"/>
Password
<input type="text"/>
<input type="checkbox"/> Enable Auto Login
<input type="button" value="LOGIN"/>
<a href="#">Forgot Password/User ID?</a>
If you're a <a href="#">copyright.com</a> user, you can login to RightsLink using your <a href="#">copyright.com</a> credentials. Already a <a href="#">RightsLink</a> user or want to <a href="#">learn more?</a>

**PERMISSION/LICENSE IS GRANTED FOR YOUR ORDER AT NO CHARGE**

This type of permission/license, instead of the standard Terms & Conditions, is sent to you because no fee is being charged for your order. Please note the following:

- Permission is granted for your request in both print and electronic formats, and translations.
- If figures and/or tables were requested, they may be adapted or used in part.
- Please print this page for your records and send a copy of it to your publisher/graduate school.
- Appropriate credit for the requested material should be given as follows: "Reprinted (adapted) with permission from (COMPLETE REFERENCE CITATION). Copyright (YEAR) American Chemical Society." Insert appropriate information in place of the capitalized words.
- One-time permission is granted only for the use specified in your request. No additional uses are granted (such as derivative works or other editions). For any other uses, please submit a new request.

## **Vita Auctoris**

**Name:** Michael Stephen Miller

**Place of Birth:** Windsor, Ontario, Canada

**Education:**

**Ph.D. Chemistry**

Department of Chemistry and Biochemistry, University of Windsor,  
Windsor, Ontario, Canada. 2013.

**B.Sc. Honours Chemistry with Thesis**

Department of Chemistry and Biochemistry, University of Windsor,  
Windsor, Ontario, Canada. 2008.

St Joseph's Secondary School, Windsor, Ontario, Canada. 2000-2004.

**Work Experience:**

**Research Assistant**

Department of Chemistry and Biochemistry, University of Windsor,  
Windsor, Ontario, Canada. September 2005 - August 2013.

**Graduate Assistant**

Department of Chemistry and Biochemistry, University of Windsor,  
Windsor, Ontario, Canada. September 2008 - April 2013.

**Honours and Awards:**

NSERC CGS-D (2010-2013)

Ontario Graduate Scholarship (2008-2010)

American Chemical Society Award (2008)

NSERC USRA (2008)

CSC Silver Medal (2007)

University of Windsor Outstanding Scholar Award (2004-2008)

University of Windsor Entrance Scholarship (2004-2008)

Inorganic Discussion weekend Top Poster Prize (2006)

CIS Academic All-Canadian (2005-2009)

## Publications:

1. **Miller, M. S.**; San Juan, R. R.; Ferrato, M.-A.; Carmichael, T. B. “The Unusual Self-Organization of Dialkyldithiophosphinic Acid Self-Assembled Monolayers on Ultrasoother Gold”. **2013**, Submitted (*J. Am. Chem. Soc.*) ID: ja-2013-11140j.
2. **Miller, M. S.**; O’Kane, J. C.; Niec, A.; Carmichael, R. S.; Carmichael, T. B. “Silver Nanowire/Optical Adhesive Coatings as Transparent Electrodes for Flexible Electronics” *ACS Appl. Mater. Interfaces* **2013**, 5, 10165-10172.
3. San Juan, R. R.; **Miller, M. S.**; Ferrato, M.-A.; Carmichael, T. B.; “Influence of Alkyl Chain Length on the Structure of Dialkyldithiophosphinic Acid Self-Assembled Monolayers on Gold” *Langmuir* **2012**, 28, 13253-13260.
4. **Miller, M. S.**; San Juan, R. R.; Ferrato, M.-A.; Carmichael, T. B. “New Dialkyldithiophosphinic Acid Self-Assembled Monolayers (SAMs): Influence of Gold Substrate Morphology on Adsorbate Binding and SAM Structure” *Langmuir* **2011**, 27, 10019-10026.
5. **Miller, M. S.**; Filiatrault, H. L.; Davidson, G. J. E.; Luo, M.; Carmichael, T. B. “Selectively Metallized Polymeric Substrates by Microcontact Printing an Aluminum(III) Porphyrin Complex” *J. Am. Chem. Soc.* **2010**, 132, 765-772.
6. **Miller, M. S.**; Davidson, G. J. E.; Carmichael, T. B. “Templated Self Assembly of Glass Microspheres into Ordered Two-Dimensional Arrays under Dry Conditions” *Langmuir* **2010**, 26, 5286-90.
7. **Miller, M. S.**; Davidson, G. J. E.; Sahli, B. J.; Mailloux, C. M.; Carmichael, T. B.; “Fabrication of Elastomeric Wires by Selective Electroless Metallization of Poly(dimethylsiloxane)” *Adv. Mater.* **2008**, 20, 59-64

**Conference and Poster Presentations (\* denotes presenting author):**

**Miller, M. S.;**\* San Juan, R. R.; Ferrato, M.-A.; Carmichael, T. B. “Self-Assembled Monolayers (SAMs) of Dialkyldithiophosphinic Acids (DTPAs) on Gold: The Effect of Alkyl Chain Length on SAM Properties”. The 243rd ACS National Meeting in San Diego, CA, USA. Oral Presentation (2012).

San Juan, R. R.;

**Miller, M. S.;** Carmichael, T. B. “New Class of Self-Assembled Monolayers (SAMs) Based on Dithiophosphinic Acids (DTPAs)” The 243rd ACS National Meeting in San Diego, CA, USA. Oral Presentation (2012).

Carmichael, T. B.;

**Miller, M. S.;** San Juan, R. R.; Ferrato, M.-A. “Self-Assembled Monolayers (SAMs) of Dialkyldithiophosphinic Acids (DTPAs): Manipulating Gold Substrate Morphology and DTPA Chemistry to Control SAM Properties” 94th Canadian Chemistry Conference in Montreal, ON, Canada. Oral Presentation (2011).

**Miller, M. S.;**\* Carmichael, T. B. “Chemical Mechanical Polishing of Gold: The Role of Substrate Morphology in Controlling the Structure and Charge Transport Properties of n-Alkanethiolate Self-Assembled Monolayers” 94th Canadian Chemistry Conference in Montreal, ON, Canada. Oral Presentation (2011).

Carmichael, T. B.;

**Miller, M. S.;** San Juan, R. R. “Directing the Binding and Structure of Dithiophosphinic acid (DTPA) Self-Assembled Monolayers Using Substrate Morphology” 93rd Canadian Chemistry Conference in Toronto, ON, Canada. Oral Presentation (2010).

**Miller, M. S.;**\* Carmichael, T. B. (2010) “Low-Defect Alkanethiolate Self-Assembled Monolayers on Ultra-Smooth Gold Substrates Prepared by Chemical Mechanical Planarization” 93rd Canadian Chemistry Conference in Toronto, ON, Canada. Poster Presentation (2010).

Davidson, G. J. E.; **Miller, M. S.;** Filiatrault, H. L.; Carmichael, T. B.\* “Simple, Low-Cost Methods for the Fabrication of Flexible Devices” 92nd Canadian Chemistry Conference in Hamilton, ON, Canada. Oral Presentation (2009).

San Juan, R. R.;\*, Muller, J.; **Miller, M. S.**; Carmichael, T. B. “New Self-Assembled Monolayers (SAMs) on Gold with Nanoscale Structural Control” 42nd Inorganic Discussion Weekend in Guelph, ON, Canada. Oral Presentation (2009).

Carmichael, T. B.;\*, Davidson G. J. E.; and **Miller, M. S.** (“A Simple, Low-Cost Approach to Selective Metal Deposition on Polymeric Substrate”. MRS Fall Meeting in Boston, MA, USA. Oral Presentation (2008).

**Miller, M. S.**;\* Davidson, G. J. E.; Carmichael, T. B. “Selective Self-Assembly of Micron-Scale Components Under Dry Conditions” 91st Canadian Chemistry Conference in Edmonton, AB, Canada. Poster Presentation (2008).

**Miller, M. S.**;\* Davidson, G. J. E.; Carmichael, T. B. “New, Low-Cost Fabrication Methods for Polymer-Based Electronic Devices” Inorganic Discussion Weekend in Toronto, ON, Canada. Poster Presentation (2007).

Carmichael, T. B.;\* Mailloux, C. M.; **Miller, M. S.**; Sahli, B. J. “Selective Electroless Metallization of Elastomeric Substrates” The 233rd ACS National Meeting in Boston, MA, USA. Oral Presentation (2007).